2021

School of Engineering
Howard College Campus
Durban

HYDROTHERMAL LIQUEFACTION OF MARINE MACROALGAE

By:

Deslin Nadar

MSc Chemical Engineering
2021

A dissertation submitted to the School of Engineering
University of KwaZulu-Natal
Durban
In fulfilment of the requirements of the degree of Master of Science in Engineering

DECLARATION

The work presented in this dissertation was undertaken at the School of Engineering, University of KwaZulu-Natal, Howard College Campus in Durban, South Africa, from February 2018 until December 2019.

All work presented in this dissertation is original unless otherwise stated. It has neither in whole nor part been submitted previously to any other University or Institute as part of a degree.

I, Deslin Nadar, declare that

1. The research reported in this thesis, except where otherwise indicated, is my original research.

2. This thesis has not been submitted for any degree or examination at any other university.

3. This thesis does not contain other persons‟ data, pictures, graphs or other information, unless specifically acknowledged as being sourced from other persons.

4. This thesis does not contain other persons' writing, unless specifically acknowledged as being sourced from other researchers. Where other written sources have been quoted, then:

a. Their words have been re-written but the general information attributed to them has been referenced

b. Where their exact words have been used, then their writing has been placed in italics and inside quotation marks, and referenced.

5. This thesis does not contain text, graphics or tables copied and pasted from the Internet, unless specifically acknowledged, and the source being detailed in the thesis and in the References sections.

_____

Deslin Nadar

As the candidate’s supervisor hereby certify that I find this work to be suitable for submission for the degree of Master of Science in Chemical Engineering.

_____

Prof. David Lokhat

ACKNOWLEDGEMENTS

I would like to take this opportunity to acknowledge and show my deepest gratitude to the following people who have all greatly contributed to the completion of this dissertation:

Firstly, I would like to thank my parents, my brother, my family, friends, and God for giving me the motivation, support, and strength to pursue my Master of Science degree and other endeavours in life.

My supervisor, Professor David Lokhat, for imparting to me his invaluable expertise, vast knowledge, and guidance for the entirety of the project.

The lab technicians: Ms. Xoli Hadebe and Ms. Thobekile Mofokeng, and the chemical engineering technical staff: Mr. Sanjay Deeraj, Mr. Danny Singh, Mr. Sanil Mahabeer, and Mr. Gerald Addieah. Thank you for your valuable expertise and assistance throughout my laboratory work.

Postgraduate student, Ethan Hammond, and undergraduate student, Alyssa Murray, for their assistance with the kinetic modeling of the experimental data.

ABSTRACT

The biofuel industry has experienced substantial growth during the past decade due to the extreme demands placed on the fossil fuel industry and the limited availability of fossil fuels. Biofuels are seen as a renewable source of energy while reducing the effects on the environment significantly. Renewable biofuels are made through the use or conversion of biomass such as algae and lignocellulosic biomass. Biomass is seen as a viable alternative to produce biofuel as it is readily available, and has a relatively low cost. Marine macroalgae (seaweed) may be considered as a feedstock for biofuel production due to their low cost, fast growth rate, and they do not cause land-use and fuel-vs-food conflicts. Hydrothermal liquefaction is a thermochemical process that utilises water as a reaction medium under high pressures and temperatures to produce bio-oils from biomass. Hydrothermal liquefaction is different from most other conversion techniques as it uses a wet feedstock and does not require an energy-consuming drying step.

In this work, hydrothermal liquefaction of marine macroalgae for the production of bio-oil was studied at various reaction conditions. The effect of the mass of seaweed, temperature, pressure, solids loading and reaction time were examined. A kinetic model of dissolution was developed and regressed against the experimental temporal data to obtain the kinetics of dissolution. A measured quantity of marine macroalgae and water were placed within the Parr reaction vessel and exposed to high temperatures and pressures for a set time. The resulting solution was filtered, to separate the algae from the liquid (water and bio-oil solution), and mixed with dichloromethane, to selectively separate the bio-oil from the water. The dichloromethane mixture was transferred to the rotary evaporator and the dichloromethane was evaporated to ensure only the bio-oil remained. The bio-oil was measured and transferred to the GC/MS for a more in-depth compositional analysis.

Bio-oil was formed for every variation of the process variables and every run conducted. The highest bio-oil yield obtained was for the 10g 10wt% run at the high reaction conditions (250°C and 4000 KPa) and a time of 30 minutes, with a bio-oil yield of 34.67%. This was for the highest manipulation of every process variable. The lowest bio-oil yield (not including the induction period) was obtained for the 6g 10wt% run at the low reaction conditions (200°C and 1500 KPa) and a time of 5 minutes, with a bio-oil yield of 18.14%. The bio-oil yield formed during the induction period ranged from 0.11% to 26.58%. A higher mass loading was observed to provide a higher dissolution and a higher bio-oil yield (ranging from 29.59% to 34.67% for a mass loading of 10g)). Higher temperatures and pressures were also found to increase the mass dissolution and bio-oil yield obtained. The higher solids loading of 10wt% observed a larger bio-oil yield (ranging from 27.96% to 32.62%) than a solids loading of 5wt% (ranging from 22.81% to 26.53%). The bio-oil yield was found to increase for an increase in the reaction time for every variation of the process variable.

The assessment of the quality of bio-oil through GC/MS analysis determined that the main compounds formed during the hydrothermal liquefaction process were hexanedioic acid (adipic acid), cyclopentene, hexadecenoic acid, phenol, butanone, ethanone, tetrapentacontane, furancarboxaldehyde, cyclohexane, and hexanedioic acid- bis (2-ethyhexyl) ester. A kinetic model was applied to the data obtained to determine the kinetic parameters of dissolution. The dynamic model was identified with the aid of MATLAB programming software. The kinetic models for the conversion of solids to bio-oil and the conversion of solids to the aqueous product have the same formula. The simplified model is expressed by the mass fraction of the solid biomass multiplied by the kinetic rate constant and then multiplied again by the exponential of the negation of the inhibition constant over the mass fraction of the solid biomass. Utilising both the non-linear least squares regression and the ode15s variable-step, variable-order solver, the kinetic reaction rates were determined to be 0.0059 g/g/s (k_1) for the conversion from solids biomass to bio-oil and 0.0103 g/g/s (k_2) for the conversion from solid biomass to the aqueous-phase product. The inhibition constants (k_3 and k_4) were determined to be the same at a value of 4.44e-14.

The overall results of this work validate that the hydrothermal liquefaction of marine algae produces an adequate amount of bio-oil that may be further processed to produce biofuel. It was observed that higher process conditions resulted in higher bio-oil yields being obtained and that a kinetic model may be determined for the mass dissolution from the algae and bio-oil yield formed. The maximum yield of 34.67% obtained in this work was amongst the higher yield results for research in this section, while utilizing lower temperatures and a slightly higher reaction time, thereby requiring a lower amount of energy. The results of this work imply that enough bio-oil is formed from the hydrothermal liquefaction of marine macroalgae to allow for scale-up of the process to produce a cleaner biofuel fuel that may alleviate the demands placed on fossil fuels.

TABLE OF CONTENTS

LIST OF FIGURES

LIST OF TABLES

NOMENCLATURE

Symbol	Definition	Unit
M_b	Mass of bio-oil	g
$M_{d,f}$	Final dry mass of seaweed	g
$M_{d,i}$	Initial dry mass of seaweed	g
$M_{d,l}$	Total dry mass of seaweed lost	g
$M_{w,f}$	Final wet mass of seaweed	g
$M_{w,i}$	Initial wet mass of seaweed	g
MC_f	Final moisture content	%
MC_i	Initial moisture content	%
MD	Mass dissolution	%
Y	Yield	%
k_1, k_2	Kinetic rate constants	g/g/s
k_3, k_4	Inhibition constants	-

CHAPTER 1: INTRODUCTION

1.1. Motivation of research

The biofuel industry has experienced substantial growth over the past decade due to the extreme demands placed on the fossil fuel industry and the environmental impacts of fossil fuels (Popp et al., 2014). Fossil fuels satisfy the majority of the energy demands of the planet and may be regarded as the world's primary source of energy, however, fossil fuels are a non-renewable resource and contribute significantly to the amount of greenhouse gases in the atmosphere. Climate change as well as the effects of global warming have made biofuels an attractive option for use as an energy source (Nadar et al., 2020). Biofuels provide a renewable source of energy while substantially reducing the effects on the environment. Biofuels are produced through the conversion of biomass. Biomass used for the production of biofuels are generally defined as organic matter derived from living plants, which are produced through the process of photosynthesis (Pang, 2016).

The use of biomass for biofuel production is assumed to be a carbon-neutral cycle as the carbon dioxide is absorbed by living biomass and expelled when the biomass is burnt for fuel (EESI, 2020). Biomass may be used to produce thermal energy, transportation fuels, and electricity. The combination of utilising biomass and fossil fuels in power stations may aid in reducing air pollutants and reduce the cost of energy. Biomass is composed of cellulose, hemicellulose, lignin, proteins (amino acids), and fats (lipids), however, the amount of the constituents varies depending on the type of biomass utilised (Gollakota et al., 2018). There are a variety of biomass sources that may be used for the production of biofuels. Types of biomass include algae, lignocellulosic biomass, agricultural crops, wood processing residues, dedicated energy crops, wet waste, and municipal waste (Office of Energy Efficiency and Renewable Energy, 2020).

Algae biomass is composed of three main components, namely, lipids (natural oils), carbohydrates, and proteins. Algae is the feedstock for third-generation biofuels (Vassilev & Vassileva, 2016). Third-generation biofuels may overcome the limitations of first- and second-generation biofuels, such as land-use conflicts and the protection and preservation of ecosystems (Nigam & Singh, 2011). Microalgae is usually considered as a source of biomass over macroalgae due to the higher content of lipids and the presence of triglycerol when it is converted to bio-oil (Wen, 2019), however, the difficulty of cultivation of microalgae makes macroalgae a viable choice for biofuel production. Algae can easily adapt and may grow in a variety of locations and climates, therefore, it may be harvested year-round and does not cause a land availability issue and fuel–food conflicts (Bharathiraja et al., 2015). Algae biomass possesses a rapid growth rate and high crop yield. Algae may grow in oceans, rivers ponds, and a variety of waste waters (Vassilev & Vassileva, 2016).

Algae do not require the addition of nutrients and fertiliser to grow, as it utilises the nutrients supplied by the source in which it is growing. They reproduce very quickly and may be known as the fastest-

growing organisms (Ullah et al., 2015). Algae may also be processed when wet so there is no energy-intensive drying step required. Biofuels produced from algae biomass are regarded as a good source of renewable energy with the potential to satisfy the long-term sustainability of the global demand for biofuels (Vassilev & Vassileva, 2016). Algae may be anaerobically digested to produce methane gas and may be utilised to produce hydrogen gas within specific growth and reaction conditions (Wen, 2019). Algal biofuels are known as an effective response to climate change that does not affect food and feed security (Vassilev & Vassileva, 2016). Algae may also be burned to produce thermal and electric energy. Algal biofuels are sustainable, renewable, and environmentally friendly.

Hydrothermal liquefaction is a thermochemical process that utilises high temperatures and pressure in a liquid reaction medium to produce biocrude from various biomass feedstocks (Valdez et al., 2014). For the hydrothermal liquefaction process, the reaction pressures range from 1.5 MPa to 20 MPa (Toor et al., 2011) and the reaction temperatures vary from 200°C to 400°C (Chen et al., 2015). The bio-oil produced from this process may be converted to a product similar to petroleum crude as the bio-oil is energy dense (Dote et al., 1994). Hydrothermal liquefaction may be considered over other conversion processes as it possesses a lower energy requirement (Zou et al., 2010). Hydrothermal liquefaction processing does not require a reaction catalyst, therefore there is no need for a catalyst separation step, thereby reducing the overall process costs (Duan & Savage, 2010). This technology may process both dry and wet feeds and as a result does not require drying of the feedstock which is known to require a lot of energy (Valdez et al., 2014). A further advantage of this technology is that it is possible to recycle the reaction medium (in most cases water), which is nutrient-rich and possesses elements such as magnesium, iron, and potassium (Biller et al., 2012)

1.2. Research questions

The overall aim of the study is to consider the performance of the hydrothermal liquefaction process for conversion of marine macroalgae and attempt to extract kinetic data for the process. The study will address the following two research questions:

1. How do the process variables (reaction time, mass, solids loading, temperature, and pressure) affect the production and quality of bio-oil from the hydrothermal liquefaction of marine macroalgae?

2. Can a kinetic model be applied to the mass dissolution data obtained, and if so, what are the kinetic parameters?

1.3. Objectives

The objectives are the main tasks that will accomplish the overall aim of the study. The following objectives will address the overall aim of this study:

1. Provide an in-depth theoretical background of biomass (specifically algae) and the hydrothermal liquefaction process in the production of bio-oil.

2. Design and compile process methodology and equipment and identify operating conditions to achieve the desired hydrothermal processing.

3. Determine if bio-oil can be formed from the hydrothermal liquefaction of marine macroalgae and determine the amount of bio-oil formed from the hydrothermal liquefaction process at different reaction times, masses of seaweed, solids loading, and the temperature and pressure.

4. Analyse the quality of the bio-oil formed through Gas Chromatography-Mass Spectrometry (GCMS) analysis.

5. Develop a kinetic model to accurately represent the mass dissolution and formation of bio-oil from marine macroalgae during hydrothermal processing.

1.4. Outline of dissertation

This dissertation was divided into six chapters to provide a complete understanding of the experimental research conducted.

Chapter 1 consists of the motivation of the research and outlines the research questions, objectives, and aims.

Chapter 2 provides a literature review on the information relevant to the research topic, including background and understanding of biomass and its use in the biofuel industry, as well as an in-depth understanding of the hydrothermal liquefaction process and its application in producing bio-oil.

Chapter 3 describes the experimental design and methodology of the process and the equipment used in the research.

Chapter 4 consists of the analysis of the results and an in-depth discussion on the results and the development and analysis of the kinetic model obtained.

Chapter 5 describes the main conclusions from the research conducted and the extent to which objectives were completed and the research questions answered.

Chapter 6 states possible recommendations that may be applied to the experimental work to achieve a more efficient process and higher bio-oil yields.

CHAPTER 2: LITERATURE REVIEW

The literature review will provide an analysis on biomass, its role in the biofuel industry, and its potential to alleviate the demands placed on fossil fuels, with a specific focus on marine macroalgae (seaweed) and its current potential in the biofuel industry. It will also provide a review of thermochemical conversion technologies, specifically a branch of liquefaction (hydrothermal liquefaction) and its reaction conditions and reaction mechanism.

2.1. Biomass for energy and fuel applications

Biomass is organic matter that is animal or plant in origin, marine and terrestrial, produced indirectly or directly through photosynthesis (Bonechi et al., 2017). Biomass for the production of energy refers to residues, crops, and biological materials that may be utilized as an alternative to fossil fuels (EESI, 2020). It may be defined as anything that consists of an organic matrix (Bonechi et al., 2017). Living biomass is known to consume carbon dioxide as it grows (photosynthesis) and expels the carbon dioxide when it is used for the production of energy (Pang, S., 2018). This results in a cycle that is close to carbon-neutral(Pang, S., 2018). The composition of biomass permits the development of an extensive bioindustry through the utilisation of the various components of biomass (Nadar et al., 2020). Biomass can be used to produce biocrude or bio-oil which may be applied to generate thermal energy, renewable electricity, and transportation fuels (EESI, 2020). It is a highly available resource and is seen as a renewable source of energy (Nadar et al., 2020). The use of biomass along with fossil fuels in power plants may provide a low-cost means for reducing air pollutants and greenhouse gas emissions. The use of biomass is a strategic response to the increasing deficiency of traditional energy sources (Bonechi et al., 2017). The use of biomass could help alleviate the excessive demands placed on fossil fuels and reduce the price of energy. The value of biomass is enhanced through the utilisation of the various components present within the biomass, permitting the development of a large-scale bioindustry to utilise all the components.

2.1.1. Elemental composition of biomass

The composition of biomass is dependent on whether lignocellulosic, woody (fibrous), or algae is being used for processing. Different biomasses have different elemental compositions depending on a variety of factors, including, area of origin and growth conditions. The general elemental composition of biomass consists of a few important elements such as carbon (C), oxygen (O), nitrogen (N), hydrogen (H), sulphur (S). An overview of these elements is presented below.

Carbon (C)

Carbon is the most important component of biomass (Gollakota et al., 2018). The carbon is obtained from atmospheric carbon dioxide that is absorbed into the plant matter during photosynthesis. During photosynthesis, plants use sunlight and carbon dioxide (along with water and chlorophyll) to produce

oxygen. Carbon represents a main contribution to the overall heating value of biomass (Gollakota et al., 2018). The carbon molecules are converted into carbon dioxide during the combustion process, and released into the atmosphere (Wang et al., 2011). This results in a net zero greenhouse gas emission as carbon dioxide is used by the plant to produce oxygen and is expelled from the plant when it is burned for fuel. During most combustion processes, a portion of the carbon does not combust completely and is emitted into the atmosphere as other gases such as carbon monoxide (Vallero, 2008). The carbon content of biofuel is generally estimated using the composition of cellulose, lignin, and hemicellulose (Gollakota et al., 2018).

Oxygen (O)

Oxygen is an important element in the chemical composition of plant matter (Gollakota et al., 2018). Oxygen is produced during photosynthesis in green plants and released into the atmosphere. Oxygen is also absorbed into the plant biomass in the form of water and carbon dioxide. The oxygen content controls the heating value of the biocrude that is formed from the processing of biomass (Elliot, 2011). A decrease in the oxygen content results in an increase in the heating value of the biocrude (Huber et al., 2006). The majority of bio crudes are limited in their use as they possess an excess oxygen content (Gollakota et al., 2018)).

Nitrogen (N)

Nitrogen is an important element in plant matter. Nitrogen forms part of the proteins and nucleic acid of plants. Nitrogen is utilized in fertilizers for soil and improves the growth of plants (Gollakota et al., 2018). Due to the continual application of nitrogen-based fertilizer in modern agriculture, woody biomass has a lower nitrogen content than herbaceous biomass (Hirel et al., 2011). Although nitrogen aids in the growth of plants, the presence of nitrogen contributes to the degradation during biological processes such as fermentation (Gollakota et al., 2018).

Hydrogen (H)

Hydrogen is another main element in biomass due to the chemical composition of the phenolic polymers and carbohydrates (Gollakota et al., 2018). During the combustion of biomass, the hydrogen within the biomass is converted to water resulting in hydrogen contributing significantly to the overall heating value of the biomass combustion (Kreith and Goswami, 2007). An increase in the hydrogen content of the bio-crude formed from biomass processing results in an increase in its heating value (Huber et al., 2006). Woody biomass has a hydrogen content of approximately 6-8% by weight, which is slightly higher than the hydrogen content of herbaceous biomass, which has a hydrogen content of approximately 5.5-6% by weight (Gollakota et al., 2018).

Sulphur (S)

Sulphur forms part of proteins and amino acids in plants and aids in the growth of the plant (Gollakota et al., 2018). The substantial growth rate of herbaceous biomass compared to woody biomass could imply that herbaceous biomass contains a larger concentration of sulphur (Gollakota et al., 2018). The most important aspect of sulphur relates to biomass processing, as sulphur impacts gaseous emissions. The presence of sulphur in syngas requires an extra step of cleaning the syngas of sulphur before further processing. Sulphur is also corrosive to many upgrading procedures and needs to be reduced to an acceptable level.

2.1.2. Chemical composition of biomass

2.1.2.1. Cellulose

Cellulose may be considered a valuable component in plant matter as it stores large quantities of the energy conserved by photosynthesis (Nadar et al., 2020). It has a high degree of polymerisation and is a long-chain polysaccharide (Gollakota et al., 2018). Cellulose is a polymer of glucose. Cellulose that is obtained from biomass is a type of celluboise, which is made up of two glucose molecules (Harmsen et al., 2010). Cellulose possesses a crystalline structure due to the nature of the hydrogen bonds between the molecules, however, at higher temperatures cellulose becomes soluble as the increase in energy is sufficient to break the intermolecular hydrogen bonds (Harmsen et al., 2010).

2.1.2.2. Hemicellulose

Hemicellulose is a hetero polymer that possesses a branched and amorphous structure (Gollakota et al., 2018). Hemicellulose represents a group of polysaccharides found in the cell wall of the plant (Harmsen et al., 2010). The hemicellulose compositions differ depending on the type of biomass. Grassy biomass contains hemicellulose that is composed of galactan, mannan, and glucan, and woody biomass possesses hemicellulose that contains xylan (Delmer and Amor, 1995). Hemicellulose has a weaker structure than cellulose and may disintegrate more easily due to the weaker intermolecular forces (Peterson et al., 2008).

2.1.2.3. Lignin

Lignin is a complex natural polymer and may be regarded as an aromatic compound (Harmsen et al., 2010). It is an amorphous polymer that is composed predominantly of phenyl-propane as its building blocks (Harmsen et al., 2010). Lignin is resistant to forms of biological degradation and possesses a low decay rate (Gollakota et al., 2018). Lignin has a high energy content and a high heating value (Wahyudiono et al., 2007). Lignin has a solubility comparable to that of cellulose and it possesses a hydrophobic nature (Gollakota et al., 2018). It is composed of fibrous contents to help strengthen the structure of the cell wall (Osada et al., 2006).

2.1.2.4. Proteins/ Amino acids

Protein is one of the main components of algae or microbial biomass (Gollakota et al., 2018). Proteins are composed of amino acids and are highly heterogenous (Gollakota et al., 2018). The heterogenous nature of amino acids makes the degradation of amino acids a challenging and complex process. Hydrothermal processing of the peptide chains of proteins results in the protein experiencing deamination and decarboxylation reactions which forms amines, acids, aldehydes, and hydrocarbons (Toor et al., 2011). Further processing of proteins results in propionic acid, acetic acid, iso-butyric acid, and carboxylic acid (Gollakota et al., 2018).

2.1.2.5. Lipids/ Fats

Lipids are non-polar compounds that are hydrophobic in nature (Gollakota et al., 2018). It is commonly referred to as triglycerides which are triesters of glycerol and fatty acids (Bühler et al., 2002). Fats are insoluble in solvents at ambient conditions. A change in the temperature of the fats may allow them to be converted to polar compounds (Gollakota et al., 2018). The stability of the structure of triglycerides leads to glycerol being formed, which is a by-product of biodiesel production (Gollakota et al., 2018). This is a combination of methanol, salts, and fatty acids (Gollakota et al., 2018).

2.2. Types of biomass

There are a variety of biomass sources that may be considered as potential sources for chemical feed stocks and fuels (Toor et al., 2013). The types of biomass include agricultural crops, dedicated energy crops, algae, forestry residues, wood processing residues, wet waste, and municipal waste.

2.2.1. Agricultural crop residue

Agricultural crop residues are diverse, abundant, and widely distributed. Agricultural crop residues generally contain approximately 35wt% cellulose, approximately 24wt% hemicellulose, and approximately 22wt% lignin (Cheng et al., 2020). Types of agricultural crop residues include wheat straw, sorghum stubble, oat straw, and corn stover (Office of Energy Efficiency and Renewable Energy, 2020). The main obstacle of using agricultural crop residues as a biomass source is the interference with the production of fibre, feed, and food, as land use for food crops is prioritised over biomass.

2.2.2. Dedicated energy crops

Dedicated energy crops can be defined as non-food crops that may be grown on land not suitable for traditional food crops (such as soybeans and corn) specifically for use as biomass (Office of Energy Efficiency and Renewable Energy, 2020). Dedicated energy crops may be woody biomass or herbaceous biomass. Woody biomass used as dedicated food crops is usually fast-growing hardwood trees (Office of Energy Efficiency and Renewable Energy, 2020). These trees are generally harvested within 8 years of planting. Types of woody biomass crops that are used as dedicated energy crops include hybrid willow, green ash, and sweetgum (Office of Energy Efficiency and Renewable Energy,

2020). Herbaceous biomass is plants that have a lifespan greater than two years and take approximately two to three years to reach full productivity (Office of Energy Efficiency and Renewable Energy, 2020). Herbaceous crops include bamboo, switch grass, and sweet sorghum. Dedicated plants that are grown for energy production usually have more cellulose (greater than 38wt%) and less lignin (approximately 19wt%) (Cheng et al., 2020).

2.2.3. Algae

Algae are organisms that can grow in a variety of aquatic environments. Algae use carbon dioxide, nutrients, and sunlight to produce biomass which contains proteins, carbohydrates, and lipids (Office of Energy Efficiency and Renewable Energy, 2020). Algae may be classified as microalgae or macroalgae. Microalgae are unicellular and generally measured in micrometres. Microalgae usually grow in suspension in a body of water (Wen, 2019). Macroalgae are unicellular or multicellular and are large organisms that are often measured in centimetres or metres (depending on the size of the algae). The largest macroalgae are called seaweed, for example, the giant kelp plant may reach lengths greater than 30 metres (Office of Energy Efficiency and Renewable Energy, 2020). Macroalgae are usually seen growing in ponds.

2.2.4. Forestry residues

Forestry biomass can fall into two categories. The first category is trees and crops harvested specifically for use as biomass and the second category is forest residues that remain following the logging of trees for timber (Office of Energy Efficiency and Renewable Energy, 2020). Forest residues that fall in category one include black maple, hybrid poplar, and silver maple and forestry residues that fall under category two include the tops, and limbs of trees and culled trees and their components that are generally unsellable (Office of Energy Efficiency and Renewable Energy, 2020). Category two trees may also include poorly formed, diseased or dead trees that remain following the harvesting of trees as these trees are usually unmerchantable (Office of Energy Efficiency and Renewable Energy, 2020). These leftover forestry residues and unwanted trees may be used for energy production while ensuring that there are adequate trees left behind for proper nutrient maintenance and to provide habitats. The use of excess or left-over wood biomass for bioenergy production would not negatively impact the stability and health of the forest and may reduce the risk of forest fires and aid in forest productivity, vitality, and restoration.

2.2.5. Wood processing residues

Wood processing residues are the waste streams and by-products produced from the processing of wood for various products. Biomass from wood processing is seen as a comparatively inexpensive and convenient source of biomass as the wood processing residues are already collected in the wood processing plant (Office of Energy Efficiency and Renewable Energy, 2020). Leaves, bark, sawdust,

and branches are examples of the residues remaining from the processing of wood, and these materials have a high energy potential.

2.2.6. Wet waste

The use of wet waste as a source of biomass can help resolve waste disposal problems and may create additional revenues for rural communities by converting waste streams into bioenergy. There are a variety of waste feedstocks that may be used in bioenergy production, these include organic wastes from industrial processes, food wastes, biogas (gas formed by the decomposition of organic compounds, organic-rich biosolids (for example treated sewage sludge), and manure slurries (Office of Energy Efficiency and Renewable Energy, 2020).

2.2.7. Municipal waste

Municipal waste is any form of refuse from residential and commercial areas that may be used as a source for energy production. Municipal waste as a source of biomass has the potential to reduce commercial waste and residential waste by converting waste that was meant for landfills into bioenergy. Types of municipal waste include rubber, paper, yard, and tree trimmings, textiles, food waste, and plastics (Office of Energy Efficiency and Renewable Energy, 2020).

2.3. Biomass as a fuel source

2.3.1. Background of the biofuel industry

The fossil fuel industry is known as the largest contributor of carbon dioxide (a greenhouse gas) in the atmosphere (Wyman et al., 2005). As a result, there is a need for a more environmentally friendly source of fuel that can be produced from renewable resources to reduce the greenhouse effect, which is a leading cause of climate change and global warming (Little, 2000). The use of an alternative source of fuel provides a possible solution to partially solve environmental pollution through fossil fuels.

The effects of climate change and global warming have made biofuels an attractive option for the future. Biofuels are produced through the conversion or use of biomass. Biomass is seen as an attractive alternative to produce biofuels as it is seen as an abundant renewable resource, it is readily available and has a relatively low. Depending on the type of conversion technology used, biomass may be used to produce liquid biofuels (such as ethanol and bio-oils) and biogas (for example methane) (Hoekman, 2009). Biomass can be converted into chemicals, as well as solid, gaseous, and liquid biofuels for generating energy. The use of sustainable biofuels that would protect ecosystems and reduce greenhouse gas emissions would require plants that are grown on land of low quality, lignocellulosic material, algae, non-agricultural feedstocks (e.g., residues and wastes) and integration with food production (Farrell and Gopal, 2008). The replacement of fossil fuels with biofuels is an effective strategy to reduce global greenhouse gas emissions (specifically carbon emissions from the combustion of fossil fuels) and meet future energy demands (Ullah et al., 2015). Biofuels are seen as a more environmentally friendly source of fuel compared to fossil fuels (Chen et al., 2015b), however, a potential constraint for the use of

biofuels is the argument for energy balances, and sustainable development and cultivation of biomass (the land-use conflict) (Ullah et al., 2015).

2.3.2. Biofuels

Liquid biofuels (such as biodiesel, bio-oil, and bioethanol), gaseous biofuels (such as syngas and biomethane), and solid (such as biomass) biofuels obtained from liquefaction, anaerobic digestion, gasification, fermentation, genetically modified organisms, or pyrolysis may be categorised based on the origin of the biomass into first, second, third or fourth generation biofuels (Abbasi and Abbasi, 2010).

First-generation biofuels are usually produced from edible feedstock (feed and food crops) consisting mainly of starch, seeds, sugar, oils (sunflower, sugarcane, soybean, corn, and animal fat), and grains. These biofuels cannot meet the rising energy demand as they are inefficient, inadequate, and unsustainable (Ross et al., 2010), and their use causes controversial debates over the food versus fuel conflict as it affects food prices and global food security (Singh et al., 2011). Second-generation biofuels provide a greater potential compared to first-generation biofuels (Ullah et al., 2015).

Second-generation biofuels are made from non-edible crops and they are typically based on lignocellulosic feedstock which originates from industrial organic waste such as grass, straw, forest residues, sewage sludge, municipal solid waste and wood, and agriculture and forest residues (Anto et al., 2019). These biofuels are more advantageous than first-generation biofuels as they have lower land requirements, produce higher yields, and do not compete with feed and food supplies (Ross et al., 2010). Second-generation biofuels are also inadequate and inefficient to meet the global energy requirements due to the concerns over land availability, the protection of the global ecosystem, and the lack of efficient and effective technologies for commercial applications (Nigam and Singh, 2011)

Third-generation biofuels are generated from algae biomass as the feedstock (Vassilev and Vassileva, 2016). Algae as a source of biomass to produce biochemicals and biofuels have received a lot of attention (Sambusiti et al., 2015). Third-generation biofuels are a viable source of energy that can overcome the limitations experienced with first- and second-generation biofuels (Noraini et al., 2014). The remnants of algae following oil extraction may be used as fertilisers or fish feed (Anto et al., 2019) Algae has not been produced on large scale commercially as the production costs are high (Bharathiraja et al., 2015).

Fourth-generation biofuels are produced from genetically modified microalgae, yeast, microbes, and fungi that absorbed carbon dioxide and convert it directly to fuel (Raslavicius et al., 2014). These genetically modified microorganisms may also alter the capability of organisms to store oil (Gust et al.,

2008). Artificial photosynthesis can be employed to produce genetically reengineered biofuels (Gust et al., 2008).

2.3.3. Advantages and disadvantages of biomass as a source of fuel

2.3.3.1. Advantages

Biomass is available globally and as a result, it is a strategic resource in the increasing possibility of a shortage of current energy resources. Unexploited biomass could satisfy approximately 10%-20% of the primary energy demand of the planet (Bonechi et al., 2017). The energy produced from biofuels may reduce the energy costs and reduce the demand placed on fossil fuels. The use of biofuels could also reduce the emissions of greenhouse gases as the complete cycle of the biomass (production, processing, and use) theoretically have a zero net carbon dioxide emission (Bonechi et al., 2017). Biomass and bioenergy have been acknowledged as important elements of many energy scenarios and can contribute to environmental, economic, and social goals (Farrell and Gopal, 2008).

2.3.3.2. Disadvantages

There have been no definite guidelines developed for the use of biomass by modern technologies. This is due to biomass being the residual part of various crops and these crops differ structurally, molecularly, and macroscopically (Bonechi et al., 2017). Biomass obtained from crop residues and food industry residues usually possess bioactive compounds such as carotenoids, lignans, flavonoids, and antioxidants that should be removed. The removal of the bioactive compounds would depend on the cost and the environmental sustainability of removing, purifying, and reusing these compounds (Bonechi et al., 2017).

2.4. Algae biomass

Algae utilise carbon dioxide and sunlight to biomass, and oxygen as a by-product, and may be regarded as aquatic organisms as it grows in aquatic environments (Wen, 2019). Algae is composed of carbohydrates, proteins, and lipids (Office of Energy Efficiency and Renewable Energy, 2020). Algae can grow in seawater, freshwater groundwater, and surface water sources and may also be found in agricultural and municipal wastewater and treated industrial wastewater (Office of Energy Efficiency and Renewable Energy, 2020). It is considered an important organism for carbon dioxide consumption and sustainable biofuel production due to its photosynthetic abilities (Chapman, 2010). The oil that is used today is obtained majorly from deposits of marine algae (Chapman, 2010). It is a source of fuel and food and produces oxygen for humans to breathe. Algae that are found in rivers, lakes, and oceans produce approximately 50% of the oxygen on the planet (Chapman, 2010). There are two types of algae, which are microalgae and macroalgae. Macroalgae (commonly referred to as seaweeds) are multicellular organisms that can be seen with the naked eye (American Scientist, 2020). There are three main types of macroalgae, namely, green algae, brown algae, and red algae (American Scientist, 2020).

There are approximately 1800 different green algae, 6200 species of red algae, and 1800 different species of brown algae (American Scientist, 2020). Microalgae are commonly referred to as phytoplankton and are microscopic organisms (Chapman, 2010). Microalgae are unicellular organisms that possess a high lip content and rapid growth rate (Wen, 2019). Types of microalgae include blue-green algae, diatoms, red algae, green algae, and dinoflagellates (Chapman, 2010).

2.4.1. Types of Algae

2.4.1.1. Green algae

Figure 2-1: Green algae (The Seaweed Site: information on marine algae, 2020).

Green algae are commonly referred to as Chlorophyta (Chapman, 2010). Green algae may consist of one cell (unicellular) or many cells (multicellular) and may be microscopic or several meters long (Chapman, 2010). These algae may be composed of a large cell that does not have cross walls (coenocytic) or may live as an aggregation of cells (colonial) (The Seaweed Site: information on marine algae, 2020). The green colour of the algae comes from the chloroplasts that contain chlorophyll which is present within the algae. The chloroplasts are membrane-bound (The Seaweed Site: information on marine algae, 2020). The chlorophyll aids in the absorption of carbon dioxide from the atmosphere and the expulsion of oxygen into the atmosphere. The majority of green algae are aquatic and may be found in marine habitats and freshwater. Terrestrial green algae may be found on rocks, trees, and soil. The food reserves of green algae are oils, fats, and starch (The Seaweed Site: information on marine algae, 2020). There are over 6000 species of green algae with approximately 90% being freshwater as opposed

to marine (Chapman, 2010). Types of green algae include chlamydomonas, spirogyra, and chlorella (The Seaweed Site: information on marine algae, 2020).

2.4.1.2. Brown algae

Figure 2-2: Brown algae (The Seaweed Site: information on marine algae, 2020).

Brown algae are also known as Phaeophyta (Chapman, 2010). Brown algae may be multicellular and coenocytic. The brown colour of the algae is due to fucoxanthin (which is a xanthophylls pigment), as this is dominant over the other pigments such as chlorophyll and beta-carotene (The Seaweed Site: information on marine algae, 2020). The main food reserves of this type of algae are sugars and polysaccharides. Brown algae include all types of giant kelp, as well as smaller, intertidal seaweeds (Chapman, 2010). The walls of brown algae are composed of alginic acid and cellulose, and the kelps may reach up to 70 meters in length and are the most complex of the brown algae (The Seaweed Site: information on marine algae, 2020). Alginates that are made from alginic acids are utilised as a binding agent, moulding agent, or emulsifying agent to make soaps, tinned meats, toothpaste, and ice cream (The Seaweed Site: information on marine algae, 2020). There are more than 1500 different species of brown algae, with the majority of the species being marine water algae (Chapman, 2010). Types of

brown algae include saccharina, laminaria, and sargassum (The Seaweed Site: information on marine algae, 2020).

2.4.1.3. Red algae

Figure 2-3: Red algae (Ask nature, 2020).

Red algae are also known as Rhodophyta (Chapman, 2010). The red colour comes from the pigments phycocyanin and phycoerythrin present within the cells of the algae (The Seaweed Site: information on marine algae, 2020). The presence of these pigments is dominant over the green colour of chlorophyll. The majority of red algae are macroscopic; however, some may be unicellular and microscopic (Chapman, 2010). The algae walls are composed of long chain polysaccharides, namely, carrageenans, cellulose, and agars (Chapman, 2020). The main food reserves of red algae are floridoside and floridean starch (The Seaweed Site: information on marine algae, 2020). Several types of red algae may be eaten. Carrageenan of red algae is used in chocolate milk, yoghurts, and some puddings (The Seaweed Site: information on marine algae, 2020). Agars may be used in biotechnological and food applications and may be utilised as a growth medium for microorganisms (The Seaweed Site: information on marine algae, 2020). There are approximately 4000 species of red algae and 90% of red algae are marine species (Chapman, 2010). Examples of red algae are delesseria, chondrus, and palmaria (The Seaweed Site: information on marine algae, 2020).

2.4.2. Current potential of algae biomass as a biofuel source

Fuels made from algae biomass are considered to be the best source of renewable energy that has the capacity and capability to sustain the global demand for biofuels in the long term and are regarded as the most environmentally friendly, renewable, sustainable, and effective response to food-fee security and the growing climate change problem (Vassilev and Vassileva, 2016). Algae biomass is composed of three main components, namely, lipids (natural oils), carbohydrates, and proteins. Algae biomass can be converted to both bioethanol and biodiesel (Anto et al., 2019). The majority of natural oil produced from microalgae is tricygylcerol, which is the most suitable oil for making biodiesel (Wen, 2019). Therefore, the bulk of microalgae is focused solely on the conversion to biodiesel. Algae biomass may be burned like coal or wood to produce electricity and heat. Algae can also produce hydrogen gas under certain growth conditions. Algae can be anaerobically digested to created methane biogas which may also be used to generate heat and electricity (Wen, 2019). Current data displays that the large contents of inorganic matter that possess unwanted modes of elemental occurrences, such as sulphates, oxalates, phosphates, chlorides, carbonates, and oxyhydroxides, in algae ash and algae negatively affect the environmental challenges and critical technological challenges during the processing of algae biomass to produce biofuels, specifically during the thermochemical conversion of algae to biofuel (Vassilev and Vassileva, 2016).

There are many advantages to using algae as a source for biofuel production. Algae are easily adaptable as they may grow in a wide variety of climate conditions which enables continuous cultivation throughout the year (Bharathiraja et al., 2015). Algae are known as the fastest-growing organisms as they only take hours to reproduce (Ullah et al., 2015). It has a large greenhouse gas uptake, and a higher carbon dioxide capture with extra oxygen release during growing than most biomass sources (Vassilev and Vassileva, 2016). Algae has high productivity, a rapid growth rate, and a high crop yield. Algae do not require the addition of fertiliser and other costly nutrients to grow. They grow using the nutrient supplied by the location in which they grow. Algae biomass as a source of biofuel does not cause land-use conflicts as they do not require environmentally sensitive or agricultural productive land grow and may grow in oceans, ponds, and municipal, industrial and agricultural waste waters (Vassilev and Vassileva, 2016). Most algae species are mostly non-edible and non-toxic resources and may prevent pollution and eutrophication in aquatic ecosystems. They also have the highest growth rate at the higher altitudes (Faeth et al., 2013). Algae may also be processed when wet so there is no energy intensive drying step required.

Although there are many advantages to the use of algae as a source of biofuel, there are also some disadvantages that need to be taken into consideration. The cost of cultivation and harvesting of large algae sources is high due to the wide variety of locations that algae may grow, as different locations would need different methods of harvesting, requiring a variety of equipment before harvesting and

cultivation can take place (Vassilev and Vassileva, 2016). The cultivation of algae may also damage the environment. There is also a lack of monitoring and control of fuel production using algae. The transportation, storage, collection, and pretreatment of algae is expensive, resulting in a low-cost efficiency with a high initial capital cost (Vassilev and Vassileva, 2016). The combustion and gasification of algae are limited due to the algae ash chemistry (Vassilev and Vassileva, 2016). Certain thermochemical conversion techniques may experience corrosion, agglomeration, or erosion when processing algae.

2.5. Liquefaction

Liquefaction is a thermochemical process whereby the feedstock (e.g., biomass or coal) undergoes thermal degradation and complex chemical reactions within a solvent medium to produce liquid biofuels (Zhang et al., 2019). According to Akhtar and Amin (2011), the utilisation of appropriate particle size during the liquefaction process could allow for a greater contact surface area, reduced energy consumption by decreasing the amount of grinding needed, and a reduced limitation of mass and heat transfer.

The oil formed from liquefaction is highly viscous and can cause handling problems. Organic solvents (for example, acetone, butanol, and propanol) are typically added to highly viscous oils. Catalytic aqueous liquefaction can produce a higher bio-oil yield than non-catalytic aqueous liquefaction (Naik et al., 2010). The bio-oils produced from the liquefaction process typically contain large contents of volatile organic esters, acids, ketones, aldehydes, ethers, and alcohols, along with non-volatile components (Zhang et al., 2019). The components of the oil may be catalytically converted to produce an organic product that has useful chemicals and is rich in hydrocarbons. The bio-oil produced from liquefaction is more viscous than bio-oil formed from pyrolysis and the bio-oil yield is much higher with the pyrolysis process than with the liquefaction process (Naik et al., 2010).

2.5.1. Hydrothermal liquefaction

Hydrothermal liquefaction can be regarded as one of the most effective methods to produce biofuels and value-added chemicals from biomass (Beims et al., 2020). Hydrothermal liquefaction is a thermochemical process that utilises high pressures and high temperatures in a water reaction medium (either supercritical or subcritical water) to produce bio-oils from a biomass feedstock (Valdez et al., 2014; Chen et al., 2015). Over the last decade, there has been a growing interest in the use of subcritical and supercritical water as a reaction medium and solvent for biomass conversion (Toor et al., 2013). This process breaks down the solid biopolymeric structure into mostly liquid components (Elliot et al., 2015).

Biomass is placed inside a reactor along with a set amount of water. This mixture is exposed to high temperatures and pressures, in the presence of inert gas, to allow the water to permeate the biomass and extract the oil. The process temperatures range from 200°C to 400°C (Chen et al., 2015) and the process

pressures range from 1.5 MPa to 20 MPa (Toor et al., 2011). Once the gas has been vented and the product filtered to recover the remaining solid biomass, the filtered solution (product) is usually mixed with an organic solvent to separate the bio-oil from the solution (Barreiro et al., 2015). The use of the organic solvent could cause the transfer of organic molecules from the aqueous phase to the biocrude oil phase (Barreiro et al., 2015). The organic solvent is selective with the bio-oil and dissolves it from the product solution. The resulting solution is centrifuged or left to settle until both phases are observed (Barreiro et al., 2015). Following the separation of the water from the organic solvent, the solvent is evaporated and recovered to ensure only the bio-oil remains.

The overall aim of the hydrothermal liquefaction of biomass is to produce a product that has a high energy density through the removal of oxygen (Elliot et al., 2015). The products formed from the hydrothermal liquefaction process include a bio-crude/ bio-oil fraction, a solid fraction, a gas fraction, and an aqueous fraction consisting of inorganic and organic compounds (Toor et al., 2011). Bio-crude (or bio-oil) is the main product of hydrothermal liquefaction and is compromised of aromatic compounds, hydrocarbon compounds, and oxygenated compounds that reduce the high heating value (HHV) (Beims et al., 2020). The bio-oil or biocrude formed is an energy dense bio-oil (Dote et al., 1994) that may be catalytically converted to a product that is similar to petroleum crude. Possible biocrude products include cyclic ketones, alcohols, phenols, acids, benzofurans, and naphthols (Elliot et al., 2015).

The energy requirement from the hydrothermal liquefaction process is low when compared to other biomass processing technologies (Zou et al., 2010). A major advantage of the hydrothermal liquefaction process is that it can process both wet and dry biomass feedstock, therefore there is no need for an energy-intensive drying procedure before processing (Valdez et al., 2014). Another advantage of this process is the possibility to recycle the process water, which is rich in polar organics, elements such as potassium, magnesium, calcium, and iron, nutrients (for example, phosphorus and nitrogen), and other mineral matters (Biller et al., 2012). Hydrothermal liquefaction does not require a catalyst which reduces the overall cost of processing (Duan and Savage, 2010). A benefit of the hydrothermal liquefaction processing of microalgae is the possibility of producing bio-oil and value-added polysaccharides simultaneously and preserving the nutritional value of the solid algae biomass as an additive for animal feedstock (Toor et al., 2013).

At the process conditions of the hydrothermal liquefaction process, water remains in the liquid phase and has many exotic properties. Water acts as a reactant and reaction medium, therefore biomass may be converted to biofuels without requiring an energy-demanding drying step (Bridgwater et al., 1999). The effect of the particle size of the biomass is negligible as the water reaction medium (solvent) acts as a heat transfer medium and an extractant (Deng et al., 2015). Water aids the complex biomass

molecules in breaking down into smaller molecules which may repolymerise to form oily compounds (Peterson et al., 2008).

The industrial application of hydrothermal liquefaction technologies faces various challenges due to the feedstocks and process conditions used. The high operating pressures and temperatures place difficult requirements on process components (for example, feed pumps), and corrosion and erosion hindrances require expensive alloys to be used (Toor et al., 2011). The high cost of the initial investment is another main factor affecting the commercialisation of this process.

The chemistry and mechanism of hydrothermal liquefaction are complex and highly dependent on the substrate (Toor et al., 2011). This process allows access to ionic reaction conditions by ensuring a liquid water medium is maintained (Elliot et al., 2015). The temperature of the hydrothermal liquefaction process is adequate to initiate a pyrolytic mechanism in the biopolymers and the pressure is appropriate to maintain a liquid reaction medium (Elliot et al., 2015). Although the hydrothermal liquefaction process occurs through pyrolytic reaction mechanisms, the biocrude product formed is more deoxygenated than the fast pyrolysis process, through condensation reactions of light components produced from the biomass (Elliot et al, 2015). Hydrothermal liquefaction is seen as one of the best processes for converting algal biomass to value-added chemicals and bio-oil (Gu et al., 2020).

2.5.2. Fundamentals of the hydrothermal liquefaction of algae biomass to bio-oil.

Hydrothermal liquefaction is theorised to mimic the geological processes involved in the formation of fossil fuels, as the fossil fuels (such as coal, petroleum, and natural gas) are exposed to high pressures and temperatures for millions of years (www.energy.gov, 2020). Hydrothermal liquefaction comprises reactions undertaken in a compressed hot water system (Gu et al., 2020). Unlike biological processes, hydrothermal liquefaction converts the feedstock to mainly oil with some by-products. The bio-oil (or biocrude) formed has a higher energy content than the alcohol or syngas formed from biological processes (Barreiro et al., 2015).

The overall process may be summarised into two stages. The first stage is the hydrothermal liquefaction of the algae to bio-oil and the second stage is the upgrading of the bio-oil to a more viable source of fuel (Xu et al., 2018). The hydrothermal liquefaction of algae may be carried out at a variety of temperatures of pressures and the method of upgrading the biocrude is dependent on the composition of the biocrude formed. The hydrothermal liquefaction of algae results in four main products i.e., a biocrude fraction, a gaseous fraction, a solid residue, and an aqueous fraction (Ramirez et al., 2015). The aqueous phase from the hydrothermal pretreatment may be used in algae cultivation as it contains important nutrients (e.g., potassium, phosphorus, and nitrogen), however, the toxic components need to be removed (Xu et al., 2018).

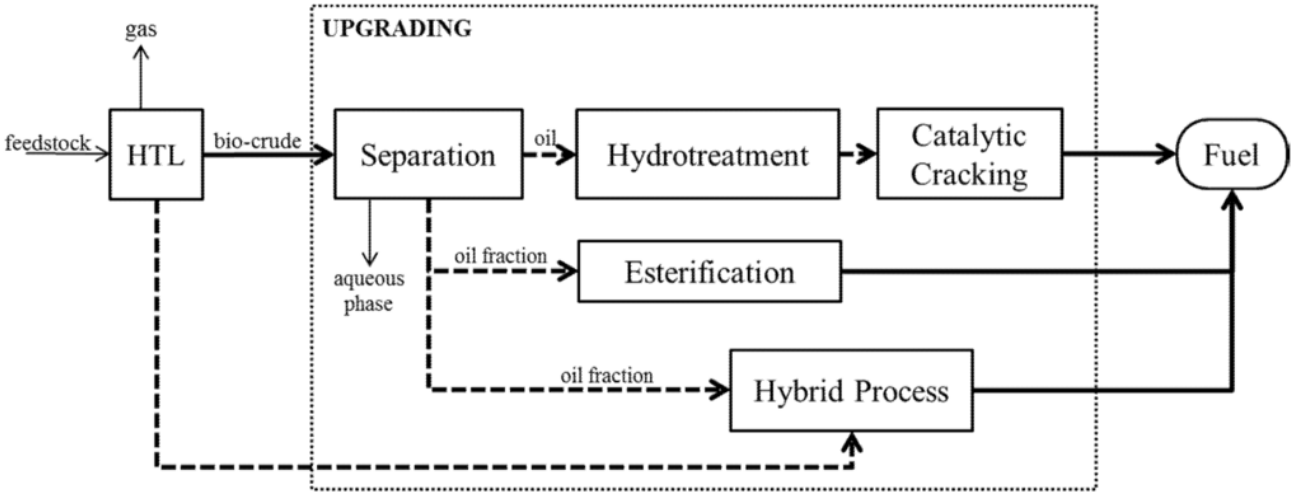

Figure 2-4: Basic flow diagram of the hydrothermal conversion of algae to fuel (Ramirez et al., 2015).

Figure 2-4 shows the potential conversion routes for the production of bio-oil from the hydrothermal liquefaction of algae biomass. According to figure 4, following the hydrothermal liquefaction of algae, the resulting biocrude undergoes a separation process to separate the various products formed for further analysis. The separation processes also aid in the isolation of valuable products, which may be further processed to produce fuel, along with various high-value products (Ramirez et al., 2015). Possible separation processes include solvent extraction and distillation (Ramirez et al., 2015).

Solvent extraction is performed by adding a solvent to the liquid product (the liquid fraction and liquid-aqueous fraction) to enhance the separation and extraction of these components. The resulting liquid mixture may be separated into the oil and aqueous fractions (Ramirez et al., 2015). The solvent selection is based on the immiscibility with water and the maximisation of the bio-oil yield. A polar solvent may be better suited for bio-oil extraction due to the large number of polar compounds found in bio-oil (Garcia-Perez et al., 2007). According to Garcia-Perez et al., dichloromethane and ethyl acetate provide an adequate extraction and a large bio-oil yield from the aqueous mixture. The solvent extraction method is appropriate for small-scale processes and low volumes, as the use of solvent extraction in large-scale processes has negative economic and environmental effects (Xu et al., 2018).

Distillation is a physical separation process that separates components based on their boiling points or relative volatility (Smith and Jobson, 2000). There are many types of distillation and the distillation method used depends on the chemical and physical properties of the feed components (Ramirez et al., 2015). Common (or fractional) distillation separates components based on their boiling points. Steam distillation uses the addition of steam to reduce the partial pressure of the feed, which in turn decreases

the boiling points of the feed components (Ramirez et al., 2015). Extractive distillation uses a solvent to aid in the separation of components with close boiling points and requires two columns. Molecular distillation utilises a pressure of less than 1 Pa to ensure separation occurs without pressure applied by the gaseous phase (Schaschke, 2014). Molecular distillation depends on the differences in the free paths of the components (Guo et al., 2010). Vacuum distillation utilises lower pressures, which reduces the boiling points of the feed components and allows lower temperatures to be used (Ramirez et al., 2015). The use of lower temperatures prevents decomposition and cracking from occurring (Ramirez et al., 2015). The main advantages of distillation over other separation processes are the capability to deal with a large variety of flow rates; the ability to separate a large variety of feed concentrations and the ability to generate products with higher purity (Smith and Jobson, 2000). Distillation is more suited for large-scale and industrial processes (Ramirez et al., 2015).

The main biocrude fraction undergoes hydrotreatment processes such as hydrogenation. Hydrogenation is a refining process in the petroleum industry that is used to remove compounds such as oxygen, nitrogen, and sulphur and to increase the amount of hydrocarbons present within the bio-oil (Ramirez et al., 2015). Hydrogen and oxygen are directly related to the heating value of the bio-oil. An increase in the hydrogen content and a decrease in the oxygen content improve the heating value of the bio-oil (Huber et al., 2006). Therefore, hydrogenation increases the heating value of the bio-oil. Hydrogenation prevents the deactivation of the catalyst during further processing which results in a higher quality of bio-oil and a minimisation of coking during processing (Alfke et al., 2008). The hydrotreated bio-oil undergoes further processing to refine the bio-oil to acceptable standards. Bio-crudes that are highly oxygenated have a high potential for coking (Melero et al., 2011), therefore thermal cracking is not a viable technique for the cracking of bio-crudes (Ramirez et al., 2015). Catalytic cracking is used following the hydrotreating step to produce lighter hydrocarbon products. Catalytic cracking decreases the formation of by-products, such as coke, by utilising milder processing conditions (Melero et al., 2011). The catalysts used include crystalline zeolites, natural clay materials, and synthetic silica-alumina (Alfke et al., 2008). The addition of hydrogen during catalytic cracking is referred to as hydrocracking. Hydrocracking differs from typical hydrotreatment as the bio-crude is processed under more severe conditions (Alfke et al., 2008).

Esterification is an alternative process to upgrade bio-crude. Esterification is the addition of alcohol to the biocrude to alter the composition and enhance the physical properties of the bio-crude (Ramirez et al., 2015). The alcohols react with organic acids within the bio-crude to form esters, which are similar to those found in biodiesel (Ramirez et al., 2015). Bio-oils that have undergone esterification have displayed improved density, viscosity, and a higher heating value (Ramirez et al., 2015). Hybrid processes employ the combination of various features of other upgrading techniques into a single process to convert the biocrude to a high purity bio-oil product. The objective of the hybrid process is

to reduce undesirable reactions and products while maximising the yield and increasing the purity. An example of a hybrid process would be a reactive-distillation process which would be utilised to simultaneously separate the biocrude from the aqueous phase and alter the physical properties and chemical characteristics of the biocrude (Ramirez et al., 2015).

2.5.3. Effects of process conditions on the performance of hydrothermal liquefaction on algal biomass

The effects of the process conditions are vital to ensure the maximum possible yield is obtained from the hydrothermal liquefaction process. Temperature is a major factor affecting the bio-oil yield and bio-oil properties (Reddy et al., 2016). It is the property that influenced the distribution of products the most (Djandja et al., 2020). An increase in temperature is likely to increase the bio-oil yield, however, the pattern of increase differs between the types of algae due to the varying chemical composition of each alga (Reddy et al., 2016). Due to the closed system of hydrothermal liquefaction, the pressure is seen to increase with an increase in temperature. A lower initial pressure may be more favourable for a higher bio-oil yield, as gasification is more distinct for higher initial pressures, which would cause a higher conversion to a gaseous fraction (Djandja et al., 2020). The reaction time is the time the biomass undergoes hydrothermal liquefaction once the required reaction conditions have stabilised. An increase in the reaction time up to 30 minutes is seen as favourable (Djandja et al., 2020). A reaction time greater than 30 minutes causes the energy dense bio-oil molecules to undergo polymerisation or condensation and form tar-like substances (Djandja et al., 2020, Yuan et al., 2019).

2.5.4. Reaction mechanism for the production of bio-oil from algae through hydrothermal liquefaction conversion.

The hydrothermal liquefaction process has the ability to chemically convert algae that possess a high moisture content into a biocrude product that has a low coke yield, whilst requiring less energy when compared to other algae conversion processes (Yang et al., 2015). During hydrothermal liquefaction, the molecules within the biomass are hydrolysed into smaller components which are reactive and unstable and may rearrange into large molecules (Toor et al., 2011). The hydrothermal liquefaction process is effective in obtaining elements such as hydrogen and carbon and restructuring elements such as nitrogen and oxygen into different products (Tian et al., 2014). The algal biomass depolymerises and breaks down into smaller components over a short period of time. However, these components may be rearranged to form bio-oil over a long period through repolymerisation and condensation reactions (Zou et al., 2010, b). The reaction mechanism includes the formation of a bio-oil product (light biocrude or heavy biocrude) and an aqueous product (Valdez et al., 2013). Initially, the aqueous product is produced and after some time the aqueous product is consumed to produce a biocrude product (Valdez et al., 2013). Throughout the algae hydrothermal liquefaction process, the proteins, lipids, and carbohydrates undergo depolymerization, repolymerization, isomerization, and reforming reactions, which produce the bio-oil (Yang et al., 2015). The route from algae biomass to bio-oil signifies the breaking down of

the algae cell wall, the hydrolysis of the internal components, and the rearranging and reforming of the subsequent small molecules (Valdez et al., 2012). The formation of the gas product fraction is generally much lower than the bio-oil product and aqueous phase product (Valdez et al., 2013). The intermediate products of the hydrolysis process initiate multiple reactions including oxidation, cracking, substitution, addition, isomerization, polymerization, and hydrogenation reactions (Xu et al., 2018). The bio-oil resulting from this process is a complex mixture that contains a lot of compounds and possesses a broad distribution of the molecular weights of the compounds (Vardon et al, 2011). The bio-oil usually possesses a large number of cyclic compounds which contain oxygen and nitrogen (Xu et al., 2018). There may also exist an exchange of components between the aqueous phase and the bio-oil phase, thus creating a reaction pathway between the bio-oil product and the aqueous phase (Valdez et al., 2013).

The reaction mechanism of the hydrothermal liquefaction of algae biomass occurs in three main stages. The initial stage is the hydrolysis of the main components (proteins, carbohydrates, and lipids) of the algae biomass (Xu et al., 2018). The hydrolysis of proteins produces various peptides (through peptide bond fracture) and amino acids (Xu et al., 2018). The hydrolysis of the carbohydrate forms a polysaccharide or monosaccharide, and the hydrolysis of lipids results in three fatty acid molecules and one glycerol molecule (Xu et al., 2018). The second stage of the reaction mechanism is a parallel reaction of the hydrolysis monomer, which includes a cracking reaction and dehydration reaction (Xu et al., 2018). The third stage of the reaction mechanism is a cross-reaction of the intermediate products, for example, the dehydration reaction of ammonia and fatty acid, and the Maillard reaction between the amino compounds and the carbonyl compounds (Xu et al., 2018). The Maillard reaction (non-enzymatic browning) is a complex chemical reaction between proteins and reducing sugars through the use of heat (Feiner, 2006). The reducing sugars of the carbohydrates increase the transformation of amino acids (Peterson et al., 2010). The amino from the amino acid and the carbonyl group of the sugar take part in the Maillard reaction resulting in an increase of cyclic-oxygen and cyclic-nitrogen compounds (Peterson et al., 2010). The algae biomass undergoes intricate chemical reactions to get rid of the hydrophilic groups such as the carboxyl and hydroxyl groups and produce lipophilic compounds, which increases the bio-oil yield (Xu et al., 2018).

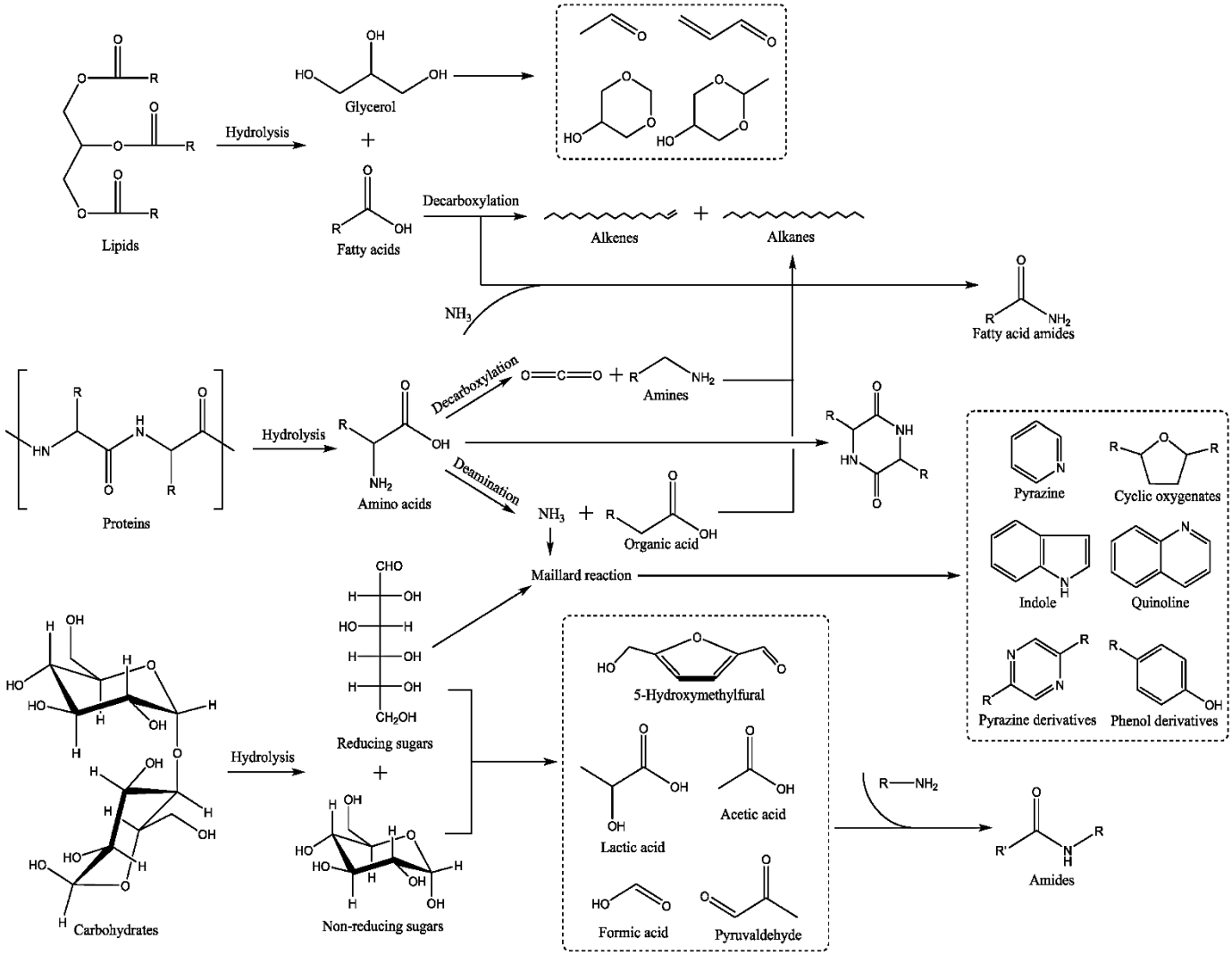

Figure 2-5: Reaction mechanism for the production of bio-oil from algae biomass (Xu et al., 2018)

2.5.5. Structural change of seaweed during hydrothermal liquefaction

There exist structural differences between brown, green, and red algae. The primary cell wall components of green algae and red algae are mannan, xylan, and cellulose (polysaccharides), while the primary cell wall of brown algae is composed of cellulose (Kloareg et al., 1988). Red and green algae may also possess a skeletal backbone of the cell wall formed from crystalline xylan and mannan (Kloareg et al., 1988). These polysaccharides generally form microfibrils that have varying structural configurations and orientations based on the species, having either a structure that is randomly distributed within each layer or an organised structure (Hurd et al., 2014). These microfibrils may include carboxylic or sulphated polysaccharides depending on the species (Synytsya et al., 2015). An example is sulphated fucans which aid in the interlocking of the cellulosic backbone of the cell wall (Deniaud-Bouet et al., 2014). In brown algae, it was found that proteins were also associated with phenols and sulphated fucans (Deniaud-Bouet et al., 2014). The bond between the alginates and phenols plays an important role in the rigidity of the algae cell wall.

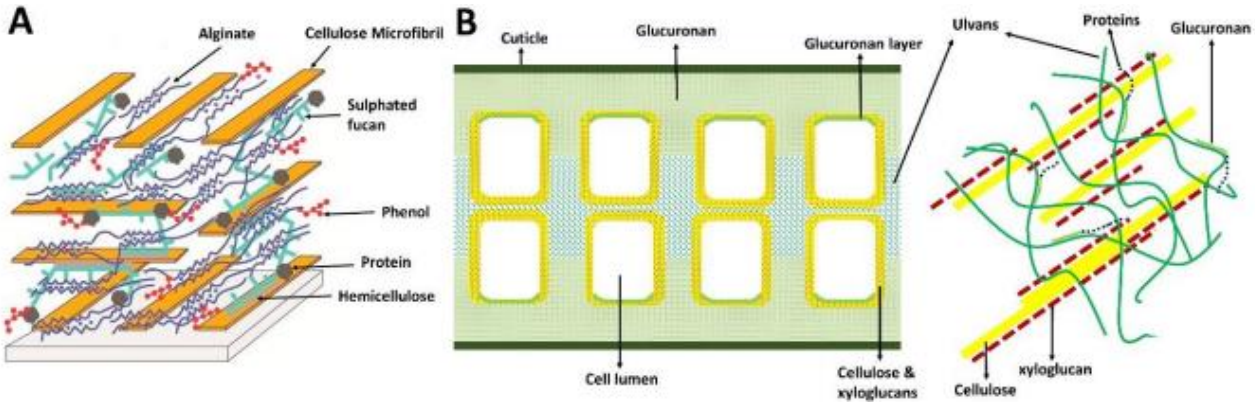

(a) (b)

Figure 2-6: (a) Simplified cell structure of brown macroalgae and (b) Simplified cell wall distribution in green algae, with closer interactions displayed on the far right (Maneein et al., 2018).

Alginates found in brown algae can be relatively resistant to degradation and may limit biodegradation of, and the access to, the polysaccharides within the algae, specifically cellulose (Maneein et al., 2018). Carrageenans found in red algae and ulvans in green algae play a similar role to the alginates found in brown algae (Maneein et al., 2018). The structure of the cell walls in seaweed may be similar to the structure of the cell walls in land-based plants (lignocellulosic plants), where chains of glucose molecules are surrounded by crystalline cellulose microfibrils help provide structural support. This layer is protected from hydrolysis to glucose by natural microorganisms (sulphated fucans, alginates, carrageenans, and ulvans) (Bobin-Dubigeon et al., 1997). Land-based plants (typically lignocellulosic plants) are protected by a layer of lignin, with cellulose and hemicellulose within the cell.

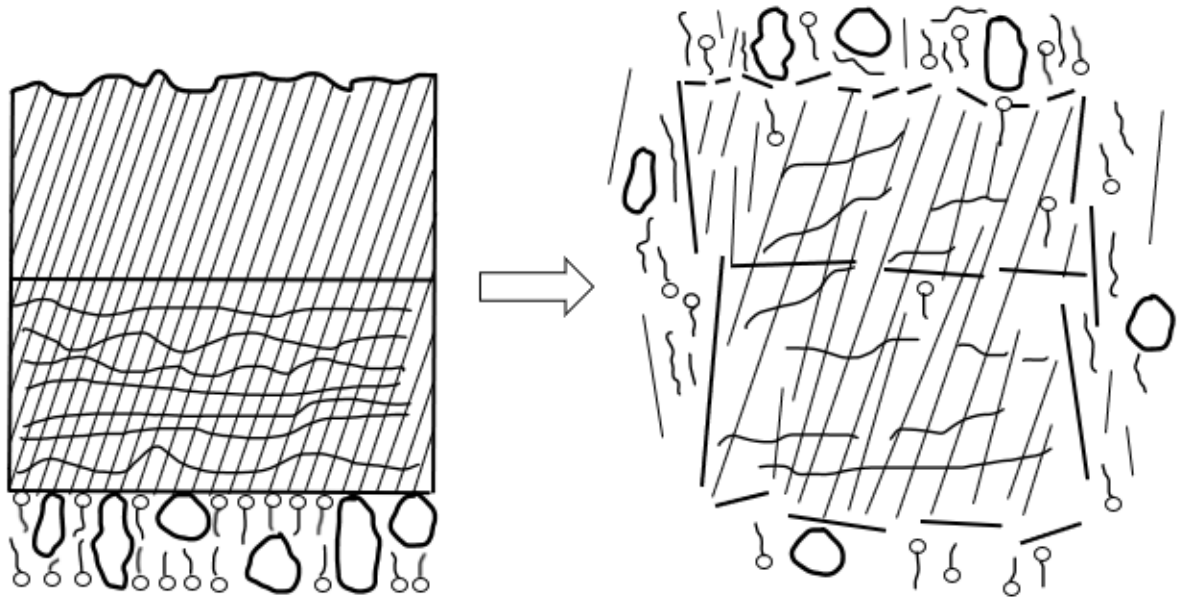

(a) (b)

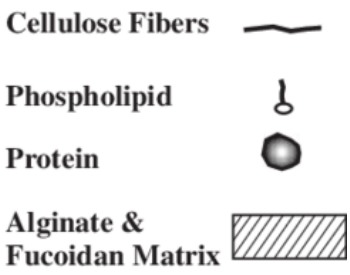

(c)

Figure 2-7: (a) Structure of algae cell before hydrothermal liquefaction (Diagram adapted from Maneein et al., 2018), (b) Structure of algae cell after hydrothermal liquefaction, and (c) key for the diagram (Maneein et al., 2018).

The hydrothermal liquefaction process would have to break the outer cell walls of the algae to gain access to valuable materials within the algae cell. The hydrothermal liquefaction would disrupt the alginate and fucoidan matrix and allow permeation within the algae cell. The cellulose fibres, phospholipids, and proteins, along with a portion of the alginate and fucoidan matrix, would be able to move through the breakages in the cell walls and be absorbed into the water medium of the hydrothermal liquefaction process.

2.5.6. The role of water in hydrothermal liquefaction

Water plays an important role in the hydrothermal liquefaction process; therefore, it is vital to understand the chemistry of water at high temperatures. Under normal environmental conditions (a pressure of 101,325 KPa and temperature 25°C) water may not react with the organic molecules of the feedstock. An increase in the temperature of water results in a decrease in its relative permittivity (Han et al., 2019). As the temperature and thermal energy rise, the kinetic energy of the atoms (hydrogen and oxygen) of the water molecule increases causing the hydrogen bonds of the water molecule to break apart (Molnar and Gair, 2015). This results in the electronegativity of the oxygen molecule decreasing due to the shared electron of the hydrogen and oxygen atoms spinning more evenly (Han et al., 2019). The increased solubility of water should favour the ionic reactions of the organic molecules. This would also result in an increase in the solubility of hydrocarbons in the water and hence accelerate the process of hydrothermal liquefaction (Han et al., 2019).

The changes in the chemical and physical properties of water, as a result of the increase in the temperature favour organic chemical reactions. Water can also cause cleavage, hydrolysis, and condensation reactions to take place and can affect selective ionic chemistry. During hydrothermal liquefaction, water serves the purpose of both the reactant and catalyst, which hydrolytically decomposes the carbohydrates, proteins, and lipids within the cells of the algae biomass (Valdez et al., 2014). At the conditions near the critical point, water possesses a high solubility of organic substance

and a low viscosity, resulting in subcritical water being a good medium for efficient, homogenous, and fast reactions (Krammer and Vogel, 2000).

2.6. Other thermochemical processes

2.6.1. Pyrolysis

Pyrolysis is a thermochemical process that causes the decomposition of the feedstock using high temperatures (temperatures ranging from 800°C to 1300°C) or medium temperatures (temperatures ranging from 300°C to 800°C) in an inert atmosphere (Zhang et al., 2017). The products formed from the pyrolysis of biomass are liquids (bio-oil), solids (biochar), and gases (syngas) (Zhang et al., 2019).

Pyrolysis has many advantages compared to other thermochemical processes. The bio-oil formed is the main product of the process and the yield can be as high as 75% (Zhang et al., 2019). The bio-oil may have low contents of sulphur and nitrogen and a high content of carbon. The desired product (be it the bio-oil, syngas, or biochar) may be produced by altering the process conditions (Azizi et al., 2018). The pyrolysis process has a short residence time and this may reduce the operational cost.

Pyrolysis may be classified according to the operating parameters, such as residence time, reaction temperature, and heating rate, into three groups namely, fast pyrolysis, slow pyrolysis, and flash pyrolysis (Zhang et al., 2019).

Fast pyrolysis has a residence time between 0.5s – 20s, a heating rate between 10°C/s to 300°C/s and a reaction temperature ranging from 550°C - 1250°C. Slow pyrolysis has a residence time of greater than 450s, a heating rate of less than 1°C/s, and a reaction temperature between 300°C and 700°C. Flash pyrolysis has a residence time of less than 0.5s, a heating rate greater than 1000°C/s and a reaction temperature between 800°C and 1300°C (Zhang et al., 2017).

Fast and slow pyrolysis usually produce bio-oils that contain high amounts of oxygen and water, which result in the bio-oils being incompatible with conventional forms of fuels (Deng et al., 2015). It is vital to reduce the water and oxygen contents to upgrade the quality of the bio-oils. This results in an extra step and an added expense of reducing the oxygen and water contents. The process to upgrade the bio-oil may use up to 84 wt% of the initial amount of the bio-oil (Deng et al., 2015)

2.6.2. Fischer-Tropsch

The use of Fischer-Tropsch synthesis to convert biomass to liquid fuels is gaining interest from industry as it is possible to produce carbon-neutral fuels that are environmentally friendly. The Fischer-Tropsch process is a group of catalytic processes that may be utilised to produce liquid fuels and valuable chemicals from synthetic gas (a gaseous mixture of carbon dioxide and hydrogen), which may be produced from biomass, natural gas, or coal (Hu et al., 2012).

The typical Fischer-Tropsch synthesis process is a multistep process for converting biomass to fuels. The process has three main stages that occur following the preparation of the feedstock. The first main

step is the conversion of the biomass feedstock to syngas via a gasification process. The second step is the cleaning of syngas to remove contaminants and impurities before it is catalytically converted to meet the Fischer-Tropsch synthesis requirements (Evans and Smith, 2012). The final step is the Fischer-Tropsch synthesis in a catalytic reactor to produce biodiesel and other biofuels (Hu et al., 2012). At low-temperature Fischer-Tropsch synthesis, a waxy hydrocarbon may be formed. This waxy hydrocarbon is typically sent for hydrocracking, where it is broken down into smaller molecular weight liquid hydrocarbons, to upgrade the waxy hydrocarbon to the required final product (Mahmoudi et al., 2017).

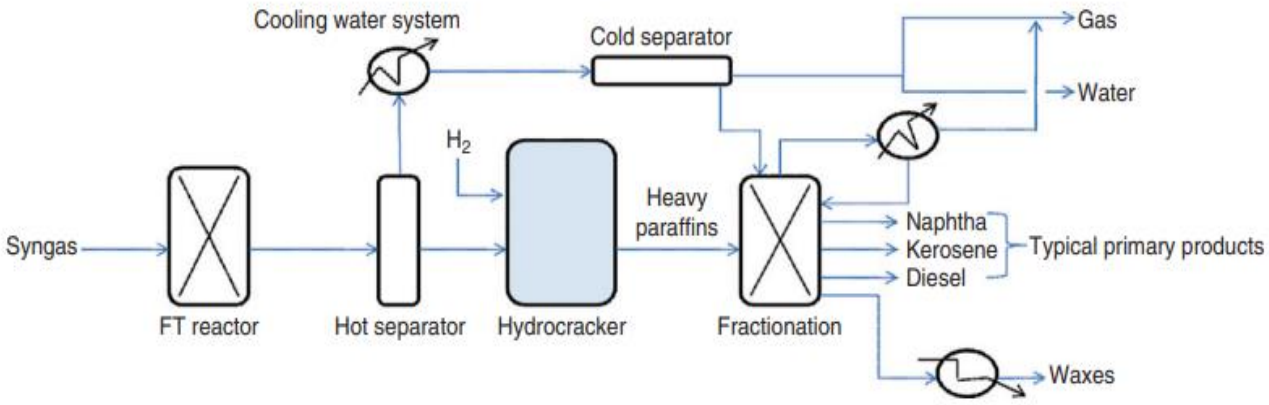

Figure 2-8: Simplified process flow diagram of the Fischer-Tropsch process (Evans and Smith, 2012).

2.6.3. Gasification

Gasification is a thermochemical process that produces syngas through reactions between a gasification agent and feedstock (Zhang et al., 2019). The syngas that is formed generally contains hydrogen, carbon monoxide, carbon dioxide, nitrogen, some hydrocarbons (for example, methane, ethane, and ethylene) and may also contain very small amounts of ammonia, hydrogen sulphide, and possibly tars (Zhang et al., 2015). Gasification produces gaseous fuel products through the process of partial oxidation at high temperatures (Toor et al., 2011). Gasification converts biomass (carbon containing feedstock) in a high-temperature environment into synthetic gas (for energy production) and valuable products such as chemicals (detergents, adhesives, surfactants, and plasticizers) (Lozano and Lozano, 2018).

Biomass gasification processes may be classified based on the type of gasification agent used. According to Zhang et al. (2019), types of gasification include air gasification, steam gasification, oxygen gasification, carbon dioxide gasification, and supercritical water gasification. Air gasification is the most widely used and studied gasification process as the reaction process is easy, the structure of the reactor is simple, and the gasification agent (air) is cheap and readily available. Steam gasification, supercritical water gasification, carbon dioxide gasification, and oxygen gasification generally produce higher HHVs (higher heating value) than air gasification (Zhang et al., 2019).

For oxygen gasification and air gasification, the overall reaction can be exothermic or endothermic and these reactions may be controlled by varying the oxygen and air content. Typically, certain oxygen or air content relates to a specific gasification temperature if there is no external heat, however, if a higher temperature is needed then higher oxygen or air content is needed, or an external heating source may be applied (Zhang et al., 2011).

Gasification processes occur inside a gasifier. The type of gasifier used is an important factor as it affects the reactions, processes, and products formed (Zhang et al., 2019). Gasifiers may be categorized into three groups: fluidised bed gasifiers, fixed bed (moving bed) gasifiers, and entrained flow gasifiers (Zhang et al., 2015). Types of fluidised bed gasifiers include circulating fluidised bed and bubbling fluids bed gasifiers. Examples of fixed bed gasifiers include horizontal draft and downdraft gasifiers. The majority of the gasifiers manufactured are downdraft fixed bed gasifiers and the second most manufactured gasifier is the fluidised bed gasifier (Balat et al., 2009).

2.7. Summary

Table 2-1 displays the various types of biomass and their potential as a source for biofuel production. It also shows why algae may be a favourable biomass resource and more suitable for biofuel production.

Table 2-1: Summary of types of biomass

Types of biomasses	Summary
Agricultural crop residue	Agricultural crops are a diverse and abundant resource and include sorghum stubble, corn stove, wheat straw, and oat straw. The main difficulty of using agricultural crops as a source of energy is the use of these crops for food and feed production and the land-use conflict.
Dedicated energy crops	Dedicated food crops are non-food crops grown explicitly to be used as a source of biomass (such as woody and herbaceous biomass) on land not suitable for traditional food crops. This resource does not cause land-use and food vs fuel conflicts; however, it may take years before the biomass reaches full productivity for cultivation. The long period before cultivations means this type of biomass would not meet global energy demands.
Forestry residues	Forestry residues may be defined as the by-products and residues of the logging of trees and may also be trees and crops grown specifically for utilisation as biomass. The use of unwanted and unsellable residues does not negatively affect the environment and may reduce the risk of forest fires. The limitation of this form of biomass is ensuring there are sufficient trees for ecological maintenance in terms of habitats and nutrient maintenance. Another limitation is that the quantity of resources available for energy conversion and the period of the collection depends highly on the operation of the logging industry
Wood processing residues	Wood processing residues are the waste and by-products from the processing of wood (bark, sawdust, leaves, and branches). This form of biomass is generally inexpensive and convenient, as the collection is done by the processing plant and does not cause land-use conflicts. However, it cannot meet global energy demands as the number of resources available for bioenergy conversion, and the time taken to acquire resources, depends highly on the operation of the wood processing industry.
Wet waste	Wet waste includes manure slurries, biogas, organic waste, and treated sewage sludge, and may help to alleviate waste disposal problems and generate revenue streams for communities employing the conversion of this waste to bioenergy. However, the separation

	and processing of the different forms of waste require large capital costs, a lot of manpower, and various processing technologies.
Municipal waste	Municipal waste may be defined as waste from commercial and residential areas that has the potential to be converted to energy (paper, plastics, food wastes, and rubber), and the use of this resource as a source of biomass can reduce waste meant for landfills, however, different forms of waste have to be processed in different ways, requiring a lot of resources, capital, and technology.
Algae	Algae is aquatic biomass and may be classified based on their size, as microalgae or macroalgae. Algae can grow in a variety of aquatic locations (such as ocean, river, lake, and pond) and under a variety of conditions. A limitation of using algae as a source for energy conversion on a large scale is the high productions costs, however, algae have many positives which makes them a viable and attractive source for energy conversion. Algae do not cause land-use conflicts as grows in aquatic environments and it does not cause food vs fuel conflicts as algae is not a main source of food globally. Algae is also fast-growing and may be cultivated many times throughout the year, especially due to its ability to grow under various conditions and in various environments.

Table 2-2 displays the various thermochemical process options available for the processing of biomass, primarily to convert biomass to a biofuel product. The summary also shows why hydrothermal liquefaction may be more beneficial than the other thermochemical processing techniques.

Table 2-2: Summary of thermochemical processing techniques

Technique	Summary
Pyrolysis	Pyrolysis is a thermochemical process that triggers the decomposition of feed through the use of an inert atmosphere and medium to high temperatures (300°C to 1300°C). Pyrolysis can be classified based on the operating conditions (such as reaction temperature, residence time, and heating rate) into three groups: flash pyrolysis, fast pyrolysis, and slow pyrolysis. Pyrolysis of biomass produces bio-oil, biochar, and syngas. The main advantage of pyrolysis is that generally, the main product formed is bio-oil, with a possible yield of up to 75%. The bio-oil produced may have a high concentration of carbon and low concentrations of sulphur and nitrogen. Pyrolysis has a short residence time and thus a lower operational cost.
Fischer-Tropsch	Fischer-Tropsch synthesis is a cluster of catalytic processes used for the conversion of synthetic gas to liquid fuels and valuable chemicals products. Fischer-Tropsch synthesis is a multistep process (with three main stages) utilised for the conversion of feedstock (biomass) to fuels. The initial step is a gasification process to convert the biomass feedstock to syngas. The next step is the removal of contaminants and impurities to clean the syngas. The final step is the catalytic conversion of the syngas, within a catalytic reactor, to produce biodiesel and other biofuels. Low temperature Fischer-Tropsch synthesis may produce a waxy hydrocarbon that is sent for hydrocracking to break it down into smaller liquid hydrocarbons. The Fischer-Tropsch process has the ability to produce carbon-neutral fuels that are environmentally friendly.
Gasification	Gasification is a thermochemical process that involves the reaction between a gasification agent and a feedstock to produce syngas. Gasification utilises partial oxidation in high temperature environments to convert biomass to gaseous fuel products and valuable chemical products (adhesives, detergents, and plasticizers).

	The syngas that is produced contains carbon dioxide, hydrogen, nitrogen, hydrocarbons (methane, ethane, and ethylene), and possibly small amounts of ammonia, tar, and hydrogen sulphide. Gasification processes are classified based on the type of gasification agent used. Types of gasification processes include air, steam, oxygen, and supercritical water gasification. Gasification occurs within a gasifier and the type of gasifier used affects the reactions, processes, and types of products formed. There are three categories of gasifiers: fluidised bed, fixed bed, and entrained flow gasifiers.
Liquefaction	Liquefaction is a thermochemical process that causes thermal degradation of feedstock in a liquid reaction medium. This triggers complex chemical reactions that produce liquid biofuels and other valuable chemical products. The components formed from this process may be catalytically converted to organic products that are rich in hydrocarbons. The utilisation of a suitable feedstock particle size would provide a higher contact surface area and reduce the limitation of mass and heat transfer. The bio-oil produced contains volatile organic esters, ketones, acids, alcohols, and aldehydes. Liquefaction may produce a higher bio-oil yield than the pyrolysis and gasification processes, with the bio-oil being a more viscous product.
Hydrothermal Liquefaction	Hydrothermal liquefaction is a thermochemical process and a category of the liquefaction process. It uses high pressures and temperatures within a liquid reaction medium (generally water) to convert biomass to bio-oils. The high pressures and temperatures allow the water to permeate the biomass and extract the bio-oil. The main aim is to produce a bio-oil product that possesses a high energy density through the removal of oxygen. The process pressures range from 1.5 MPa to 20 MPa and the process temperatures range from 200°C to 400°C. The products formed from the hydrothermal liquefaction process include a bio-crude/ bio-oil fraction, a gas fraction, a solid fraction, and an aqueous fraction. This process has a low energy requirement when compared to other processing technologies as it can process both wet and dry feedstocks negating the need for an energy intensive drying step. Hydrothermal liquefaction does not require a catalyst thereby reducing the overall cost of processing. This process may occur through pyrolytic means, however, the biocrude product formed is generally more deoxygenated than the pyrolysis process.

CHAPTER 3: MATERIALS AND METHODS

3.1. Materials and Equipment

3.1.1. Materials

Marine macroalgae

Figure 3-1: Marine macroalgae utilised for experimentation.

Marine macroalgae was the source of biomass used for this investigation. Marine macroalgae is an aquatic biomass resource that grows in a variety of conditions and locations, making it a useful source of biomass for biofuel production. The analysis of the bio-oil yield and mass dissolution of the algae was the main objective of this study. The marine macroalgae used for this investigation was seaweed from the Taurus Cape Kelp company located in Western Cape, South Africa. The type of seaweed used was brown algae (also known as *Ecklonia Maxima*). The seaweed was dried, ground, and crushed to produce the sample of seaweed used. The sample size of the seaweed was stated to be 3mm.

Water

Water was used for various purposes throughout the experiment. The main purpose of water was for the use as a reactant and catalyst during the hydrothermal liquefaction process. Deionized water was used inside the reactor to permeate the seaweed through the aid of high temperatures and pressures and extract the oil within. Reaction conditions were selected to ensure the water inside the reactor did not vaporize and no product was lost.

Nitrogen

Nitrogen was obtained from Afrox (located in South Africa). It was supplied in a standard gas cylinder at a purity of 99.99%.

Dichloromethane

Dichloromethane is a colourless and volatile polar liquid that has a sweet-smelling odour. Dichloromethane was obtained from Merck (Pty) Ltd located in Gauteng, South Africa at a percentage of 99%. Dichloromethane was used to separate the bio-oil from the water solution following the hydrothermal liquefaction process. There is an abundance of literature that states that dichloromethane is selective with oil and not with water. According to Han et al. (2019), dichloromethane provides adequate separation of the bio-oil from water. Dichloromethane was added to the solution after the filtering process, and it was also used to rinse the reaction vessel and filtration equipment to absorb any residual oil. Distinct layers were formed when dichloromethane was mixed with the aqueous phase.

3.1.2. Equipment

Parr reactor vessel

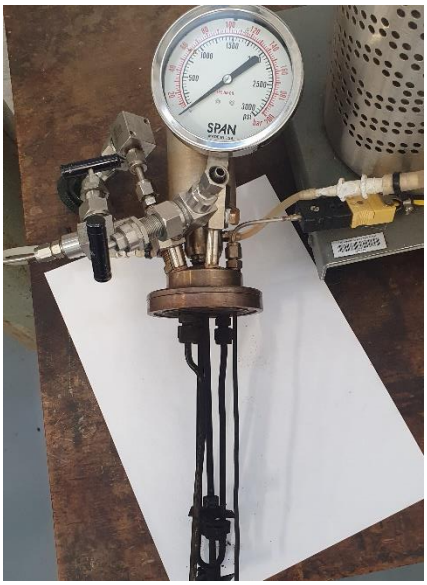

Figure 3-2: Reaction vessel internals

The Parr reactor vessel was the instrument where the batch hydrothermal liquefaction process occurred. The Parr reaction vessel was also designed and manufactured by the Parr Instrument Company. The reactor vessel is composed of the cylindrical vessel (194 mm long, with an inner diameter of 64 mm and a thickness of 5.5 mm) and the lid (diameter 75 mm) joined together with a casing that encompasses the part of the lid and the vessel that are in contact. The casing has six bolts to ensure that the reaction vessel is sealed, and no pressure and components escape the reactor. The reactor vessel was designed to fit into the heating mantle. The base and the lid are composed of 316 stainless steel to withstand the corrosive nature of any components within the pressure vessel. The lid possesses many valves attached to it to allow for the inlet and outlet flow of compounds. The nitrogen inlet gas line to pressurize the reactor and the pressure relief valve are both attached to the reactor vessel lid. The inlet gas line has an inner diameter of 1/8 inch (x mm) and is fabricated of stainless steel. The water inlet and outlet lines were also attached to the reactor vessel lid. The water lines were composed of silicon and were attached

to the batch reactor vessel to ensure that the central components did not seize up due to the high temperatures. At the centre of the lid, there was an attachment to join the stirrer controller (from the reactor controller) to the stirrer. The stirrer is attached to the reactor lid and is 185 mm long and is made of 316 stainless steel to withstand the corrosive properties of compounds placed inside the reactor vessel. The stirrer has two impellers positioned at 10 mm and 47 mm from the bottom of the stirrer. The impellers used are pitched blade impellers, each composed of four individual slanted blades, to promote axial flow within the reactor.

Reactor controller

Figure 3-3: Reactor controller used to control temperature and agitation speed.

The Parr Model 4848 reactor controller was designed to be used with Parr laboratory reactors and pressure vessels. It was designed and built by the Parr Instrument Company located in Illinois, USA. The reactor controller consists of a temperature controller unit, that is assembled with appropriate power, pilot lights, switches, and safety relays, along with a heating mantle and an overhead stirrer. The temperature controller contains the controls to regulate the reactor temperature based on the inputs set. The temperature controller is programmable and may be used as a setpoint mode or to automatically alter the temperature at specific time intervals with the 'ramp and soak' method. The reactor controller also has an analogue control for regulating the stirrer speed within the reaction vessel. The temperature controller unit has a height of 235 mm and is 279 mm long, with a width of 280 mm. The temperature controller possesses a J-type thermocouple, which is used to measure the temperature inside the Parr reactor.

The heating mantle serves the purpose of heating up the reactor vessel based on the inputs set in the temperature controller unit. The heating mantle is fabricated from aluminium to withstand the high temperatures. The mantle base has a height of 50 mm, with a length of 200mm and a width of 234 mm. The mantle has a height of 200 mm, with an inner diameter of 80 mm and an outer diameter of 120 mm.

The heating mantle possesses an outer layer placed 30 mm away from the outer diameter of the mantle (150mm in diameter from the centre of the mantle) for an added safety measure.

Mass Scale

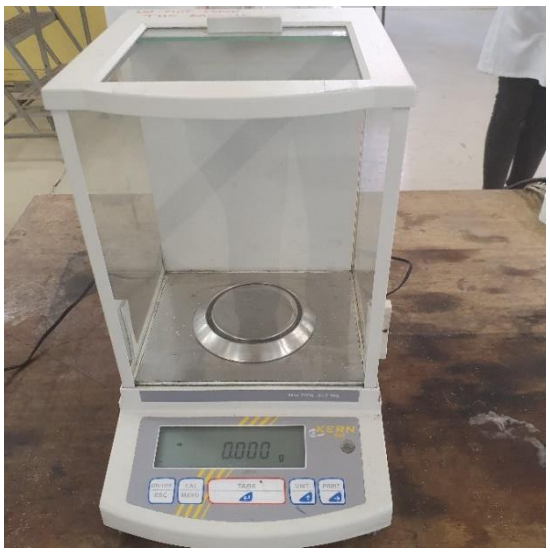

Figure 3-4: Mass scale used to measure seaweed before and after hydrothermal liquefaction.

The gravimetric scale was used to determine the mass of the seaweed before the hydrolysis and following the filtration process. The scale was also used to determine the mass of oil formed from hydrolysis, by measuring the mass of a glass vial with and without the bio-oil and subtracting these values. All measurements were recorded in grams. The gravimetric scale used was the Ohaus Adventurer TM manufactured in New Jersey, USA, and had an uncertainty of +/-0.001g.

Moisture Analyser

Figure 3-5: Moisture analyser

The moisture analyser was used to determine the moisture content of the seaweed, before the hydrolysis process and after filtering the product of the hydrolysis process, to analyse the total mass lost (mass dissolution) on a dry basis. This was done as the seaweed used (although dried, ground and crushed) was determined to contain a percentage of moisture when removed from the sample bag. An aluminium tray was used in the moisture analyser to place the seaweed sample for analysis. The moisture analyser was set to operate at a temperature of 100°C, with an automatic time limit, to determine the total moisture present within the seaweed. The moisture analyser was a Boeco model BM035 manufactured in Hamburg, Germany.

Vacuum pump

Figure 3-6: Vacuum pump

The vacuum pump was used in the filtration setup to induce vacuum filtration and efficiently separate the solution from the seaweed following the hydrothermal liquefaction process. The vacuum pump used was the Rocker 300 vacuum pump manufactured by Rocker Scientific Co., Ltd in Taiwan. The vacuum pump is 186 mm long, 90 mm wide, and 100 mm high. The pump sucks in air through the pump and expels it from the back of the pump, by attaching the suction end of the pump to the Buchner flask and filter funnel (with a filter paper placed inside). The pump easily and effectively separates solids and liquids, pulling the liquids through the filter paper while the solids or solid residue remains on top of the filter paper. The filter funnel used is a large ceramic filter funnel with a diameter of 152 mm and the filter paper had a diameter of 150 mm and was of grade 3hw. The vacuum pump possesses an internal filter to ensure that any solid particles or residue small enough to go through the filter paper and into the pump does not damage the pump internally or affect the efficiency of the pump.

Separating funnel

The separating funnel was used to separate liquids of different densities (specific gravity). The liquids with the higher density will sink to the bottom of the funnel and the liquids with the lower density will float to the top. The funnel has a tap on the bottom where the heaviest liquid sits. When the tap is turned

90 degrees, the liquid flows out of the bottom of the funnel. This allows for the separation of the different fluids. The funnel is made of glass (therefore transparent) which allows the user to separate the fluids based on sight. The separating funnel was used to separate the dichloromethane and oil mixture from the water. The water was the top layer and the dichloromethane and oil mixture was the denser or heavier liquid that sank to the bottom.

Rotary Evaporator

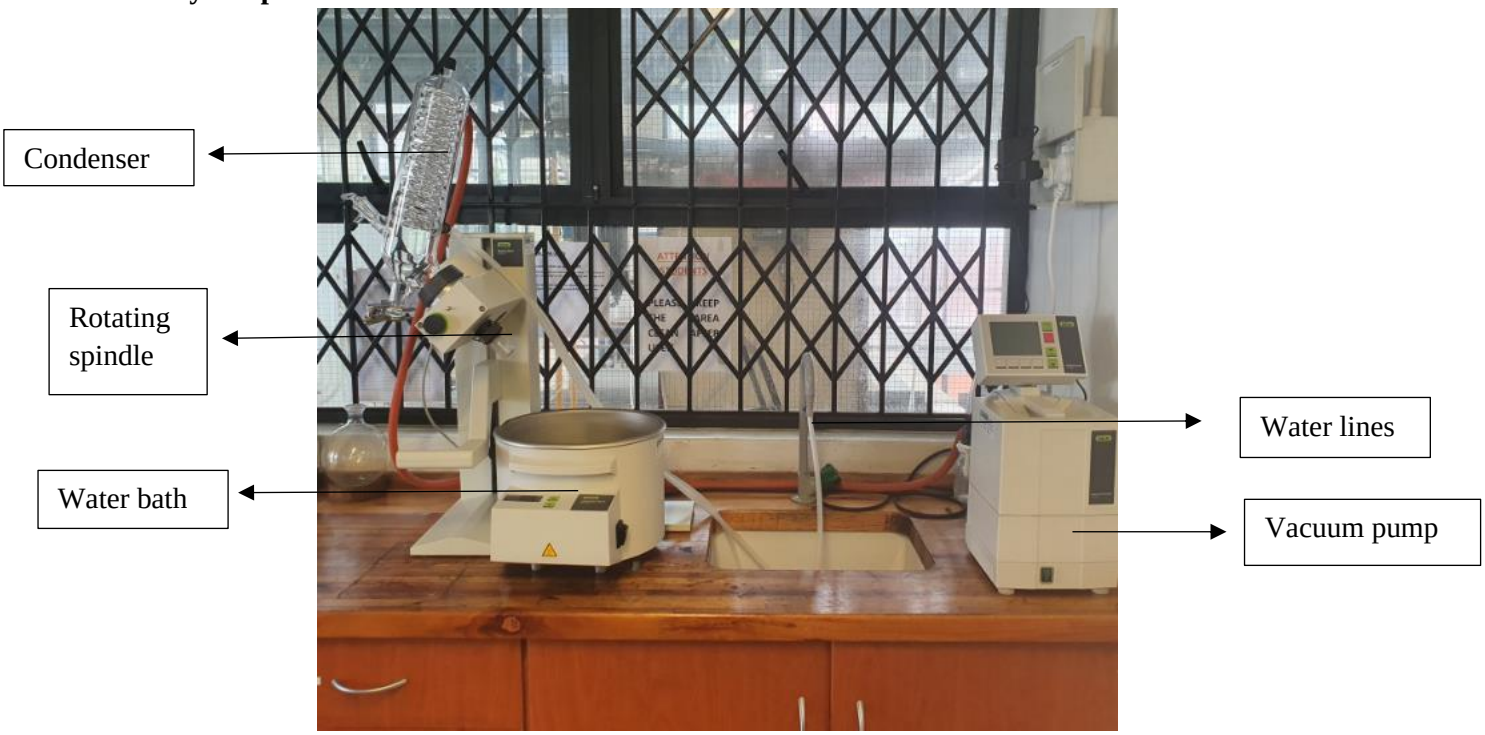

Figure 3-7: Rotary evaporation setup

A rotary evaporator is used to separate liquid mixtures that contain liquids that have different boiling points. The liquid with the lower boiling point is the liquid that is evaporated. The rotary evaporator setup is composed of a water bath, a pump, two glass flasks, a condenser, and the central body to which all the components attach to. One glass flask is used as an evaporation flask and has a diameter of 130 mm. The second flask is used as a condenser flask and has a diameter of 130 mm. The water bath is filled with water and heated up to set the evaporation temperature. The pump is used to set the appropriate evaporation pressure. Both the water bath temperature and pump pressure are manually set and dependent on the component being evaporated. Two silicon tubes are attached to the inlet and outlet of the condenser to allow for the flow of water through the condenser to cool and condense the component being evaporated. The end of the silicon tube attached to the inlet of the condenser was attached to a tap to provide a source of water (cooling medium) to cool the component being evaporated. The end of the silicon tube that is attached to the condenser outlet was placed in a sink to send the water coming out of the condenser to a drain. The condenser flask was attached to the bottom of the condenser

and was used to collect the component being evaporated. The evaporated flask was attached to the spindle on the central body. This spindle was at a 45-degree angle and allowed for the rotation of the evaporation flask to ensure even evaporation within the reaction flask. The central body can move vertically to allow for the optimum placement of the evaporation flask in the water bath. All major components (Rotavapor R-100, Vacuum pump V-100, Heating bath B-100 and Interface I-100) were manufactured by Buchi Labortechnik AG in Switzerland.

Gas Chromatograph – Mass Spectrometer (GC-MS)

Figure 3-8: GCMS setup for sample injection and analysis

A Shimadzu autosampler GC (gas chromatograph) 2010 Plus was attached to a GCMS–QP2010SE (gas chromatograph-mass spectrometer). The apparatus was used to determine the composition of the bio-oil formed from the hydrothermal liquefaction process. The GCMS contained a Shimadzu SH-Rxi-5ms non-polar capillary column (5% phenyl/ 95% dimethyl polysiloxane). The capillary column was 30 meters in length and had an inner diameter of 0.25mm and a wall thickness of 0.25µm. The carrier gas used was helium. The helium gas may also serve as a makeup gas to increase the flow of the gas over the detector within the column. The GCMS autosampler was used to inject the sample into the column. The autosampler syringe was prerinsed two times with solvent (dichloromethane) and then rinsed three times with the sample before injecting the sample into the column, to ensure that only the sample and no impurities entered the column. Following the injection of the sample, the autosampler was rinsed three times with the solvent. An injection volume of 2ml was used to ensure that a sufficient amount of the entered the column for analysis. The split ratio ensured that broad and tailing peaks are not formed. The split ratio functions whereby the hot gas sample is mixed with the carrier gas and split into specified flows based on the ratio. The split stream is vented and the stream containing the carrier gas enters the column.

3.2. Experimental Setup

To carry out this investigation on the bio-oil production from the hydrothermal liquefaction of marine macroalgae, the appropriate equipment had to be sourced and assembled to form a functioning reactor setup, filtration system, and evaporation system. The setup was assembled taking into account all safety factors and precautions.

Hydrothermal liquefaction setup

Figure 3-9: Hydrothermal liquefaction setup

The nitrogen gas cylinder was placed in a bracket that was attached to the wall to ensure it was secured. The outlet gas valve was attached to the top of the gas cylinder. The gas lines were connected to the outlet gas valve at one end and the reactor vessel lid at the other end. The reactor controller and heating mantle were placed adjacent to each other on a desk and all cords were connected. The thermocouple was connected from the reactor controller to the reactor vessel lid. Two silicone tubes were connected to the t water inlet and outlet ports. Once filled with the required materials, the reactor vessel lid was placed on the vessel and sealed. The reaction vessel was placed inside the heating mantle. The stirrer attachment from the reactor controller was then connected to the central stirring component and the reaction conditions were inputted to the controller before commencing with the run.

Experimental procedure diagram

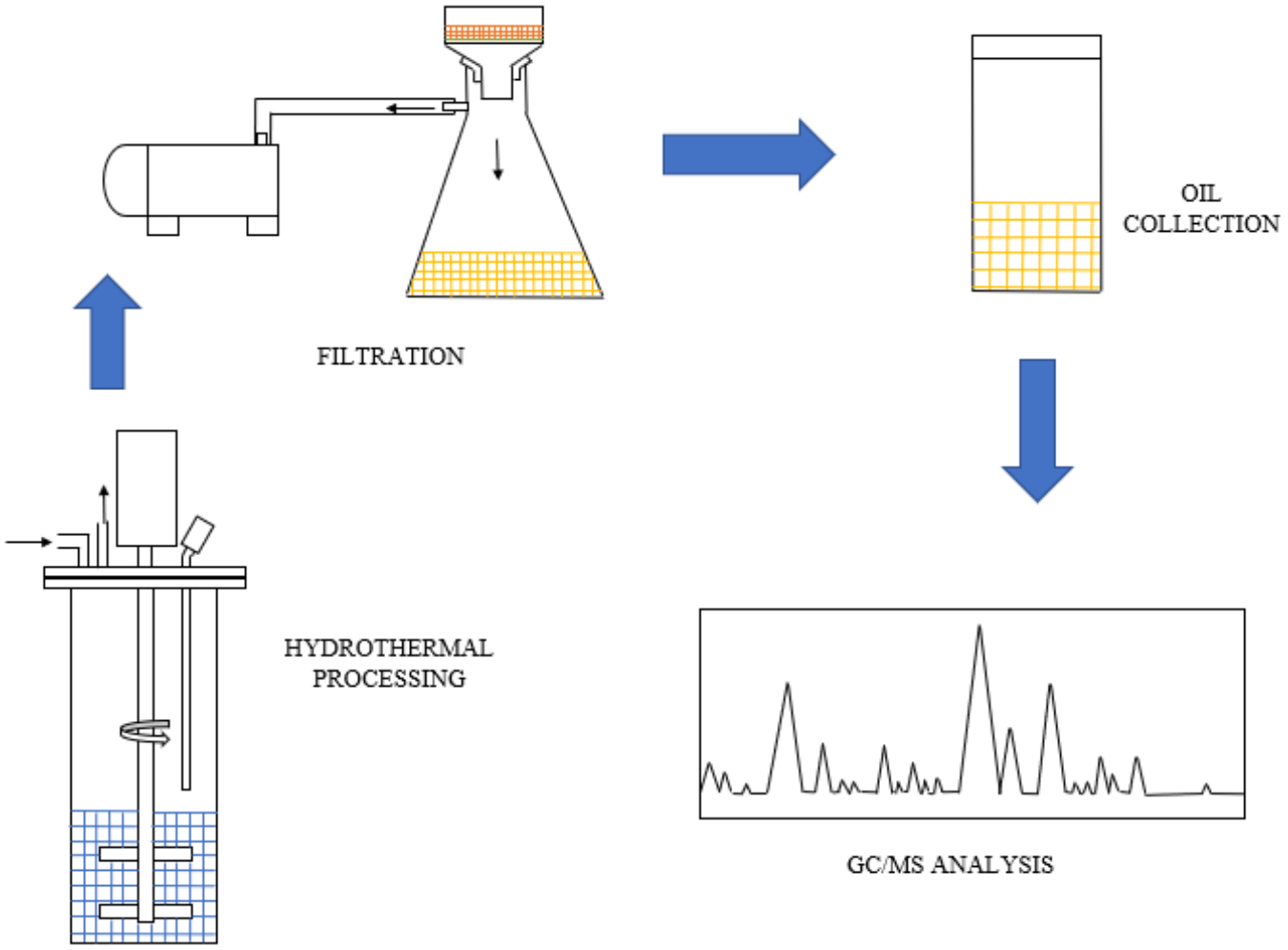

Figure 3-10: Graphical representation of experimental procedure

3.3. Experimental procedure

A multistep procedure was used to determine the amount of bio-oil formed from the hydrothermal liquefaction of marine macroalgae. To reduced uncertainty and ensure accuracy, all of the experimental runs were approached in the same manner with only the selected variable being altered for each data set. The experimental apparatus was cleaned before and after each run (with boiling water and soap followed by an acetone rinse) to ensure no residue remained in the apparatus and to ensure the accuracy of the experimental results. It was observed that the seaweed used for processing contained a percentage of moisture before the commencement of the run. To account for the actual mass lost from the seaweed, all mass dissolution results were determined on a dry basis. The moisture percentage was measured prior to each run, as this provided the most accurate account for the moisture in the seaweed due to the moisture varying dependent on the ambient conditions present when undertaking the run. The procedure was composed of four main parts. These were: hydrothermal liquefaction, filtration, liquid-liquid separation, and evaporation.

Hydrothermal liquefaction

Gravimetric measurements were required to determine the total mass of seaweed lost. The mass of a watch glass was measured, and the required amount of seaweed was measured before being placed in the Parr reactor and the initial moisture percentage was subtracted from the mass of seaweed to determine the initial dry mass of seaweed. Water was filled into the reactor with the seaweed. The amount of water filled in the reactor was determined by the required solids loading and mass of seaweed used. The lid was placed on the reactor and the reactor was sealed to ensure no pressure, seaweed or water escaped from the reactor during processing. All six bolts on the seal were tightened to lock the seal in place. The sealed reactor vessel was transferred to the Parr heating mantle.

All non-essential valves on the reactor were closed to ensure only one inlet for gas into the reactor. The nitrogen gas cylinder was opened, and nitrogen was fed to the reactor through the stainless-steel gas line attached to the one-way valve on the lid of the reactor. According to Boyle's law and Charle's law, the pressure will increase with an increase in temperature. Taking this into account, the reactor was initially pressurised with a low pressure of 4 KPa gauge pressure, as the pressure increased to the required reaction pressure during heat up. The reactor controller was used to set the required reaction temperature and the heating element was set to the highest setting. Various agitation speeds were examined and an agitation speed of 330 rpm was selected based on the effective mixing of the contents of the reaction vessel (to ensure efficient contact between the seaweed and water) without vortexing and clogging the impellers with biomass. The reaction vessel was allowed to heat up to the required reaction conditions. The inlet valve was closed so that no product was pushed back through the gas lines towards the nitrogen tank.

The time taken to reach the required reaction conditions was noted for each run. Once the required reaction temperature and pressure were reached, the reactor was maintained at these conditions for the allocated time, ranging from 5 minutes to 30 minutes in steps of 5 minutes, for each set of reaction conditions. When the allocated time was reached, the heating element was switched off, the stirrer was stopped, and the reaction vessel was quenched (transferred to an ice bath) immediately to stop any further reaction or process from taking place. When the reactor was completely cooled, the gaseous product was vented into the atmosphere to depressurise the reaction vessel. All six bolts of the seal were loosened and removed, and the seal was subsequently removed. The reactor lid was removed and any residual liquid on the stirrer blade was drained into the main reaction vessel.

Filtration

The filter paper was weighed and placed in the ceramic filter funnel. The vacuum pump was switched on and the suction was tested. The contents from the reaction vessel (the solution and seaweed) were transferred to the filter funnel and underwent filtration until all the liquid was separated from the seaweed. The large surface area of the filter funnel allowed for a quicker filtration process. The mass of a watch glass was measured. The filter paper and seaweed were transferred to the watch glass and the mass of the watch glass with the seaweed and filtered paper was measured. This determined the final wet mass of the seaweed. To determine the total mass lost on a dry basis, a portion of the seaweed was placed in an aluminium tray and transferred to the moisture analyser to determine the moisture content of the seaweed following the hydrothermal liquefaction process.

Liquid-liquid separation

The liquid solution from the filtration process was transferred from the Buchner flask to a 500ml volumetric flask. 100 ml of dichloromethane (DCM) was measured into a measuring cylinder. Approximately 75% of the dichloromethane was poured directly into the volumetric flask. The remaining 25% of dichloromethane was poured into the reaction vessel and the Buchner flask to remove any residual bio-oil remaining in these vessels. The dichloromethane from the reaction vessel and Buchner flask were then poured into the volumetric flask. The volumetric flask was shaken to ensure thorough mixing of the dichloromethane with the solution. The resulting mixture was allowed to settle and separate into the distinct phases overnight (through gravity separation). The solution is separated into two distinct phases, a layer of water and an oil-DCM mixture layer, with a thin aqueous layer between the two solutions.

The resulting solution was transferred to a liquid-liquid separating funnel. Approximately 20ml of dichloromethane was used to remove any remaining oil from the volumetric flask and this was added to the liquid-liquid separation funnel. The funnel separates liquids based on the density or specific gravity of the liquid., hence it was determined that the oil-DCM layer was the bottom layer due to the higher density. The

oil-DCM layer was separated from the water layer and transferred directly to the evaporation flask. The water and aqueous layers were discarded into a waste bottle.

Evaporation

The water bath was filled with water and allowed to reach the desired temperature of 42°C. The vacuum pump was switched on and set to the required pressure of 148.39KPa. The evaporation conditions were determined based on the component being evaporated (in this investigation the dichloromethane was evaporated to obtain bio-oil) and were based on the vapour pressure of the solvent (Appendix C, Figure C-1). Grease was placed on the lip of the evaporation flask before connecting it to the spindle attachment of the evaporation setup to ensure the evaporation flask did not seal to the spindle and to allow for easy removal of the flask following evaporation. The evaporation flask containing the oil-DCM mixture was connected to the spindle, which was at a 45° angle and allowed for an adjustable rotational speed. Silicon tubing was connected to the condenser to provide a source of coolant (water) for the condenser to cool the liquid being evaporated (DCM). Lube grease was also placed on the lip of the condenser flask before attaching it to the bottom of the condenser to ensure the condenser flask did not seal to the condenser during the evaporation and condensing processes.

A portion of the evaporation flask was submerged in the water bath until the entire oil-DCM solution was well within the water bath. The evaporation flask was set to rotate, as this provided an even distribution of heat for evaporation. Evaporation was done until the condensation of dichloromethane stopped, indicating that all the dichloromethane had evaporated. The evaporated dichloromethane was recovered in the condenser flask. The evaporation flask was subsequently removed from the water bath and the rotating speed set to zero. The mass of a glass vial (with lid) was measured. The evaporation flask was carefully removed while ensuring no spilling of the oil, and the oil was transferred to the glass vial. The mass of the glass vial with the oil was measured to determine the total mass of oil formed. The condenser flask was carefully removed from the condenser and the recovered dichloromethane was transferred to a waste bottle.

GCMS sampling and analysis

The GCMS equipment was switched on and autotuned to ensure the accuracy of the results analysed. The oil from the glass vial was transferred to a syringe and injected through a microfilter (0.45 micrometres) and into the GCMS vial. To ensure no bio-oil remained in the glass vial, the glass vial was rinsed with a small amount of dichloromethane. The GCMS method used included a solvent cut time of 3 minutes to ensure that the solvent did not show in the GCMS results. The GCMS vial was placed in the autosampler tray and analysed when the GCMS equipment stabilised and the desired analysis conditions were reached. Following analysis of the sample by the equipment, the resulting peaks were analysed and selected based

on the height and width (area) of the peak. The peaks with the highest relative area were selected as the main components formed.

3.4. Experimental design

The importance of experimental design is generating the type of experimental data that will be used for the performance analysis and kinetic study. The experimental design also ensures that the most amount of information is collected with the least resources and time expended.

Experimental variables

The experiment examined the effects of mass of algae, temperature, and pressure (reaction conditions), solids loading and reaction time on the hydrothermal liquefaction of marine macroalgae. The experiments were conducted to ensure that when one experimental variable was varied, the remaining variables were kept constant.

The independent variables are variables that do not change as a result of altering another variable and remain constant during the run. The independent variables for this experiment were: mass (5g, 6g, 10g), solids loading (5% and 10%), reaction time (5 minutes to 30 minutes in steps of 5 minutes), stirrer speed (330 rpm), type of inert gas used (nitrogen), and temperature (200°C and 250°C) and pressure (1500 KPa and 4000 KPa). The dependent variables are affected by the values of the independent variables stated previously. The dependent variables were: The final (wet) mass of the seaweed, the final moisture content, the percentage of mass dissolution, and the amount of bio-oil formed.

The staple mass selected to be used was 6g as this provided adequate dissolution and formation of bio-oil while taking into account the size of the reaction vessel (500ml) used and the position of the two impellers of the overhead stirrer. The type of impellers used were the pitch blade impeller (also known as the axial flow impeller), which consists of four individual slanted blades that are used to induce axial flow. The effect of mass on the yield of bio-oil was examined by varying the mass above (10g) and below (5g) the staple mass used throughout experimentation.

The solids loading was selected to provide an adequate bio-oil yield following the hydrothermal liquefaction. A solids loading of 10wt% provided an adequate amount of bio-oil following the hydrothermal liquefaction process. To examine the effect of solids loading on the mass dissolution and bio-oil formation, the solids loading was reduced to 5wt%. A lower solids loading is assumed to provide a lower yield of bio-oil.

The temperature and pressure were selected based on the vapour pressure of water to ensure it did not vaporize during the hydrothermal liquefaction process. The reaction pressures had to correspond to the reaction temperatures selected. The reaction conditions selected were a temperature of 250°C and a corresponding pressure of 4000KPa. For the analysis of how the reaction conditions affect the bio-oil yield, a lower reaction temperature of 200°C was selected, with a corresponding reaction pressure of 15.33KPa. A Harris pressure gauge and outlet gas flow nozzle (pressure range: 0KPa to 6000KPa) were used to evaluate the reaction pressure.

The reaction times selected were 5 minutes to 30 minutes in steps of 5 minutes. These time intervals are started after the induction period. Separate experimental runs were conducted for each time interval (from 5 minutes to 30 minutes), therefore six experimental runs were conducted for each reaction set. These times were selected to determine the kinetic regime and kinetic parameters of dissolution over a uniform time difference while ensuring multiple points for a more accurate measurement. The induction time (time to heat up to the desired reaction conditions) was also considered, as it was assumed that mass dissolution and bio-oil formation would take place during the induction time as well. Preliminary runs indicated that the induction time was on average 60 minutes when the heating element of the Parr reactor was set to its highest level. The induction period runs were only conducted for the control conditions, which was a mass of 6g, and a solids loading of 10wt%. The temperature and pressure for the induction period will vary for every time interval as the reactor is heating up to the desired reaction conditions. The pre-set temperature (before beginning the heat up) for every run of the induction period was set to 250°C to ensure the same heating rate for every run.

Table 3-1: Experimental Design for stabilised reaction conditions

Run	Time (minutes)	Mass of seaweed (g)	Temperature (°C)	Pressure (KPa)	Solids loading (wt%)
1	5	5	250	4000	10
2	10	5	250	4000	10
3	15	5	250	4000	10
4	20	5	250	4000	10
5	25	5	250	4000	10
6	30	5	250	4000	10
7	5	6	250	4000	10
8	10	6	250	4000	10
9	15	6	250	4000	10
10	20	6	250	4000	10
11	25	6	250	4000	10
12	30	6	250	4000	10
13	5	10	250	4000	10
14	10	10	250	4000	10
15	15	10	250	4000	10
16	20	10	250	4000	10
17	25	10	250	4000	10
18	30	10	250	4000	10
19	5	6	250	4000	5
20	10	6	250	4000	5
21	15	6	250	4000	5
22	20	6	250	4000	5
23	25	6	250	4000	5
24	30	6	250	4000	5
25	5	6	200	1533	10
26	10	6	200	153	10
27	15	6	200	1533	10
28	20	6	200	1533	10
29	25	6	200	1533	10
30	30	6	200	1533	10

Table 3-2: Experimental Design for induction period.

Run	Time (minutes)	Mass of seaweed (g)	Solids loading (wt%)
31	5	6	10
32	10	6	10
33	15	6	10
34	20	6	10
35	25	6	10
36	30	6	10
37	35	6	10
38	40	6	10
39	45	6	10
40	50	6	10
41	55	6	10
42	60	6	10

CHAPTER 4: RESULTS AND DISCUSSION

The production of bio-oil from marine macroalgae was quantified at varying masses of seaweed, reaction times, solids loading, and reaction conditions. The algae biomass was stated to be 3mm in size, however, further analysis determined that the size of the algae ranged between 1mm to 3mm. Gravimetric measurements and moisture analysis were performed prior to and after the hydrothermal liquefaction process to determine the total mass lost from the algae and the total amount of bio-oil formed. The gravimetric scale possessed an uncertainty of approximately +/- 0.04g, which was applied to all calculations. The fraction of mass lost from the algae was assumed to be a part of the aqueous solution and bio-oil formed. The light brown colour of the hydrolysate was assumed to be due to the brown pigmentation of the seaweed mixing with the liquefied proteins, lipids, and carbohydrates from the macroalgae. In this study, the control conditions were noted to be a seaweed mass of 6g, a solids loading of 10%, a temperature of 200°C, and a pressure of 4000 KPa. Gas Chromatography-Mass Spectrometry (GCMS) analysis was conducted to determine the composition of the bio-oil and ensure that the correct components for biofuel production were forming. A kinetic model was developed based on the mass dissolution and production of bio-oil.

4.1. Characterisation of the algae

Moisture analysis and proximate analysis were done to determine the average moisture content, average ash content, and average volatiles content of the seaweed. The moisture analysis was completed in a moisture analyser and the ash content was determined by placing 6g of seaweed into a muffle furnace at 700°C for 1 hour and measuring the ash formed. The volatiles content was also measured by placing 6g of the seaweed into the muffle furnace at 900°C.

Table 4.1: Analysis of algae used

Analysis	**Run 1**	**Run 2**	**Run 3**	**Average**
Moisture content	12.55%	12.49%	12.59%	12.54%
Ash content	1.637%	1.727%	1.655%	1.673%
Volatile's content	0.196%	0.265%	0.229%	0.230%

The average moisture content of the feedstock was determined to be 12.54%, the average ash content was determined to be 1.673% and the average volatiles content was determined to be 0.230%.

4.2. Effect of mass

The effect of varying mass on the formation of bio-oil from marine macroalgae was examined in this study. Masses of 5g, 6g, and 10g were selected to categorise the difference between a low mass yield and a high mass yield. These masses were also selected to ensure the reactor had a sufficient volume to facilitate hydrothermal liquefaction and to ensure an adequate amount of bio-oil could be extracted and measured. The solids loading was fixed at 10% and as such the amount of water was adjusted based

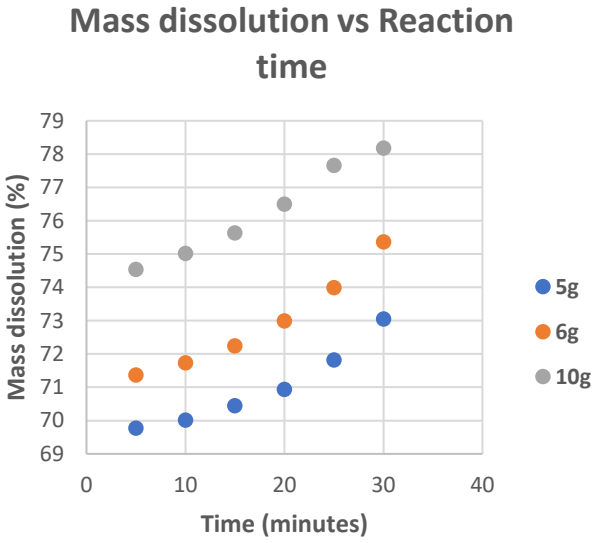

(a)

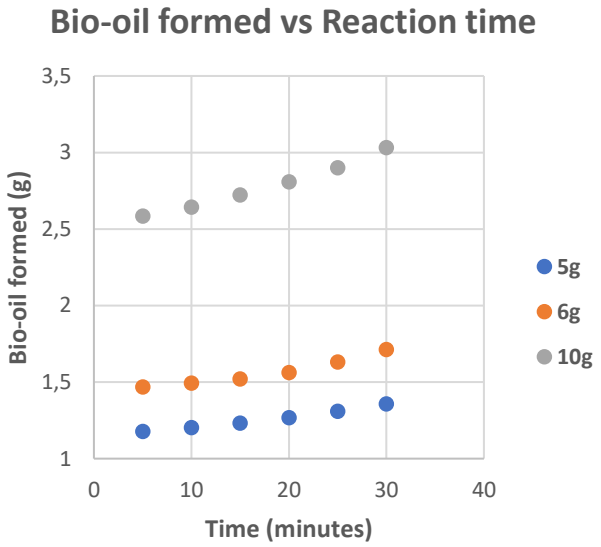

(b)

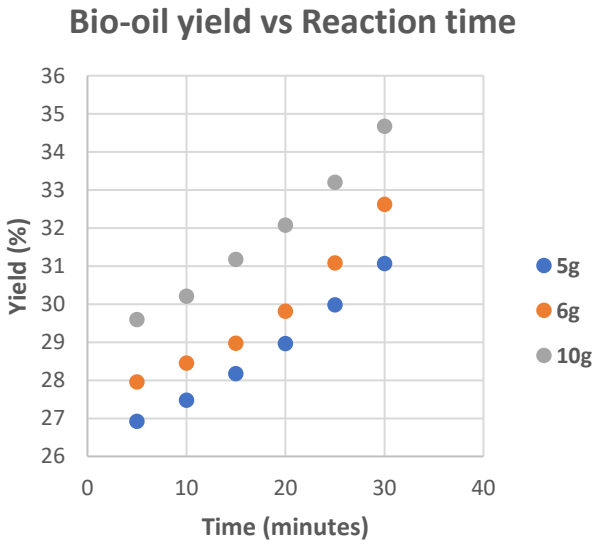

(c)

Figure 4-1: (a) Effect of mass on the mass dissolution of marine macroalgae, (b) Effect of mass on the amount of bio-oil formed and (c) Effect of mass on the bio-oil yield obtained from hydrothermal liquefaction.

Figure 4-1 (a) shows the effect of varying mass on the mass dissolution of macroalgae. It is observed that the mass dissolution increases with an increase in the mass of macroalgae used. The highest mass dissolution of 78.18% is observed for a mass of 10g, at a reaction time of 30 minutes. The lowest mass dissolution of 69.78% is seen for a mass of 5g, at a reaction time of 5 minutes. The mass dissolution for the mass of 5g ranges from 69.78% to 73.05%, for a mass of 6g the mass dissolution ranges from 71.37% to 75.37%, and for a mass of 10g the mass dissolution ranges from 74.54% to 78.18%. The average difference in mass dissolution between the masses of 5g and 6g is 1.94%, between the masses of 5g and 10g is 5.25% and between the masses of 6g and 10g is 3.31%.

Figure 4-1 (b) displays the trend for bio-oil production at varying masses. It is observed that the amount of bio-oil formed increases with an increase in the mass of seaweed used for hydrothermal liquefaction. The largest amount of bio-oil formed was 3.03g for the 10g, 30-minute run and the lowest amount of bio-oil formed was 1.18g for the 5g, 5-minute run. The amount of bio-oil formed ranges from 1.28g to 1.46g for a mass of 5g, from 1.47g to 1.71g for a mass of 6g, and from 2.59g to 3.03g for a mass of 10g. The average difference in the amount of bio-oil formed between the masses of 5g and 6g is 0.32g, between the masses of 5g and 10g is 1.54g and between the masses of 6g and 10g is 1.22g. This is due to the overall presence of more bio-oil within the reactor due to the larger mass used.

Figure 4-1 (c) shows the effect of varying the mass on the bio-oil yield. It is seen that the bio-oil yield increases with an increase in the mass used. The largest bio-oil yield of 34.67% was produced for the mass of 10g and at a reaction time of 30 minutes. The smallest bio-oil yield of 26.92% was produced for a mass of 5g and a reaction time of 5 minutes. The bio-oil yield ranges from 26.92% to 32.35% for a mass of 5g, from 27.96% to 32.62% for a mass of 6g, and from 29.59% to 34.67% for a mass of 10g. The average difference in the bio-oil yield between the masses of 5g and 6g is 1.05%, between the masses of 5g and 10g is 3.05% and between the masses of 6g and 10g is 2.00%. The observed results indicate that scale-up of the process, in terms of the amount of mass used, would result in a higher production of bio-oil to be used for biofuel production.

In figure 4-1 (a) and 4-1 (b) it is observed that the data does not converge for the various starting masses i.e., the trends are almost parallel, therefore, within this range of starting masses, temperatures, and reaction times, there is no limiting effect of increasing the quantity of the biomass relative to the amount of water

being used. The parallel trends also indicate that the mechanism of liquefaction is unaffected by the increase in biomass content.

4.3. Effect of solids loading

The effect of varying the solids loading was examined on the mass dissolution from macroalgae and the production of bio-oil. Solids loadings of 5wt% and 10wt% were used to quantify the effects of solids loading on the hydrothermal liquefaction process. These solids loadings were selected to ensure the macroalgae was completely submerged in the water medium to increase the contact surface area and facilitate effective hydrothermal processing. A mass of 6g was used for both solids loadings.

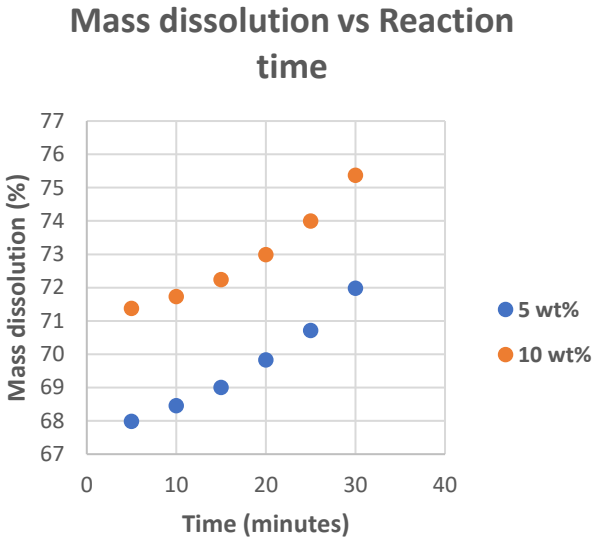

(a)

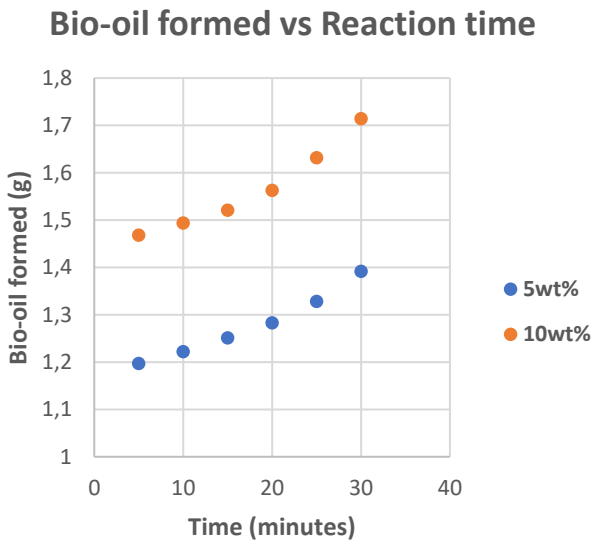

(b)

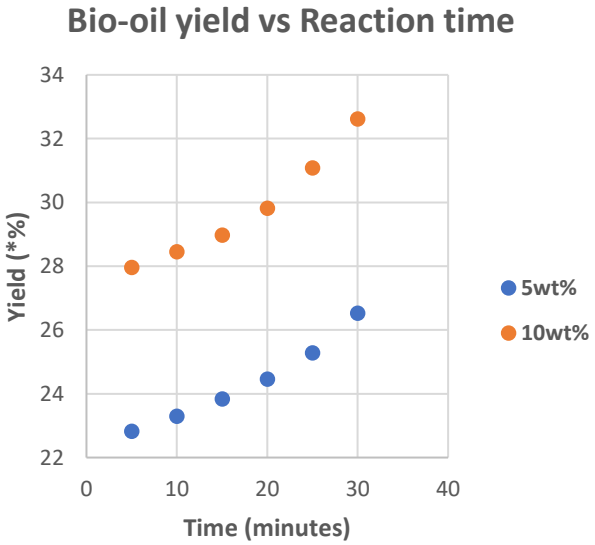

(c)

Figure 4-2: (a) Effect of solids loading on the mass dissolution of marine macroalgae, (b) Effect of solids loading on the amount of bio-oil formed and (c) Effect of solids loading on the bio-oil yield obtained from hydrothermal liquefaction.

Figure 4-2 (a) displays the trend for the mass dissolution of marine macroalgae for varying solids loadings. It was observed that the solids loading of 10wt% provided a larger amount of dissolution than the solids loading of 5wt%. The highest mass dissolution of 75.37% is observed for a solids loading of 10wt% and a reaction time of 30 minutes and the lowest mass dissolution of 67.98% is observed for a solids loading of 5wt% with a reaction time of 5 minutes. The mass dissolution for the solids loading of 5wt% varies from 67.98% to 71.98% and the mass dissolution for a solids loading of 10wt% varies from 71.37% to 75.37%. The average mass dissolution between a solids loading of 5wt% and a solids loading of 10wt% is 3.29%. This shows that a higher solids loading provides a higher mass dissolution during the hydrothermal liquefaction process at every reaction time interval.

Figure 4-2 (b) shows the effects the solids loading has on the production of bio-oil. The results display that an increase in the solids loading provides an increase in the amount of bio-oil formed. The largest amount of bio-oil formed was 1.71g, which was produced from a solids loading of 10wt% and a reaction time of 30 minutes. The lowest amount of bio-oil formed was 1.20g, which was observed for a solids loading of 5wt% and a reaction time of 5 minutes. The amount of bio-oil produced for the solids loading of 5wt% ranges from 1.20g to 1.39g and the amount of bio-oil produced for the solids loading of 10wt% ranges from 1.47g to 1.71g. The average difference in the amount of bio-oil produced between the solids loading of 5wt% and the solids loading of 10wt% was 0.29g.

Figure 4-2 (c) shows the bio-oil yield produced from varying solids loadings. The bio-oil yield is observed to increase with an increase in the solids loading. The highest yield of 32.62% was produced for the solids loading of 10wt% and a reaction time of 30 minutes and the lowest yield of 22.82% was produced for a solids loading of 5wt% and a reaction time of 5 minutes. The bio-oil yield for the solids loading of 5wt% varies from 22.81% to 26.53% and the bio-oil yield for the solids loading of 10wt% ranges from 27.96% to 32.62%. The average difference in the bio-oil yield between the solids loading of 5wt% and 10wt% was 5.49%.

The increase in the solids loading produced more bio-oil due to the higher ratio of solids to water within the batch reactor. The limitation with altering the solids loading is that there needs to be enough water to completely submerge the solid algae to ensure that there is sufficient contact surface area for the water to fully permeate the algae to ensure liquefaction occurs.

4.4. Effect of temperature and pressure

The effect of altering the reaction conditions was examined on the hydrothermal liquefaction process to understand how it affects mass dissolution and bio-oil production. The reaction conditions were selected using the phase diagram of water (Appendix C, Figure C-1) to ensure that the water does not vaporise during the reaction process. This also assumes that the bio-oil content in the water does not significantly affect its phase behaviour. The first set of reactions conditions was a temperature of 250°C and a pressure of 4000 KPa (high reaction conditions) and the second set of reaction conditions were a temperature of 200°C and a pressure of 1500 KPa (low reaction conditions). The temperatures were also selected in the range where liquefaction is prominent, based on literature data. Both sets of reaction conditions were elected to ensure hydrothermal liquefaction of the macroalgae would occur and processing safety standards were maintained.

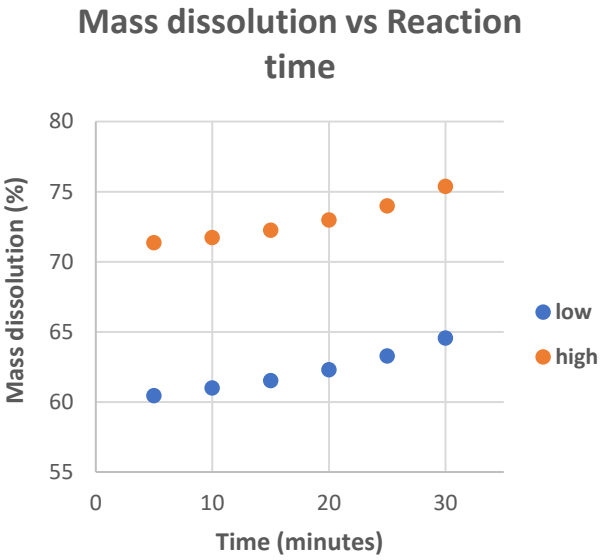

(a)

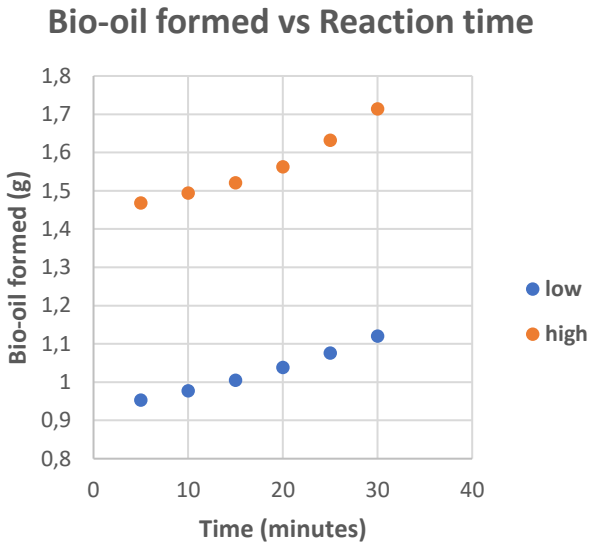

(b)

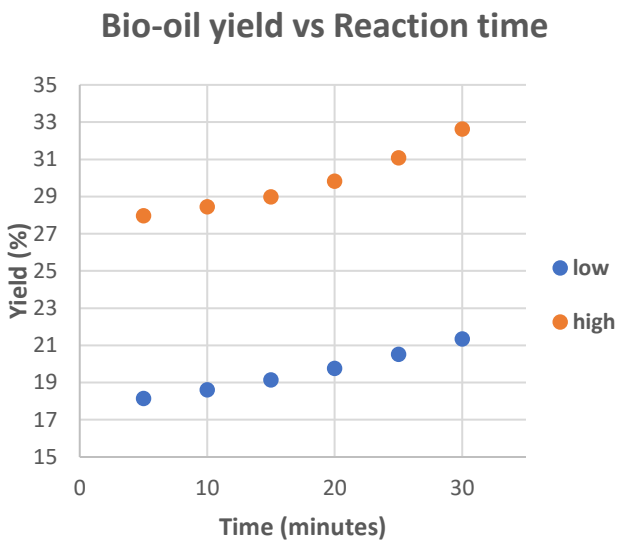

(c)

Figure 4-3: (a) Effect of reaction conditions (temperature and pressure) on the mass dissolution of marine macroalgae, (b) Effect of reaction conditions on the amount of bio-oil formed and (c) Effect of reaction conditions on the bio-oil yield obtained from hydrothermal liquefaction.

Figure 4-3 (a) reflects the trend of varying the reaction conditions on the mass dissolution of marine macroalgae. It was observed that an increase in the reaction conditions resulted in an increase in mass dissolution. The largest mass dissolution of 75.36% was observed for the higher reaction conditions at a reaction time of 30 minutes. The lowest mass dissolution of 60.44% was observed for the lower reaction conditions at a reaction time of 5 minutes. The mass dissolution for the lower reaction conditions ranges from 60.44% to 64.55% and the mass dissolution for the higher reaction conditions ranges from 71.37% to 75.37%. The average mass dissolution between the higher reaction conditions and lower reaction conditions is 10.77%. this indicates that an increase in the reaction temperature by 50°C and an increase in the reaction pressure by 2500 KPa results in a 10.77% increase in the mass dissolution.

Figure 4-3 (b) displays the results for altering the reaction conditions on the bio-oil production from marine macroalgae. It was observed that an increase in the reaction conditions increases the amount of bio-oil produced. The largest amount of bio-oil produced was 1.71g, which was produced from the higher reaction conditions at a reaction time of 30 minutes. The lowest amount of bio-oil produced was 0.95g, which was produced from the lower reaction conditions at a reaction time of 5 minutes. The quantity of bio-oil produced from the lower reaction conditions ranges from 1.95g to 1.12g and the quantity of bio-oil produced

from the higher reaction conditions ranges from 1.7g to 1.71g. The average difference in the amount of bio-oil formed from the low reaction conditions and high reaction conditions was 0.54g.

Figure 4-3 (c) depicts the bio-oil yield for low and high reaction conditions during specific time intervals. It is observed that the bio-oil yield increases with an increase in temperature and pressure. The largest bio-oil yield of 32.62% was obtained for the high reaction conditions, at a reaction time of 30 minutes. The lowest bio-oil yield was observed for the low reaction conditions, at a reaction time of 5 minutes. The bio-oil yield produced from the lower reaction conditions ranges from 18.14% to 21.35% and the bio-oil yield formed from the higher reaction conditions ranges from 27.96% to 32.62%. The average difference in the bio-oil yield between the low and high reaction conditions is 10.23%.

It is observed that the higher temperature increases the overall rate of dissolution and must be accompanied by an increase in pressure to maintain a liquid phase. This is the trade-off that has to be made in regard to process performance and process costs. This depicts that an increase in the reaction temperature by 50°C and an increase in the reaction pressure by 2500 KPa results in a 10.23% increase in the yield produced. The higher reaction conditions allow for a deeper and more throughout permeation of the algae and therefore a greater degree of removal of the bio-oil.

4.5. Effect of reaction time

The effect of varying reaction time on the hydrothermal liquefaction process was examined during this study. The reaction time was varied from 5 minutes to 30 minutes in steps of 5 minutes to get an accurate depiction of the dissolution of mass and formation of oil from the algae. The reaction time intervals were measured only when the desired reaction conditions were reached and maintained. It was observed that bio-oil was produced during the induction period (heat-up), therefore supplementary runs were conducted to determine the bio-oil formed during the induction period in steps of 5 minutes. The induction period may be defined as the period from the initial moment of heating to the stabilisation of the reaction conditions (temperature and pressure). The induction period was determined to be 60 minutes. The induction period

runs were conducted with a mass of 6g, a solids loading of 10wt%, and the higher reaction conditions of 250°C and 4000 KPa.

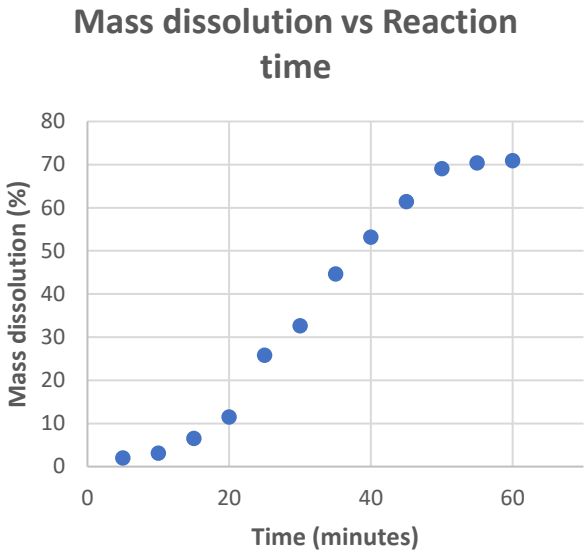

(a)

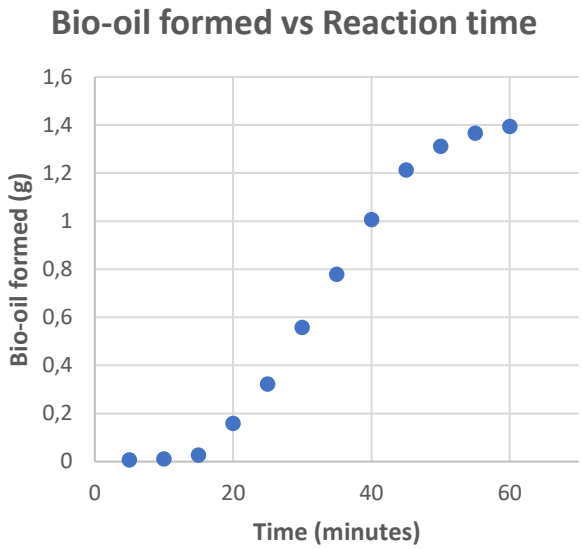

(b)

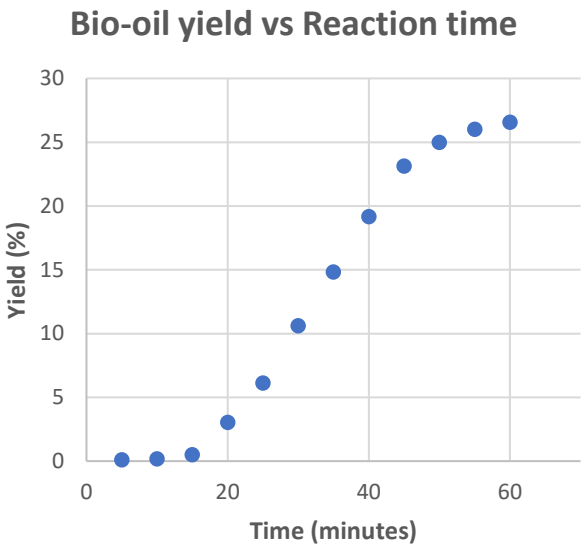

(c)

Figure 4-4: (a) Effect of reaction time on the mass dissolution during the Induction period, (b) Effect of reaction time on the amount of bio-oil formed during the Induction period and (c) Effect of reaction time on the bio-oil yield obtained during the Induction period.

Figure 4-4 (a) depicts the effect of reaction time on the mass dissolution during the induction period. The mass dissolution is seen to increase with an increase in the reaction time. There is a gradual increase between 5 minutes to 20 minutes with the mass dissolution ranging from 1.98% to 11.46%. This is followed by a sharp increase from 20 minutes to 50 minutes as the mass dissolution increases by approximately 9.59% per time interval to a mass dissolution of 68.99% at a time of 50 minutes. Between 50 minutes and 60 minutes, there is a gradual increase in the dissolution percentage with the mass dissolution increasing less than 2% between this time interval (from a mass dissolution of 68.99% to 70.87%). The gradual increase in the mass dissolution between 50 minutes to 60 minutes may be due to the small increase in temperature and pressure (from 229°C to 249°C and 3200 KPa to 3900 KPa, respectively). The sharp increase observed between 20 minutes to 50 minutes could be due to the heating rate between this time interval as the temperature and pressure increase from 137°C to 229°C and from 800 KPa to 3200 KPa, respectively.

The three distinct areas of the mass dissolution graph (figure 4-4 (a)) may be related to the physical mechanism of dissolution. During the initial stages, the hydrothermal solution will be acting on the dense outer layers of the biomass and hence the dissolution will be low. Once the hydrothermal solution has reached the main components of the biomass the dissolution rapidly increases. Eventually, the solid material that is easily accessible to the dissolution solvent is rapidly consumed, and then the denser material is left without significant change.

Figure 4-4 (b) shows the effects of reaction time on the production of bio-oil during the induction period. It is seen that there is an increase in the production of bio-oil with an increase in the reaction time. There is initially a gradual increase in the bio-oil formed between 5 minutes and 15 minutes. This could indicate that the initial heat up (below 15 minutes) provides ineffective formation of bio-oil due to the low temperatures and pressures. Between 15 minutes to 45 minutes, there exists an almost constant increase as the bio-oil formed increases approximately 0.2g per time interval (from 0.027g to 1.213g). There is a gradual decrease in the average increase of bio-oil production between 50 – 60 minutes (1.31g to 1.394g), compared to the 15 – 45 minutes interval. This gradual increase could be attributed to the slight increase in temperature and pressure between 50 minutes and 60 minutes compared to the sharp increase in temperature and pressure between 15minutes and 45 minutes (104°C to 220°C and 500 KPa to 2700 KPa).

The effect of reaction time on the bio-oil yield during the induction period is shown in figure 4-4 (c). From the graph, it is observed that the bio-oil yield increases as the reaction time increases. There is initially a small increase in the bio-oil yield between 5 minutes to 15 minutes, with the yield ranging from 0.01% to 0.5%. Between 15 minutes and 45 minutes, there exists a sharp increase as the bio-oil yield rises to 23.13%, with an average increase of approximately 3.77% between each time interval. Between 45 minutes to 60 minutes, the average increase is lower than the time interval of 15 minutes to 45 minutes, as the bio-oil yield increases from 23.13% to 26.58%. The low initial bio-oil yield may be due to the low temperatures and pressures as the reaction conditions were not sufficient to induce adequate hydrothermal liquefaction. The sharp increase between 15 minutes and 45 minutes may be noted to be due to the high heating rate and pressure increase present within this reaction time interval. The gradual increase between 45 minutes to 60 minutes is due to the gradual temperature and pressure increase from 220°C to 249°C and 2700 KPa to 3900 KPa respectively.

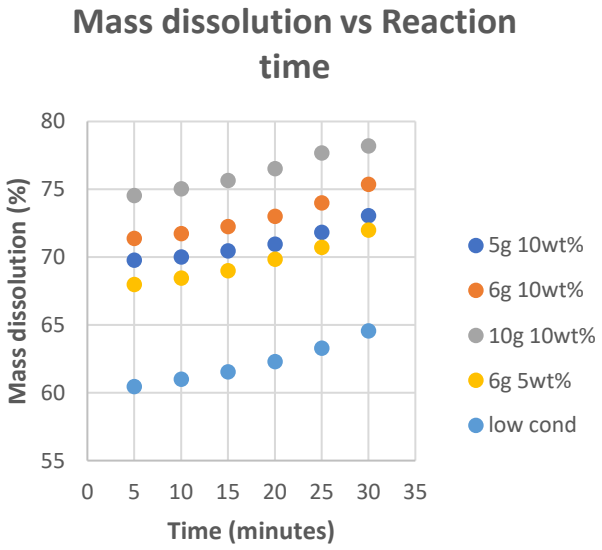

(a)

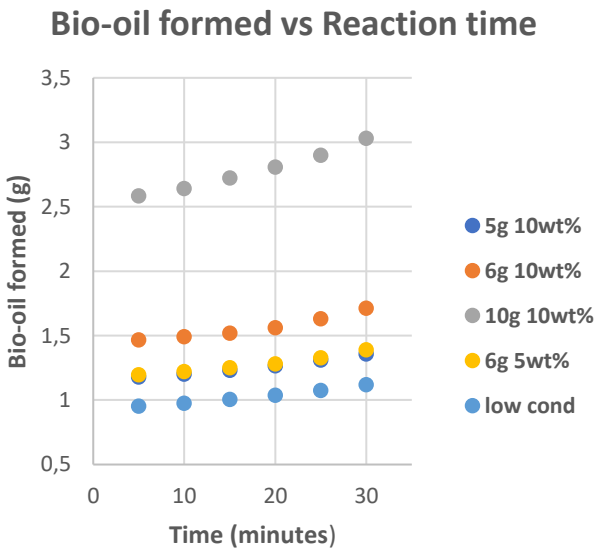

(b)

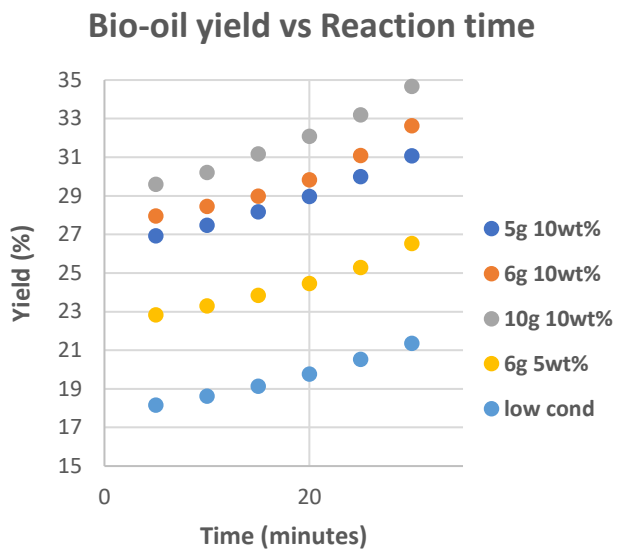

(c)

Figure 4-5: (a) Effect of reaction time on the mass dissolution, (b) Effect of reaction time on the amount of bio-oil formed and (c) Effect of reaction time on the bio-oil yield obtained from hydrothermal liquefaction.

The reaction time graphs show the effects of all the process variables compared to each other to give us an overall view of the best and worst results for the hydrothermal liquefaction process. Figure 4-5 (a) displays the mass dissolution for varying reaction times. It is observed that for all the process variables, the mass dissolution increased with an increase in the reaction time. The 10g 10wt% condition provided the highest dissolution at every reaction time interval, with the highest dissolution of 78.18% observed at the 30-minute interval. The low reaction conditions of 200°C and 1500 KPa provided the lowest dissolution at every time interval, with the lowest mass dissolution of 60.44% being observed for the 5-minute interval. The difference in the mass dissolution between each time interval ranges from 0.24% to 1.23% for a mass of 5g, 0.36% to 1.37% for a mass of 6g, 0.48% to 1.16% for a mass of 10g, 0.47% to 1.27% for a solids loading of 5wt% and from 0.55% to 1.26% for the low reaction conditions.

Figure 4-5 (b) shows the effects of reaction time on the production of bio-oil from macroalgae. The graph of the bio-oil formed against the reaction times for the stabilised hydrothermal liquefaction process displays an increase in the amount of bio-oil formed for an increase in reaction time. At each interval, the amount of bio-oil formed increases for every manipulation of the process variables. The 10g 10wt% reaction set provided the highest amount of bio-oil at every time interval and the largest amount of bio-oil of 3.03g was formed for the 10g 10wt% high reaction conditions run, at a reaction time of 30 minutes. the 6g 10wt% low reaction set provided the lowest amount of bio-oil at every time interval and the lowest amount of bio-oil

of 0.95g was produced for the 6g 10wt%, low reaction conditions run, at a time of 5 minutes. The difference in the amount of bio-oil produced between each time interval ranges from 0.024g to 0.047g for a mass of 5g, from 0.026g to 0.082g for a mass of 6g, from 0.057g to 0.131g for a mass of 10g, from 0.025g to 0.064g for a solids loading of 5wt% and from 0.024g to 0.044g for the low reaction conditions.

Figure 4-5 (c) displays the effects of reaction time on the bio-oil yield obtained from the hydrothermal liquefaction of macroalgae. It is observed that the bio-oil yield increases for an increase in the reaction time for every variation of the process variables. The 10g 10wt% reaction set provided the highest bio-oil yield for every time interval, with the highest bio-oil yield of 34.67% formed for a reaction time of 30 minutes. The low reaction condition (at a mass of 6g 10wt%) provided the lowest bio-oil yield at every time interval, with the lowest yield of 18.14% observed for a reaction time of 5 minutes. The difference in the bio-oil yield obtained between each time interval ranges from 0.56% to 1.08% for a mass of 5g, from 0.49% to 1.54% for a mass of 6g, from 0.62% to 1.47% for a mass of 10g, from 0.47% to 1.24% for a solids loading of 5wt% and from 0.47% to 0.83% for the low reaction conditions. The results obtained indicate that the bio-oil formed should continually increase as time increases, however, the limitation is that there exists a finite amount of oil in the macroalgae.

4.6. Comparison of Bio-oil Yield obtained from the Hydrothermal Liquefaction of Macroalgae

Studies have been conducted on the hydrothermal liquefaction of the various types of macroalgae. A comparative analysis allows the determination of how well the process performed compared to other types of algae and process conditions.

Table 4-2: Comparative analysis of maximum bio-oil yields formed from hydrothermal liquefaction

Reaction conditions	Bio-oil yield	Additional comments	Reference
A temperature of 250°C and a pressure of 4000 KPa, with a reaction time of 30 minutes (this study).	34.67% (dry basis)	The type of algae used was *Euklonia Maxima*, with a mass loading of 10g.	-[1]
A temperature of 350°C and a reaction time of 15 minutes.	19.3% (dry ash free)	The type of algae used was *L. saccharina*.	(Anastasakis and Ross, 2011)
A temperature of 340°C and a reaction time of 15 minutes.	32.1%	The type of algae used was *Sargassum*.	(Li et al., 2012)

[1] No reference in this row as these are the results for this study

Reaction temperatures ranging from 220°C to 320°C.	23.0% (dry basis)	-	(Zhou et al., 2010)
A temperature of 300°C and a solids loading of 10%.	47.5%	The type of algae used was *Nannochloropsis sp*.	(Reddy et al., 2016)
A temperature of 300°C and a solids loading of 10%.	32.5%	The type of algae used was *Chlorella sp*.	(Reddy et al., 2016)
A temperature of 350°C and a reaction time of 15 minutes.	79% (dry basis)	The type of algae used was *L. saccharina* and a heating rate of 585°C /minute was utilised.	(Bach et al., 2014)

Considering the variation in mass, solids loading and reaction temperature, and pressure, the maximum yield of 34.67% obtained from this study is satisfactory compared to the other studies and a sufficient amount of bio-oil is produced to recommend up-scaling the process for biofuel production. The bio-oil yield of 34.67% is comparatively amongst the average yields obtained from research in this field, while utilising a lower reaction temperature and slightly higher reaction time, thereby requiring less energy for the process. The highest yield of 79% obtained by Bach et al. (2014) is an outlier compared to other research in this field and may be due to the high heating rate of 585°C/minute. Not considering the outlier, the yield of 34.67% is the second highest yield of this comparative analysis and further validates the purpose of this study. The implications of this mean that enough bio-oil is formed to allow for further processing into a cleaner biofuel product, and further validates the feasibility of scale-up of this process, as enough biofuel would be produced to reduce some of the demands placed on fossil fuels.

4.7. Qualitative analysis of the crude bio-oil

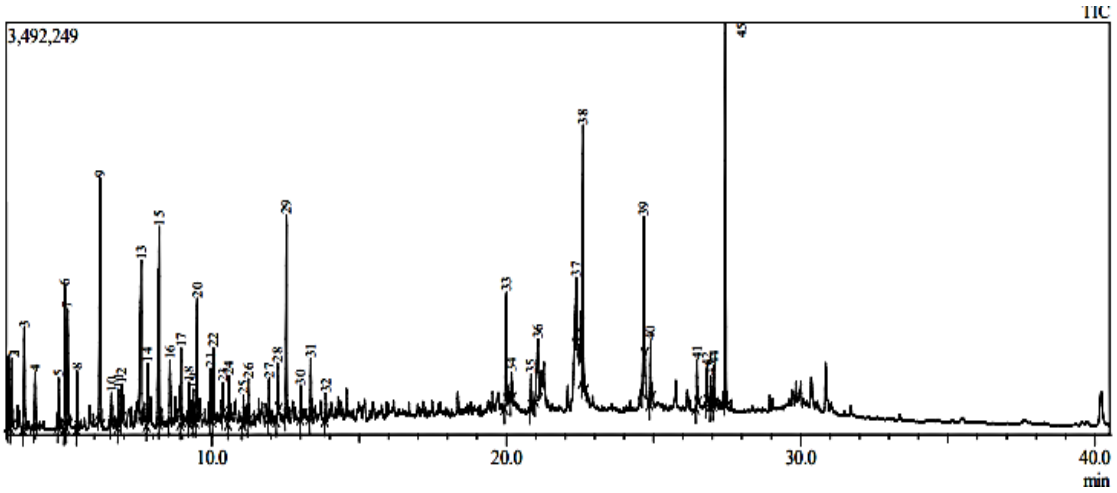

Figure 4-6: Gas Chromatograph-Mass Spectrometry graph obtained for the bio-oil obtained following the hydrothermal liquefaction process for a mass of 6g, high reaction conditions, a solids loading of 10wt%, and a reaction time of 30 minutes.

GCMS analysis was carried out to determine the composition of the bio-oil. A solvent cut time of 3 minutes was implemented to ensure the solvent was not shown in the results. The split ratio was selected to ensure that there were no tail-ending peaks present during analysis. GCMS analysis was conducted for every run, with major focus on the main peaks. As seen in Appendix D, Table D-12, a variety of components were formed during the hydrothermal liquefaction of marine macroalgae. These components include acids, esters, ketones, alkanes, alkenes, aldehydes, phenols, and cyclic compounds. The main compound that was formed for most runs during hydrothermal liquefaction processing was hexanedioic acid (adipic acid). This is a precursor to the production of nylon polymers. The high quantity of hexandioic acid could possibly be due to the plastic pollution of oceans which contaminates macroalgae sources within oceans (Hongthong et al., 2021). Other main components include hexadecanoic acid, 2-cyclopentene-1-one, propanoic acid, cyclohexane, etanone, butanone, phenol, 2-furancarboxaldehyde, octadecanoic acid, hexanedioic acid- bis (2-ethyhexyl) ester, tetrapentacontane, palmitoleic acid. The components that are produced during hydrothermal liquefaction may be further processed using techniques such as esterification and hydrocracking to form biofuels such as biodiesel and other valuable chemicals that may be used in the production of food additives, solvents, thermoplastics, and pharmaceutical medication. This concluded that the bio-oil formed from the hydrothermal liquefaction of marine macroalgae may be further processed and refined to produce biofuel.

4.8. Kinetic model development and identification

The hydrothermal liquefaction of *Euklonia Maxima* at high temperatures and pressures proceeds via the breakdown of the seaweed into a bio-oil phase, aqueous phase, and the remaining solid fraction. The development of the model needs to accurately correlate the effects of the change in time and temperature on the product yield fractions obtained from hydrothermal liquefaction. The reaction network used in this study was developed by modifying the reaction network depicted by Valdez et al. (2014). The reaction network used by Valdez et al. (2014) incorporated the biochemical composition of the seaweed and treated each pathway as a first order reaction.

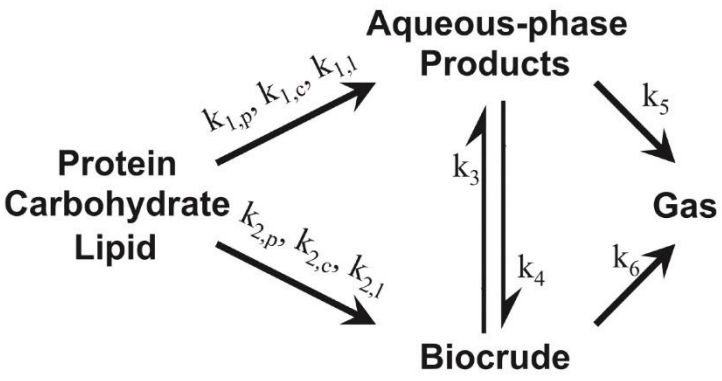

Figure 4-7: Hydrothermal liquefaction reaction network incorporating biochemical content (Valdez et al., 2014).

The breakdown of the seaweed molecules into the subcomponents requires a large amount of energy, hence, the very high reaction temperature used to obtain bio-oil conversion. According to Valdez et al. (2014), the seaweed may undergo decomposition reactions to simultaneously form an aqueous product and a bio-crude product with interphase transfer between the bio-crude and aqueous phases. The bio-crude and aqueous phase may also be converted further to a gaseous product. Valdez et al. (2013) displayed similar product yield graphs to the results obtained in this study and stated that the amount of gas produced during the hydrothermal liquefaction process was negligible. Biochemical analysis of the marine macroalgae was not determined and all components of the algae were analysed together. Various assumptions and modifications were applied to the reaction system developed by Valdez et al. (2014) to develop the reaction system used for the kinetic modeling; these were:

Assumptions:

The interphase transfer between the bio-oil and aqueous phase was neglected.
The mass fraction of the aqueous solution was assumed to be the difference between the initial solids fraction and the combined mass fraction of the remaining solids and bio-oil formed.
Modifications:

The production of gas phase products was neglected. (Valdez et al, 2013)
The lipids, proteins, and carbohydrates were lumped together in the analysis of all reactants (solids biomass) and products (bio-oil, aqueous solution, and remaining solid biomass).
The modified reaction pathway utilized for the development of the kinetic model was:

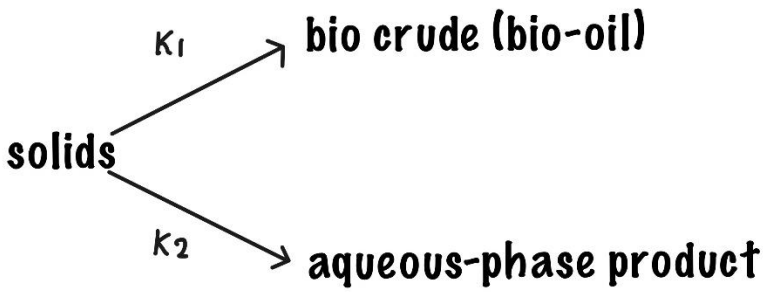

Figure 4-8: Simplified hydrothermal liquefaction reaction pathway

Where k_1 represents the kinetic rate constant for the conversion from solids to a bio-oil product and k_2 represents the kinetic rate constants for the conversion from solids to an aqueous phase product.

A variety of reaction orders were tested and examined to determine which reaction order most fit the experimental data obtained. It was determined that a first order reaction best fit the data obtained and hence, each reaction pathway is treated as a first order reaction. Therefore, the reactions occurring are:

$$Solids \rightarrow Bio-oil\text{: } r_1 = k_1 w_s \qquad \text{Equation 4-1}$$

$$Solids \rightarrow Aqueous-phase\ product\text{: } r_2 = k_2 w_s \qquad \text{Equation 4-2}$$

Where w_s represents the initial mass fraction of the solids in the reaction vessel.

It was observed that there were three distinct regions of dissolution over the 90-minute period, which was regarded as the saturation of the biomass dissolution with time. Inhibition constants (k_3 and k_4) were introduced to each reaction rate expression to account for the observed saturation of the mass dissolution with time. Combining the material balances of the batch reactor with the reaction pathways and considering the inhibition constants and the effect it has on the reaction rates, the following reaction rate expressions were developed:

$$Solids \rightarrow Bio-oil\text{: } r_1 = k_1 \times w_s \times exp\left(-\frac{k_3}{w_s}\right) \qquad \text{Equation 4-3}$$

$$Solids \rightarrow Aqueous-phase\ product\text{: } r_2 = k_2 \times w_s \times exp\left(-\frac{k_4}{w_s}\right) \qquad \text{Equation 4-4}$$

The dynamic models to predict the mass dissolution of the solid seaweed and the production of the bio-oil and aqueous-phase solution may be simplified using the differential mass balance over the reaction system for each component.

$$\text{Change in Solids: } \frac{dx_s}{dt} = -r_1 - r_2 = -(k_1 + k_2) w_s exp\left(-\frac{k_3 + k_4}{w_s}\right) \quad \text{Equation 4-5}$$

$$\text{Change in Bio} - \text{oil: } \frac{dx_o}{dt} = r_1 = k_1 w_s exp\left(-\frac{k_3}{w_s}\right) \quad \text{Equation 4-6}$$

$$\text{Change in Aqueous} - \text{phase product: } \frac{dx_A}{dt} = r_2 = k_2 w_s exp\left(-\frac{k_4}{w_s}\right) \quad \text{Equation 4-7}$$

The ordinary differential equations above were solved using the initial product fractions (Appendix A, Table A-8) and final product yield fractions (Appendix A, Table A-9) while simultaneously estimating the value of the kinetic rate constants (k_1 and k_2) and the inhibition constants (k_3 and k_4) at various temperatures (Appendix A, Table A-5) along the reaction path. The estimation was determined by minimising the least square error between the experimental data obtained and the calculated data points for each product fraction yield at each reaction time for every species (Valdez et al., 2014) while utilising the ode15s variable-step, variable- order solver to produce the predicted values. The estimated kinetic reaction rates are shown in Table 4-3.

Table 4-3: Estimated kinetic reaction rates

Kinetic rate constant	**Value [g/g/s]**
k_1	0.0059
k_2	0.0103

The reaction rate for the production of bio-oil from the macroalgae was determined to be 0.0059 g/g/s and the reaction rate for the production of the aqueous-phase product from macroalgae was determined to be 0.0103 g/g/s. It was observed that the production of the aqueous product possessed a higher reaction rate than the production of bio-oil for the hydrothermal liquefaction process. The estimated inhibition constants are shown in Table 4-4.

Table 4-4: Estimated inhibition constants

Inhibition constant	**Value**
k_3	4.44e-14
k_4	4.44e-14

It was observed that initially, the inhibition constants for the production of bio-oil and the production of the aqueous product were very close. It was decided to lump both terms into one overall inhibition constant.

Therefore, both inhibition constants were determined to be 4.44e-14. The small value of the inhibition constant does not significantly impact the overall reaction rate for both reactions and the reactions mainly depend on the driving force of the reaction.

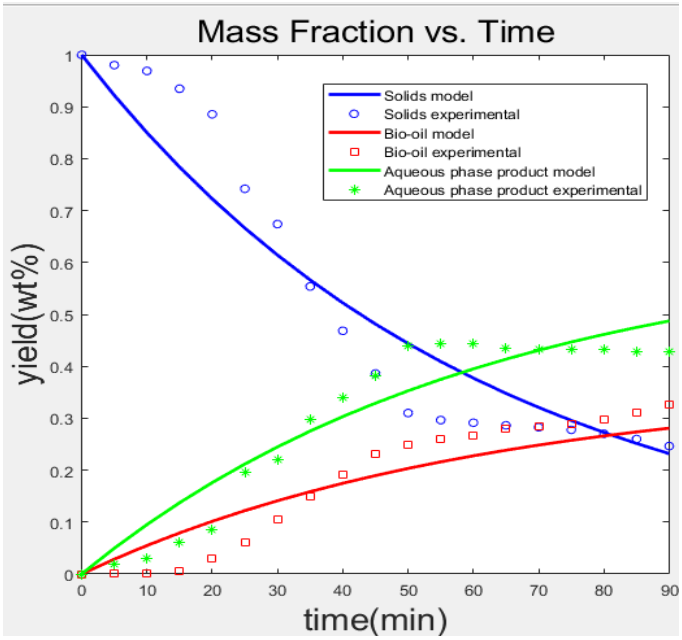

Figure 4-9: Yield fraction plot produced on MATLAB for a mass loading of 6g, a solids loading of 10wt%, reaction temperatures ranging from 0°C to 250°C, and reaction pressures ranging from 0KPa to 4000KPa.

The product yield fraction plot shows how accurately the estimated data from the model compares to the actual experimental data obtained. The experimental data is shown by discrete points and the estimated data is shown by continuous lines. It was observed that the models are fairly accurate as they observed the general trends for dissolution of the macroalgae and the production of the aqueous-phase product and the bio-oil.

Parity plot

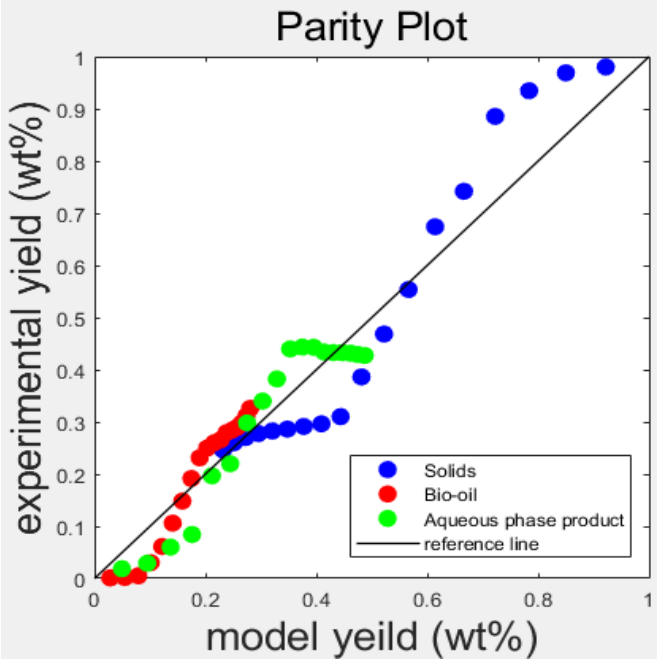

Figure 4-10: Parity plot developed on MATLAB

A parity plot was done to further validate the accuracy of the kinetic model. A parity plot compares the experimental data to the actual data. A line with a slope of 1 may be added as a reference and is referred to as the line of parity. The clustering of data points close to the line of parity verifies whether the model was satisfactory at estimating the product fraction yields and how well it correlates to the experimental data. It was observed that the data points for the production of bio-oil are clustered close to the line of parity indicating a good agreement between the experimental yield and model yield. The data points for the production of the aqueous-phase product were also clustered close to the line of parity, however, the experimental yield seems to decrease slightly towards the end which may indicate deviation in the theoretical data. The data points for the mass dissolution of the macroalgae (solids) were the least clustered to the reference line, however, all were fairly closely clustered to the line of parity and spread evenly around the reference line.

CHAPTER 5: CONCLUSION

The main aim of this study was to examine the effect of process variables on the performance of the hydrothermal liquefaction of marine macroalgae and to determine kinetic parameters of dissolution. The following conclusions were established based on the research conducted and the objectives set:

Bio-oil was produced for every run conducted and of every variation of the process variables, with bio-oil yields ranging from 18.14% to 34.67%. Bio-oil was also formed during the induction period (for 6g 10wt%) at every time interval with bio-oil yields ranging from 0.11% to 26.58% for the induction period.

The largest bio-oil yield obtained was for the 10g 10wt% run at the high process conditions (a temperature of 250°C and a pressure of 4000 KPa) and a reaction time of 30 minutes, with a bio-oil yield of 34.67%. This high bio-oil yield was due to the high reaction and process conditions. The high reaction temperature accelerates the dissolution resulting in more bio-oil being removed from the seaweed. Increasing the mass of seaweed used and increasing the solids loading both increased the driving force for the dissolution of the seaweed. This results in a higher mass lost and more bio-oil being produced. The longer reaction time allowed for more contact time between the seaweed and water under the desired reaction conditions resulting in a fuller dissolution occurring. According to this study, these conditions allow for the potential for large-scale processes to be pursued, as it allows the processing of more biomass per batch (up to a 10wt% solids loading) without encountering any problems with mixing.

The assessment of the quality of the bio-oil formed was another objective of this study. The bio-oil produced from the hydrothermal liquefaction process underwent Gas Chromatograph-Mass Spectrometry analysis to determine its composition. The main component (component with the highest area) formed for every run conducted was determined to be hexanedioic acid (adipic acid). This is a precursor to the production of nylon polymers. The high presence of hexandioic acid may be due to the plastic pollution of oceans, and therefore the contamination of macroalgae sources within the ocean. The other main components formed from the hydrothermal liquefaction process were cyclohexane, propanoic acid, hexadecenoic acid, etanone, phenol, cyclopentene, octadecanoic acid, butanone, palmitoleic acid, tetrapentacontane, and hexanedioic acid- bis (2-ethyhexyl) ester. The products formed from the hydrothermal liquefaction of brown macroalgae are precursors to biofuels and may be further processed through methods such as hydrocracking and esterification to produced valuable chemical products and biofuels (e.g., biodiesel). This implies that the biofuels may be produced from the bio-oil obtained from the hydrothermal liquefaction of marine macroalgae.

A simplified kinetic model of the liquefaction process was developed, based on the rigorous model of Valdez et al. (2014). The kinetic parameters were identified based on the experimental observations. The basic kinetic model was modified to account for the saturation of the biomass dissolution with time. An inhibition term was added to each of the reaction rate expressions. The kinetic rates of reaction determined from the MATLAB code were found to be 0.0059 g/g/s for k_1 and 0.0103 g/g/s for k_2. The inhibition constants were calculated to be 4.44e-14 for k_3 and 4.44e-14 for k_4. The kinetic parameters obtained were able to satisfactory capture the change in solids, bio-oil, and aqueous phase products. The model and experimental observations showed that the rate of production of the aqueous product is higher than that of the bio-oil, at the specific conditions used. The model could be used for preliminary simulation and scale-up of the process.

The overall results of this work validate that the hydrothermal liquefaction of marine algae produces an adequate amount of bio-oil that may be further processed to produce a cleaner biofuel product. It was determined that higher process conditions resulted in higher bio-oil yields being obtained and that a kinetic model may be determined for the bio-oil yield formed and mass dissolution from the algae to aid in further development of research in this section. The maximum bio-oil yield of 34.67% obtained in this report was amongst the higher yield results for research in this section and required an overall lower amount of energy as it used a lower reaction temperature and slightly higher reaction time. The results of this work imply that enough bio-oil is formed from this process to allow for the feasibility of scale-up of the process to produce a biofuel that would reduce the increasing demands placed on fossil fuels and provide a cleaner source of fuel that does not significantly harm the environment.

CHAPTER 6: RECOMMENDATIONS

Based on the research conducted and the results obtained in this dissertation, the following recommendations should be considered to expand on and enhance the study:

- Scale-up studies can be conducted using a large reaction vessel and with higher solids loadings to determine the saturation value, i.e., the maximum solids loading beyond which no increase in dissolution is observed.

- Using an alternative solvent (reaction medium) such as an alcohol-water mixture, compared to water alone during the hydrothermal liquefaction process may produce higher bio-oil yields. According to Brand et al. (2014), supercritical alcohols provide a more adequate solubility of the organic intermediates, higher bio-oil yields, and an easier separation as a result of the low boiling point and hydrogen donor properties.

References

Abbasi, T. and Abbasi S. A. 2010. Biomass energy and the environmental impacts associated with its production and utilization. *Renewable and Sustainable Energy Reviews*, 14(3), 919-937.

Akhtar, J. and Amin, N. A. S. 2011. A review on process conditions for optimum bio-oil yield in hydrothermal liquefaction of biomass. *Renewable and Sustainable Energy Reviews*. 15(3), 1615-1624.

Alfke, G., Irion, W. W. and Neuwirth, O. S. 2008. Oil Refining. In *Handbook of Fuels: Energy Sources for Transportation*; Elvers, B., Ed.; Wiley-VCH: Weinheim, Germany.

American Scientist. 2020. *The Science of Seaweeds*. https://www.americanscientist.org/article/the-science-of-seaweeds. Date of access: 16 November 2020

Anto, S., Mukherjee, S. S., Muthappa, R., Mathimani, T., Deviram, G., Kumar, S. S., Verma, T. N., and Pugazhendhi, A. 2019. Algae as a green energy reserve: Technological outlook on biofuel production. *Chemosphere*, 125079.

Ask nature. 2020. *Biofilm-inhibiting Chemical Protects Surfaces*. https://asknature.org/strategy/biofilm-inhibiting-chemical-protects-surfaces/ Date of access: 18 November 2020

Azizi, K., Moraveji, M. K. and Najafabadi, H. A. 2018. A review on bio-fuel production from microalgal biomass by using pyrolysis method. *Renewable and Sustainable Energy Reviews*, 82, 3046-3059.

Balat, M., Balat, M., Elif, K. and Balat, H. 2009. Main routes for the thermo-conversion of biomass into fuels and chemicals, Part 2: gasification systems. *Energy Conversion and Management*, 50, 3158-3168.

Barreiro, D. L., Reide, S., Hornung, U., Kruse, A. and Prins, W. 2015. Hydrothermal liquefaction of microalgae: Effect on the product yields of the addition of an organic solvent to separate the aqueous phase and the biocrude oil. *Algal Research*, 12, 206-212.

Beims, R. F., Hu, Y., Shui, H., Xu, C. (C.). 2020. Hydrothermal liquefaction of biomass to fuels and value-added chemicals: Products applications and challenges to develop large-scale operations. *Biomass and Bioenergy*, 135, 105510.

Bharathiraja, B., Chakravarthy, M., Kumar, R. R., Yogendran, D., Yuvaraj, D., Jayamuthunagai, J., Kumar, R. P. and Palani, S. 2015. Aquatic biomass (algae) as a future feed stock for bio-refineries: A review on cultivation, processing and products. *Renewable and Sustainable Energy Reviews*, 47, 634–653.

Biller, P., Ross, A. B., Skill, S. C., Lea-Langton, A., Balasundaram, B., Hall, C., Riley, R., and Llewellyn, C. A., 2012. Nutrient recycling of aqueous phase for microalgae cultivation from the hydrothermal liquefaction process. *Algal Research*, 1, 70–76.

Bobin-Dubigeon, C., Lahaye, M., Guillon, F., Barry, J. L. and Gallant, D. J. 1997. Factors limiting the biodegradation of Ulva sp. Cell-wall polysaccharides. *Journal of the Science of Food and Agriculture*, 75, 341-351.

Bonechi, C., Donati, M., Leone, G., Magnani, A., Tamasi, G. and Rossi, C. 2017. Biomass: An overview. *Bioenergy Systems of the Future*, 3-42.

Bridgwater, A. 1990. A survey of thermochemical biomass processing activities. *Biomass*, 22, 279-292.

Bridgwater, A. V., Meier, D. and Radlein, D. 1999. An overview of fast pyrolysis of biomass. *Organic Geochemistry*, 30, 1479 – 1493.

Bühler, W., Dinjus, E., Ederer, H. J. Kruse, A. and Mas, C. 2002. Ionic reactions and pyrolysis of glycerol as competing reaction pathways in near- and supercritical water. *The Journal of Supercritical Fluids*, 22, 37-53.

CarbonBrief. 2018. *The Carbon Brief Profile: South Africa*. https://www.carbonbrief.org/the-carbon-brief-profile-south-africa Date of access: 14 December 2020

Chapman, R. L. 2010. Algae: the world's most important "plants"- an introduction. *Mitigation and Adaption Strategies for Global Change*, 18(1), 5-12.

Chen, H., Zhou, D., Luo, G., Zhang, S., and Chen, J. 2015a. Macroalgae for biofuels production: progress and perspectives. *Renewable and Sustainable Energy Reviews*, 47, 427-437

Chen, W.-H., Lin, B.-J., Huang, M.-Y. and Chang, J.-S. 2015b. Thermochemical conversion of microalgal biomass into biofuels: a review. *Bioresource Technology*, 184, 314-327.

Cheng, F., Bayat, H., Umakanta, J., and Brewer, C. E. 2020. Impact of feedstock composition on pyrolysis of low-cost, protein- and lignin-rich biomass: A review. *Journal of Analytical and Applied Pyrolysis*, 147, 104780

David T. A., Volesky, B. and Mucci, A. 2003. A review of the biochemistry of heavy metal biosorption by brown algae. *Water Research*, 37(18), 0-4430

Delmer, D. P. and Amor, Y. 1995. Cellulose biosynthesis. *THE PLANT CELL ONLINE*, 7, 987-1000.

Deng, H., Meredith, W., Uguna, C. N. and Snape, C. E. 2015. Impact of solvent type and condition on biomass liquefaction to produce heavy oils in high yield with low oxygen contents. *Journal of Analytical and Applied Pyrolysis*, 113, 340-348.

Deniaud-Bouet, E., Kervarec, N., Michel, G., Tonon, T., Kloareg, B and Herve, C. 2014. Chemical and enzymatic fractionation of cell walls from Fucales: Insights into the structure of the extracellular matrix of brown algae. *Annals of Botany*, 114, 1203-1216.

Djandja, O. S., Wang, Z., Chen, L., Wang, F., Xu, Y. -P. and Duan, P. -G. 2020. Progress in Hydrothermal Liquefaction of Algal Biomass and Hydrothermal Upgrading of the Subsequent Crude bio-oil: A Mini Review. *Energy & Fuels*, 1-69.

Dote, Y., Sawayama, S., Inoue, S., Minowa, T., Yokoyama, S. 1994. Recovery of liquid fuel from hydrocarbon-rich microalgae by thermochemical liquefaction. *Fuel*, 73, 1855-1857.

Duan, P. and Savage, P.E. 2010. Hydrothermal liquefaction of a microalga with heterogeneous catalysts. *Industrial and Engineering Chemical Research*, 50(1), 52-61.

Elliot, D. (2011). In *Thermochemical processing of biomass*. John Wiley and Sons Ltd, Chichester, UK.

Elliot, D. C., Biller, P., Ross, A. B., Schmidt, A. J. and Jones, S. B. 2015. Hydrothermal liquefaction of biomass: Developments from batch to continuous process. *Bioresource Technology*, 178, 147-156.

Office of Energy Efficiency and Renewable Energy. 2020. *Biomass Resources*. https://www.energy.gov/eere/bioenergy/biomass-resources Date of access: 10 December 2020.

EESI (Environmental and Energy Study Institute). 2020. *Bioenergy (Biofuels and Biomass)*. https://www.eesi.org/topics/bioenergy-biofuels-biomass/description Date of access: 19 November 2020

Evans, G. and Smith, C. 2012. Biomass to Liquids Technology. *Comprehensive renewable energy*, 5, 156-183.

Farrell, A. E. and Gopal, A. R. 2008. Bioenergy research needs for heat, electricity, and liquid fuels. MRS Bulletin, 33, 373–380.

Faeth, J. L., Valdez, P. J. and Savage, P. E. 2013. Fast Hydrothermal Liquefaction of Nannochloropsis sp. to Produce Biocrude, *Energy and Fuels*, 27, 1391–1398.

Feiner, G. 2006. Definitions of terms used in meat science and technology. *Meat Products Handbook*, 46-76.

Gollakota, A. R. K., Kawale, H. D., Kishore, N. and Gu, S. 2018. A Review on Hydrothermal Liquefaction of Biomass. *Renewable and Sustainable Energy Reviews*, 81, 1378 – 1392

Guo, Z., Wang, S., Gu, Y., Xu, G., Li, X. and Luo, Z. 2010. Separation characteristics of biomass pyrolysis oil in molecular distillation, *Separation and Purification Technology*, 76, 52-57.

Gu, X., Martinez-Fernandez, J. S., Pang, N., Fu, X., and Chen, S. 2020. Recent development of hydrothermal liquefaction for algal biorefinery. *Renewable and Sustainable Energy Reviews*, 121, 109707.

Gust, D., Kramer, D., Moore, A., Moore, T. A. and Vermaas, W. 2008. Engineered and Artificial Photosynthesis: Human Ingenuity Enters the Game. MRS Bulletin, 33, 383–387.

Han Y., Hoekman, S., Cui, Z., Jena, U. and Das, P. 2019. Hydrothermal liquefaction of marine microalgae biomass using co-solvents. *Algal Research*, 38, 101412

Harmsen, P., Huijgen, W., Bermudez, L., and Bakker, R. 2010. Literature Review of the Physical and Chemical Pretreatment Processes for Lignocellulosic Biomass, 1st ed.; Wageningen UR Food & Biobased Research: Wageningen, The Netherlands, 6–30.

Hirel, B., Tétu, T., Lea, P. J. and Dubois, F. 2011. Improving Nitrogen Use Efficiency in Crops for Sustainable Agriculture. *Sustainability*, 3(9), 1452-1485

Hoekman, S. K. 2009. Biofuels in the U.S. – Challenges and Opportunities. *Renewable Energy*, 34(1), 14-22.

Hongthong, S., Leese, H. S., Allen, M. J. and Chuck, C. J. 2021. Assessing the Conversion of Various Nylon Polymers in the Hydrothermal Liquefaction of Macroalgae. *Environments*, 8, 1-17

Hu, J., Yu, F., and Lu, H. 2012. Application of Fischer-Tropsch Synthesis in Biomass to Liquid Conversion. *Catalysts*, 2, 303-326.

Huber, G. W., Iborra, S. and Corma, A. 2006. Synthesis of transportation fuels from biomass: Chemistry, catalysts, and engineering. *Chemical Reviews*, 106, 4044-4098.

Hurd, C. L., Harrison, P. J., Bischof, K. and Lobban, C. S. 2014. Seaweed Ecology and Physiology, 2nd ed.; Cambridge University Press: Cambridge, UK; ISBN 0521145953

Kloareg, B. and Quatrano, R. S. 1988. Structure of the cell walls of marine algae and ecophysiological functions of the matrix polysaccharides, Oceanography and Marine Biology: *An Annual Review*, 26, 259-315.

Krammer, P. and Vogel, H. 2000. Hydrolysis of esters in subcritical and supercritical water. *Journal of Supercritical Fluids*, 16, 189 – 206.

Kreith, F. and Goswami, D. Y. 2007. In *Handbook of energy efficiency and renewable energy*. Taylor and Francis, Boca Raton, Florida.

Kumar, S. and Gupta, R. B. 2008. Hydrolysis of microcrystalline cellulose in subcritical and supercritical water in a continuous flow reactor. *Industrial and Engineering Chemical Research*, 47, 9321-9329.

Little, A. D. 2000. Study into the Potential Impact of Changes in Technology on the Development of Air Transport in the UK. Final report for department of the environment transport and regions (DETR), Cambridge.

Lozano, F. J., and Lozano, R. 2018. Assessing the potential sustainability benefits of agricultural residues; Biomass conversion to syngas for energy generation or to chemicals production. *Journal of Cleaner Production*, 172, 4162-4169.

Mahmoudi, H., Mahmoudi, M., Doustdar, O., Jahangiri, H., Tsolakis, A., Gu, S., and LechWyszynski, M. 2017. A review of Fischer Tropsch synthesis process, mechanism, surface chemistry and catalyst formulation. *Biofuels Engineering*, 2, 11-31.

Maneein, S., Milledge, J. J., Nielsen, B. V. and Harvey, P. J. 2018. A Review of Seaweed Pre-Treatment Methods for Enhanced Biofuel Production by Anaerobic Digestion or Fermentation. *Fermentation*, 1-31

Melero, J. A., Garcia, A. and Iglesias, J. 2011. Biomass catalysts in conventional refineries. In *Advances in Clean Hydrocarbon Fuel Processing*; Khan, M. R., Ed.; Woodhead Publishing: Cambridge, UK, 199-240.

Molnar, C. and Gair, J. 2015. Concepts of Biology – 1st Canadian Edition. BCcampus. https://opentextbc.ca/biology/ Date of access: 14 January 2021

Nadar, D., Naicker, K. and Lokhat, D. 2020. Ultrasonically-Assisted Dissolution of Sugarcane Bagasse during Dilute Acid Pretreatment: Experiments and Kinetic Modeling, *Energies*, 13, 5627.

Naik, S. N., Goud, V. V., Rout, P. K. and Dalai, A. K. 2010. Production of first and second generation biofuels: a comprehensive review. *Renewable and Sustainable Energy Reviews*, 14 (2), 578 - 597

Nigam, P. S., and Singh, A. 2011. Production of liquid biofuels from renewable resources. *Progress in Energy and Combustion Science*, 37, 52 – 68.

Noraini, M. Y., Ong, H. C., Badrul, M. J. and Chong, W. T. 2014. A review on potential enzymatic reaction for biofuel production from algae. *Renewable and Sustainable Energy Reviews*, 39, 24–34.

Osada, M., Sato, T., Watanabe, M., Shirai, M. and Arai, K. 2006. Catalytic gasification of wood biomass in subcritical and supercritical water. *Combustion Science and Technology*, 178, 537-552.

Pang, Shusheng. 2018. Advances in thermochemical conversion of woody biomass to energy, fuels and chemicals. *Biotechnology Advances*, 1-30.

Peterson, A. A., Vogel, F., Lachance, R. P., Froling, M., Antal, M. J. and Tester, J. W. 2008. Thermochemical biofuel production in hydrothermal media: a review of sub- and supercritical water technologies. *Energy and Environmental Science*, 1, 32 – 65.

Peterson, A. A., Lachance, R. P. and Tester, J. W. 2010. Kinetic Evidence of the Maillard Reaction in Hydrothermal Biomass Processing: Glucose-Glycine Interactions in High-Temperature, High-Pressure Water. *Industrial and Engineering Chemistry Research*, 49, 2107-2117.

Popp, J., Lakner, Z., Harangi-Rakos, M. and Fari, M. 2014. The effect of bioenergy expansion: Food, energy, and environment. *Renewable and Sustainable Energy Reviews*, 32, 559 – 578.

Pradhan, A. and Mbohwa, C. 2014. Development of biofuels in South Africa: Challenges and opportunities. *Renewable and Sustainable Energy Reviews*, 39, 1089 – 1100.

Ramirez, J. A., Brown, R. J., and Rainey, T. J. 2015. A Review of Hydrothermal Liquefaction Bio-Crude Properties and Prospects for Upgrading to Transport Fuels. *Energies*, 8, 6765-6794.

Raslavicius, L., Semenov, V. G., Chernova, N. I., Kersys, A. and Kopeyka, A. K. 2014. Producing transportation fuels from algae: in search of synergy. *Renewable and Sustainable Energy Reviews*, 40, 133–142.

Reddy, H. K., Muppaneni, T., Ponnusamy, S., Sudasinghe, N., Pegallapati, A., Selvaratnam, T., Seger, M., Dungan, B., Nirmalakhandan, N., Schaub, T., Holguin, F. O., Lammers, P., Voorhies, W. and Deng, S. 2016. Temperature effect on hydrothermal liquefaction of Nannochloropsis gaditana and Chlorella sp., *Applied Energy*, 165, 943-951.

Ross, A. B., Biller, P., Kubacki, M. L., Lea-Langton, A. and Jones, J. M. 2010. Hydrothermal processing of microalgae using alkali and organic acids. *Fuel*. 89, 2234–2243.

Sambusiti, C., Bellucci, M., Zabaniotou, A., Beneduce, L. and Monlau, F. 2015. Algae as promising feedstocks for fermentative biohydrogen production according to a biorefinery approach: a comprehensive review. *Renewable and Sustainable Energy Reviews*, 44, 20–36.

Schaschke, C. A. 2014. Dictionary of Chemical Engineering; Oxford University Press, UK.

Singh, A., Nigam P. S. and Murphy, J. D. 2011. Renewable fuels from algae: an answer to debatable land based fuels. *Bioresource Technology*, 102, 10–16.

Smith, R. and Jobson, M. 2000. DISTILLATION. *Encyclopedia of Separation Science*, 84-103.

Stack Exchange. 2019. *Phase diagram of water*. https://physics.stackexchange.com/questions/346750/phase-diagram-of-water. Date of access: 15 June 2019

Synytsya, A., Copikova, J., Kim, W. J. and Park, Y. 2015. Cell Wall Polysaccharides of Marine Algae. In *Springer Handbook of Marine Biotechnology*; Kim, S. K., Ed.; Springer: Berlin/Heidelberg, Germany, 543-590.

The Seaweed Site: information of marine algae. 2020. *Chlorophyta: Green Algae*. https://www.seaweed.ie/algae/chlorophyta.php Date of access: 18 November 2020.

The Seaweed Site: information of marine algae. 2020. *Phaeophyceae: Brown Algae*. https://www.seaweed.ie/algae/phaeophyta.php Date of access: 18 November 2020.

The Seaweed Site: information of marine algae. 2020. *Rhodophyta: Red algae*. https://www.seaweed.ie/algae/rhodophyta.php Date of access: 18 November 2020.

Tian, C., Li, B., Liu, Z., Zhang, Y., and Lu, H. 2014. Hydrothermal liquefaction for algal biorefinery: a critical review. *Renewable and Sustainable Energy Reviews*, 38, 933–950.

Toor, S. S., Rosendahl, L. and Rudolf, A. 2011. Hydrothermal liquefaction of biomass: A review of subcritical water technologies. *Energy*, 36, 2328-2342.

Toor, S. S., Reddy, H., Deng, S., Hoffman, J., Spangsmark, D., Madsen, L. B., Holm-Nielsen, J. B. and Rosendendahl, L. A. 2013. Hydrothermal liquefaction of Spirulina and Nannochloropsis salina under subcritical and supercritical water conditions. *Bioresource Technology*, 131, 413-419.

Ullah, K., Ahmad, M., Sofia, Sharma, V. K., Lu, P., Harvey, A., Zafar, M., and Sultana, S. 2015. Assessing the potential of algal biomass opportunities for bioenergy industry: a review. *Fuel*, 143, 414–423.

Valdez, P. J., Tocco, V. J. and Savage, P. E. 2014. A general model for the hydrothermal liquefaction of microalgae. *Bioresource Technology*, 163, 123-127

Valdez, P. J., Nelson, M. C., Wang, H. Y., Lin, X. N. and Savage, P. E. 2012. Hydrothermal liquefaction of Nannochloropsis sp. Systematic study of process variables and analysis of the product fractions. *Biomass and Bioenergy*, 46, 317–331.

Valdez, P. J. and Savage, P. E. 2013. A reaction network for the hydrothermal liquefaction of Nannochloropsis sp. *Algal Research*, 2, 416-425

Vallero, D. 2008. In *Fundamentals of air pollution*, 4th ed., Elsevier Inc, San Diego.

Vardon, D. R., Sharma, B. K., Scott, J., Guo, Y., Wang, Z. and Schideman, L. 2011. Chemical properties of biocrude oil from the hydrothermal liquefaction of Spirulina algae, swine manure, and digested anaerobic sludge. *Bioresource Technology*, 102, 8295–8303.

Vassilev, S. V., & Vassileva, C. G. 2016. Composition, properties and challenges of algae biomass for biofuel application: An overview. *Fuel*, 181, 1–33.

Vlaskin, M., Grigorenko, A. V., Chernova, N. I., Kiseleva, S. V. and Kumar, V. 2018. Bio-oil production by hydrothermal liquefaction of microalgae biomass. *Alternative Energy and Ecology*, 68-79.

Wahyudiono, Kanetake, T., Sasaki, M. and Goto, M. 2007. Decomposition of a lignin model compound under hydrothermal conditions. *Chemical Engineering and Technology*, 30(8), 1113-1122.

Wang, W., Kuang, Y. and Huang, N. 2011. Study on the decomposition of factors affecting energy-related carbon emissions in Guangdong province, China. *Energies*, 4, 2249-2272.

Wen, Z. 2019. *Algae for Biofuel Production*. https://farm-energy.extension.org/algae-for-biofuel-production/ Date of access: 21 November 2020

Wyman, C. E., Dale, B. E., Elander, R.T., Holtzapple, M., Ladisch, M. R. and Lee, Y. Y. 2005. Coordinated development of leading biomass pretreatment technologies. *Bioresource Technology*, 96(18), 1959-1966.

Xu, D., Lin, G., Guo, S., Wang, S., Guo, Y. and Jing, Z. 2018. Catalytic hydrothermal liquefaction of algae and upgrading of biocrude: a critical review. *Renewable and Sustainable Energy Reviews*, 97, 103-118

Yang, G., Yeh, T., Song, W., Xu, D. and Wang, S. 2015. A review of bio-oil production from hydrothermal liquefaction of algae. *Renewable and Sustainable Energy Reviews*, 48, 776-790.

Yuan, C., Wang, S., Cao, B., Hu, Y., Abomohra, A. E.-F., Wang, Q., Qian, L., Liu, L., Liu, X., He, Z., Sun, C., Feng, Y. and Zhang, B. 2019. Optimization of hydrothermal co-liquefaction of seaweeds with lignocellulosic biomass: Merging 2nd and 3rd generation feedstocks for enhanced bio-oil production, *Energy*. doi:10.1016/j.energy.2019.02.091

Zhang, Y., Cui, Y., Chen, P., Lui, S., Zhou, N., Ding, K., Fan, L., Peng, P., Min, M., Cheng, Y., Wang, Y., Wan, Y., Lui, Y., Li, B. and Ruan, R. 2019. Chapter 14 – Gasification Technologies and Their Energy Potentials. *Sustainable Resource Recovery and Zero Waste Approaches*, 193-206

Zhang, Y., Li, B., Li, H. and Lui, H. 2011. Thermodynamic evaluation of biomass gasification with air in autothermal gasifiers. *Thermochimica Acta*, 519, 65-71.

Zhang, Y., Chen, P., Lui, S., Peng, P., Min, M., Cheng, Y., Anderson, E., Zhou, N., Fan, I., Lui, C., Chen, G., Lui, Y., Lei, H., Ruan, R. and Lei, H. 2017. Effects of feedstock characteristics on microwave-assisted pyrolysis – a review. *Bioresource Technology*, 230, 143-151.

Zhang, Y., Zhao, Y., Gao, X., Li, B. and Huang, J. 2015. Energy and energy analyses of syngas produced from rice husk gasification in an entrained flow reactor. *Journal of Cleaner Production*. 95, 273-280.

Zou, S., Wu, Y., Yang, M., Imdad, K., Li, C. and Tong, J. 2010a. Production and characterization of bio-oil from hydrothermal liquefaction of microalgae Dunaliella tertiolecta cake. *Energy*, 35, 5406–5411.

Zou, S., Wu, Y., Yang, M., Li, C. and Tong, J. 2010b. Bio-oil production from sub- and supercritical water liquefaction of microalgae Dunaliella tertiolecta and related properties. *Energy and Environmental Science*, 3, 1073–1078.

Appendix A: Raw Data

A.1) Raw data

Table A-1: Mass dissolution raw data for the variation of the process variables

Condition	Time (min)	Initial wet mass (g)	Initial moisture (%)	Initial dry mass (g) (Equation B-1)	Final wet mass (g)	Final moisture (%)	Final dry mass (g) (Equation B-2)	Mass Dissolution (%) (Equation B-4)
5g 10% 4000 KPa 250°C	5	5,003	12,46	4,380	8,618	84,64	1,324	69,776
	10	5,005	12,52	4,378	8,866	85,19	1,313	70,010
	15	5,001	12,55	4,373	8,629	85,02	1,293	70,443
	20	5,002	12,49	4,377	8,883	85,68	1,272	70,940
	25	5,001	12,57	4,372	9,105	86,47	1,232	71,825
	30	5,002	12,61	4,371	8,897	86,76	1,178	73,052
6g 10% 4000 KPa 250°C	5	6,003	12,53	5,251	11,441	86,86	1,503	71,369
	10	6,001	12,49	5,251	11,895	87,52	1,484	71,732
	15	6,003	12,55	5,250	11,253	87,05	1,457	72,241
	20	6,000	12,63	5,242	11,131	87,28	1,416	72,991
	25	6,002	12,52	5,251	11,781	88,41	1,365	73,993
	30	6,004	12,48	5,255	11,896	89,12	1,294	75,369
10g 10% 4000 KPa 250°C	5	10,001	12,62	8,739	18,297	87,84	2,225	74,540
	10	10,001	12,52	8,749	18,986	88,49	2,185	75,022
	15	10,003	12,67	8,736	18,065	88,22	2,128	75,639
	20	10,005	12,46	8,758	18,228	88,71	2,058	76,503
	25	10,002	12,63	8,739	19,102	89,78	1,952	77,660
	30	10,003	12,57	8,746	18,511	89,69	1,908	78,178
6g 5% 4000 KPa 250°C	5	6,002	12,61	5,245	11,21	85,02	1,679	67,985
	10	6,000	12,55	5,247	11,807	85,98	1,655	68,452
	15	6,000	12,52	5,249	11,323	85,63	1,627	69,000
	20	6,001	12,58	5,246	10,637	85,12	1,583	69,829
	25	6,002	12,48	5,253	11,551	86,68	1,539	70,710
	30	6,001	12,55	5,248	10,861	86,46	1,471	71,978
6g 10% 1500 KPa	5	6,001	12,47	5,253	11,627	82,13	2,078	60,444
	10	6,004	12,56	5,250	10,974	81,34	2,048	60,995
	15	6,002	12,49	5,252	11,385	82,25	2,021	61,525
	20	6,002	12,51	5,251	11,169	82,27	1,980	62,289

200°C	25	6,001	12,62	5,244	11,563	83,35	1,925	63,285
	30	6,001	12,58	5,246	11,495	83,82	1,860	64,547

Table A-2: Bio-oil formed and bio-oil yield for the variation of the process variables

Condition	**Time (min)**	**Mass of glass vial (g)**	**Mass of oil and vial (g)**	**Mass of oil (g)**	**Yield (%)** (Equation B-5)
5g 10% 4000 KPa 250°C	5	12,242	13,421	1,179	26,920
	10	12,144	13,347	1,203	27,476
	15	12,065	13,297	1,232	28,170
	20	12,087	13,355	1,268	28,968
	25	12,305	13,616	1,311	29,984
	30	12,107	13,465	1,358	31,067
6g 10% 4000 KPa 250°C	5	11,958	13,426	1,468	27,958
	10	12,024	13,518	1,494	28,449
	15	12,21	13,731	1,521	28,974
	20	12,224	13,787	1,563	29,816
	25	11,984	13,616	1,632	31,082
	30	12,015	13,729	1,714	32,618
10g 10% 4000 KPa 250°C	5	12,062	14,648	2,586	29,592
	10	12,140	14,783	2,643	30,210
	15	12,088	14,811	2,723	31,171
	20	11,992	14,801	2,809	32,072
	25	12,131	15,032	2,901	33,197
	30	12,086	15,118	3,032	34,669
6g 5% 4000 KPa 250°C	5	12,009	13,206	1,197	22,821
	10	12,206	13,428	1,222	23,289
	15	11,991	13,242	1,251	23,834
	20	12,181	13,464	1,283	24,456
	25	12,042	13,370	1,328	25,281
	30	12,113	13,505	1,392	26,525
6g 10% 1500 KPa 200°C	5	12,109	13,062	0,953	18,143
	10	12,163	13,14	0,977	18,610
	15	12,001	13,006	1,005	19,134
	20	11,969	13,007	1,038	19,767
	25	12,105	13,181	1,076	20,520
	30	11,995	13,115	1,12	21,349

Table A-3: Mass dissolution raw data for the Induction Period

Condition	**Time (min)**	**Initial wet mass (g)**	**Initial moisture (%)**	**Initial dry mass (g)** (Equation B-1)	**Final wet mass (g)**	**Final moisture (%)**	**Final dry mass (g)** (Equation B-2)	**Mass Dissolution (%)** (Equation B-4)
6g 10%	5	6,002	12,56	5,248	38,621	86,68	5,144	1,978
	10	6,000	12,6	5,244	40,294	87,39	5,081	3,107
	15	6,000	12,52	5,249	42,517	88,46	4,906	6,522
	20	6,001	12,51	5,250	36,72	87,34	4,649	11,457
	25	6,000	12,49	5,251	31,545	87,65	3,896	25,803
	30	6,003	12,57	5,248	27,682	87,22	3,538	32,594
	35	6,001	12,56	5,247	25,115	88,43	2,906	44,623
	40	6,001	12,52	5,250	19,928	87,66	2,459	53,157
	45	6,002	12,63	5,244	15,059	86,55	2,025	61,376
	50	6,000	12,59	5,245	10,983	85,19	1,627	68,986
	55	6,002	12,52	5,251	11,476	86,44	1,556	70,362
	60	6,001	12,61	5,244	11,634	86,87	1,528	70,872

Table A-4: Bio-oil formed and bio-oil yield for the induction period

Condition	**Time (min)**	**Mass of glass vial (g)**	**Mass of oil and vial (g)**	**Mass of oil (g)**	**Yield (%)** (Equation B-5)
6g 10%	5	12,045	12,051	0,006	0,114
	10	12,206	12,216	0,010	0,191
	15	12,142	12,169	0,027	0,514
	20	11,992	12,151	0,159	3,028
	25	12,007	12,329	0,322	6,133
	30	12,135	12,692	0,557	10,619
	35	12,086	12,864	0,778	14,827
	40	12,187	13,193	1,006	19,163
	45	12,212	13,425	1,213	23,131
	50	12,008	13,319	1,311	24,997
	55	12,096	13,462	1,366	26,016
	60	12,224	13,618	1,394	26,581

Table A-5: Temperature and Pressure change during induction period

Time (min)	**Temperature(°C)**	**Pressure (KPa)**	**Mass Dissolution (%)** (Equation B-4)	**Bio-oil mass (g)**	**Yield (%)** (Equation B-5)
5	34	100	1,978	0,006	0,114
10	53	200	3,107	0,01	0,191
15	104	500	6,522	0,027	0,514
20	137	800	11,457	0,159	3,028
25	153	1200	25,803	0,322	6,133
30	175	1600	32,594	0,557	10,613
35	191	2000	44,623	0,778	14,827
40	206	2400	53,157	1,006	19,163
45	220	2700	61,376	1,213	23,131
50	229	3200	68,986	1,311	24,997
55	240	3700	70,362	1,366	26,016
60	249	3900	70,872	1,394	26,581

Table A-6: Initial mass observed for each time

Time (min)	**0**	**5**	**10**	**15**	**20**	**25**	**30**	**35**	**40**	**45**
Solids	5,2490	5,2481	5,244	5,2488	5,2502749	5,2506	5,2484	5,2473	5,2497	5,2439
Bio-oil	0	0	0	0	0	0	0	0	0	0
Aqueous	0	0	0	0	0	0	0	0	0	0
Time (min)	**50**	**55**	**60**	**65**	**70**	**75**	**80**	**85**	**90**	
Solids	5,2446	5,2505	5,2443	5,2508	5,2515	5,2496	5,2422	5,2505	5,2547	
Bio-oil	0	0	0	0	0	0	0	0	0	
Aqueous	0	0	0	0	0	0	0	0	0	

Table A-7: Final mass observed for each time

Time (min)	**0**	**5**	**10**	**15**	**20**	**25**	**30**	**35**	**40**	**45**
Solids	5,2490	5,1443	5,0811	4,9065	4,6488	3,8958	3,5378	2,9058	2,4591	2,0254
Bio-oil	0	0,0060	0,010	0,0270	0,1590	0,3220	0,5570	0,7780	1,0060	1,2130
Aqueous	0	0,0978	0,1529	0,3153	0,4425	1,0328	1,1537	1,5634	1,7846	2,0055
Time (min)	**50**	**55**	**60**	**65**	**70**	**75**	**80**	**85**	**90**	
Solids	1,6266	1,5561	1,5275	1,5033	1,4845	1,4573	1,4159	1,3654	1,2943	
Bio-oil	1,3110	1,3660	1,3940	1,4680	1,4940	1,5210	1,5630	1,6320	1,7140	
Aqueous	2,3070	2,3284	2,3228	2,2795	2,2730	2,2714	2,2633	2,2531	2,2464	

Table A-8: Initial mass fractions observed for each time

Time (min)	**0**	**5**	**10**	**15**	**20**	**25**	**30**	**35**	**40**	**45**
Solids	1	1	1	1	1	1	1	1	1	1
Bio-oil	0	0	0	0	0	0	0	0	0	0
Aqueous	0	0	0	0	0	0	0	0	0	0
Time (min)	**50**	**55**	**60**	**65**	**70**	**75**	**80**	**85**	**90**	
Solids	1	1	1	1	1	1	1	1	1	
Bio-oil	0	0	0	0	0	0	0	0	0	
Aqueous	0	0	0	0	0	0	0	0	0	

Table A-9: Final mass observed for each time

Time (min)	**0**	**5**	**10**	**15**	**20**	**25**	**30**	**35**	**40**	**45**
Solids	1	0,9802	0,9689	0,9348	0,8854	0,7420	0,6741	0,5538	0,4684	0,3862
Bio-oil	0	0,0011	0,0019	0,0051	0,0303	0,0613	0,1061	0,1483	0,1916	0,2313
Aqueous	0	0,0186	0,0292	0,0601	0,0843	0,1967	0,2198	0,2980	0,3399	0,3824
Time (min)	**50**	**55**	**60**	**65**	**70**	**75**	**80**	**85**	**90**	
Solids	0,3101	0,2964	0,2913	0,28631	0,2827	0,2776	0,2701	0,2601	0,2463	
Bio-oil	0,2500	0,2602	0,2658	0,2796	0,2845	0,2897	0,2982	0,3108	0,3262	
Aqueous	0,4399	0,4434	0,4429	0,4341	0,4328	0,4327	0,4318	0,4291	0,4275	

Table A-10: Ash content raw data

Initial mass	**Final mass**	**% Difference** (Equation B-6)
28,39	27,93	1,637
34,49	33,89	1,727
28,05	27,58	1,655
Average		**1,673**

Table A-11: Volatile content raw data

Initial mass	**Final mass**	**% Difference** (Equation B-7)
30,65	30,59	0,196
30,16	30,08	0,265
30,58	30,51	0,229
Average		**0,229**

Appendix B: Sample calculations

All moisture content analysis was done at 100℃ with an automatic time limit. This was done to ensure the optimal effect of the moisture analysis.

Results shown are for the experimental run with a mass of 6g, a solids loading of 10wt%, a temperature of 250°C, a pressure of 4000KPa, and a reaction time of 30 minutes.

Table B-1: Initial biomass conditions

Mass of initial wet seaweed ($M_{w,i}$)	6.004g
Initial moisture content (MC_i)	12.48%

Initial dry mass of seaweed ($M_{d,i}$):

$$= M_{w,i} - \left(M_{w,i} \times \frac{MC_i}{100}\right) \quad \text{(Equation B-1)}$$

$$= 5.255\text{g}$$

Table B-2: Final biomass conditions

Mass of final wet seaweed ($M_{w,f}$)	11.896g
Final moisture content (MC_f)	89.12%

Final dry mass of seaweed ($M_{d,f}$):

$$= M_{w,f} - \left(M_{w,f} \times \frac{MC_f}{100}\right) \quad \text{(Equation B-2)}$$

$$= 1.294\text{g}$$

Total dry mass lost $(M_{d,l})$:

$$= M_{d,i} - M_{d,f} \quad \text{(Equation B-3)}$$

$$= 5.255 - 1.294$$

$$= 3.961\text{g}$$

Mass dissolution (MD):

$$= \frac{M_{d,l}}{M_{d,i}} \times 100 \quad \text{(Equation B-4)}$$

$$= \frac{3.961}{5.255} \times 100$$

$$= 75.38\%$$

Mass of bio-oil formed ($\boldsymbol{M_b}$) = 1.714g (measured on scale)

Yield (*Y*):

$$= \frac{M_b}{M_{d,i}} \times 100 \quad \text{(Equation B-5)}$$

$$= \frac{1.714}{5.255} \times 100$$

$$= 32.62\%$$

Proximate analysis:

Ash content:

The ash content was determined by placing 6g of seaweed into a muffle furnace at 700°C for 1 hour and measuring the remaining mass. Calculations are shown for Run 1.

$$= \frac{\text{initial mass} - \text{final mass}}{\text{initial mass}} \times 100 \quad \text{(Equation B-6)}$$

$$= \frac{28.3916 - 27.9268}{28.3916} \times 100$$

$$= 1.637\%$$

Volatile content:

The volatiles content was also measured by placing 6g of the seaweed into the muffle furnace at 900°C and measuring the remaining mass. Calculations are shown for Run 1.

$$= \frac{\text{initial mass} - \text{final mass}}{\text{initial mass}} \times 100 \quad \text{(Equation B-7)}$$

$$= \frac{30.65 - 30.59}{30.65} \times 100$$

$$= 0.1958\%$$

Appendix C: Phase diagram of water

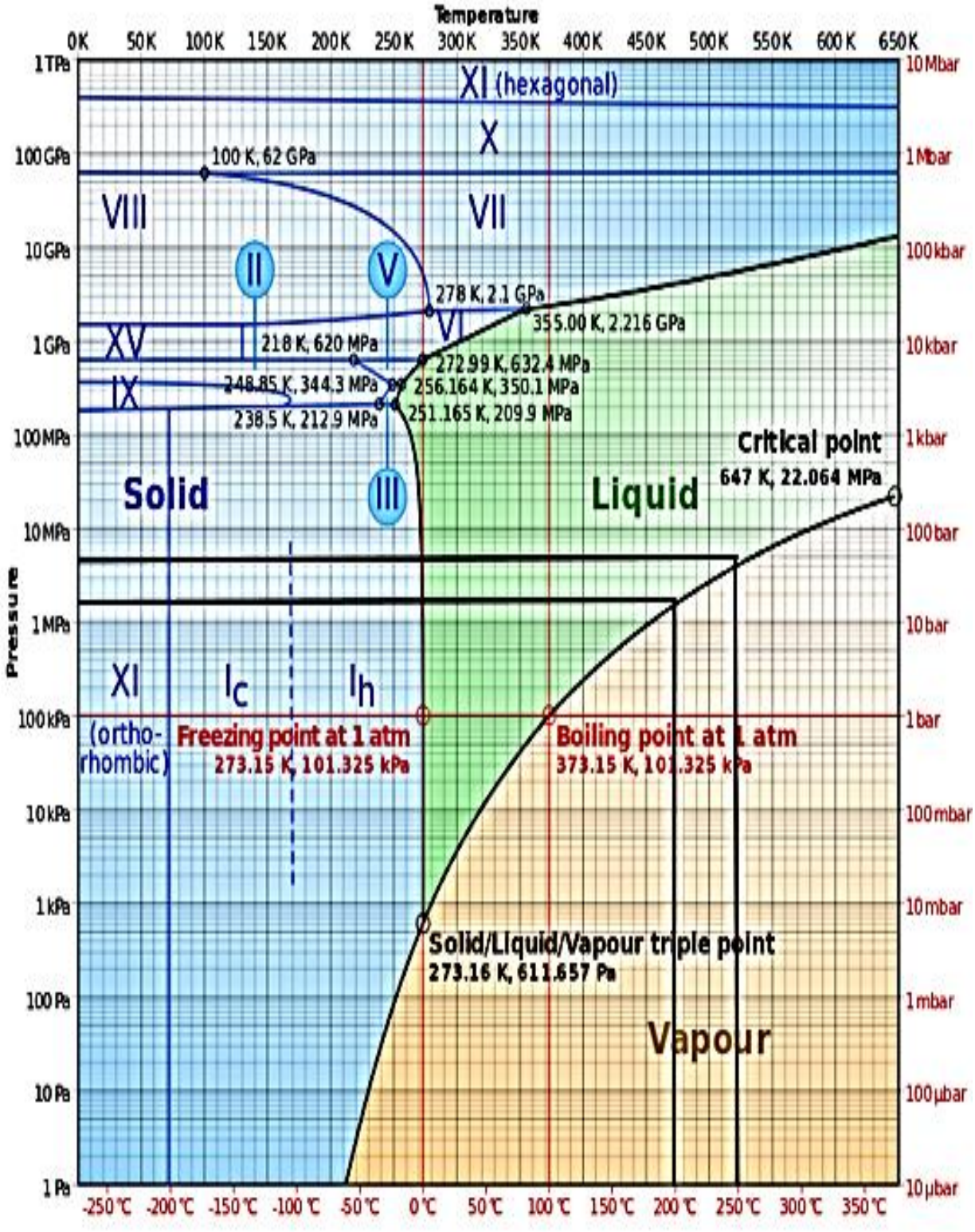

Figure C-1: Phase diagram of water showing temperatures and pressures used (Stack Exchange, 2019).

Appendix D: Gas Chromatography-Mass Spectrometry (GC-MS) Analysis

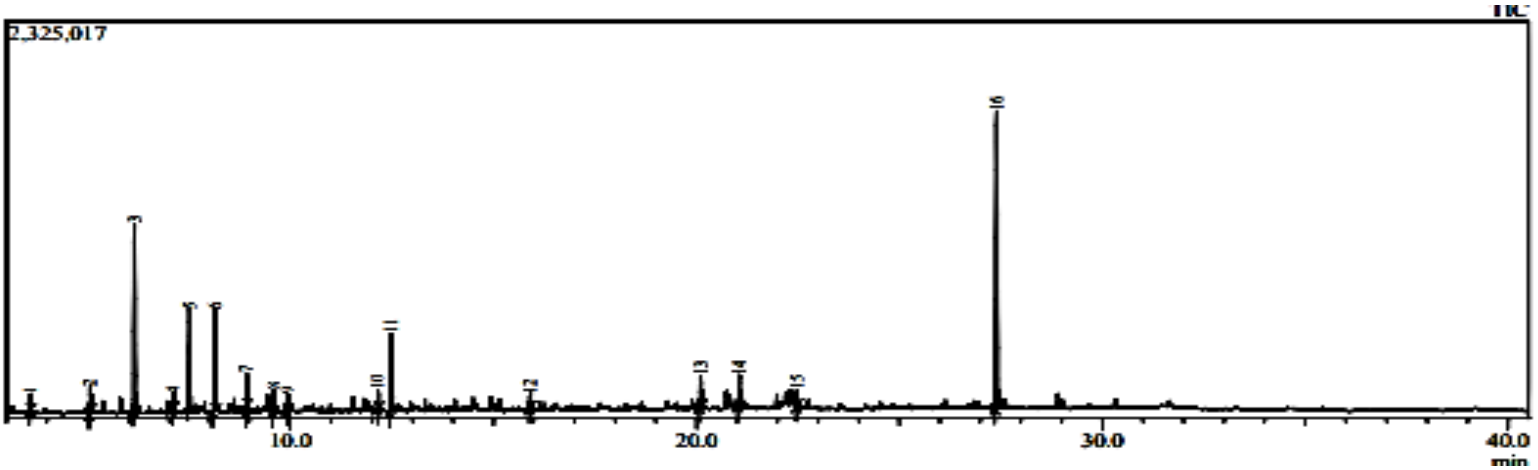

Figure D-1: GCMS analysis for the 5g 10wt% 5 minutes run.

Table D-1: GCMS results for the 5g 10wt% 5 minutes run

Peak#	R. Time	Area	Area%	Name	Similarity	Base m/z
1	3.583	135450	1.27	Furfural	96	96.05
2	5.063	246875	2.32	Ethanone, 1-(2-furanyl)-	95	95.00
3	6.154	1834376	17.21	2-Furancarboxaldehyde, 5-methyl-	96	110.05
4	7.110	157734	1.48	1H-Pyrrole-2-carboxaldehyde	97	95.00
5	7.518	1166365	10.94	2-Cyclopenten-1-one, 2-hydroxy-3-methyl-	97	112.05
6	8.133	1247552	11.71	2-Cyclopenten-1-one, 3-ethyl-2-hydroxy-	90	126.10
7	8.918	315891	2.96	2-Cyclopenten-1-one, 3-ethyl-2-hydroxy-	93	126.10
8	9.579	205448	1.93	2(3H)-Furanone, 5-acetyldihydro-	95	85.05
9	9.919	145628	1.37	Cyclopentane, 1-acetyl-1,2-epoxy-	84	55.05
10	12.153	156193	1.47	1,2-Benzenediol, 3-methyl-	96	124.05
11	12.486	750346	7.04	Ethanone, 1-(2,5-dihydroxyphenyl)-	93	137.00
12	15.905	110466	1.04	Bicyclo[3.3.1]nona-2,6-diene, 2,6-bis(acetoxy)-	80	152.05
13	20.105	340861	3.20	4-Methyldaphnetin	73	192.00
14	21.060	386450	3.63	Cyclo(L-prolyl-L-valine)	73	156.05

15	22.477	144173	1.35	n-Hexadecanoic acid	95	73.00
16	27.399	3313617	31.09	Hexanedioic acid, bis(2-ethylhexyl) ester	98	129.05
		10657425	100.00			

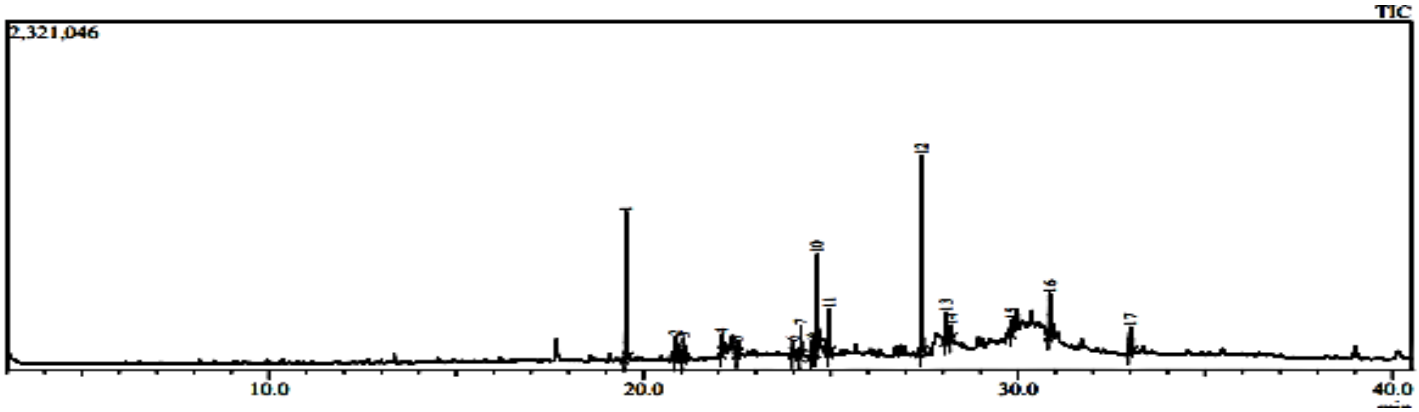

Figure D-2: GCMS analysis for the 5g 10wt% 10 minutes run.

Table D-2: GCMS results for the 5g 10wt% 10 minutes run

Peak#	R Time	Area	Area%	Name	Similarity	Base m/z
1	19.536	1737446	16.10	Cyclohexane, 1,3,5-triphenyl-	82	91.10
2	20.866	472582	4.38	7-Ethyl-4,6-heptadecandione	75	156.10
3	21.071	309104	2.86	Cyclo(L-prolyl-L-valine)	82	154.05
4	22.097	178386	1.65	Hexadecanoic acid, methyl ester	91	74.05
5	22.513	161104	1.49	n-Hexadecanoic acid	89	73.05
6	23.991	119316	1.11	n-Nonadecanol-1	97	83.10
7	24.201	343043	3.18	9-Octadecenoic acid, methyl ester, (E)-	95	55.05
8	24.485	167081	1.55	Methyl stearate	95	74.05
9	24.567	171153	1.59	Octadecadienoic acid (Z,Z)-	70	73.00
10	24.644	1548540	14.35	Oleic Acid	95	55.05
11	24.960	497756	4.61	Ethyl Oleate	95	55.05
12	27.433	2436006	22.57	Hexanedioic acid, bis(2-ethylhexyl) ester	98	129.05
13	28.079	358146	3.32	Cyclohexane, 1,3,5-triphenyl-	87	91.10
14	28.212	156134	1.45 9-	9-Octadecenoic acid (Z)-, oxiranylmethyl ester	93	55.05
15	29.837	233054	2.16	Pentatriacontane	86	57.05
16	30.851	1285033	11.91	Pentatriacontane	86	57.10
17	33.001	620090	5.74	Z,E-3,13-Octadecadien-1-ol	76	173.00
		10793974	100.00			

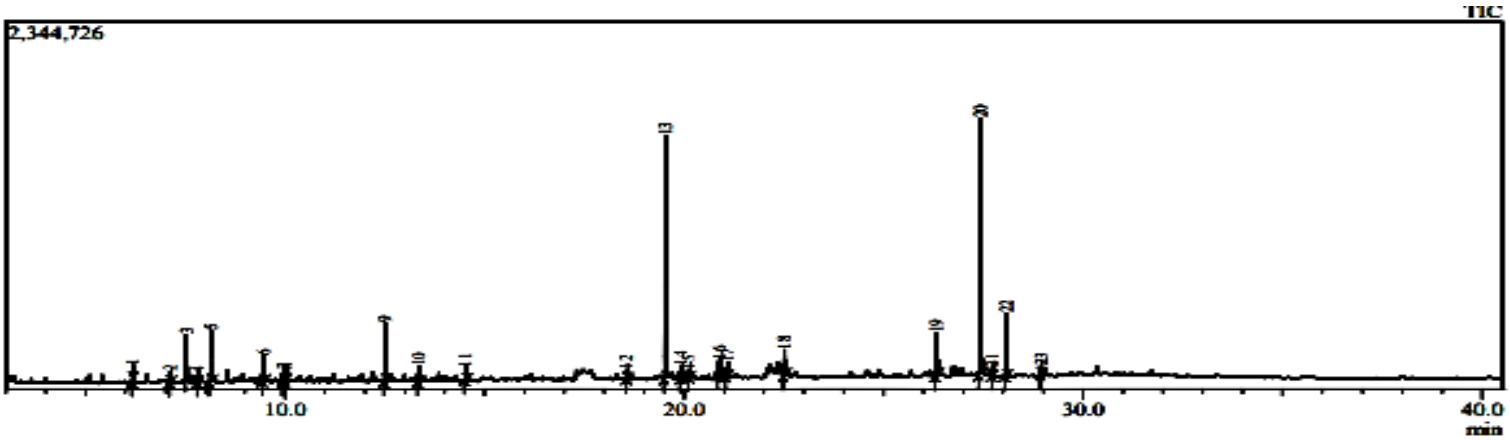

Figure D-3: GCMS analysis for the 5g 10wt% 15 minutes run.

Table D-3: GCMS results for the 5g 10wt% 15 minutes run

Peak#	R. Time	Area	Area%	Name	Similarity	Base m/z
1	6.179	122018	1.08	2-Furancarboxaldehyde, 5-methyl-	95	110.10
2	7.126	111645	0.99	1H-Pyrrole-2-carboxaldehyde	96	95.05
3	7.526	472336	4.19	2-Cyclopenten-1-one, 2-hydroxy-3-methyl-	97	112.10
4	7.811	76367	0.68	2-Cyclopenten-1-one, 2,3-dimethyl-	93	67.10
5	8.146	641940	5.69	2-Cyclopenten-1-one, 3-ethyl-2-hydroxy-	89	126.10
6	9.461	259579	2.30	2-Cyclopenten-1-one, 3-ethyl-2-hydroxy-	95	126.10
7	9.945	120469	1.07	3,4-Dimethyl-1,2-cyclopentadione	83	55.05
8	10.024	97799	0.87 cis-77 94.05	Cyclohexanone, 5-methyl-2-(1-methylethyl)-, cis-	77	94.05
9	12.510	591278	5.24	Ethanone, 1-(2,5-dihydroxyphenyl)-	94	137.05
10	13.347	176902	1.57	3,4,5,6,7,8-Hexahydro-2H-chromene	69	138.05
11	14.527	184319	1.63	Phenol, 2,3,5-trimethyl-	81	136.10
12	18.574	85850	0.76	Benzene, 1,1'-(1,3-propanediyl)bis-	95	92.10
13	19.538	2819737	25.01	Cyclohexane, 1,3,5-triphenyl-	82	91.10
14	19.933	161543	1.43	Tetradecanoic acid	88	73.05
15	20.128	87654	0.78	4-(5-Amino-2H-1,2,4-triazol-3-yl)benzene-1,3-diol	70	192.00
16	20.880	330894	2.93	7-Ethyl-4,6-heptadecandione	79	156.10
17	21.083	180724	1.60	Cyclo(L-prolyl-L-valine)	72	156.10
18	22.517	297481	2.64	n-Hexadecanoic acid	95	73.05
19	26.327	528343	4.69	9-Octadecenoic acid, 12-hydroxy-, methyl ester, [R-(Z)]-	90	55.05

20	27.434	3024611	26.82	Hexanedioic acid, bis(2-ethylhexyl) ester	98	129.05
21	27.735	86352	0.77	Phenol, 2,2'-methylenebis[6-(1,1-dimethylethyl)-4-methyl-	92	177.15
22	28.079	731805	6.49	Cyclohexane, 1,3,5-triphenyl-	93	91.05
23	28.945	85979	0.76	Bis(2-ethylhexyl) phthalate	95	149.05
		11275625	100.00			

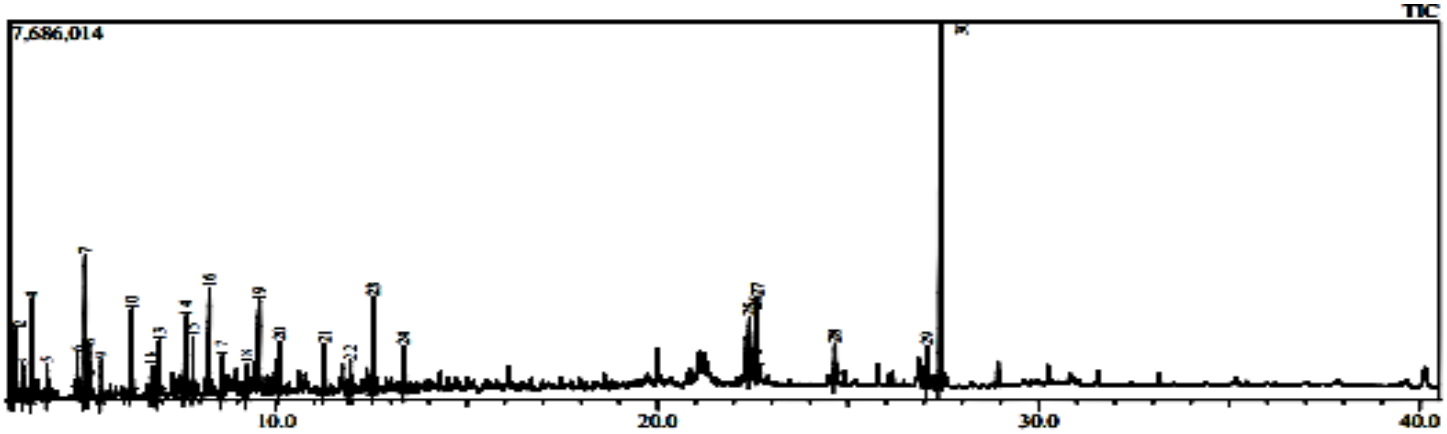

Figure D-4: GCMS analysis for the 5g 10wt% 20 minutes run.

Table D-4: GCMS results for the 5g 10wt% 20 minutes run

Peak#	R. Time	Area	Area%	Name	Similarity	Base m/z
1	3.054	2548729	2.98	3-Hydroxy-3-methyl-2-butanone	90	59.00
2	3.164	2501560	2.92	2-Hydroxy-3-pentanone	96	45.05
3	3.352	1085255	1.27	3-Pentanone, 2,4-dimethyl-	93	43.05
4	3.593	3592137	4.20	2-Cyclopenten-1-one	95	82.05
5	3.989	1341542	1.57	3-Furanmethanol	85	43.05
6	4.783	1065270	1.25	4-Hydroxy-3-hexanone	94	59.00
7	4.990	5256142	6.14	2-Cyclopenten-1-one, 2-methyl-	94	96.00
8	5.086	1721924	2.01	Ethanone, 1-(2-furanyl)-	91	94.95
9	5.412	1274877	1.49	2,5-Hexanedione	98	43.00
10	6.208	4217471	4.93	2-Cyclopenten-1-one, 3-methyl-	84	96.05
11	6.724	997950	1.17	Phenol	91	94.00
12	6.815	725985	0.85	2-Cyclopenten-1-one, 3,4-dimethyl-	96	95.00
13	6.930	2075446	2.43	2-Cyclopenten-1-one, 2,3-dimethyl-	93	67.00
14	7.644	5332547	6.23	2-Cyclopenten-1-one, 2-hydroxy-3-methyl-	98	112.00
15	7.816	1872260	2.19	2-Cyclopenten-1-one, 2,3-dimethyl-	95	110.05
16	8.249	5351262	6.26	2-Cyclopenten-1-one, 3-ethyl-2-hydroxy-	86	126.05
17	8.582	1819052	2.13 84 110.05	4H-1,3-Benzodioxin-4-one, hexahydro-4a,5-dimethyl-, [4as-(4a.alpha.,5.beta.,8a.beta.)]-	84	110.05

18	9.230	1342734	1.57	2,5-Cyclohexadiene-1,4-dione, 2,5-dimethyl-	78	136.00
19	9.556	5239594	6.13	2-Cyclopenten-1-one, 3-ethyl-2-hydroxy-	96	126.05
20	10.090	1716365	2.01	1,3-Cyclopentanedione, 2-ethyl-2-methyl-	79	94.00
21	11.262	1904687	2.23	2-Hydroxy-3-propyl-2-cyclopenten-1-one	80	125.00
22	11.946	1241740	1.45	2-Cyclohexen-1-one, 4-(1-methylethyl)-	83	43.00
23	12.553	3410658	3.99	Ethanone, 1-(2,5-dihydroxyphenyl)-	93	137.00
24	13.361	1420216	1.66	3,4,5,6,7,8-Hexahydro-2H-chromene	80	110.00
25	22.413	2668453	3.12	5,10-Diethoxy-2,3,7,8-tetrahydro-1H,6H-dipyrrolo[1,2-a:1',2'-d]pyrazine	75	70.05
26	22.576	2027210	2.37	Hexahydro-3-(1-methylpropyl)pyrrolo[1,2-a]pyrazine-1,4-dione	86	154.00
27	22.611	1972293	2.31	27 22.611 1972293 2n-Hexadecanoic acid	96	73.00
28	24.658	1597387	1.87	Oleic Acid	94	55.00
29	27.088	1716821	2.01	9-Octadecenamide, (Z)-	70	91.00
30	27.428	16501661	19.29	Hexanedioic acid, bis(2-ethylhexyl) ester	97	129.00
		85539228	100.00			

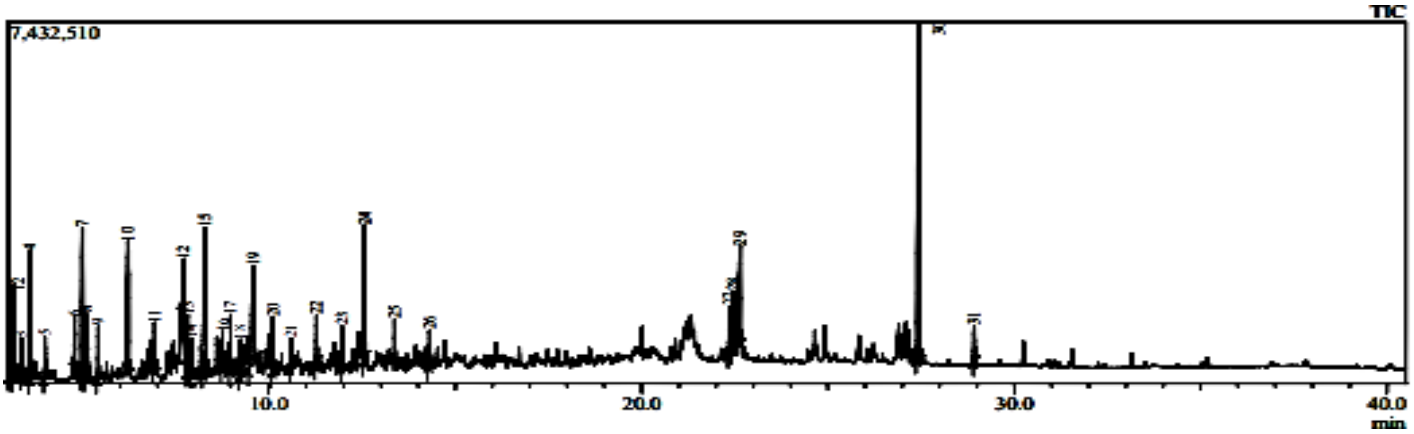

Figure D-5: GCMS analysis for the 5g 10wt% 25 minutes run.

Table D-5: GCMS results for the 5g 10wt% 25 minutes run

Peak#	R. Time	Area	Area%	Name	Similarity	Base m/z
1	3.058	4285590	3.59	3-Hydroxy-3-methyl-2-butanone	90	59.05
2	3.171	4263430	3.57	2-Hydroxy-3-pentanone	96	45.10
3	3.355	1603977	1.34	3-Pentanone, 2,4-dimethyl-	93	43.10
4	3.602	5563701	4.66	2-Cyclopenten-1-one	93	82.10

5	3.993	2389096	2.00	1-Hexene, 4,5-dimethyl-	83	43.10
6	4.788	2131717	1.79	Hydroxy-3-hexanone	94	59.10
7	4.997	6569690	5.50	2-Cyclopenten-1-one, 3-methyl-	93	96.10
8	5.091	3764301	3.15	Ethanone, 1-(2-furanyl)-	92	95.05
9	5.419	2064062	1.73	2,5-Hexanedione	98	43.05
10	6.222	8478503	7.10	2-Furancarboxaldehyde, 5-methyl-	93	110.05
11	6.933	1659685	1.39	2-Cyclopenten-1-one, 2,3-dimethyl-	91	67.05
12	7.718	3823176	3.20	2-Cyclopenten-1-one, 2-hydroxy-3-methyl-	96	112.10
13	7.830	2661520	2.23	2-Cyclopenten-1-one, 2,3-dimethyl-	95	110.10
14	7.936	1306580	1.09	1H-Pyrazole-4-carboxaldehyde, 1,5-dimethyl-	83	124.10
15	8.289	9049270	7.58	2-Cyclopenten-1-one, 3-ethyl-2-hydroxy-	80	126.10
16	8.756	1733252	1.45	2-Acetylcyclopentanone	71	108.10
17	8.965	1937852	1.62	2-Cyclopenten-1-one, 3-ethyl-2-hydroxy-	91	126.10
18	9.232	1534283	1.29	1,2-Cyclohexanedicarboxaldehyde	71	112.10
19	9.590	8036240	6.73	2-Cyclopenten-1-one, 3-ethyl-2-hydroxy-	95	126.10
20	10.111	2416682	2.02	1,3-Cyclopentanedione, 2-ethyl-2-methyl-	77	94.05
21	10.586	1573905	1.32	Cyclohexanone, 5-methyl-2-(1-methylethylidene)-	83	152.10
22	11.279	1961434	1.64	2-Hydroxy-3-propyl-2-cyclopenten-1-one	87	125.10
23	11.965	1851992	1.55	2-Cyclohexen-1-one, 4-(1-methylethyl)-	85	96.10
24	12.571	6022759	5.05	Ethanone, 1-(2,5-dihydroxyphenyl)-	94	137.05
25	13.373	1541707	1.29	3,4,5,6,7,8-Hexahydro-2H-chromene	78	110.10
26	14.309	1468501	1.23	2,5-Dihydroxypropiophenone	91	137.05
27	22.368	3026915	2.54	Pyrrolo[1,2-a]pyrazine-1,4-dione, hexahydro-3-(2-methylpropyl)-	88	154.05
28	22.446	3370302	2.82	Octahydrodipyrrolo[1,2-a:1',2'-d]pyrazine-5,10-dione-, (5aR,10aR) (isomer 1)	89	70.10
29	22.643	5808875	4.87	n-Hexadecanoic acid	83	73.05
30	27.427	16016529	13.42	Hexanedioic acid, bis(2-ethylhexyl) ester	95	129.10
31	28.924	1444185	1.21	Bis(2-ethylhexyl) phthalate	81	149.00
		119359711	100.00			

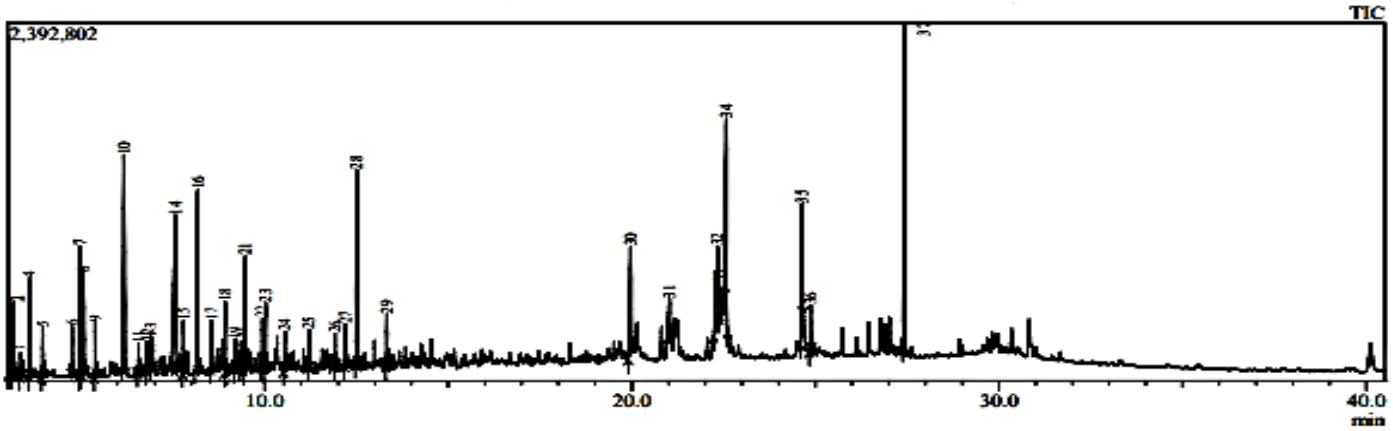

Figure D-6: GCMS analysis for the 5g 10wt% 30 minutes run.

Table D-6: GCMS results for the 5g 10wt% 30 minutes run

Peak#	R. Time	Area	Area%	Name	Similarity	Base m/z
1	3.054	870967	1.89	Propanoic acid, 2-hydroxy-2-methyl-	91	59.05
2	3.162	879718	1.91	2-Hydroxy-3-pentanone	96	45.05
3	3.354	262421	0.57	Pentane, 2-nitro-	90	43.10
4	3.591	1211901	2.63	2-Cyclopenten-1-one	90	82.05
5	3.961	714444	1.55	2-Furanmethanol	88	43.05
6	4.759	451526	0.98	4-Hydroxy-3-hexanone	95	59.05
7	4.970	1498370	3.25	2-Cyclopenten-1-one, 2-methyl-	94	96.10
8	5.069	1755741	3.81	Ethanone, 1-(2-furanyl)-	87	95.00
9	5.386	602464	1.31	2,5-Hexanedione	98	43.05
10	6.171	3078527	6.67	2-Furancarboxaldehyde, 5-methyl-	96	110.05
11	6.569	448014	0.97	Phenol	89	94.05
12	6.798	279874	0.61	2-Cyclopenten-1-one, 3,4-dimethyl-	96	95.05
13	6.909	290465	0.63	2-Cyclopenten-1-one, 2,3-dimethyl-	89	67.05
14	7.569	3197117	6.93	2-Cyclopenten-1-one, 2-hydroxy-3-methyl-	98	112.05
15	7.788	584489	1.27	2-Cyclopenten-1-one, 2,3-dimethyl-	95	67.05
16	8.183	4086956	8.86	2-Cyclopenten-1-one, 3-ethyl-2-hydroxy-	90 1	126.10
17	8.547	930152	2.02	4H-1,3-Benzodioxin-4-one, hexahydro-4a,5-dimethyl-, [4as-(4a.alpha.,5.beta.,8a.beta.)]-	80	110.10
18	8.928	880381	1.91	2-Cyclopenten-1-one, 3-ethyl-2-hydroxy-	92	126.10
19	9.198	517621	1.12	Bicyclo[3.2.1]octan-3-one, 6-hydroxy-, exo-(.+-.)-	73	112.05

20	9.348	283040	0.61	Phenylethyl Alcohol	87	91.05
21	9.475	1693872	3.67	2-Cyclopenten-1-one, 3-ethyl-2-hydroxy-	94	126.10
22	9.937	747770	1.62	2-Hydroxy-3-propyl-2-cyclopenten-1-one	82	55.00
23	10.027	768634	1.67	Cyclohexanone, 5-methyl-2-(1-methylethyl)-, cis-	78	94.05
24	10.556	593010	1.29	4,4-Dimethyl-2-propenylcyclopentanone	83	152.10
25	11.211	376120	0.82	2-Hydroxy-3-propyl-2-cyclopenten-1-one	86	125.05
26	11.918	302966	0.66	2-Cyclohexen-1-one, 4-(1-methylethyl)-	83	43.05
27	12.206	619485	1.34	1,2-Benzenediol, 3-methyl-	95	124.05
28	12.505	2306256	5.00	Ethanone, 1-(2,5-dihydroxyphenyl)-	93	137.05
29	13.333	648102	1.41	3,4,5,6,7,8-Hexahydro-2H-chromene	76	110.05
30	19.968	1982948	4.30	Tetradecanoic acid	96	73.05
31	21.022	880009	1.91	Butylamine, N,N-dipentyl-	76	156.10
32	22.339	2563879	5.56	Palmitoleic acid	79	170.10
33	22.388	386240	0.84	Octahydrodipyrrolo[1,2-a:1',2'-d]pyrazine-5,10-dione-, (5aR,10aR) (isomer 1)	74	70.10
34	22.572	3124326	6.77	n-Hexadecanoic acid	95	73.05
35	24.639	1786509	3.87	Oleic Acid	94	55.05
36	24.868	624220	1.35	Octadecanoic acid	89	43.05
37	27.414	3894429	8.44	Hexanedioic acid, bis(2-ethylhexyl) ester	97	129.05
		46122963	100.00			

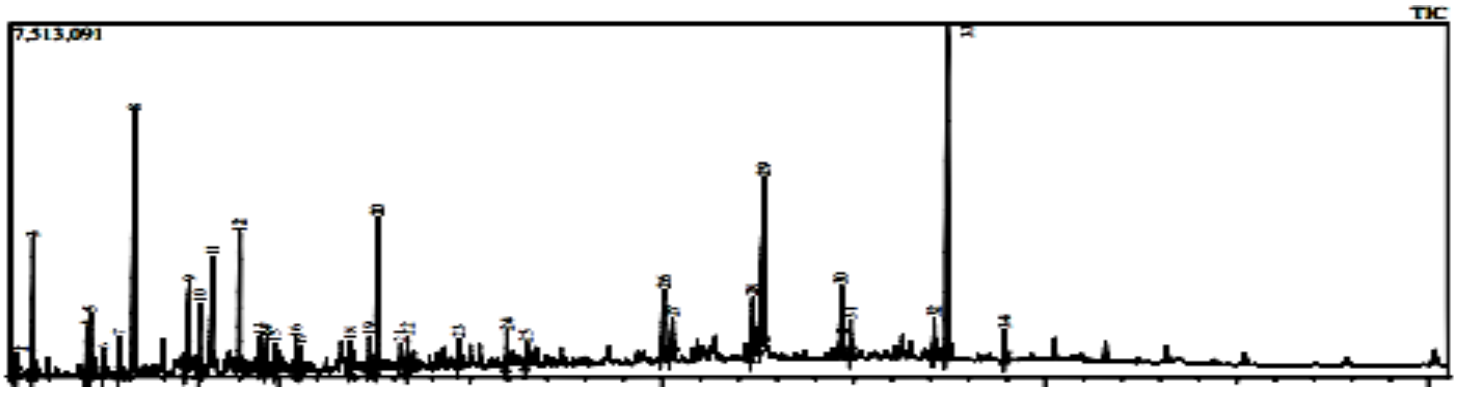

Figure D-7: GCMS analysis for the 6g 10wt% 5 minutes run.

Table D-7: GCMS results for the 6g 10wt% 5 minutes run

Peak#	R. Time	Area	Area%	Name	Similarity	Base m/z
1	3.053	632484	0.50	Propanoic acid, 2-hydroxy-2-methyl-, ethyl ester 8	89	59.00

2	3.163	700782	0.55	2-Hydroxy-3-pentanone	96	45.05
3	3.598	5634005	4.45	Furfural	94	96.00
4	4.985	1789366	1.41	1H-Imidazole-4-carboxylic acid	81	112.05
5	5.089	2383081	1.88	Ethanone, 1-(2-furanyl)-	95	95.00
6	5.415	902798	0.71	2,5-Hexanedione	98	43.00
7	5.829	1551342	1.22	3(2H)-Furanone, 2-(1-hydroxy-1-methyl-2-oxopropyl)-2,5-dimethyl-	83	112.05
8	6.252	19747914	15.59	2-Furancarboxaldehyde, 5-methyl-	96	110.05
9	7.673	8543499	6.74	2-Cyclopenten-1-one, 2-hydroxy-3-methyl-	98	112.05
10	7.938	2879664	2.27	Benzenemethanethiol	77	91.05
11	8.266	6413082	5.06	2-Cyclopenten-1-one, 3-ethyl-2-hydroxy-	86	126.05
12	8.978	5566789	4.39	2-Cyclopenten-1-one, 3-ethyl-2-hydroxy-	93	126.05
13	9.514	1.13	1.13	2-Cyclopenten-1-one, 3-ethyl-2-hydroxy-	88	126.05
14	9.683	1347924	1.06	2(3H)-Furanone, 5-acetyldihydro-	95	85.00
15	9.890	708520	0.56	1,4-Benzenediol, 2,6-dimethyl-	77	138.05
16	10.445	1287791	1.02	2,3-Dihydroxybenzaldehyde	94	138.00
17	10.582	946086	0.75	4,4-Dimethyl-2-propenylcyclopentanone	83	152.05
18	11.866	1014760	0.80	4-Acetyl-1-methylcyclohexene	84	138.05
19	12.366	1501910	1.19	1,2-Benzenediol, 3-methyl-	97	124.05
20	12.573	7428618	5.86	Ethanone, 1-(2,5-dihydroxyphenyl)-	93	137.00
21	13.182	943749	0.75	Benzaldehyde, 3-hydroxy-	83	122.05
22	13.368	1203606	0.95	6R,7aS)-3,6-Dimethyl-5,6,7,7a-tetrahydrobenzofuran-2(4H)-one	77	166.00
23	14.696	1313328	1.04	Benzaldehyde, 3-methoxy-	88	136.05
24	15.954	1219694	0.96	Bicyclo[3.3.1]nona-2,6-diene, 2,6-bis(acetoxy)-	79	152.00
25	16.465	0.82	0.82	Benzoic acid, 3-hydroxy-, 1-methylpropyl ester	83	121.00
26	20.045	4168506	3.29	Tetradecanoic acid	96	73.00
27	20.271	2788052	2.20	2,3-Diketo-6-methoxybenzo[b]pyran	73	191.95
28	22.371	3382669	2.67	6-Pentadecenoic acid, 13-methyl-, (6Z)-	85	55.05
29	22.663	15740976	12.43	n-Hexadecanoic acid	96	73.00
30	24.679	2468735	1.95	Oleic Acid	94	55.00
31	24.915	1239476	0.98	Octadecanoic acid	95	73.00

32	27.099	1860930	1.47	9-Octadecenamide, (Z)-	87	59.00
33	27.436	15649298	12.35	Hexanedioic acid, bis(2-ethylhexyl) ester	97	129.05
34	28.938	1246427	0.98	Bis(2-ethylhexyl) phthalate	68	149.00
		126675820	100.00			

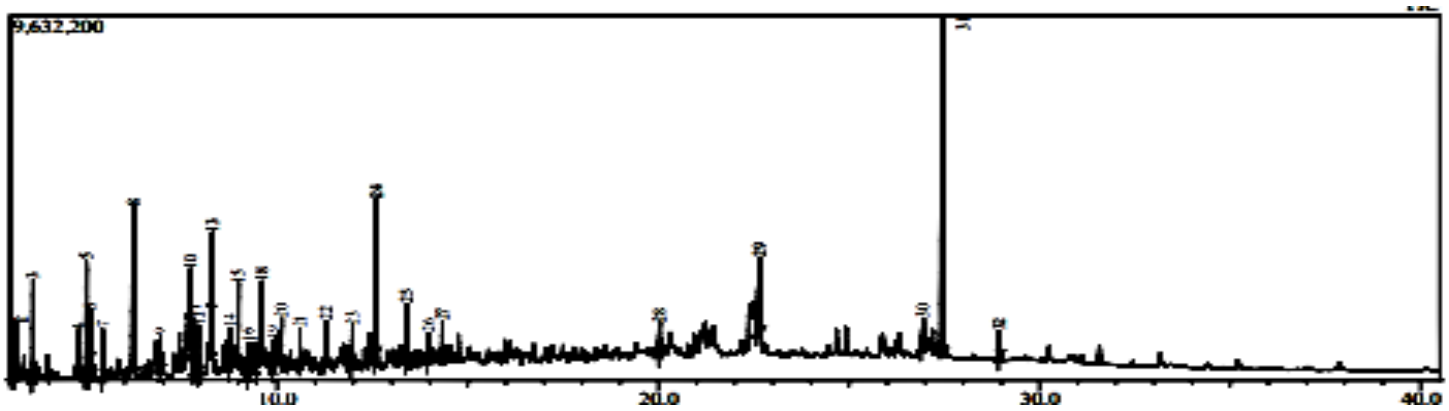

Figure D-8: GCMS analysis for the 6g 10wt% 10 minutes run.

Table D-8: GCMS results for the 6g 10wt% 10 minutes run

Peak#	R. Time	Area	Area%	Name	Similarity	Base m/z
1	3.055	2696463	2.07	Propanoic acid, 2-hydroxy-2-methyl-, ethyl ester	90	59.00
2	3.167	2750133	2.12	2-Hydroxy-3-pentanone	96	45.05
3	3.599	5060305	3.89	2-Cyclopenten-1-one	87	82.05
4	4.789	1967036	1.51	4-Hydroxy-3-hexanone	94	59.05
5	4.995	5829038	4.48	2-Cyclopenten-1-one, 2-methyl-	93	96.05
6	5.095	3045415	2.34	Ethanone, 1-(2-furanyl)-	93	95.00
7	5.421	2411168	1.85	2,5-Hexanedione	98	43.00
8	6.241	14606643	11.24	2-Furancarboxaldehyde, 5-methyl-	94	110.00
9	6.934	1.01	1.01	2-Cyclopenten-1-one, 2,3-dimethyl-	92	67.05
10	7.721	3668675	2.82	2-Cyclopenten-1-one, 2-hydroxy-3-methyl-	96	112.05
11	7.834	2997063	2.31	2-Cyclopenten-1-one, 2,3-dimethyl-	93	110.05
12	7.947	2253056	1.73	1H-Pyrazole-4-carboxaldehyde, 1,5-dimethyl-	79	124.05
13	8.303	4012840	3.09	2-Cyclohexen-1-one, 2-hydroxy-3-methyl-6-(1-methylethyl)-	77	126.05
14	8.769	2498615	1.92	2-Acetylcyclopentanone	70	110.95
15	8.983	3504724	2.70	2-Cyclopenten-1-one, 3-ethyl-2-hydroxy-	91	126.05

16	9.238	1602161	1.23	2-[(2-Oxocycloheptyl)methyl]cycloheptan-1-one (isomer 2)	72	112.00
17	9.341	1257275	0.97	2,3-Dimethyl-4-hydroxy-2-butenoic lactone	82	55.05
18	9.595	8459207	6.51	2-Cyclopenten-1-one, 3-ethyl-2-hydroxy-	95	126.05
19	9.903	1284896	0.99	Cyclohexanone, 3-vinyl-3-methyl-	77	138.00
20	10.124	2116852	1.63	1,3-Cyclopentanedione, 2-ethyl-2-methyl-	77	94.00
21	10.599	2232084	1.72	Cyclohexanone, 5-methyl-2-(1-methylethylidene)-	83	152.05
22	11.291	1810355	1.39	2-Hydroxy-3-propyl-2-cyclopenten-1-one	88	125.05
23	11.976	2450789	1.89	2-Cyclohexen-1-one, 4-(1-methylethyl)-	86	43.00
24	12.598	10464266	8.05	Ethanone, 1-(2,5-dihydroxyphenyl)-	93	137.00
25	13.386	3022060	2.32	1,8(2H,5H)-Naphthalenedione, hexahydro-	78	110.05
26	13.963	1382958	1.06	7-Hydroxy-1-indanone	88	148.00
27	14.331	1633976	1.26	2,5-Dihydroxypropiophenone	92	137.00
28	20.039	1879577	1.45	Tetradecanoic acid	95	73.00
29	22.668	7802859	6.00	n-Hexadecanoic acid	81	170.05
30	26.947	2625144	2.02	Phe-Leu-OH	91	91.05
31	27.447	20189516	15.53	Hexanedioic acid, bis(2-ethylhexyl) ester	96	129.05
32	28.942	1166159	0.90	Bis(2-ethylhexyl) phthalate	80	149.00
		129992711	100.00			

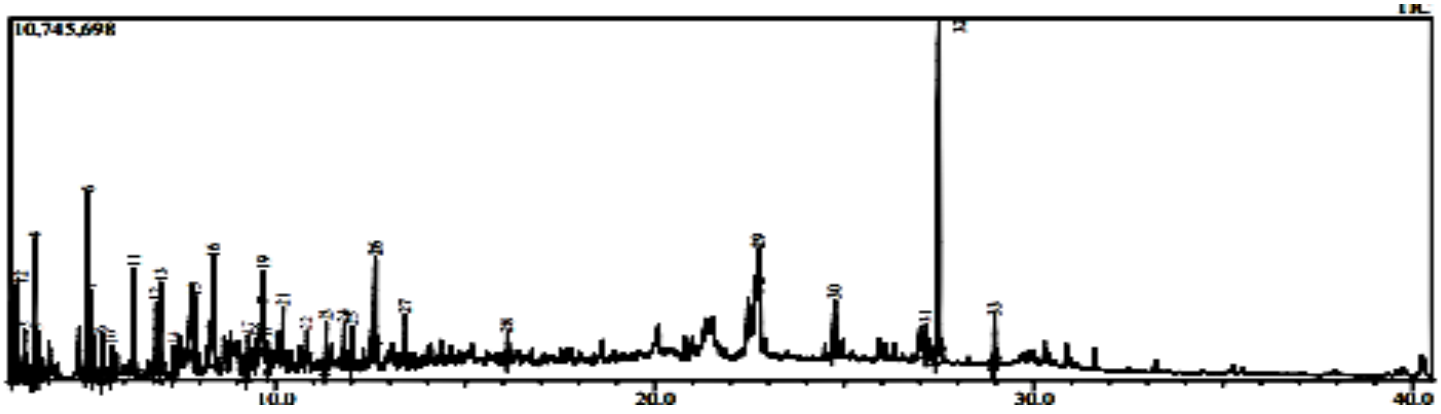

Figure D-9: GCMS analysis for the 6g 10wt% 15 minutes run.

Table D-9: GCMS results for the 6g 10wt% 15 minutes run

Peak#	R. Time	Area	Area%	Name	Similarity	Base m/z
1	3.085	6946384	4.23	Oxirane, tetramethyl-	90	59.05
2	3.198	5641385	3.44	2-Hydroxy-3-pentanone	97	45.05

3	3.379	2487248	1.52	1-Hydroxy-3-methyl-2-butanone	93	43.05
4	3.634	9852117	6.00	2-Cyclopenten-1-one	95	82.05
5	3.744	1923722	1.17	Cyclopentanone, 2-methyl-	98	42.05
6	5.043	15171824	9.24	2-Cyclopenten-1-one, 2-methyl-	93	96.05
7	5.127	3404354	2.07	Ethanone, 1-(2-furanyl)-	96	95.00
8	5.195	2178716	1.33	Pentanal, 2,3-dimethyl-	78	58.00
9	5.447	2278258	1.39	2,5-Hexanedione	98	43.00
10	5.670	1648430	1.00	2-Cyclopenten-1-one, 2,3-dimethyl-	88	67.05
11	6.261	10056083	6.13	2-Cyclopenten-1-one, 3-methyl-	83	96.05
12	6.845	5113127	3.12	2-Cyclopenten-1-one, 3,4-dimethyl-	89	95.05
13	6.968	5146663	3.14	2-Cyclopenten-1-one, 2,3-dimethyl-	95	67.05
14	7.312	1810230	1.10	3-n-Propyl-5-methylhexan-2-one	85	71.05
15	7.866	7.866	2.53	2-Cyclopenten-1-one, 2,3-dimethyl-	92	110.10
16	8.367	6265973	3.82	3-Cyclopentylpropionic acid, 2-methylphenyl ester	77	108.05
17	9.273	2764958	1.68	2,5-Cyclohexadiene-1,4-dione, 2,5-dimethyl-	78	136.05
18	9.469	1742340	1.06	Phenylethyl Alcohol	96	91.05
19	9.681	3445195	2.10	2-Cyclopenten-1-one, 3-ethyl-2-hydroxy	94	126.10
20	9.798	1403687	0.86	2-Ethyl-3-methylcyclopent-2-en-1-one	84	124.10
21	10.196	3711691	2.26	Cyclohexanone, 5-methyl-2-(1-methylethyl)-, cis-	78	94.05
22	10.824	1513620	0.92	2-Acetonylcyclopentanone	82	43.00
23	11.339	3424777	2.09	2-Hydroxy-3-propyl-2-cyclopenten-1-one	87	125.05
24	11.808	2366788	1.44	2-Cyclohexen-1-one, 2-hydroxy-3-methyl-6-(1-methylethyl)-	83	126.10
25	12.010	2655653	1.62	2-Cyclohexen-1-one, 4-(1-methylethyl)-	43.00	43.00
26	12.630	6771023	4.13	Ethanone, 1-(2,5-dihydroxyphenyl)-	92	137.05
27	13.421	2880418	1.76	3,4,5,6,7,8-Hexahydro-2H-chromene	79	110.05
28	16.118	1377474	0.84	Cycloheptasiloxane, tetradecamethyl-	93	281.05
29	22.749	2267438	1.38	n-Hexadecanoic acid	94	73.05
30	24.750	4923238	3.00	9-Octadecenoic acid, (E)-	94	55.00
31	27.161	1465763	0.89	9-Octadecenamide, (Z)-	94	59.00

32	27.503	34542242	21.05	Hexanedioic acid, bis(2-ethylhexyl) ester	96	129.10
33	28.967	2772938	1.69	Bis(2-ethylhexyl) phthalate	75	149.00
		164111107	100.00			

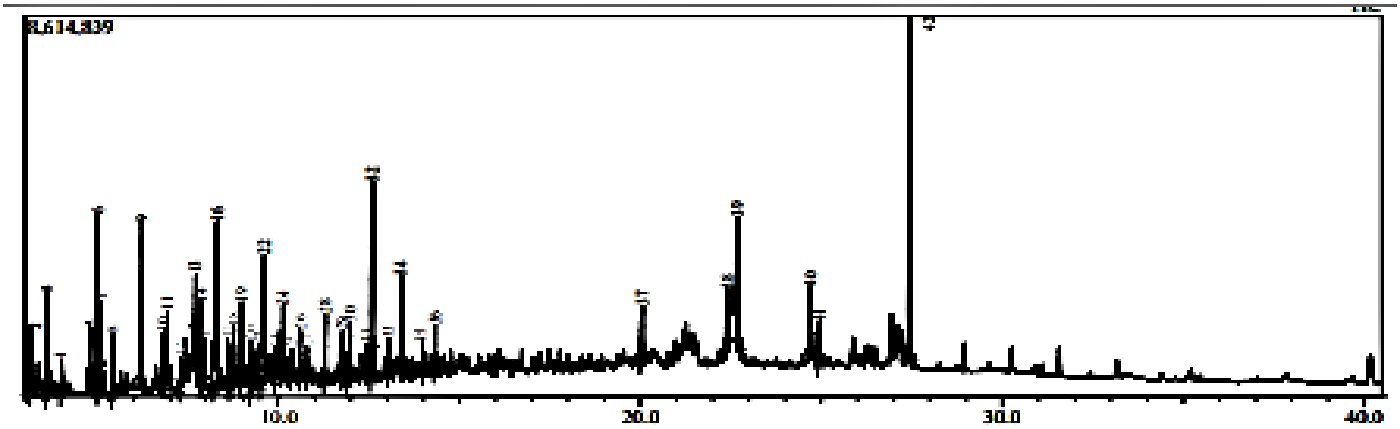

Figure D-10: GCMS analysis for the 6g 10wt% 20 minutes run.

Table D-10: GCMS results for the 6g 10wt% 20 minutes run

Peak#	R. Time	Area	Area%	Name	Similarity	Base m/z
1	3.067	3273834	1.92	3-Hydroxy-3-methyl-2-butanone	90	59.00
2	3.178	3237902	1.90	2-Hydroxy-3-pentanone	96	45.05
3	3.607	5208506	3.05	2-Cyclopenten-1-one	94	82.05
4	3.996	2084666	1.22	1-Hydroxy-2-pentanone	88	43.05
5	4.803	2676266	1.57	4-Hydroxy-3-hexanone	94	59.00
6	5.009	9032857	5.30	2-Cyclopenten-1-one, 2-methyl-	93	93 96.05
7	5.104	4213169	2.47	Ethanone, 1-(2-furanyl)-	93	95.00
8	5.429	2647475	1.55	2,5-Hexanedione	98	43.00
9	6.235	11688030	6.86	2-Furancarboxaldehyde, 5-methyl-	92	110.00
10	6.826	2293517	1.35	2-Cyclopenten-1-one, 3,4-dimethyl-	94	95.00
11	6.940	2764691	1.62	2-Cyclopenten-1-one, 2,3-dimethyl-	92	67.05
12	7.292	1383404	0.81	Cyclopropanemethanol, .alpha.-butyl-	85	71.05
13	7.713	2408572	1.41	2-Cyclopenten-1-one, 2-hydroxy-3-methyl-	93	112.00
14	7.842	4071196	2.39	2-Cyclopenten-1-one, 2,3-dimethyl-	95	110.05
15	7.948	1564851	0.92	3,5-Dimethyl-1H-pyrazole-4-carbaldehyde	83	124.05
16	16 8.310	14837170	8.70	2-Cyclopenten-1-one, 3-ethyl-2-hydroxy-	81	126.05
17	8.607	2140177	1.26	2-Cyclopenten-1-one, 3-ethyl-	86	110.05

18	8.777	3507602	2.06	Benzene, 1-ethoxy-3-methyl-	73	108.05
19	8.983	3028275	1.78	2-Cyclopenten-1-one, 3-ethyl-2-hydroxy-	91	126.05
20	9.240	2117566	1.24	2-[(2-Oxocycloheptyl)methyl]cycloheptan-1-one (isomer 2) 7	71	112.00
21	9.438	1066499	0.63	Phenylethyl Alcohol	98	91.05
22	9.615	12902908	7.57	2-Cyclopenten-1-one, 3-ethyl-2-hydroxy-	95	126.05
23	9.907	1203751	0.71	Cyclopropane, 1,1,2-trimethyl-3-(2-methyl-1-propenyl)-	76	138.00
24	10.139	3672844	2.15	1,3-Cyclopentanedione, 2-ethyl-2-methyl-	78	94.00
25	10.369	878734	0.52	Ethanone, 1-(6-methyl-7-oxabicyclo[4.1.0]hept-1-yl)-	84	43.00
26	10.604	2697070	1.58	Cyclohexanone, 5-methyl-2-(1-methylethylidene)-	82	152.00
27	10.788	1376073	0.81	2-Acetonylcyclopentanone	89	43.00
28	11.298	3313812	1.94	2-Hydroxy-3-propyl-2-cyclopenten-1-one	87	125.05
29	11.764	1804059	1.06	2-Cyclohexen-1-one, 2-hydroxy-3-methyl-6-(1-methylethyl)-	82	126.05
30	11.979	3504999	2.06	2-Cyclohexen-1-one, 4-(1-methylethyl)-	84	43.00
31	12.456	1089554	0.64	1,2-Benzenediol, 3-methyl-	82	124.00
32	12.603	10721233	6.29	Resorcinol, 2-acetyl-	93	137.00
33	13.063	1439990	0.84	Furan, 2-[(methylthio)methyl]-	75	128.00
34	13.390	3953006	2.32	3,4,5,6,7,8-Hexahydro-2H-chromene	79	110.00
35	13.971	1366355	0.80	7-Hydroxy-1-indanone	35 88	148.00
36	14.332	2091313	1.23	2,5-Dihydroxypropiophenone	93	137.00
37	20.059	3623748	2.13	Tetradecanoic acid	94	73.00
38	22.402	3457804	2.03	6-Pentadecenoic acid, 13-methyl-, (6Z)-	94	55.05
39	22.703	4262307	2.50	Tridecanoic acid	69	170.05
40	24.703	4006152	2.35	9-Octadecenoic acid, (E)-	94	55.00
41	24.934	1685831	0.99	Octadecanoic acid	95	73.00
42	27.439	16195083	9.50	Hexanedioic acid, bis(2-ethylhexyl) ester	96	129.05
		170492851	100.00			

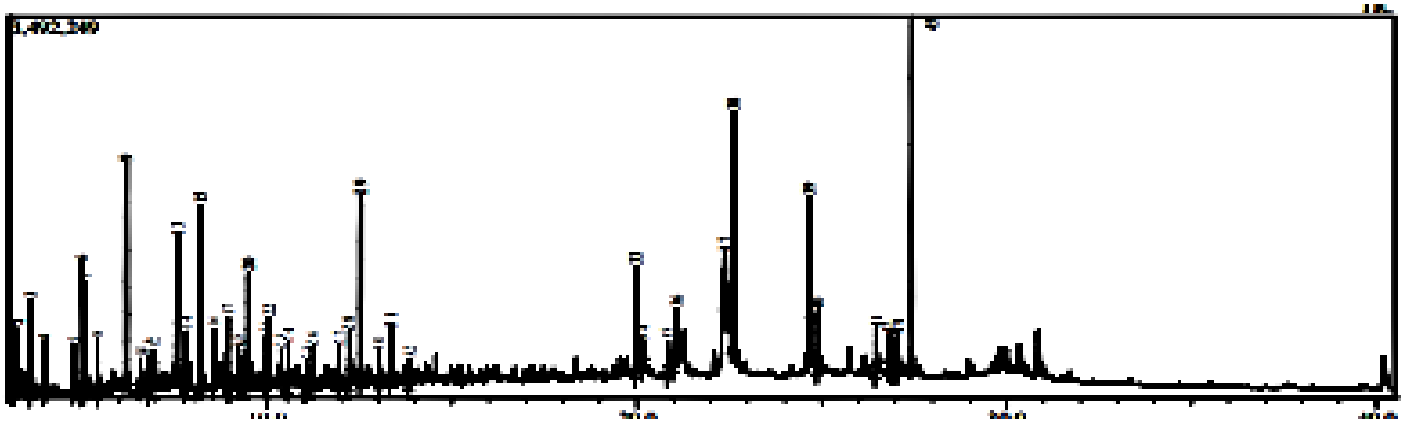

Figure D-11: GCMS analysis for the 6g 10wt% 25 minutes run.

Table D-11: GCMS results for the 6g 10wt% 25 minutes run

Peak#	R. Time	Area	Area%	Name	Similarity	Base m/z
1	3.087	1463829	2.11	Propanoic acid, 2-hydroxy-2-methyl-	90	59.05
2	3.195	1332062	1.92	2-Hydroxy-3-pentanone	96	45.05
3	3.618	2048986	2.96	2-Cyclopenten-1-one	88 8	82.05
4	3.988	1137448	1.64	3-Furanmethanol	86	43.05
5	4.784	873005	1.26	4-Hydroxy-3-hexanone	95	59.05
6	4.994	2468278	3.56	2-Cyclopenten-1-one, 2-methyl-	94	96.05
7	5.090	2724169	3.93	Ethanone, 1-(2-furanyl)-	85	95.00
8	5.409	894651	1.29	2,5-Hexanedione	98	43.05
9	6.192	4798258	6.93	2-Furancarboxaldehyde, 5-methyl-	96	110.05
10	6.584	618612	0.89	Phenol	91	94.05
11	6.817	542022	0.78	2-Cyclopenten-1-one, 3,4-dimethyl-	95	95.05
12	6.928	496307	0.72	2-Cyclopenten-1-one, 2,3-dimethyl-	89	67.10
13	7.593	4401582	6.36	2-Cyclopenten-1-one, 2-hydroxy-3-methyl-	98	112.10
14	7.808	868553	3 1.25	2-Cyclopenten-1-one, 2,3-dimethyl-	94	67.10
15	8.208	2362607	3.41	2-Cyclopenten-1-one, 3-ethyl-2-hydroxy-	90	126.10
16	8.567	1388933	2.01	4H-1,3-Benzodioxin-4-one, hexahydro-4a,5-dimethyl-, [4as-(4a.alpha.,5.beta.,8a.beta.)]-	80	110.10
17	8.948	1185501	1.71	2-Cyclopenten-1-one, 3-ethyl-2-hydroxy-	92	126.10
18	9.217	761396	1.10	2,6-Dimethyl-8-oxoocta-2,6-dienoic acid, methyl ester	71	112.05
19	9.366	530846	0.77	Phenylethyl Alcohol	79	91.05

20	9.494	2373114	3.43	2-Cyclopenten-1-one, 3-ethyl-2-hydroxy-	94	126.10
21	9.956	1061422	1.53	2-Hydroxy-3-propyl-2-cyclopenten-1-one	82	55.05
22	10.047	1073948	1.55	Cyclohexanone, 5-methyl-2-(1-methylethyl)-, cis-	77	94.05
23	10.370	421831	0.61	Naphthalene, 1,2,3,4-tetrahydro-	93	104.10
24	10.573	788878	1.14	4,4-Dimethyl-2-propenylcyclopentanone	84	152.10
25	11.065	557106	0.80	Catechol	96	110.05
26	11.230	560098	0.81	2-Hydroxy-3-propyl-2-cyclopenten-1-one	86	140.10
27	11.939	521777	0.75	2-Cyclohexen-1-one, 4-(1-methylethyl)-	84	43.00
28	12.223	1006702	1.45	1,2-Benzenediol, 3-methyl-	95	124.10
29	12.525	3112109	4.49	Resorcinol, 2-acetyl-	94	137.05
30	13.016	533505	0.77	2-Methyl-3-(methylthio) furan	70	128.05
31	31 13.352	953433	1.38	3,4,5,6,7,8-Hexahydro-2H-chromene	76	110.10
32	13.863	460767	0.67	2-Methyl-5-hydroxybenzofuran	84	148.05
33	19.999	2677430	3.87	Tetradecanoic acid	96	73.05
34	20.176	559867	0.81	6,8-Dihydroxy-3-methylisocoumarin	74	192.00
35	20.840	649918	0.94	Cyclo(L-prolyl-L-valine)	87	154.05
36	21.072	2096802	3.03	7-Ethyl-4,6-heptadecandione	79	156.10
37	22.380	717694	1.04	6-Pentadecenoic acid, 13-methyl-, (6Z)-	79	55.05
38	22.609	6071909	8.77	n-Hexadecanoic acid	95	73.05
39	24.670	2967732	4.29	Oleic Acid 94	94	55.05
40	24.899	984515	1.42	Octadecanoic acid	88	43.05
41	26.474	778511	1.12	Arachidonic acid	96	79.05
42	26.805	676041	0.98	Phe-Leu-OH	88	91.05
43	26.947	522711	0.75	Pyrrolo[1,2-a]pyrazine-1,4-dione, hexahydro-3-(phenylmethyl)-	93	125.10
44	27.054	654840	0.95	Phe-Leu-OH	88	91.05
45	27.442	5572089	8.05	Hexanedioic acid, bis(2-ethylhexyl) ester	98	129.05
		69251794	100.00			

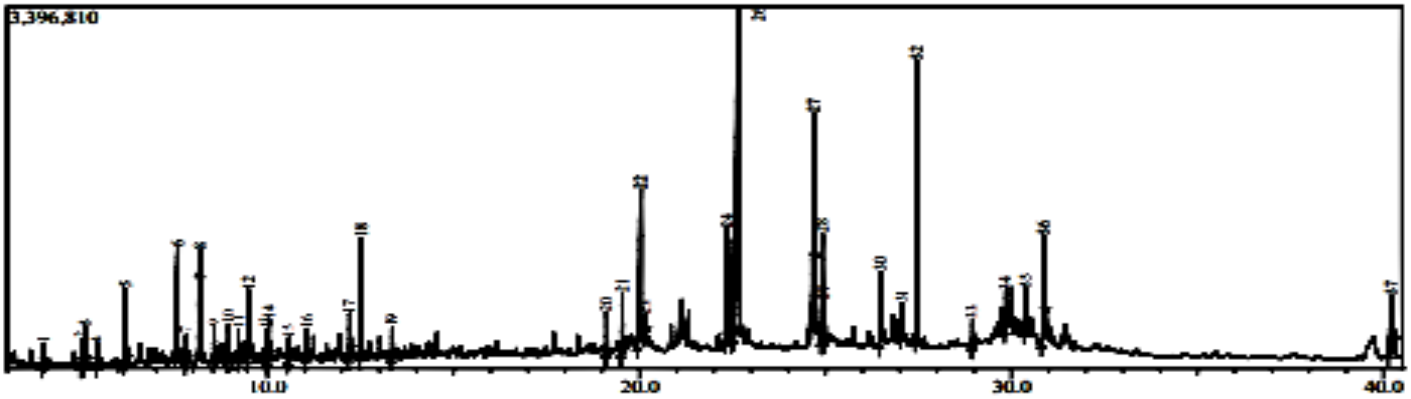

Figure D-12: GCMS analysis for the 6g 10wt% 30 minutes run.

Table D-12: GCMS results for the 6g 10wt% 30 minutes run

Peak#	R. Time	Area	Area%	Name	Similarity	Base m/z
1	3.980	417355	0.66	2-Furanmethanol	96	98.05
2	4.997	416047	0.66	2-Cyclopenten-1-one, 2-methyl-	94	6.10
3	5.092	778522	1.23	4-(Azidomethyl)-1-methylpyrazole	80	95.05
4	5.411	320273	0.51	2,5-Hexanedione	98	43.05
5	6.181	1575706	2.49	2-Furancarboxaldehyde, 5-methyl-	97	110.05
6	7.586	3422568	5.41	2-Cyclopenten-1-one, 2-hydroxy-3-methyl-	98	112.10
7	7.808	402389	0.64	2-Cyclopenten-1-one, 2,3-dimethyl-	95	67.05
8	8.193	650594	1.03	2-Cyclopenten-1-one, 3-ethyl-2-hydroxy-	90	126.10
9	8.566	882938	1.40	3-Cyclohexene-1-carboxaldehyde	77	107.05
10	8.947	543020	0.86	2-Cyclopenten-1-one, 3-ethyl-2-hydroxy-	93	126.10
11	9.219	512644	0.81	2,5-Cyclohexadiene-1,4-dione, 2,5-dimethyl-	- 76	136.05
12	9.489	1406862	2.22	2-Cyclopenten-1-one, 3-ethyl-2-hydroxy-	95	126.10
13	9.951	465476	0.74	Cyclopentane, 1-acetyl-1,2-epoxy-	85	55.05
14	10.041	603434	0.95	Cyclohexanone, 5-methyl-2-(1-methylethyl)-, cis-	77	94.05
15	10.573	459689	0.73	Cyclohexanone, 5-methyl-2-(1-methylethylidene)-	83	152.10
16	11.053	543003	0.86	Catechol	95	110.05
17	12.210	878530	1.39	1,2-Benzenediol, 3-methyl-	95	124.10
18	12.522	1954584	3.09	Ethanone, 1-(2,5-dihydroxyphenyl)-	94	137.05
19	13.352	532594	0.84	3,4,5,6,7,8-Hexahydro-2H-chromene	76	110.05
20	19.116	644593	1.02	Heptadecane	96	57.10
21	19.538	1069272	1.69	Cyclohexane, 1,3,5-triphenyl-	81	91.05
22	20.035	4766371	7.54	Tetradecanoic acid	96	73.05
23	20.171	337814	0.53	6,8-Dihydroxy-3-methylisocoumarin	73	192.00

24	22.353	3007103	4.75	6-Pentadecenoic acid, 13-methyl-, (6Z)-	84	55.05
25	22.498	1001047	1.58	Pyrrolo[1,2-a]pyrazine-1,4-dione, hexahydro-3-(2-methylpropyl)-	84	154.05
26	22.654	13753891	21.75	n-Hexadecanoic acid	97	73.05
27	24.700	4272518	6.76	Oleic Acid	94	55.05
28	24.920	2202333	3.48	Octadecanoic acid	91	73.05
29	24.970	667319	1.06	Ethyl Oleate	92	55.05
30	26.486	1251449	1.98	Arachidonic acid	96	79.10
31	27.061	596812	0.94	Phe-Leu-OH	71	91.05
32	27.445	4901304	7.75	Hexanedioic acid, bis(2-ethylhexyl) ester	98	129.05
33	28.955	411923	0.65	Bis(2-ethylhexyl) phthalate	96	149.00
34	29.851	800836	1.27	9-Methylheneicosane	90	57.10
35	30.376	1277185	2.02	Hexatriacontane	88	57.10
36	30.854	2937864	4.65	Tetrapentacontane	92	57.10
37	40.222	2581089	4.08	Stigmasta-5,24(28)-dien-3-ol, (3.beta.,24Z)-	97	314.20
		63246951	100.00			

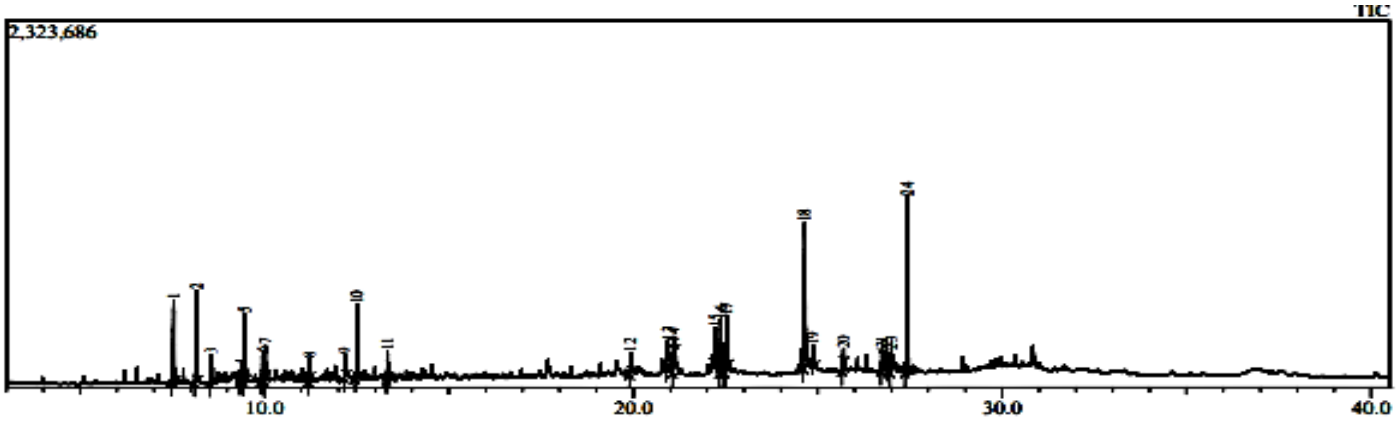

Figure D-13: GCMS analysis for the 10g 10wt% 5 minutes run.

Table D-13: GCMS results for the 10g 10wt% 5 minutes run

Peak#	R. Time	Area	Area%	Name	Similarity	Base m/z
1	7.543	1143898	7.68	2-Cyclopenten-1-one, 2-hydroxy-3-methyl-	98	112.10
2	8.161	1400119	9.40	2-Cyclopenten-1-one, 3-ethyl-2-hydroxy-	90	126.10
3	8.563	519335	519335	Phenol, 3-methyl-	84	108.10
4	9.362	145149	0.97	Phenylethyl Alcohol	94	91.10
5	9.472	817319	5.49	2-Cyclopenten-1-one, 3-ethyl-2-hydroxy-	97	97
6	9.944	330036	2.22	2-Hydroxy-3-propyl-2-cyclopenten-1-one	83	55.05

7	10.027	349215	2.34	Cyclohexanone, 5-methyl-2-(1-methylethyl)-, cis-	79	94.05
8	11.220	211330	1.42	2-Hydroxy-3-propyl-2-cyclopenten-1-one	87	112.05
9	12.194	260538	1.75	1,2-Benzenediol, 3-methyl-	95	124.10
10	12.508	794779	5.34	Ethanone, 1-(2,5-dihydroxyphenyl)-	93	137.00
11	13.340	289560	1.94	3,4,5,6,7,8-Hexahydro-2H-chromene	79	110.05
12	19.937	266126	1.79	Tetradecanoic acid	90	73.05
13	20.937	764552	5.13	7-Ethyl-4,6-heptadecandione	76	156.10
14	21.111	209971	1.41	Cyclo(L-prolyl-L-valine)	92	154.05
15	22.231	504046	3.38	Pyrrolo[1,2-a]pyrazine-1,4-dione, hexahydro-3-(2-methylpropyl)-	79	154.05
16	22.373	857232	5.75	Octahydrodipyrrolo[1,2-a:1',2'-d]pyrazine-5,10-dione-, (5aR,10aR) (isomer 2)	16 85	70.10
17	22.532	650649	4.37	n-Hexadecanoic acid	96	73.05
18	24.649	2392694	16.06	Oleic Acid	93	55.05
19	24.873	161849	1.09	Octadecanoic acid	93	73.05
20	25.694	200066	1.34	2,5-Piperazinedione, 3-benzyl-6-isopropyl-	89	91.10
21	26.745	125096	0.84	Phe-Leu-OH	88	91.10
22	26.889	188846	1.27	Pyrrolo[1,2-a]pyrazine-1,4-dione, hexahydro-3-(phenylmethyl)-	91	125.10
23	26.996	246739	1.66	Phe-Leu-OH	92	91.05
24	27.422	2067185	13.88	Hexanedioic acid, bis(2-ethylhexyl) ester	98	129.05
		14896329	100.00			

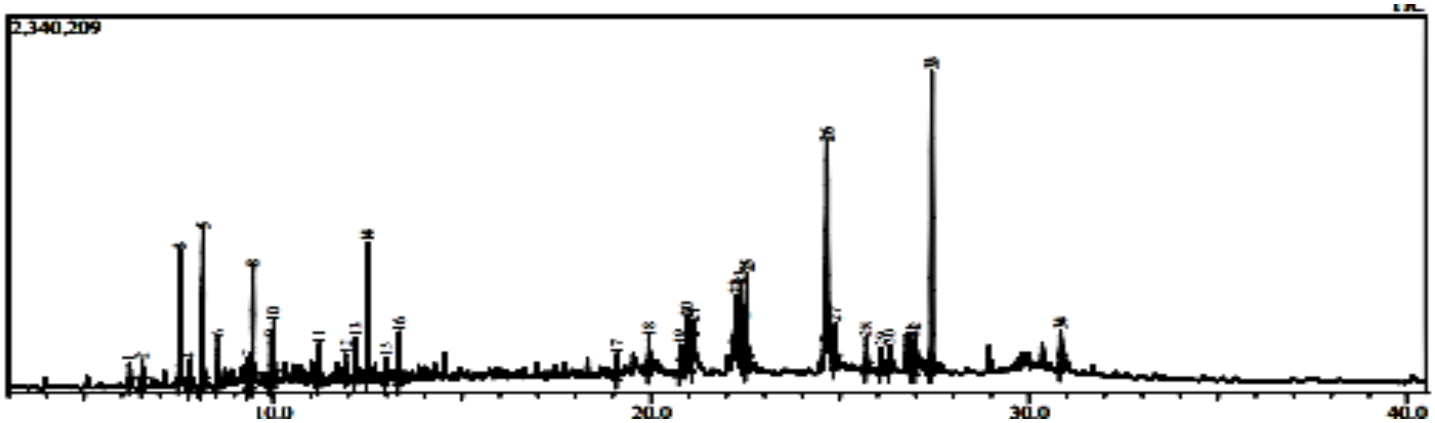

Figure D-14: GCMS analysis for the 10g 10wt% 10 minutes run.

Table D-14: GCMS results for the 10g 10wt% 10 minutes run

Peak#	R. Time	Area	Area%	Name	Similarity	Base m/z

1	6.195	160400	0.59	2-Cyclopenten-1-one, 3-methyl-	96	96.05
2	6.539	248379	0.91	Phenol	97	94.05
3	7.536	1878340	6.90	-Cyclopenten-1-one, 2-hydroxy-3-methyl-	98	112.05
4	7.791	234785	0.86	2-Cyclopenten-1-one, 2,3-dimethyl-	95	67.05
5	8.154	2403886	8.83	2-Cyclopenten-1-one, 3-ethyl-2-hydroxy-	90	126.10
6	8.552	833410	3.06	Phenol, 3-methyl-	83	108.10
7	7 9.350	207400	0.76	Phenylethyl Alcohol	94	91.05
8	9.465	1341536	4.93	2-Cyclopenten-1-one, 3-ethyl-2-hydroxy-	97	126.10
9	9.933	551507	2.02	Cyclohexanone, 2-acetyl-	83	55.05
10	10.020	601991	2.21	Cyclohexanone, 5-methyl-2-(1-methylethyl)-, cis-	76	94.05
11	11.211	336317	1.23	2-Hydroxy-3-propyl-2-cyclopenten-1-one	86	125.10
12	11.920	200162	0.73	2-Cyclohexen-1-one, 4-(1-methylethyl)-	85	43.00
13	12.190	419230	1.54	1,2-Benzenediol, 3-methyl-	93	124.05
14	12.500	1354092	4.97	Ethanone, 1-(2,5-dihydroxyphenyl)-	93	137.00
15	12.991	207886	0.76	2-Methyl-3-(methylthio) furan	71	128.05
16	13.334	502522	1.85	3,4,5,6,7,8-Hexahydro-2H-chromene	78	110.05
17	17 19.103	207119	0.76	Heptadecane	96	57.10
18	19.941	357373	1.31	Tetradecanoic acid	91	73.05
19	20.774	266286	0.98	Cyclo(L-prolyl-L-valine)	96	154.05
20	20.950	777270	2.85	7-Ethyl-4,6-heptadecandione	76	156.10
21	21.121	353554	1.30	Cyclo(L-prolyl-L-valine)	93	154.05
22	22.240	923381	3.39	Pyrrolo[1,2-a]pyrazine-1,4-dione, hexahydro-3-(2-methylpropyl)-	79	154.05
23	22.377	1319189	4.84	Octahydrodipyrrolo[1,2-a:1',2'-d]pyrazine-5,10-dione-, (5aR,10aR) (isomer 1)	87	70.10
24	22.445	825434	3.03	Hexahydro-3-(1-methylpropyl)pyrrolo[1,2-a]pyrazine-1,4-dione	92	154.05
25	22.539	1113618	4.09	n-Hexadecanoic acid	96	73.00
26	24.657	3252809	11.94	9-Octadecenoic acid, (E)-	92	55.05
27	24.879	533915	1.96	Octadecanoic acid	91	73.05
28	25.704	402179	1.48	2,5-Piperazinedione, 3-benzyl-6-isopropyl-	90	91.05
29	26.093	215474	0.79	2,5-Piperazinedione, 3-benzyl-6-isopropyl-	90	91.05
30	26.316	232824	0.85	9-Octadecenoic acid, 12-hydroxy-, methyl ester, (Z)-	90	55.05

31	26.898	422641	1.55	Pyrrolo[1,2-a]pyrazine-1,4-dione, hexahydro-3-(phenylmethyl)-	92	125.10
32	27.007	374952	1.38	Phe-Leu-OH	93	91.05
33	27.427	3579494	13.14	Hexanedioic acid, bis(2-ethylhexyl) ester	98	129.05
34	30.835	595578	2.19	Tetrapentacontane	91	57.05
		27234933	100.00			

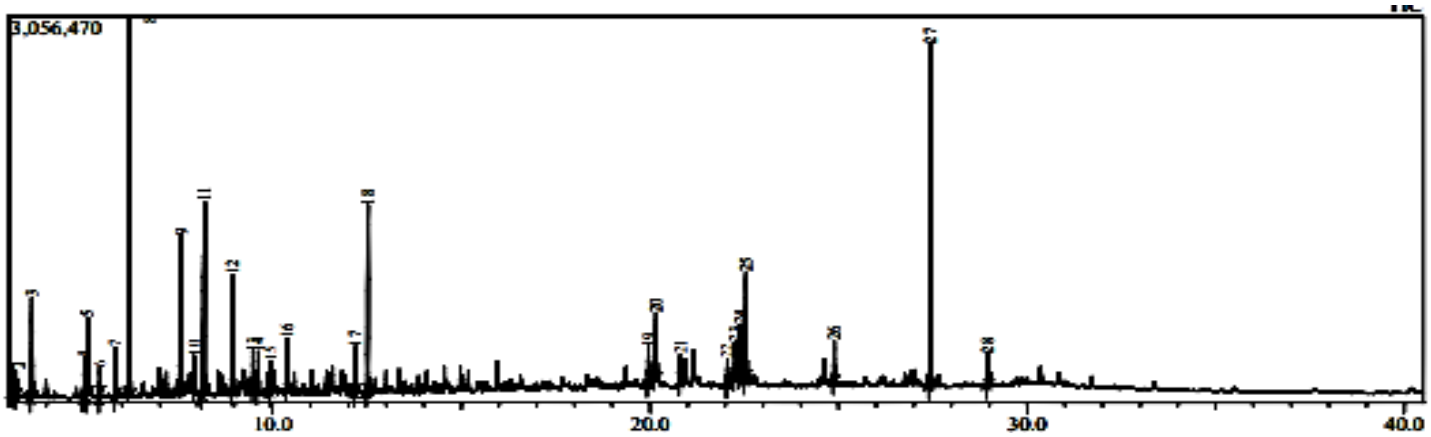

Figure D-15: GCMS analysis for the 10g 10wt% 15 minutes run.

Table D-15: GCMS results for the 10g 10wt% 15 minutes run

Peak#	R. Time	Area	Area%	Name	Similarity	Base m/z
1	3.086	375873	0.97	Propanoic acid, 2-hydroxy-2-methyl-	90	59.05
2	3.194	379794	0.98	2-Hydroxy-3-pentanone	95	45.05
3	3.611	1828634	4.74	Furfural	95	96.00
4	4.997	559747	1.45	2-Cyclopenten-1-one, 2-methyl-	83	96.10
5	5.088	1252247	3.25	Ethanone, 1-(2-furanyl)-	94	95.00
6	5.411	340576	0.88	2,5-Hexanedione	98	43.05
7	5.829	654349	1.70	2,5-Furandione, dihydro-3-methylene-	81	40.05
8	6.196	6326684	16.40	2-Furancarboxaldehyde, 5-methyl-	96	110.05
9	7.579	3553455	9 79.21	2-Cyclopenten-1-one, 2-hydroxy-3-methyl-	98	112.10
10	7.915	436111	1.13	Benzenemethanethiol	77	91.05
11	8.196	4656737	12.07	2-Cyclopenten-1-one, 3-ethyl-2-hydroxy-	89	126.10
12	8.947	1655607	4.29	2-Cyclopenten-1-one, 3-ethyl-2-hydroxy-	93	126.10
13	9.472	453368	1.	2-Cyclopenten-1-one, 3-ethyl-2-hydroxy-	94	126.05

14	9.614	512409	1.33	2(3H)-Furanone, 5-acetyldihydro-	95	85.05
15	9.946	447235	1.16	Cyclopentane, 1-acetyl-1,2-epoxy-	84	55.05
16	10.372	796592	2.07	Naphthalene, 1,2,3,4-tetrahydro-	95	104.10
17	12.198	597829	1.55	1,2-Benzenediol, 3-methyl-	96	124.05
18	12.520	2582785	6.70	Ethanone, 1-(2,5-dihydroxyphenyl)-	94	137.00
19	19.960	465576	1.21	Tetradecanoic acid	94	73.05
20	20.168	1084424	2.81	2,3-Diketo-6-methoxybenzo[b]pyran	74	192.00
21	20.811	352790	0.91	Cyclo(L-prolyl-L-valine)	95	154.05
22	22.049	365405	0.95	Hexahydro-3-(1-methylpropyl)pyrrolo[1,2-a]pyrazine-1,4-dione	95	154.05
23	22.260	541259	1.40	Pyrrolo[1,2-a]pyrazine-1,4-dione, hexahydro-3-(2-methylpropyl)-	88	154.05
24	22.400	822416	2.13	5,10-Diethoxy-2,3,7,8-tetrahydro-1H,6H-dipyrrolo[1,2-a:1',2'-d]pyrazine	80	70.10
25	22.550	1651368	4.28	n-Hexadecanoic acid	96	73.05
26	24.883	546910	1.42	Octadecanoic acid	95	73.05
27	27.441	4902736	12.71	Hexanedioic acid, bis(2-ethylhexyl) ester	98	129.05
28	28.953	423704	1.10	Bis(2-ethylhexyl) phthalate	96	149.00
		38566620	100.00			

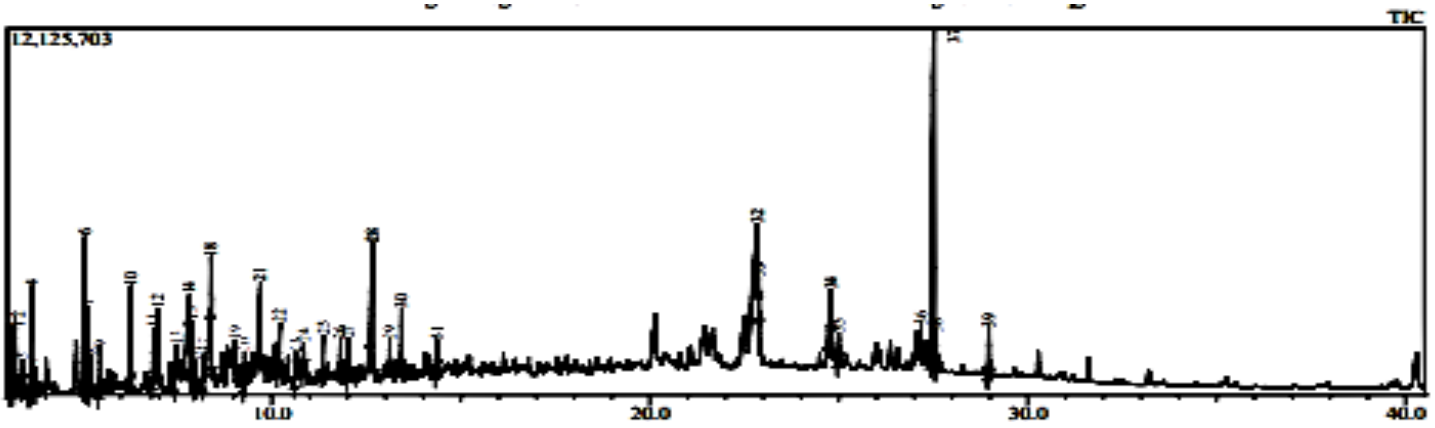

Figure D-16: GCMS analysis for the 10g 10wt% 20 minutes run.

Table D-16: GCMS results for the 10g 10wt% 20 minutes run

Peak#	R. Time	Area	Area%	Name	Similarity	Base m/z

1	3.081	6750083	6750083	Propanoic acid, 2-hydroxy-2-methyl-	90	59.00
2	3.197	6597135	3.31	2-Hydroxy-3-pentanone	96	45.05
3	3.378	1839748	0.92	3-Pentanone, 2,4-dimethyl-	93	43.05
4	3.638	8924721	4.48	2-Cyclopenten-1-one	95	82.05
5	3.747	1293775	0.65	Cyclopentanone, 2-methyl-	97	42.05
6	.049	14558813	7.31	2-Cyclopenten-1-one, 2-methyl-	92	96.05
7	5.136	8419404	4.23	Ethanone, 1-(2-furanyl)-	94	95.00
8	5.205	2489275	1.25	Pentanal, 2,3-dimethyl-	76	58.00
9	5.458	2969852	.49	2,5-Hexanedione	98	43.00
10	6.271	11351958	5.70	2-Furancarboxaldehyde, 5-methyl-	84	110.05
11	6.854	4639264	2.33	2-Cyclopenten-1-one, 3,4-dimethyl-	92	95.05
12	6.970	3889298	1.95	2-Cyclopenten-1-one, 2,3-dimethyl-	94	67.05
13	7.476	3138382	1.58	1H-Imidazole-4-carboxylic acid, 5-methyl-	77	54.05
14	7.812	2531064	1.27	2-Cyclopenten-1-one, 2-hydroxy-3-methyl-	97	112.05
15	7.880	5407320	2.72	2-Cyclopenten-1-one, 2,3-dimethyl-	93	110.05
16	7.981	1381287	0.69	3,5-Dimethyl-1H-pyrazole-4-carbaldehyde	83	124.05
17	8.208	1922154	0.97	Cyclohexanol, 2,2-dimethyl-	80	82.05
18	8.395	3831443	1.92	Phenol, 2-methyl-	79	108.05
19	9.018	1191126	0.60	2-Cyclopenten-1-one, 3-ethyl-2-hydroxy-	91	126.10
20	9.273	2280221	1.15	1,4-Diacetoxybicyclo[2.2.2]oct-2-ene	71	112.05
21	9.696	10665871	5.36	2-Cyclopenten-1-one, 3-ethyl-2-hydroxy-	95	126.10
22	10.209	4265387	2.14	Cyclohexanone, 5-methyl-2-(1-methylethyl)-, cis-	78	94.05
23	10.632	1486336	0.75	Pulegone	81	152.05
24	10.835	1836098	0.92	1,2,2,3-Tetramethylcyclopent-3-enol	79	43.00
25	11.352	3242060	1.63	2-Hydroxy-3-propyl-2-cyclopenten-1-one	87	125.10
26	11.811	2035583	1.02	2-Cyclohexen-1-one, 2-hydroxy-3-methyl-6-(1-methylethyl)-	84	126.05
27	12.021	3492170	1.75 2-	2-Cyclohexen-1-one, 4-(1-methylethyl)-	80	43.00
28	12.652	11093168	5.57	Ethanone, 1-(2,5-dihydroxyphenyl)-	92	137.05
29	13.114	1655286	0.83	2-Methyl-3-(methylthio) furan	70	128.05
30	13.433	3999065	2.01	3,4,5,6,7,8-Hexahydro-2H-chromene	79	110.05
31	14.370	2294930	1.15	2,5-Dihydroxypropiophenone	91	137.00
32	22.845	2663463	1.34	n-Hexadecanoic acid	86	73.05
33	22.878	0.43	0.43	2,5-Piperazinedione, 3,6-bis(2-methylpropyl)-	88	170.10
34	24.789	5395340	2.71 ,	9-Octadecenoic acid, (E)-	94	55.00

35	24.997	1754015	0.88	Octadecanoic acid	94	73.05
36	27.175	1592352	0.80	13-Docosenamide, (Z)-	84	59.00
37	27.512	39613620	19.90	Hexanedioic acid, bis(2-ethylhexyl) ester	96	129.05
38	27.580	2700109	.36	Cyclodecasiloxane, eicosamethyl-	70	73.05
39	28.968	3005391	1.51	Bis(2-ethylhexyl) phthalate	70	149.00
		199056033	100.00			

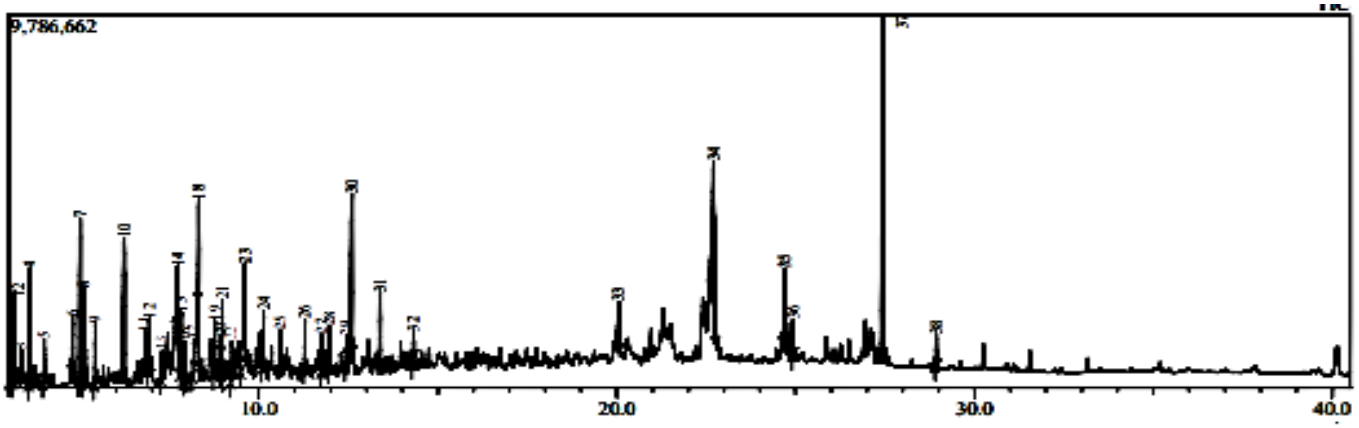

Figure D-17: GCMS analysis for the 10g 10wt% 25 minutes run.

Table D-17: GCMS results for the 10g 10wt% 25 minutes run

Peak #	R. Time	Area	Area%	Name	Similarity	Base m/z
1	3.058	5317564	2.97	3-Hydroxy-3-methyl-2-butanone	90	59.00
2	3.170	5133085	2.86	2-Hydroxy-3-pentanone	96	45.05
3	3.353	1214686	0.68	3-Pentanone, 2,4-dimethyl-	93	43.05
4	3.603	6431752	3.59	2-Cyclopenten-1-one	94	82.00
5	3.994	3248325	1.81	1-Hexene, 4,5-dimethyl-	84	43.05
6	4.791	3234472	1.80	4-Hydroxy-3-hexanone	94	59.00
7	5.004	9637591	5.38	2-Cyclopenten-1-one, 2-methyl-	93	96.00
8	5.099	7255530	4.05	Ethanone, 1-(2-furanyl)-	93	94.95
9	5.424	3165560	1.77	2,5-Hexanedione	98	43.00
10	6.230	12608249	7.03	2-Furancarboxaldehyde, 5-methyl-	92	110.00
11	6.821	1310105	0.73	2-Cyclopenten-1-one, 3,4-dimethyl-	94	95.00
12	6.935	2459033	1.37	2-Cyclopenten-1-one, 2,3-dimethyl-	91	67.00
13	7.284	1392597	0.78	Cyclopropanemethanol, .alpha.-butyl-	85	71.05
14	7.730	5917143	3.30	2-Cyclopenten-1-one, 2-hydroxy-3-methyl-	95	112.00
15	7.835	3764589	2.10	2-Cyclopenten-1-one, 2,3-dimethyl-	94	110.05
16	7.942	1893513	1.06	1H-Pyrazole-4-carboxaldehyde, 1,5-dimethyl-	82	124.00
17	8.168	1482813	0.83	Cyclohexanol	80	70.00
18	8.319	5688277	3.17	3-Cyclopentylpropionic acid, 2-methylphenyl ester	76	108.05

19	8.770	3565890	1.99	Carbamic acid, N-(3-chlorophenyl)-, 2-tolyl ester	71	108.00
20	8.917	1349788	0.75	Ethanone, 1-(3-thienyl)-	79	110.95
21	8.977	3356321	1.87	2-Cyclopenten-1-one, 3-ethyl-2-hydroxy-	92	126.00
22	9.235	1978296	1.10	1,4-Diacetoxybicyclo[2.2.2]oct-2-ene	70	112.00
23	9.608	10986831	6.13	2-Cyclopenten-1-one, 3-ethyl-2-hydroxy-	94	126.05
24	10.133	3432392	1.91	1,3-Cyclopentanedione, 2-ethyl-2-methyl-	78	94.00
25	10.596	2483224	1.38	Cyclohexanone, 5-methyl-2-(1-methylethylidene)-	83	152.00
26	11.291	2661040	1.48	2-Hydroxy-3-propyl-2-cyclopenten-1-one	87	125.00
27	11.755	2213290	1.23	2-Cyclohexen-1-one, 2-hydroxy-3-methyl-6-(1-methylethyl)-	82	126.00
28	11.973	2818213	1.57	2-Cyclohexen-1-one, 4-(1-methylethyl)-	85	43.00
29	12.445	1574065	0.88	1,2-Benzenediol, 3-methyl-	86	124.00
30	12.594	10580681	5.90	Resorcinol, 2-acetyl-	93	136.95
31	13.383	3664886	2.04	3,4,5,6,7,8-Hexahydro-2H-chromene	79	110.00
32	14.319	1373554	0.77	2,5-Dihydroxypropiophenone	90	136.95
33	20.060	2868845	1.60	Tetradecanoic acid	95	73.00
34	22.705	13651723	7.61	n-Hexadecanoic acid	92	73.00
35	24.709	5406206	3.02	9-Octadecenoic acid, (E)-	93	55.00
36	24.929	1654486	0.92	Octadecanoic acid	93	73.00
37	27.436	20855741	11.63	Hexanedioic acid, bis(2-ethylhexyl) ester	96	129.00
38	28.932	1671019	0.93	Bis(2-ethylhexyl) phthalate	74	148.95
		179301375	100.00			

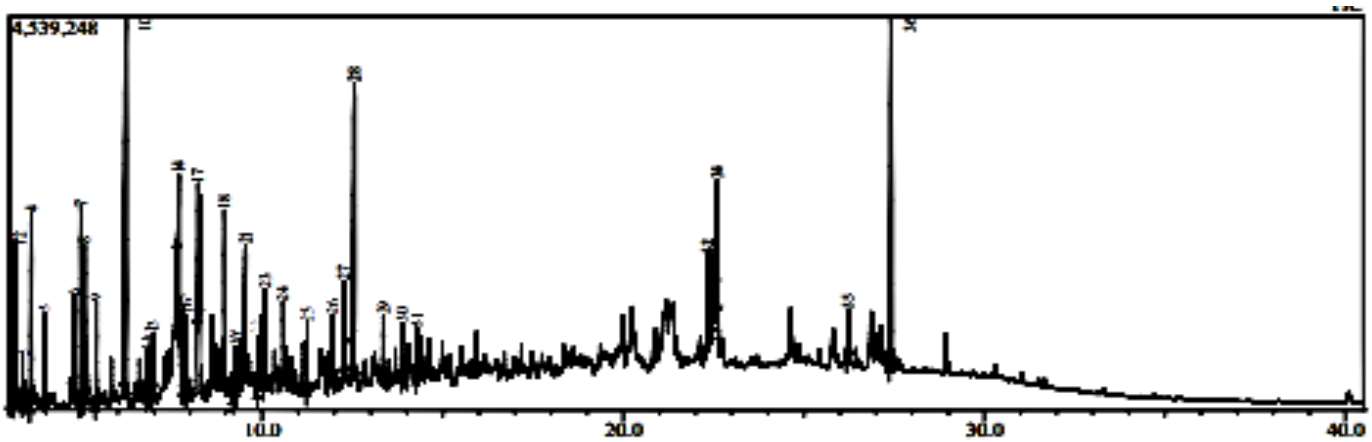

Figure D-18: GCMS analysis for the 10g 10wt% 30 minutes run.

Table D-18: GCMS results for the 10g 10wt% 30 minutes run

Peak#	R. Time	Area	Area%	Name	Similarity	Base m/z
1	3.072	4516551	4.09	Propanoic acid, 2-hydroxy-2-methyl-	90	59.05
2	3.179	3.82	3.82	2-Hydroxy-3-pentanone	96	45.05
3	3.362	1165798	1.05	Pentane, 2-nitro-	90	43.10
4	3.606	4839338	4.38	2-Cyclopenten-1-one	86	82.05
5	3.981	2247005	2.03	Cyclohexanone, 4-(1,1-dimethylpropyl)-	83	43.05
6	4.777	2348813	2.12	4-Hydroxy-3-hexanone	94	59.05
7	4.985	4636871	4.19	2-Cyclopenten-1-one, 2-methyl-	93	96.05
8	5.085	5462653	4.94	Ethanone, 1-(2-furanyl)-	92	95.00
9	5.404	2320025	2.10	2,5-Hexanedione	98	43.05
10	6.220	14405179	13.03	2-Furancarboxaldehyde, 5-methyl-	95	110.05
11	6.808	821853	0.74	2-Cyclopenten-1-one, 3,4-dimethyl-	94	95.05
12	6.919	1001945	0.91	2-Cyclopenten-1-one, 2,3-dimethyl-	87	67.05
13	6.974	1232857	1.12	2-Furanone, 2,5-dihydro-3,5-dimethyl	74	121.10
14	7.685	2010954	1.82	2-Cyclopenten-1-one, 2-hydroxy-3-methyl-	97	112.05
15	7.813	1830742	1.66	2-Cyclopenten-1-one, 2,3-dimethyl-	93	110.05
16	7.922	1752078	1.58	Orcinol	79	124.05
17	8.229	3206724	2.90	Phenol, 2-methyl-	96	108.05
18	8.960	3764237	3.41	2-Cyclopenten-1-one, 3-ethyl-2-hydroxy-	91	126.05
19	9.216	1125602	1.02	Octahydro-1H-cyclopenta[b]pyridin-4-ol	72	112.05
20	9.306	1038278	0.94	2H-Pyran-2-carboxaldehyde, 5,6-dihydro-	85	55.05
21	9.538	5245628	4.75	2-Cyclopenten-1-one, 3-ethyl-2-hydroxy-	96	126.05
22	9.879	1110083	1.00	3-Oxo-.alpha.-damascone	75	138.05
23	10.077	2348714	2.12	1,3-Cyclopentanedione, 2-ethyl-2-methyl-	75	94.00
24	10.579	1559033	1.41	4,4-Dimethyl-2-propenylcyclopentanone	85	152.05
25	11.244	1550572	1.40	2-Hydroxy-3-propyl-2-cyclopenten-1-one	85	125.05
26	11.951	1300362	1.18	2-Cyclohexen-1-one, 4-(1-methylethyl)-	86	43.00
27	12.261	2041104	1.85	1,2-Benzenediol, 3-methyl-	88	124.05
28	12.550	8396126	7.60	Ethanone, 1-(2,5-dihydroxyphenyl)-	93	137.00

29	13.355	1810430	1.64	1,8(2H,5H)-Naphthalenedione, hexahydro-	76	138.00
30	13.875	1275701	1.15	7-Hydroxy-1-indanone	82	148.00
31	14.282	1128080	1.02	2,5-Dihydroxypropiophenone	86	137.00
32	22.345	4183192	3.78	Pyrrolo[1,2-a]pyrazine-1,4-dione, hexahydro-3-(2-methylpropyl)-	82	154.05
33	22.457	2229926	2.02	Octahydrodipyrrolo[1,2-a:1',2'-d]pyrazine-5,10-dione-, (5aR,10aR) (isomer 1)	78	70.10
34	22.603	2679227	2.42	n-Hexadecanoic acid	85	73.05
35	26.245	1735518	1.57	2,5-Cyclohexadiene-1,4-dione, 2,5-diphenyl-	64	260.00
36	27.416	7995634	7.23	Hexanedioic acid, bis(2-ethylhexyl) ester	96	129.05
		110543943	100.00			

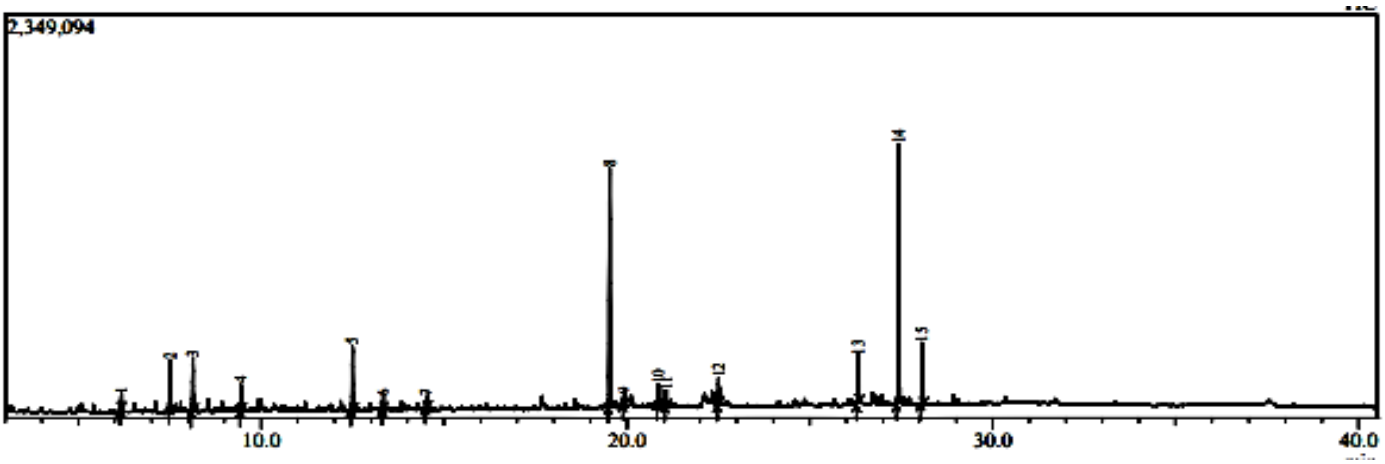

Figure D-19: GCMS analysis for the 6g 5wt% 5 minutes run.

Table D-19: GCMS results for the 6g 5wt% 5 minutes run

Peak#	R. Time	Area	Area%	Name	Similarity	Base m/z
1	6.169	113721	1.19	2-Furancarboxaldehyde, 5-methyl-	94	110.05
2	7.511	475640	4.96	2-Cyclopenten-1-one, 2-hydroxy-3-methyl-	98	112.05
3	8.131	615907	6.43	2-Cyclopenten-1-one, 3-ethyl-2-hydroxy-	89 126.10	126.10
4	9.445	250613	2.62	2-Cyclopenten-1-one, 3-ethyl-2-hydroxy-	96	126.05
5	12.495	635200	6.63	Resorcinol, 2-acetyl-	93	137.00
6	13.330	121465	1.27	3,4,5,6,7,8-Hexahydro-2H-chromene	71	110.00
7	14.512	127610	1.33	Phenol, 2,3,5-trimethyl-	136.05	136.05
8	19.527	2567902	26.80	Cyclohexane, 1,3,5-triphenyl-	82	91.05

9	19.919	93683	0.98	Tetradecanoic acid	89	73.00
10	20.854	299969	3.13	7-Ethyl-4,6-heptadecandione	77	156.05
11	21.063	196342	2.05	Cyclo(L-prolyl-L-valine)	73	156.05
12	22.503	272151	2.84	n-Hexadecanoic acid	94	73.00
13	26.318	518605	5.41	9-Octadecenoic acid, 12-hydroxy-, methyl ester, [R-(Z)]-	92	55.05
14	27.425	2597261	27.11	Hexanedioic acid, bis(2-ethylhexyl) ester	97	129.05
15	28.072	695935	7.26	Cyclohexane, 1,3,5-triphenyl-	93	93
		9582004	100.00			

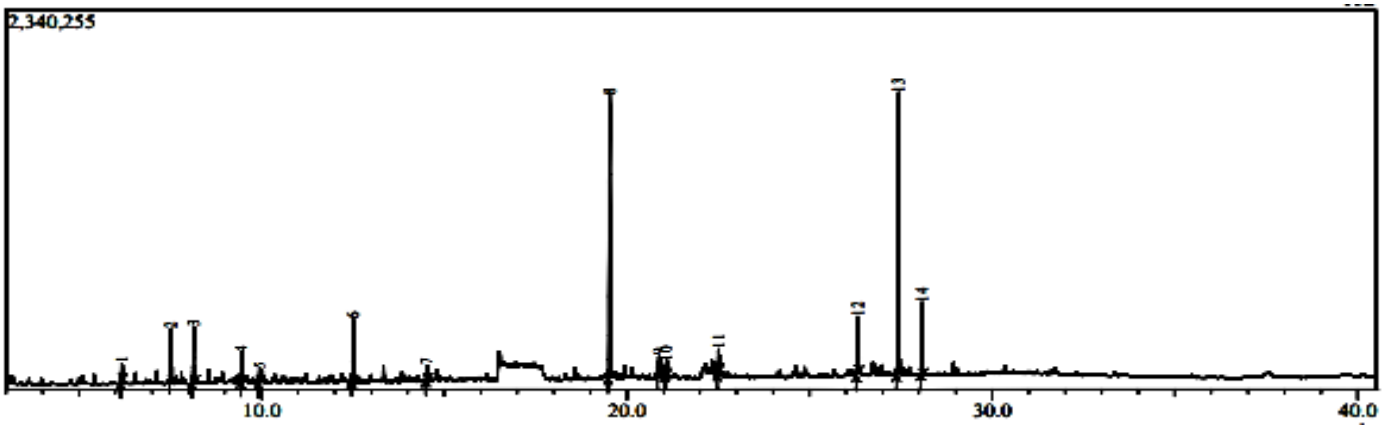

Figure D-20: GCMS analysis for the 6g 5wt% 10 minutes run.

Table D-20: GCMS results for the 6g 5wt% 10 minutes run

Peak#	R. Time	Area	Area%	Name	Similarity	Base m/z
1	6.171	174660	1.57	2-Furancarboxaldehyde, 5-methyl-	95	110.10
2	7.523	534054	4.79	2-Cyclopenten-1-one, 2-hydroxy-3-methyl-	96	112.05
3	8.141	704474	6.32	2-Cyclopenten-1-one, 3-ethyl-2-hydroxy-	90	126.10
4	9.455	293969	2.64	2-Cyclopenten-1-one, 3-ethyl-2-hydroxy-	95	126.10
5	9.940	151964	1.36	3,4-Dimethyl-1,2-cyclopentadione	83	55.05
6	12.502	615825	5.53	Resorcinol, 2-acetyl-	93	137.05
7	14.521	191435	1.72 82 136.05	3,4-Dimethylanisole	82	82 136.05
8	.531	3159239	28.35	Cyclohexane, 1,3,5-triphenyl-	82	91.05
9	20.878	281172	2.52	7-Ethyl-4,6-heptadecandione	78	156.10
10	21.080	173294	1.56	1-[(2R,5S)-2,4,5-Trimethylpiperazin-1-yl]hexan-1-one	72	156.10
11	22.511	265728	2.38	n-Hexadecanoic acid	11 95	73.00

12	26.321	626391	5.62	9-Octadecenoic acid, 12-hydroxy-, methyl ester, [R-(Z)]-	92	55.05
13	27.428	3138682	28.17	Hexanedioic acid, bis(2-ethylhexyl) ester	98	129.10
14	28.075	832793	7.47	Cyclohexane, 1,3,5-triphenyl-	93	91.05
		11143680	100.00			

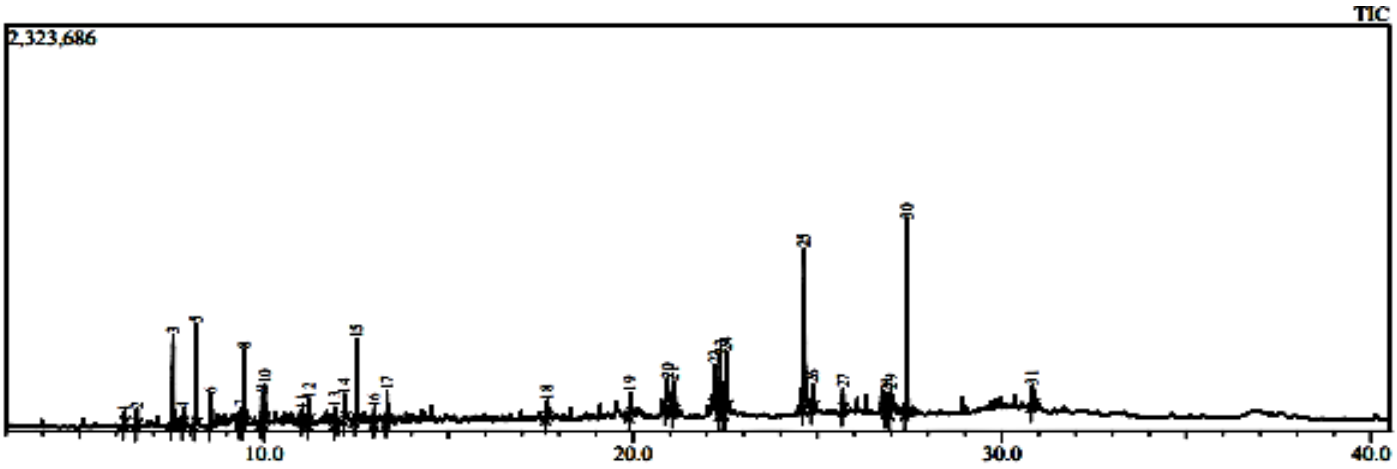

Figure D-21: GCMS analysis for the 6g 5wt% 15 minutes run.

Table D-21: GCMS results for the 6g 5wt% 15 minutes run

Peak#	R. Time	Area	Area%	Name	Similarity	Base m/z
1	6.207	106527	0.63	2-Cyclopenten-1-one, 3-methyl-	96	96.10
2	6.551	162902	0.97	Phenol	97	94.05
3	7.543	1143898	6.78	2-Cyclopenten-1-one, 2-hydroxy-3-methyl-	98	112.10
4	7.802	119668	0.71	2-Cyclopenten-1-one, 2,3-dimethyl-	95	110.10
5	8.161	1400119	8.30	2-Cyclopenten-1-one, 3-ethyl-2-hydroxy-	90	126.10
6	8.563	519335	3.08	Phenol, 3-methyl-	84	108.10
7	9.362	185325	1.10	Phenylethyl Alcohol	95	91.10
8	9.472	822637	4.88	2-Cyclopenten-1-one, 3-ethyl-2-hydroxy-	97	126.10
9	9.944	330036	1.96	2-Hydroxy-3-propyl-2-cyclopenten-1-one	83	55.05
10	10.027	349215	2.07	Cyclohexanone, 5-methyl-2-(1-methylethyl)-, cis-	79	94.05
11	11.032	86304	0.51	Catechol	95 110.05	110.05
12	11.220	211330	1.25	2-Hydroxy-3-propyl-2-cyclopenten-1-one	87	112.05
13	11.927	146409	0.87	2-Cyclohexen-1-one, 4-(1-methylethyl)-	84	43.05

14	12.194	260538	1.54	1,2-Benzenediol, 3-methyl-	95	124.10
15	12.508	794779	4.71	Ethanone, 1-(2,5-dihydroxyphenyl)-	93	137.00
16	12.996	123447	0.73	2-Penten-4-yn-1-ol, 5-(methylthio)-, (E)-	70	128.00
17	13.340	289560	1.72	3,4,5,6,7,8-Hexahydro-2H-chromene	79	110.05
18	17.677	259472	1.54	Diethyl Phthalate	92	149.00
19	19.937	266126	1.58	19 19.937 266126 1.58 Tetradecanoic acid 90 73.05	90	73.05
20	20.937	831109	4.93	7-Ethyl-4,6-heptadecandione	77	156.10
21	21.111	452257	2.68	Cyclo(L-prolyl-L-valine)	93	154.05
22	22.231	504046	2.99	Pyrrolo[1,2-a]pyrazine-1,4-dione, hexahydro-3-(2-methylpropyl)-	79	154.05
23	22.373	1000445	5.93	Octahydrodipyrrolo[1,2-a:1',2'-d]pyrazine-5,10-dione-, (5aR,10aR) (isomer 1)	86	70.10
24	22.532	650649	3.86	n-Hexadecanoic acid	96	73.05
25	24.649	2392694	14.18	Oleic Acid	93	55.05
26	24.873	282653	1.68	Octadecanoic acid	93	73.05
27	25.694	249018	1.48	2,5-Piperazinedione, 3-benzyl-6-isopropyl-	88	91.10
28	26.889	263019	1.56	Pyrrolo[1,2-a]pyrazine-1,4-dione, hexahydro-3-(phenylmethyl	92	125.10
29	26.996	246739	1.46	Phe-Leu-OH	92	91.05
30	27.422	2067185	12.25	Hexanedioic acid, bis(2-ethylhexyl) ester	98	129.05
31	30.829	350955	2.08	Tetrapentacontane	91	57.10
		16868396	100.00			

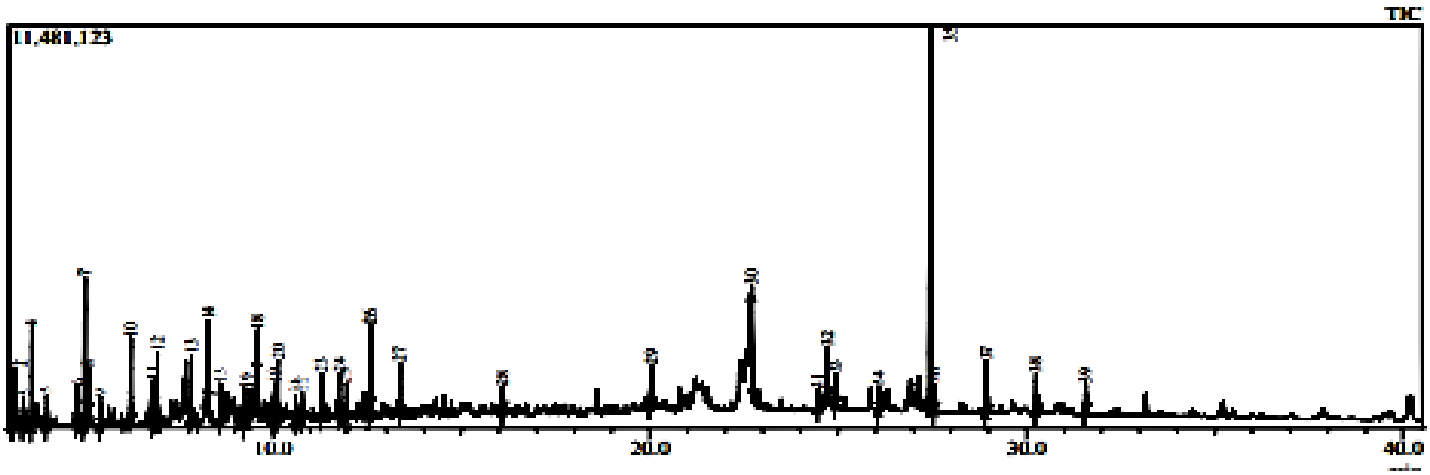

Figure D-22: GCMS analysis for the 6g 5wt% 20 minutes run.

Table D-22: GCMS results for the 6g 5wt% 20 minutes run

Peak#	R. Time	Area	Area%	Name	Similarity	Base m/z
1	3.056	3096066	2.24	3-Hydroxy-3-methyl-2-butanone	90	59.00
2	3.167	3008402	2.18	2-Hydroxy-3-pentanone	96	45.05
3	3.355	1510204	1.09	1-Hydroxy-3-methyl-2-butanone	93	43.05
4	3.599	5315602	3.85	2-Cyclopenten-1-one	96	82.05
5	3.993	2163442	1.57	3-Furanmethanol	85	43.05
6	4.790	2012486	1.46	4-Hydroxy-3-hexanone	94	59.05
7	5.003	8927009	6.47	2-Cyclopenten-1-one, 2-methyl-	93	96.05
8	5.094	1601674	1.16	Ethanone, 1-(2-furanyl)-	96	95.00
9	5.415	1406480	1.02	2,5-Hexanedione	98	43.00
10	6.220	5560205	4.03	2-Cyclopenten-1-one, 3-methyl-	87	96.05
11	6.819	2013396	1.46	2-Cyclopenten-1-one, 3,4-dimethyl-	95	95.05
12	6.941	3576393	2.59	2-Cyclopenten-1-one, 2,3-dimethyl-	93	67.05
13	7.830	3725378	2.70	2-Cyclopenten-1-one, 2,3-dimethyl-	95	110.05
14	8.291	6152197	4.46	2-Cyclopenten-1-one, 3-ethyl-2-hydroxy-	89	126.05
15	8.596	1175091	0.85	2-Cyclopenten-1-one, 3-ethyl-	85	110.05
16	9.246	2566687	1.86	2,5-Cyclohexadiene-1,4-dione, 2,5-dimethyl-	82	136.05
17	9.426	1447719	1.05	Phenylethyl Alcohol	97	91.05
18	9.602	2907940	2.11	2-Cyclopenten-1-one, 3-ethyl-2-hydroxy-	96	126.10
19	10.030	2836532	2.06	Cyclohexanone, 2-acetyl-	82	140.05
20	10.128	3830853	2.78	1,3-Cyclopentanedione, 2-ethyl-2-methyl-	77	94.00
21	10.593	1469113	1.06	Cyclohexanone, 5-methyl-2-(1-methylethylidene)-	81	152.05
22	10.781	1558569	1.13	2-Acetonylcyclopentanone	92	43.00
23	11.285	2132023	1.54	2-Hydroxy-3-propyl-2-cyclopenten-1-one	87	125.05
24	11.759	2070597	1.50	2-Cyclohexen-1-one, 2-hydroxy-3-methyl-6-(1-methylethyl)-	83	126.05
25	11.961	2031214	1.47	2-Cyclohexen-1-one, 4-(1-methylethyl)-	81	43.00
26	12.579	5053452	3.66	Resorcinol, 2-acetyl-	93	137.00
27	13.379	2429252	1.76	3,4,5,6,7,8-Hexahydro-2H-chromene	80	110.05
28	16.104	1098868	0.80	Cycloheptasiloxane, tetradecamethyl-	91	73.05
29	20.066	3418286	2.48	Tetradecanoic acid	96	73.00
30	22.716	1490535	1.08	n-Hexadecanoic acid	79	73.05

31	24.473	744919	0.54	Cyclooctasiloxane, hexadecamethyl-	86	355.00
32	24.710	3470809	2.51	Oleic Acid	95	55.05
33	24.942	1507757	1.09	Octadecanoic acid	92	73.05
34	26.079	1241588	0.90	Cyclononasiloxane, octadecamethyl-	88	73.05
35	27.464	34805466	25.22	Hexanedioic acid, bis(2-ethylhexyl) ester	96	129.05
36	27.557	1543544	1.12	Cyclodecasiloxane, eicosamethyl-	86	73.05
37	28.942	3063795	2.22	Bis(2-ethylhexyl) phthalate	65	149.00
38	30.256	2296335	1.66	Tetracosamethyl-cyclododecasiloxane	85	73.05
39	31.572	1745974	1.27	Tetracosamethyl-cyclododecasiloxane	86	73.05
		138005852	100.00			

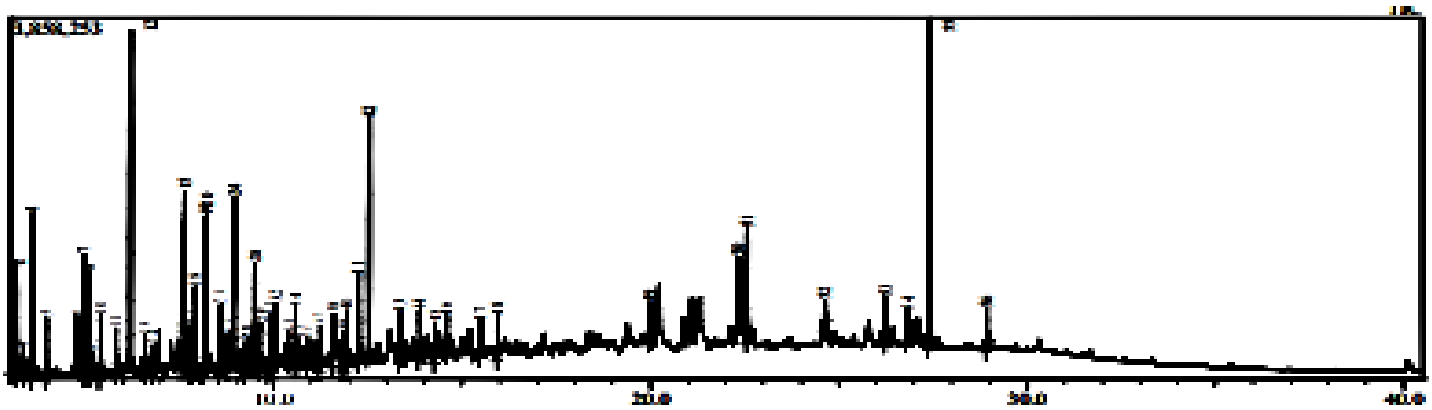

Figure D-23: GCMS analysis for the 6g 5wt% 25 minutes run.

Table D-23: GCMS results for the 6g 5wt% 25 minutes run

Peak#	R. Time	Area	Area%	Name	Similarity	Base m/z
1	3.062	2416463	2.30	Propanoic acid, 2-hydroxy-2-methyl-	90	59.05
2	3.169	2366638	2.25	2-Hydroxy-3-pentanone	96	45.05
3	3.356	485101	0.46	Pentane, 2-nitro-	90	43.10
4	3.596	3738151	3.56	3,5-Dimethylpyrazole	84	39.05
5	3.970	1417910	1.35	1,6-Heptadien-4-ol	84	43.10
6	4.765	1073413	1.02	4-Hydroxy-3-hexanone	94	59.05
7	4.976	2504301	2.38	2-Cyclopenten-1-one, 2-methyl-	89	96.10
8	5.074	2621782	2.50	Ethanone, 1-(2-furanyl)-	93	95.00
9	5.158	423533	0.40	2-Furancarboxaldehyde, 5-methyl-	88	110.05
10	5.394	1212514	1.15	2,5-Hexanedione	98 5	43.05

11	5.813	895444	0.85	3(2H)-Furanone, 2-(1-hydroxy-1-methyl-2-oxopropyl)-2,5-dimethyl-	83	40.05
12	6.204	11179694	10.64	2-Furancarboxaldehyde, 5-methyl-	96	110.05
13	6.587	821101	0.78	Butanoic acid, phenyl ester	75	94.05
14	6.804	381735	0.36	2-Cyclopenten-1-one, 3,4-dimethyl-	95	95.05
15	7.649	10043181	9.56	2-Cyclopenten-1-one, 2-hydroxy-3-methyl-		112.10
16	7.696	608709	0.58	9-Oxabicyclo[3.3.1]nonan-2-one, 6-hydroxy-	74	84.10
17	7.804	952561	0.91	2-Cyclopenten-1-one, 2,3-dimethyl-	92	67.05
18	7.914	1993351	1.90	Benzenethiol, 2-methyl-	75	124.10
19	8.194	4815341	4.58	Phenol, 2-methyl-	97	108.05
20	8.229	2711221	2.58	2-Cyclopenten-1-one, 3-ethyl-2-hydroxy-	90	126.10
21	8.579	2257392	2.15	3,4-Dimethyl-1,2-cyclopentadione	76	126.10
22	8.734	401960	0.38	Ethanone, 1-(3-thienyl)-	86	111.00
23	8.786	596772	0.57	1,4-Cyclohexanedione	86	112.05
24	8.953	3528757	3.36	2-Cyclopenten-1-one, 3-ethyl-2-hydroxy-	93	126.10
25	9.211	654863	0.62	1,4-Nonadiene, 2-nitro-, (Z)-	71	112.10
26	9.298	425056	0.40	2,3-Dimethyl-4-hydroxy-2-butenoic lactone	87	-55.05
27	9.353	452600	0.43	Cyclopentanone, 2-(2-methylpropylidene)-	74	91.05
28	9.507	3274312	3.12	2-Cyclopenten-1-one, 3-ethyl-2-hydroxy-	94	126.10
29	9.577	606926	0.58	1H-Azonine, octahydro-1-nitroso-	82	126.10
30	9.638	992707	0.95	2(3H)-Furanone, 5-acetyldihydro-	89	85.05
31	9.875	1001340	0.95	Cyclopropane, 1,1,2-trimethyl-3-(2-methyl-1-propenyl)-	76	138.10
32	10.054	1353737	1.29	Cyclohexanone, 5-methyl-2-(1-methylethyl)-, cis-	76	94.05
33	10.402	510984	0.49	2,3-Dihydroxybenzaldehyde	90	138.05
34	10.573	1406812	1.34	Cyclohexanone, 5-methyl-2-(1-methylethylidene)-	84	152.10
35	10.644	377757	0.36	Phenol, 2,3-dimethyl-	86	122.10
36	10.912	482004	0.46	1,2-Cyclooctanedione	86	55.05
37	11.233	755580	0.72	2-Hydroxy-3-propyl-2-cyclopenten-1-one	86	125.10
38	11.603	1312051	1.25	7-Octen-4-one, 2,6-dimethyl-	80	85.00
39	11.842	857475	0.82	Cyclohexanone, 2-(1-methylethylidene)-	81	43.05

40	11.945	1477778	1.41	2-Cyclohexen-1-one, 4-(1-methylethyl)-	86	43.05
41	12.244	2678624	2.55	1,2-Benzenediol, 3-methyl-	95	124.05
42	12.536	5607420	5.34	Resorcinol, 2-acetyl-	93	137.05
43	13.350	1195366	1.14	2,5-Cyclohexadiene-1,4-dione, 2-hydroxy-3,5,6-trimethyl-	79	138.05
44	13.870	980880	0.93	2-Methyl-5-hydroxybenzofuran	84	148.05
45	14.282	692990	0.66	2,5-Dihydroxypropiophenone	88	137.05
46	14.598	974547	0.93	Benzaldehyde, 3-methoxy-	87	136.05
47	15.504	973795	0.93	2,3-Dimethylhydroquinone	78	138.10
48	15.942	698305	0.66	Bicyclo[3.3.1]nona-2,6-diene, 2,6-bis(acetoxy)-	77	152.10
49	19.977	744835	0.71	Tetradecanoic acid	95	73.05
50	22.329	2394431	2.28	Pyrrolo[1,2-a]pyrazine-1,4-dione, hexahydro-3-(2-methylpropyl)-	78	154.10
51	22.573	2912851	2.77	n-Hexadecanoic acid	93	73.05
52	24.633	457672	0.44	Oleic Acid	92	55.05
53	26.243	905134	0.86	4,7,9-Trihydroxy-2-methylnaphtho[2,3-b]furan-5,8-dione	64	260.05
54	26.844	993212	0.95	Phe-Leu-OH	88	91.05
55	27.425	6793968	6.47	Hexanedioic acid, bis(2-ethylhexyl) ester	97	129.10
56	28.931	650897	0.62	Bis(2-ethylhexyl) phthalate	56 2896	149.00
		105043934	100.00			

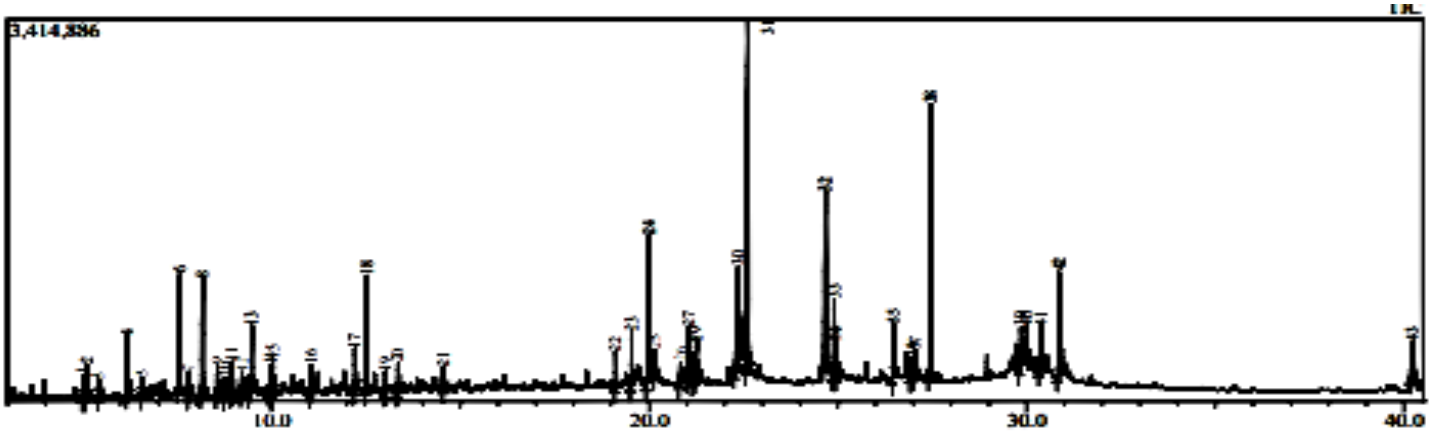

Figure D-24: GCMS analysis for the 6g 5wt% 30 minutes run.

Table D-24: GCMS results for the 6g 5wt% 30 minutes run

Peak#	R. Time	Area	Area%	Name	Similarity	Base m/z
1	4.996	0.50	0.50	2-Cyclopenten-1-one, 2-methyl-	93	96.05

2	5.091	667515	1.06	4-(Azidomethyl)-1-methylpyrazole	80	95.00
3	3 5.412	237601	0.38	2,5-Hexanedione	98	43.00
4	6.181	1292577	2.05	2-Furancarboxaldehyde, 5-methyl-	96	110.05
5	6.564	281000	0.45	Phenol	97	94.05
6	7.570	2985921	4.74	2-Cyclopenten-1-one, 2-hydroxy-3-methyl-	98	112.05
7	7.806	344909	0.55	2-Cyclopenten-1-one, 2,3-dimethyl-	94	67.05
8	8.178	2864753	4.55	2-Cyclopenten-1-one, 3-ethyl-2-hydroxy-	90	126.05
9	8.569	838095	1.33	Phenol, 3-methyl-	80	107.05
10	8.748	373333	0.59	Lactic acid, monoanhydride with 1-butaneboronic acid, cyclic ester	83	112.05
11	8.943	528081	0.84	2-Cyclopenten-1-one, 3-ethyl-2-hydroxy-	92	126.10
12	9.214	462561	0.73	2,5-Cyclohexadiene-1,4-dione, 2,5-dimethyl-	78	136.05
13	9.481	1220577	1.94	2-Cyclopenten-1-one, 3-ethyl-2-hydroxy-	96	126.05
14	9.948	486840	0.77	Cyclopentane, 1-acetyl-1,2-epoxy-	82	55.05
15	10.037	521499	0.83	Cyclohexanone, 5-methyl-2-(1-methylethyl)-, cis-	77	94.00
16	11.046	486153	0.77	Catechol	96	110.05
17	12.208	661411	1.05	1,2-Benzenediol, 3-methyl-	95	124.05
18	12.517	1758204	2.79	Ethanone, 1-(2,5-dihydroxyphenyl)-	94	137.00
19	13.012	296657	0.47	Benzaldehyde, 3-hydroxy-	68	122.05
20	13.350	479878	0.76	3,4,5,6,7,8-Hexahydro-2H-chromene	78	110.05
21	14.550	328293	0.52	Ethanone, 1-(3-hydroxyphenyl)-	80	136.05
22	19.116	562482	0.89	Heptadecane	96	57.05
23	19.538	936249	1.49	Cyclohexane, 1,3,5-triphenyl-	81	91.05
24	20.011	4451231	7.06	Tetradecanoic acid	95	73.00
25	20.160	425654	0.68	6,8-Dihydroxy-3-methylisocoumarin	73	192.00
26	20.833	506965	0.80	Cyclo(L-prolyl-L-valine)	92	154.05
27	21.063	1862838	2.96	7-Ethyl-4,6-heptadecandione	80	156.05
28	21.179	658316	1.04	Cyclo(L-prolyl-L-valine)	93	154.05
29	21.264	772553	1.23	7-Ethyl-4,6-heptadecandione	156.05	156.05
30	22.365	4472529	7.10	6-Pentadecenoic acid, 13-methyl-, (6Z)-	80	55.05
31	22.620	10281075	16.32	n-Hexadecanoic acid	96	73.05
32	24.673	4221248	6.70	Oleic Acid	94	55.05
33	24.903	1557102	2.47	Octadecanoic acid	91	43.05

34	24.968	597093	0.95	Ethyl Oleate	92	55.05
35	26.474	962513	1.53	Arachidonic acid	97	79.05
36	26.937	335069	0.53	Pyrrolo[1,2-a]pyrazine-1,4-dione, hexahydro-3-(phenylmethyl)-	93	125.10
37	27.046	549025	0.87	Phe-Leu-OH	86	91.05
38	27.442	4473931	7.10	Hexanedioic acid, bis(2-ethylhexyl) ester	97	129.05
39	29.849	845731	1.34	9-Methylheneicosane	89	57.05
40	30.005	481599	0.76	Pentatriacontane	89	57.10
41	30.375	1292175	2.05	Tetracontane	41 87	57.05
42	30.851	3406100	5.41	Tetrapentacontane	91	57.05
43	40.220	1920455	3.05	Stigmasta-5,24(28)-dien-3-ol, (3.beta.,24Z)-	96	314.20
		63003983	100.00			

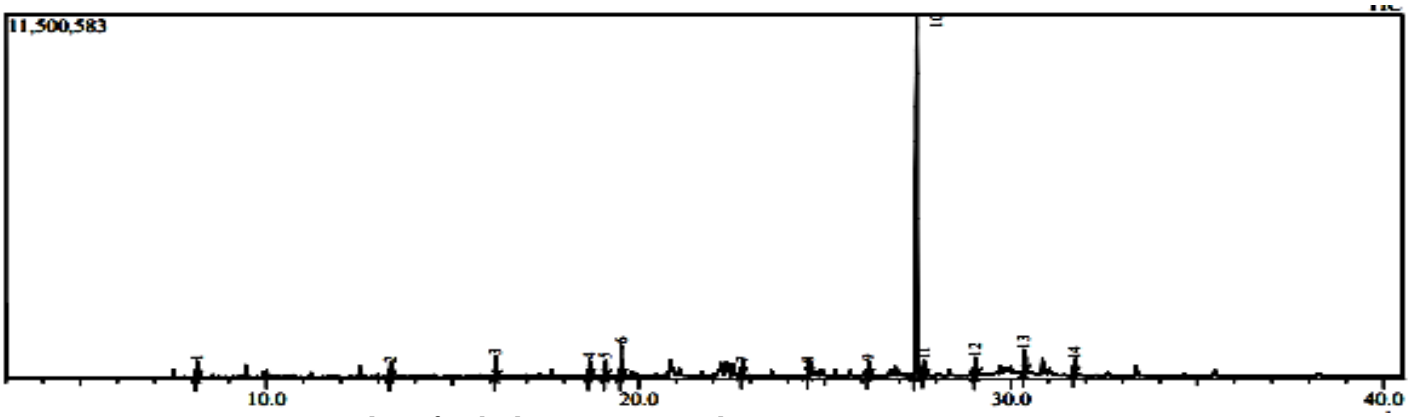

Figure D-25: GCMS analysis for the low reaction conditions 6g 10wt% 5 minutes run.

Table D-25: GCMS results for the low reaction conditions 6g 10wt% 5 minutes run

Peak#	R. Time	Area	Area%	Name	Similarity	Base m/z
1	8.140	942843	2.29	2-Cyclopenten-1-one, 3-ethyl-2-hydroxy-	91	126.10
2	13.333	688286	1.67	Cyclohexasiloxane, dodecamethyl-	58	110.10
3	16.160	1166941	2.83	Cycloheptasiloxane, tetradecamethyl-	93	281.05
4	18.675	852367	2.07	Cyclooctasiloxane, hexadecamethyl-	96	355.05
5	19.110	804202	1.95	Heptadecane	97	57.10
6	19.531	1776139	4.31	Cyclohexane, 1,3,5-triphenyl-	81	91.05
7	22.781	530563	1.29	Cyclodecasiloxane, eicosamethyl-	88	73.05
8	24.556	627377	1.52	Cyclooctasiloxane, hexadecamethyl-	84	355.10
9	26.165	748530	1.82	Cyclononasiloxane, octadecamethyl-	89 5	73.05

10	27.463	28535845	69.27	Hexanedioic acid, bis(2-ethylhexyl) ester	97	129.10
11	27.651	860798	2.09	Cyclodecasiloxane, eicosamethyl-	88	73.05
12	29.043	1116941	2.71	Cyclodecasiloxane, eicosamethyl-	85	73.05
13	30.351	1649060	4.00	Tetracosamethyl-cyclododecasiloxane	84	73.05
14	31.704	897904	2.18	Tetracosamethyl-cyclododecasiloxane	87	73.05
		41197796	100.00			

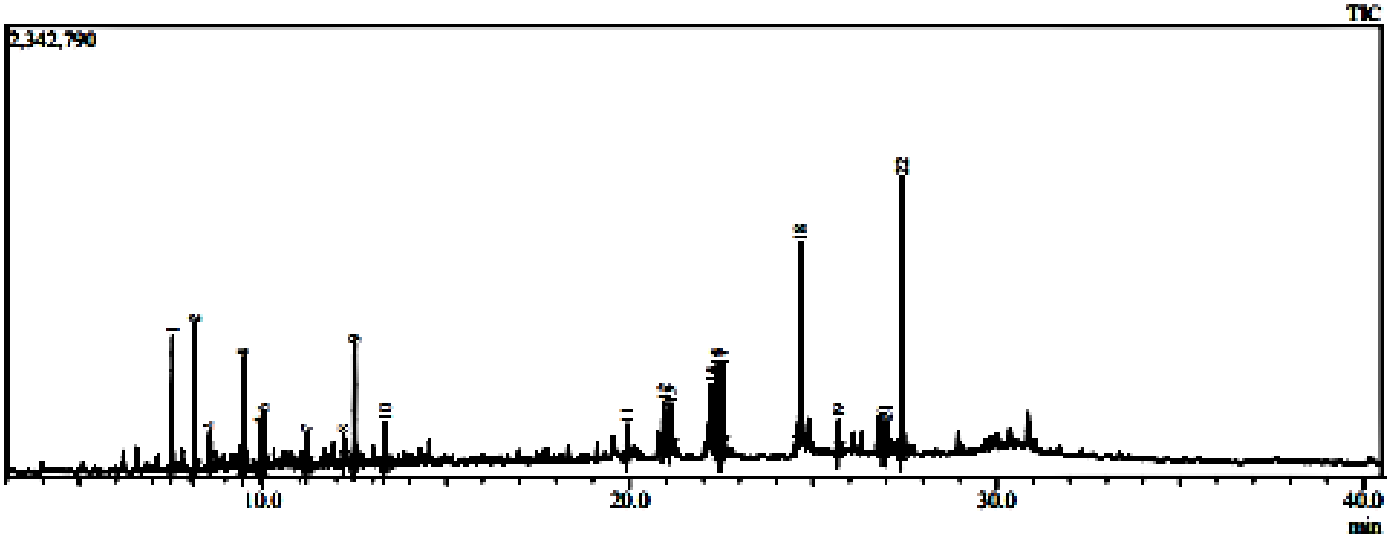

Figure D-26: GCMS analysis for the low reaction conditions 6g 10wt% 10 minutes run.

Table D-26: GCMS results for the low reaction conditions 6g 10wt% 10 minutes run

Peak#	R. Time	Area	Area%	Name	Similarity	Base m/z
1	7.543	1415142	8.07	2-Cyclopenten-1-one, 2-hydroxy-3-methyl-	98	112.05
2	8.161	1768730	10.09	2-Cyclopenten-1-one, 3-ethyl-2-hydroxy-	89	126.05
3	8.565	243410	1.39	Phenol, 3-methyl-	80	110.10
4	9.473	1041255	5.94	2-Cyclopenten-1-one, 3-ethyl-2-hydroxy-	96	126.05
5	9.948	412781	2.35	Cyclohexanone, 2-acetyl-	84	55.05
6	10.030	444849	2.54	1,3-Cyclopentanedione, 2-ethyl-2-methyl-	77	94.00
7	11.222	258800	1.48	2-Hydroxy-3-propyl-2-cyclopenten-1-one	86	125.05
8	12.202	201726	1.15	1,2-Benzenediol, 3-methyl-	93	124.05
9	12.510	1029503	5.87	Ethanone, 1-(2,5-dihydroxyphenyl)-	94	137.00

10	13.345	366558	2.09	3,4,5,6,7,8-Hexahydro-2H-chromene	79	110.05
11	19.944	290966	1.66	Tetradecanoic acid	90	73.05
12	20.941	939136	5.36	7-Ethyl-4,6-heptadecandione	77	156.05
13	21.119	664626	3.79	Cyclo(L-prolyl-L-valine)	90	70.05
14	22.239	542526	3.09	Pyrrolo[1,2-a]pyrazine-1,4-dione, hexahydro-3-(2-methylpropyl)-	82	154.05
15	22.383	947612	5.40	Octahydrodipyrrolo[1,2-a:1',2'-d]pyrazine-5,10-dione-, (5aR,10aR) (isomer 1)	87	70.05
16	22.439	403030	2.30	Hexahydro-3-(1-methylpropyl)pyrrolo[1,2-a]pyrazine-1,4-dione	92	154.05
17	22.537	776980	4.43	n-Hexadecanoic acid	96	73.00
18	24.653	2338685	13.34	Oleic Acid	93	55.05
19	25.705	282768	1.61	2,5-Piperazinedione, 3-benzyl-6-isopropyl-	90	91.05
20	26.904	253097	1.44	Pyrrolo[1,2-a]pyrazine-1,4-dione, hexahydro-3-(phenylmethyl)-	92	125.05
21	27.008	252393	1.44	Phe-Leu-OH	93	91.05
22	27.435	2660256	15.17	Hexanedioic acid, bis(2-ethylhexyl) ester	97	129.05
		17534829	100.00			

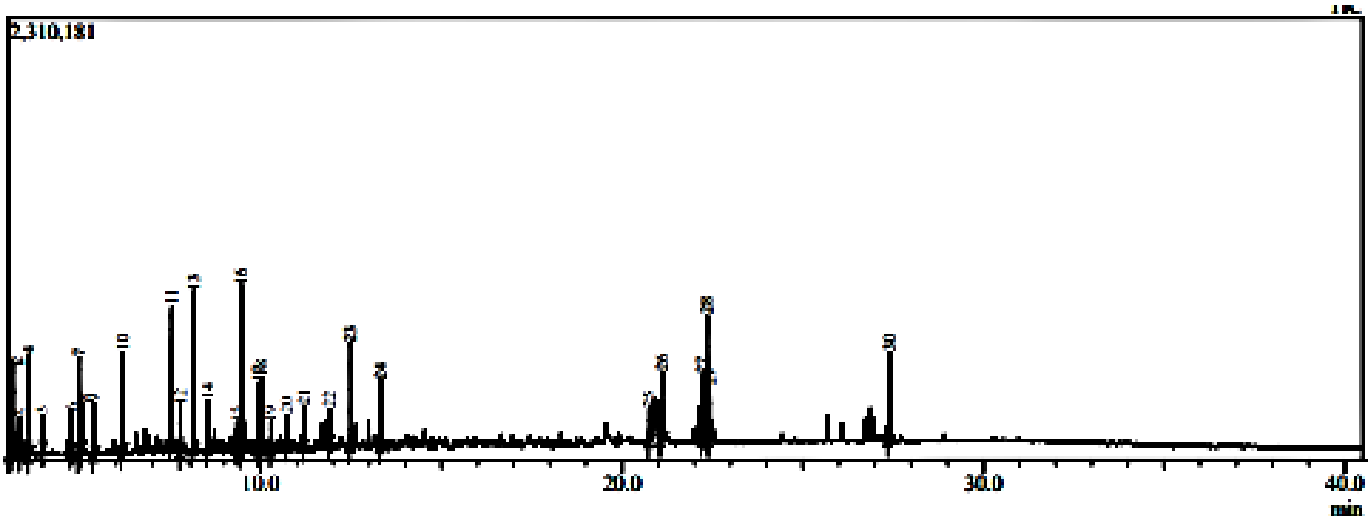

Figure D-27: GCMS analysis for the low reaction conditions 6g 10wt% 15 minutes run.

Table D-27: GCMS results for the low reaction conditions 6g 10wt% 15 minutes run

Peak#	R. Time	Area	Area%	Name	Similarity	Base m/z
1	3.053	772853	3.43	Propanoic acid, 2-hydroxy-2-methyl-	90	59.05

2	3.161	3.161	3.33	2-Hydroxy-3-pentanone	96	45.05
3	3.353	316456	1.40	Pentane, 2-nitro-	93	43.10
4	3.591	853100	3.79	2-Cyclopenten-1-one	97	82.05
5	3.961	344057	1.53	1,6-Heptadien-4-ol	84	84 43.10
6	4.758	327341	1.45	4-Hydroxy-3-hexanone	96	59.05
7	4.969	849864	3.77	2-Cyclopenten-1-one, 2-methyl-	94	96.05
8	5.073	564476	2.51	1-(Dimethylamino)pyrrole	77	42.05
9	5.385	446470	1.98	2,5-Hexanedione	98	43.05
10	6.177	976976	4.34	2-Cyclopenten-1-one, 3-methyl-	93	96.05
11	7.541	1815834	8.06	2-Cyclopenten-1-one, 2-hydroxy-3-methyl-	98	112.10
12	7.784	394983	1.75	2-Cyclopenten-1-one, 2,3-dimethyl-	95	67.05
13	8.157	2164010	9.61	2-Cyclopenten-1-one, 3-ethyl-2-hydroxy-	90	126.10
14	8.544	770801	3.42	2,4-Heptadienal, (E,E)-	80	110.10
15	9.348	279976	1.24	Phenylethyl Alcohol	98	91.05
16	9.471	1864238	8.28	2-Cyclopenten-1-one, 3-ethyl-2-hydroxy-	96	126.10
17	9.931	722167	3.21	Cyclopentane, 1-acetyl-1,2-epoxy-	85	43.05
18	10.019	639445	2.84	1,3-Cyclopentanedione, 2-ethyl-2-methyl-	78	94.05
19	10.293	218024	0.97	5,5,6-Trimethylhept-3-en-2-one	87	43.05
20	10.730	243617	1.08	2-Acetonylcyclopentanone	94	43.05
21	11.206	305482	1.36	2-Hydroxy-3-propyl-2-cyclopenten-1-one	86	125.05
22	11.914	248996	1.11 85 43.05	2-Cyclohexen-1-one, 4-(1-methylethyl)-	85	)- 85 43.05
23	12.493	972823	4.32	Ethanone, 1-(2,5-dihydroxyphenyl)-	93	137.00
24	13.328	619235	2.75	3,4,5,6,7,8-Hexahydro-2H-chromene	81	110.05
25	20.757	328630	1.46	Cyclo(L-prolyl-L-valine)	97	154.05
26	21.104	1079740	4.79	Cyclo(L-prolyl-L-valine)	86	154.05
27	22.213	780235	3.46	Pyrrolo[1,2-a]pyrazine-1,4-dione, hexahydro-3-(2-methylpropyl)-	89	154.10
28	22.360	1398896	6.21	5,10-Diethoxy-2,3,7,8-tetrahydro-1H,6H-dipyrrolo[1,2-a:1',2'-d]pyrazine	82	70.10
29	22.422	661611	2.94	Hexahydro-3-(1-methylpropyl)pyrrolo[1,2-a]pyrazine-1,4-dione	94	154.10
30	27.402	815840	3.62	Hexanedioic acid, bis(2-ethylhexyl) ester	97	129.10

		22526959	100.00			

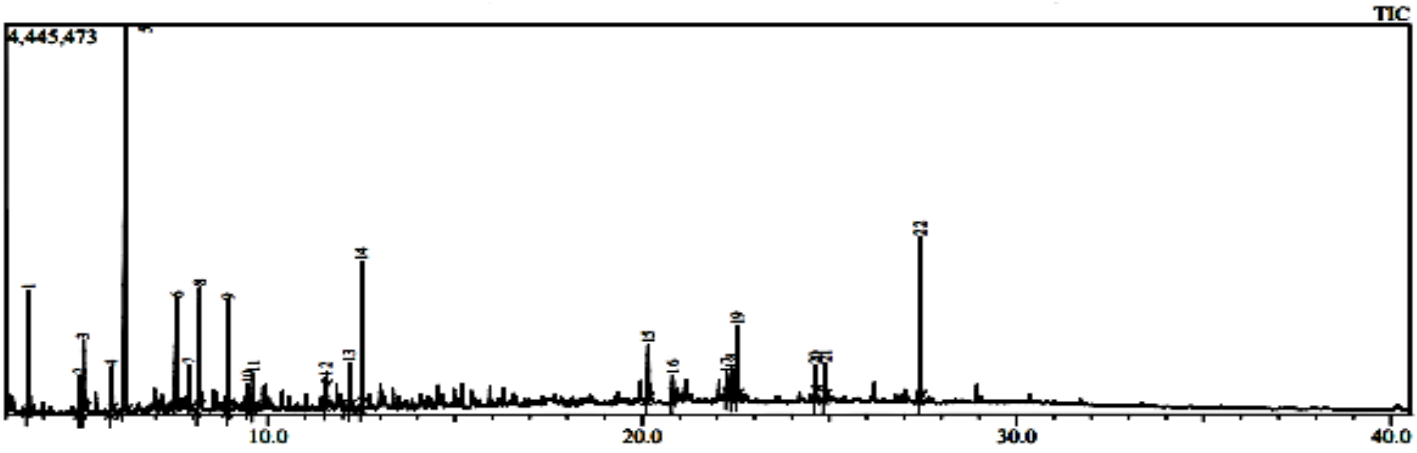

Figure D-28: GCMS analysis for the low reaction conditions 6g 10wt% 20 minutes run.

Table D-28: GCMS results for the low reaction conditions 6g 10wt% 20 minutes run

Peak#	R. Time	Area	Area%	Name	Similarity	Base m/z
1	3.604	2926167	6.89	Furfural	96	96.00
2	4.985	766876	1.81	1H-Imidazole-4-carboxylic acid	78	96.05
3	5.077	1636071	3.85	Ethanone, 1-(2-furanyl)-	95	95.00
4	5.817	927727	2.18	3(2H)-Furanone, 2-(1-hydroxy-1-methyl-2-oxopropyl)-2,5-dimethyl-	81	112.05
5	6.203	11265120	26.52	2-Furancarboxaldehyde, 5-methyl-	96	110.05
6	7.574	3671020	8.64	2-Cyclopenten-1-one, 2-hydroxy-3-methyl-	98	112.05
7	7.909	662226	1.56	Benzenethiol, 4-methyl-	78	91.05
8	8.184	4250952	10.01	2-Cyclopenten-1-one, 3-ethyl-2-hydroxy-	90	126.05
9	8.943	2244650	5.28	2-Cyclopenten-1-one, 3-ethyl-2-hydroxy-	94	126.05
10	9.464	302380	0.71	2-Cyclopenten-1-one, 3-ethyl-2-hydroxy-	91	126.05
11	9.614	631762	1.49	2(3H)-Furanone, 5-acetyldihydro-	95	85.00
12	11.561	305759	0.72	5-Hydroxymethylfurfural	94	97.00
13	12.194	793609	1.87	1,2-Benzenediol, 3-methyl-	96	124.05
14	12.518	2905437	6.84	Ethanone, 1-(2,5-dihydroxyphenyl)-	92	137.00
15	20.165	1395063	3.28	4-Methyldaphnetin	74	192.00
16	20.813	478329	1.13	Cyclo(L-prolyl-L-valine)	93	154.05

17	22.263	469613	1.11	Pyrrolo[1,2-a]pyrazine-1,4-dione, hexahydro-3-(2-methylpropyl)-	89	154.00
18	22.400	665061	1.57	Pyrrolo[1,2-a]pyrazine-1,4-dione, hexahydro-3-(2-methylpropyl)-	78	70.05
19	22.542	1607417	3.78	n-Hexadecanoic acid	97	73.00
20	24.628	571240	1.34	9-Octadecenoic acid	94	55.05
21	24.880	715344	1.68	Octadecanoic acid	95	73.00
22	27.433	3292644	7.75	Hexanedioic acid, bis(2-ethylhexyl) ester	98	129.05
		42484467	100.00			

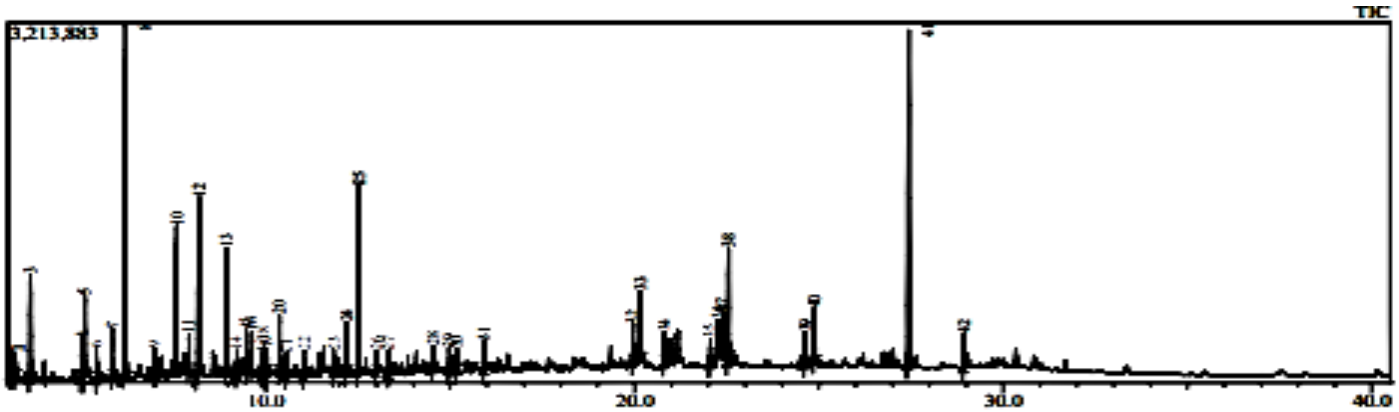

Figure D-29: GCMS analysis for the low reaction conditions 6g 10wt% 25 minutes run.

Table D-29: GCMS results for the low reaction conditions 6g 10wt% 25 minutes run

Peak#	R. Time	Area	Area%	Name	Similarity	Base m/z
1	3.080	437639	0.85	Propanoic acid, 2-hydroxy-2-methyl-	90	59.00
2	3.187	420303	0.81	2-Hydroxy-3-pentanone	94	45.05
3	3.606	2153165	4.17	Furfural	94	96.00
4	4.986	652079	1.26	2-Cyclopenten-1-one, 2-methyl-	83	96.05
5	5.080	1493712	2.90	Ethanone, 1-(2-furanyl)-	94	95.00
6	5.401	487091	0.94	2,5-Hexanedione	98	43.00
7	5.820	721591	1.40	3(2H)-Furanone, 2-(1-hydroxy-1-methyl-2-oxopropyl)-2,5-dimethyl-	82	40.05
8	6.192	7701398	14.93	2-Furancarboxaldehyde, 5-methyl-	96	110.05
9	6.972	469697	0.91	2-Furanone, 2,5-dihydro-3,5-dimethyl	92	69.05
10	7.578	4123232	7.99	2-Cyclopenten-1-one, 2-hydroxy-3-methyl-	98	112.05
11	7.908	621995	1.21	Benzenethiol, 4-methyl-	77	91.05

12	8.195	5513036	10.69	2-Cyclopenten-1-one, 3-ethyl-2-hydroxy-	89	126.05
13	8.940	1968917	3.82	2-Cyclopenten-1-one, 3-ethyl-2-hydroxy-	94	126.10
14	9.207	443297	0.86	2,5-Cyclohexadiene-1,4-dione, 2,5-dimethyl-	79	136.05
15	9.466	549902	1.07	2-Cyclopenten-1-one, 3-ethyl-2-hydroxy-	95	126.05
16	9.610	553309 00	1.07	2(3H)-Furanone, 5-acetyldihydro-	95	85.00
17	9.872	287837	0.56	Phytol	73	43.00
18	9.937	555987	1.08	Cyclopentane, 1-acetyl-1,2-epoxy-	84	55.05
19	10.025	269285	0.52	Bicyclo[2.2.1]heptane-1,2-dicarboxylic acid	77	94.00
20	10.364	1014104	1.97	Naphthalene, 1,2,3,4-tetrahydro-	94	104.10
21	10.563	473064	0.92	4,4-Dimethyl-2-propenylcyclopentanone	85	152.05
22	11.027	419963	0.81	Catechol	95	110.00
23	11.834	341634	0.66	4-Acetyl-1-methylcyclohexene	83	138.05
24	12.190	796522	1.54	1,2-Benzenediol, 3-methyl-	97	124.05
25	12.514	12.514	5.99	Ethanone, 1-(2,5-dihydroxyphenyl)-	93	137.00
26	12.998	298877	0.58	Benzaldehyde, 3-hydroxy-	88	122.05
27	13.339	405368	0.79	(6R,7aS)-3,6-Dimethyl-5,6,7,7a-tetrahydrobenzofuran-2(4H)-one	74	110.05
28	14.537	303125	0.59	Ethanone, 1-(3-hydroxyphenyl)-	77	136.05
29	14.968	344351	0.67	2-Cyclohexen-1-one,4-hydroxy-3,5,5-trimethyl-4-(1-methyl-3-oxo-1-butenyl)	81	138.05
30	15.177	315065	0.61	Spiro[4.5]decane-2,6-dione	83	166.00
31	15.929	411163	0.80	Bicyclo[3.3.1]nona-2,6-diene, 2,6-bis(acetoxy)-	80	152.05
32	19.956	632399	1.23	Tetradecanoic acid	94	73.05
33	20.163	1257346	2.44	4-Methyldaphnetin	73	192.00
34	20.808	491509	0.95	Cyclo(L-prolyl-L-valine)	95	154.05
35	22.048	452055	0.88	Hexahydro-3-(1-methylpropyl)pyrrolo[1,2-a]pyrazine-1,4-dione	94	154.05
36	22.262	557067	1.08	Pyrrolo[1,2-a]pyrazine-1,4-dione, hexahydro-3-(2-methylpropyl)-	87	154.05
37	22.394	743140	1.44	Octahydrodipyrrolo[1,2-a:1',2'-d]pyrazine-5,10-dione-, (5aR,10aR) (isomer 1)	85	70.05
38	22.546	2183422	4.23	n-Hexadecanoic acid	96	73.00

39	24.620	516204	1.00	9-Octadecenoic acid	94	55.05
40	24.875	800767	1.55	Octadecanoic acid	95	73.00
41	27.432	5770134	11.19	Hexanedioic acid, bis(2-ethylhexyl) ester	98	129.05
42	28.940	546603	1.06	Bis(2-ethylhexyl) phthalate	96	149.00
		51585688	100.00			

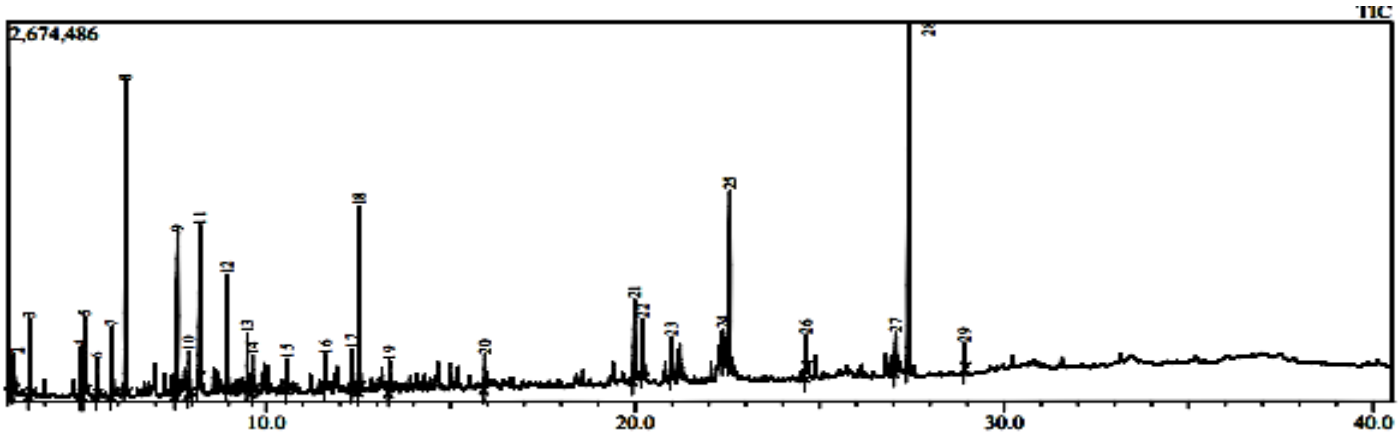

Figure D-30: GCMS analysis for the low reaction conditions 6g 10wt% 30 minutes run

Table D-30: GCMS results for the low reaction conditions 6g 10wt% 30 minutes run

Peak#	R. Time	Area	Area%	Name	Similarity	Base m/z
1	3.055	361964	1.04	Propanoic acid, 2-hydroxy-2-methyl-, ethyl ester	90	59.00
2	3.164	443401	1.28	2-Hydroxy-3-pentanone	96	45.05
3	3.590	1020159	2.94	Furfural	86	96.00
4	4.984	596843	1.72	2-Cyclopenten-1-one, 2-methyl-	89	96.00
5	5.085	1100550	3.18	Ethanone, 1-(2-furanyl)-	95	95.00
6	5.411	426519	1.23	2,5-Hexanedione	98	43.00
7	5.828	844765	2.44	3(2H)-Furanone, 2-(1-hydroxy-1-methyl-2-oxopropyl)-2,5-dimethyl-	83	40.05
8	6.198	4279598	12.35	2-Furancarboxaldehyde, 5-methyl-	96	110.00
9	7.609	3334498	9.62	2-Cyclopenten-1-one, 2-hydroxy-3-methyl-	98	112.00
10	7.920	558693	1.61	Benzoic acid, 4-(4-fluorobenzoyloxy)-, benzyl ester	75	124.00
11	8.213	2607649	7.53	2-Cyclopenten-1-one, 3-ethyl-2-hydroxy-	89	126.05
12	8.949	1361894	3.93	2-Cyclopenten-1-one, 3-ethyl-2-hydroxy-	94	126.05

13	9.495	631195	1.82	2-Cyclopenten-1-one, 3-ethyl-2-hydroxy-	94	126.05
14	9.638	428874	1.24	2(3H)-Furanone, 5-acetyldihydro-	94	85.00
15	10.571	360076	1.04	4,4-Dimethyl-2-propenylcyclopentanone	84	152.00
16	11.604	383544	1.11	7-Octen-4-one, 2,6-dimethyl-	81	85.00
17	12.332	511278	1.48	1,2-Benzenediol, 3-methyl-	96	124.00
18	12.538	2241840	6.47	Ethanone, 1-(2,5-dihydroxyphenyl)-	93	137.00
19	13.351	338621	0.98	2(4H)-Benzofuranone, 5,6,7,7a-tetrahydro-3,6-dimethyl-	78	166.00
20	15.933	404073	1.17	Bicyclo[3.3.1]nona-2,6-diene, 2,6-bis(acetoxy)-	79	152.00
21	19.984	1417133	4.09	Tetradecanoic acid	95	21 19.73.00
22	20.208	856301	2.47	6,8-Dihydroxy-3-methylisocoumarin	74	191.90
23	20.997	661740	1.91	7-Ethyl-4,6-heptadecandione	71	156.00
24	22.388	350253	1.01	l-Proline, N-butoxycarbonyl-, heptyl ester	71	70.05
25	22.568	2940264	8.49	n-Hexadecanoic acid	96	73.00
26	24.630	491198	1.42	Oleic Acid	95	55.05
27	27.067	713555	2.06	9-Octadecenamide, (Z)-	85	59.00
28	27.409	4636063	13.38	Hexanedioic acid, bis(2-ethylhexyl) ester	97	129.00
29	28.925	344836	1.00	Bis(2-ethylhexyl) phthalate	92	148.95
		34647377	100.00			

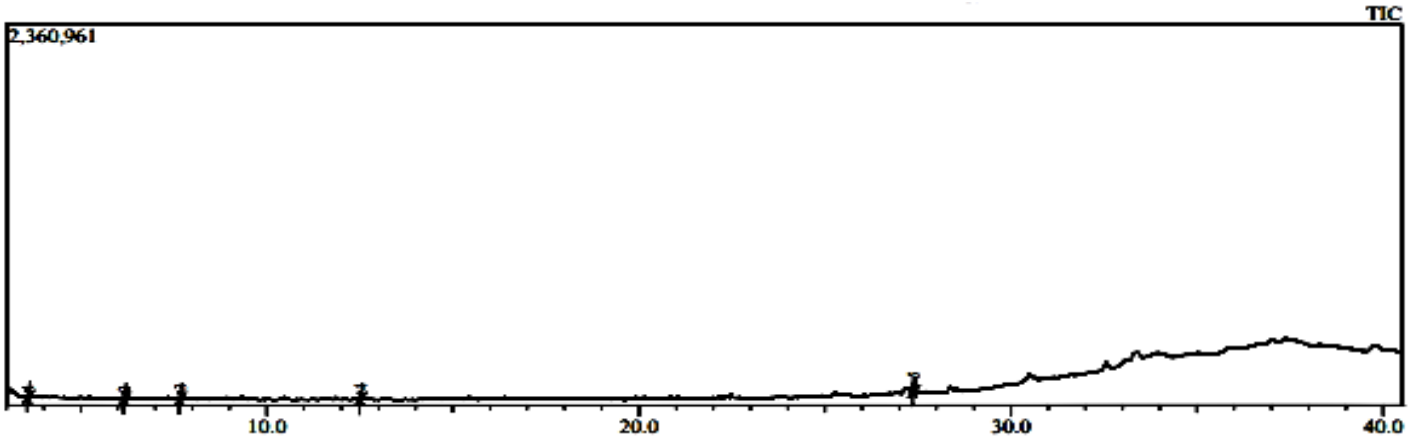

Figure D-31: GCMS analysis for the induction period 5-minute run

Table D-31: GCMS results for the induction period 5-minute run

Peak#	R. Time	Area	Area%	Name	Similarity	Base m/z
1	3.585	66936	15.53	3-Furaldehyde	95	96.05

2	6.180	60062	13.93	2-Furancarboxaldehyde, 5-methyl-	94	110.05
3	7.688	75140	17.43	2-Cyclopenten-1-one, 2-hydroxy-3-methyl-	97	112.10
4	12.533	89202	20.69	Ethanone, 1-(2,5-dihydroxyphenyl)-	92	137.00
5	27.387	139769	32.42	Hexanedioic acid, bis(2-ethylhexyl) ester	95	129.05
		431109	100.00			

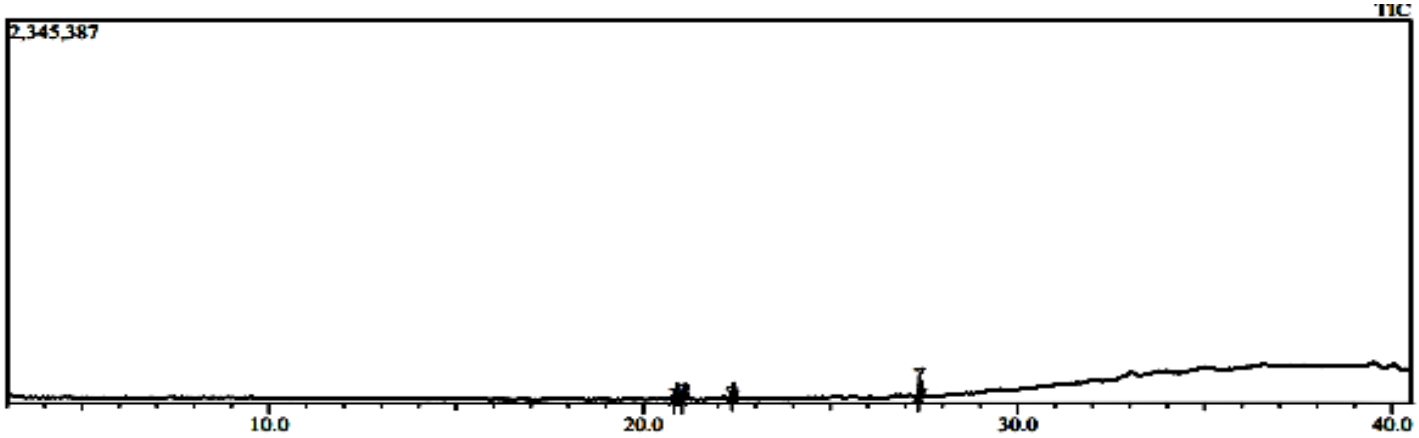

Figure D-32: GCMS analysis for the induction period 10-minute run

Table D-32: GCMS results for the induction period 10-minute run

Peak#	R. Time	Area	Area%	Name	Similarity	Base m/z
1	20.869	87917	19.62	7-Ethyl-4,6-heptadecandione	77	156.10
2	21.075	102953	22.98	Cyclo(L-prolyl-L-valine)	86	154.10
3	22.385	23911	5.34	Hexahydro-3-(1-methylpropyl)pyrrolo[1,2-a]pyrazine-1,4-dione	83	154.10
4	27.389	233216	52.06	Hexanedioic acid, bis(2-ethylhexyl) ester	97	129.10
		447997	100.00			

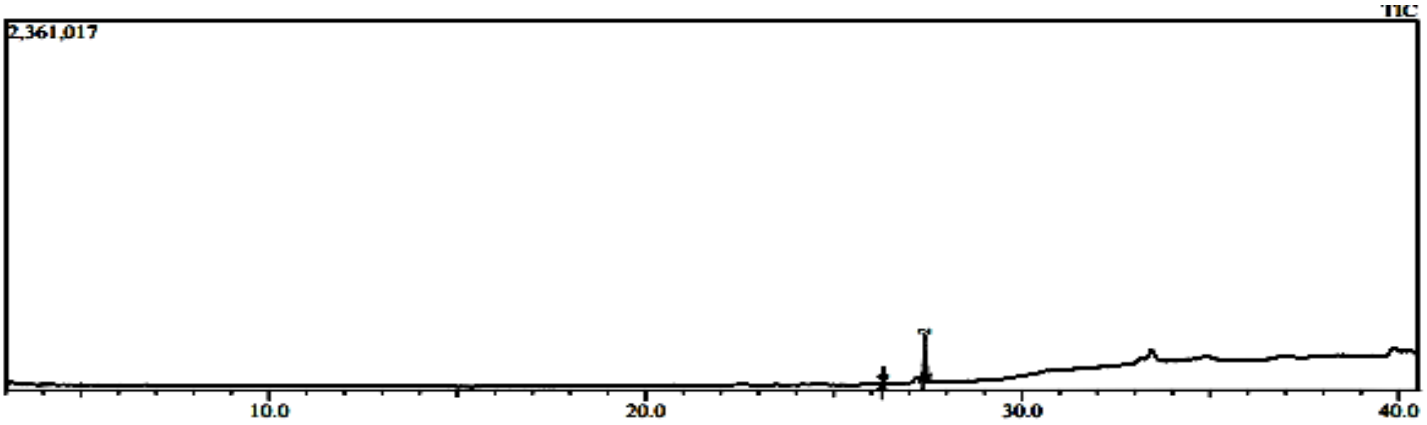

Figure D-33: GCMS analysis for the induction period 15-minute run

Table D-33: GCMS results for the induction period 15-minute run

Peak#	R. Time	Area	Area%	Name	Similarity	Base m/z
1	26.308	14808	2.68	9-Octadecenoic acid, 12-hydroxy-, methyl ester, [R-(Z)]-	79	55.00
2	27.405	537667	97.32	Hexanedioic acid, bis(2-ethylhexyl) ester	97	129.05
		552475	100.00			

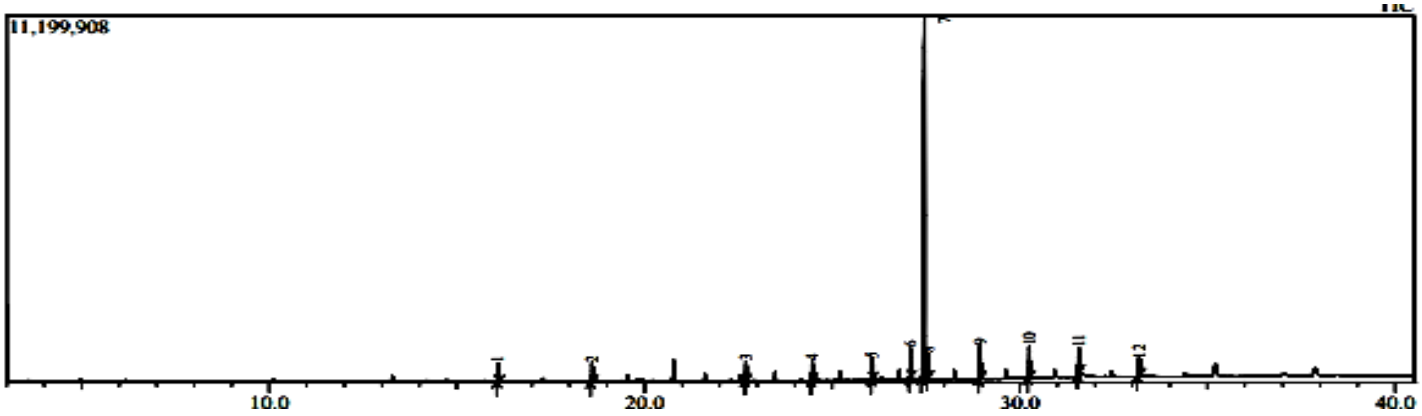

Figure D-34: GCMS analysis for the induction period 20-minute run

Table D-34: GCMS results for the induction period 20-minute run

Peak#	R. Time	Area	Area%	Name	Similarity	Base m/z
1	16.097	945516	1.86	tetradecamethyl-	96	281.00
2	18.603	1087079	2.14	Cyclooctasiloxane, hexadecamethyl-	95	355.05
3	22.699	1073045	2.11	Cyclodecasiloxane, eicosamethyl-	88	73.05

4	24.469	1046333	2.06	Cyclooctasiloxane, hexadecamethyl-	86	355.05
5	26.074	1177518	2.31	Cyclononasiloxane, octadecamethyl-	89	73.05
6	27.085	1542473	3.03	9-Octadecenamide, (Z)-	95	59.00
7	27.458	34724360	68.27	Hexanedioic acid, bis(2-ethylhexyl) ester	96	129.10
8	27.556	1339340	2.63	Cyclodecasiloxane, eicosamethyl- 87 73.05		
9	28.942	2407568	4.73	Tetracosamethyl-cyclododecasiloxane	77	355.05
10	30.251	2031989	3.99	Tetracosamethyl-cyclododecasiloxane	88	73.05
11	31.570	1795043	3.53	Tetracosamethyl-cyclododecasiloxane	86	73.05
12	33.171	1694944	3.33	Tetracosamethyl-cyclododecasiloxane	86	73.05
		50865208	100.00			

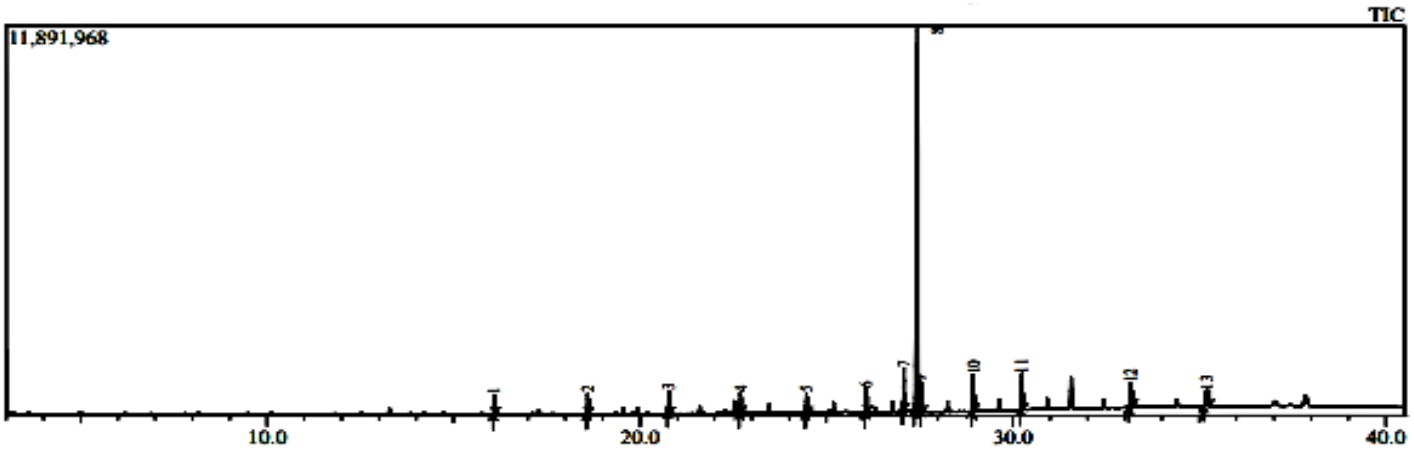

Figure D-35: GCMS analysis for the induction period 25-minute run

Table D-35: GCMS results for the induction period 25-minute run

Peak#	R. Time	Area	Area%	Name	Similarity	Base m/z
1	16.094	964921	1.64	Cycloheptasiloxane, tetradecamethyl-	96	73.00
2	18.600	1123504	1.91	Cyclooctasiloxane, hexadecamethyl-	95	354.85
3	20.766	1115909	1.90	3 20.766 1115909 1.90 Cyclononasiloxane, octadecamethyl- 91 73.00	91	73.00
4	22.696	1168444	1.99	Cyclodecasiloxane, eicosamethyl-	87	73.00
5	24.464	1190900	2.02	Cyclooctasiloxane, hexadecamethyl-	86	73.00

6	26.070	1413592	2.40	Cyclononasiloxane, octadecamethyl-	88	73.00
7	27.075	2228319	3.79	9-Octadecenamide, (Z)-	7 27.075 95	59.00
8	27.449	38472838	65.39	Hexanedioic acid, bis(2-ethylhexyl) ester	96	129.00
9	27.551	1642282	2.79	Cyclodecasiloxane, eicosamethyl-	87	73.00
10	28.939	2767630	4.70	Tetracosamethyl-cyclododecasiloxane	82	73.00
11	30.246	2346428	3.99	Tetracosamethyl-cyclododecasiloxane	87	73.00
12	33.164	2289980	3.89	Tetracosamethyl-cyclododecasiloxane	86	220.95
13	35.201	2111350	3.59	Tetracosamethyl-cyclododecasiloxane	87	220.95
		58836097	100.00			

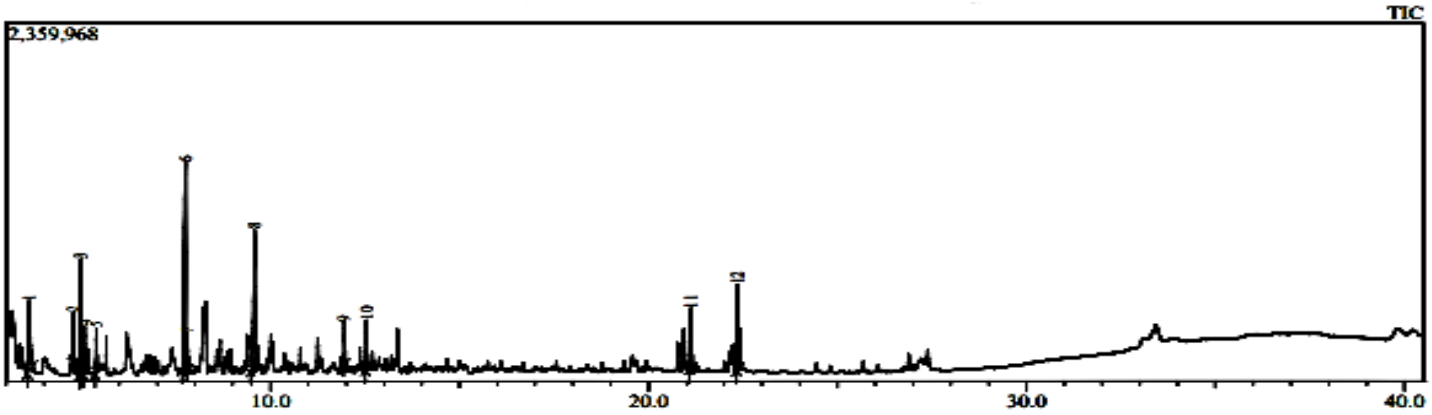

Figure D-36: GCMS analysis for the induction period 30-minute run

Table D-36: GCMS results for the induction period 30-minute run

Peak#	R. Time	Area	Area%	Name	Similarity	Base m/z
1	3.603	1651913	10.84	2-Cyclopenten-1-one	96	82.00
2	4.782	640459	4.20	4-Hydroxy-3-hexanone	94	59.00
3	4.985	1489960	9.78	2-Cyclopenten-1-one, 2-methyl-	95	96.00
4	5.085	726189	4.77	1-(3H-Imidazol-4-yl)-ethanone	83	94.95
5	5.389	482449	3.17	Butyrolactone	94	42.05
6	7.745	4103104	26.93	2-Cyclopenten-1-one, 2-hydroxy-3-methyl-	98	112.00
7	7.806	404133	2.65	2-Cyclopenten-1-one, 2,3-dimethyl-	93	67.00
8	9.574	2588408	16.99	2-Cyclopenten-1-one, 3-ethyl-2-hydroxy-	97	126.00
9	11.956	384397	2.52	2-Cyclohexen-1-one, 4-(1-methylethyl)-	85	43.00

10	12.541	624886	4.10	Ethanone, 1-(2,5-dihydroxyphenyl)-	93	137.00
11	21.122	947470	6.22	Cyclo(L-prolyl-L-valine)	85	154.00
12	22.364	1191797	7.82	5,10-Diethoxy-2,3,7,8-tetrahydro-1H,6H-dipyrrolo[1,2-a:1',2'-d]pyrazine	85	70.05
		15235165	100.00			

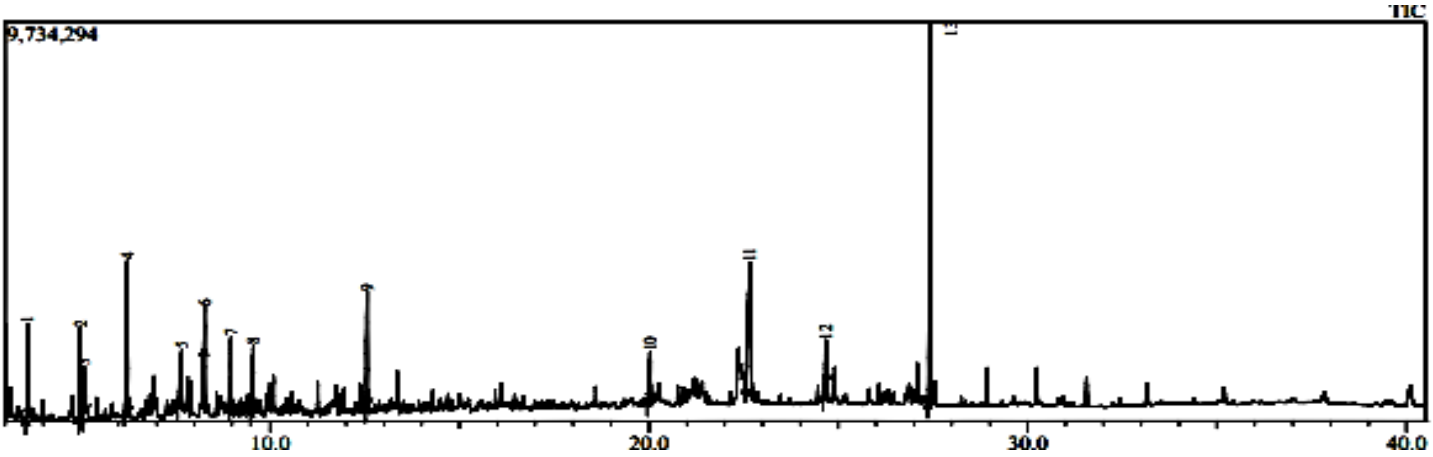

Figure D-37: GCMS analysis for the induction period 35-minute run

Table D-37: GCMS results for the induction period 35-minute run

Peak#	R. Time	Area	Area%	Name	Similarity	Base m/z
1	3.595	4788622	5.08	3-Cyclopentene-1-acetaldehyde, 2-oxo-	84	82.05
2	2 4.987	4531288	4.81	2-Cyclopenten-1-one, 2-methyl-	92	96.10
3	5.086	2844637	3.02	Ethanone, 1-(2-furanyl)-	92	95.05
4	6.228	12160502	12.91	2-Furancarboxaldehyde, 5-methyl-	96	110.05
5	7.668	5416835	5.75	2-Cyclopenten-1-one, 2-hydroxy-3-methyl-	98	112.05
6	8.266	1959317	2.08	2-Cyclohexen-1-one, 2-hydroxy-3-methyl-6-(1-methylethyl)-	78	126.10
7	8.964	3.28	3.28	2-Cyclopenten-1-one, 3-ethyl-2-hydroxy-	92	126.05
8	9.554	5221305	5.54	2-Cyclopenten-1-one, 3-ethyl-2-hydroxy-	96	126.05
9	12.562	6126571	6.50	Resorcinol, 2-acetyl-	94	137.00
10	20.037	3836048	4.07	Tetradecanoic acid	95	73.05
11	22.673	16182434	17.18	n-Hexadecanoic acid	93	73.05
12	24.676	2904969	3.08	9-Octadecenoic acid, (E)-	94	55.05
13	27.438	25136670	26.68	Hexanedioic acid, bis(2-ethylhexyl) ester	95	129.05

		94197786	100.00			

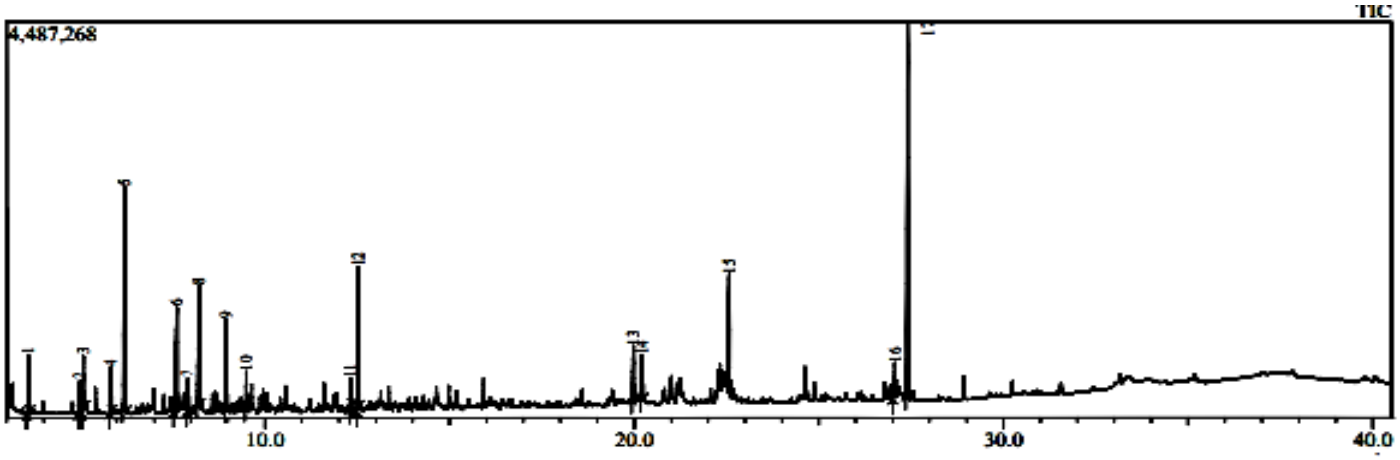

Figure D-38: GCMS analysis for the induction period 40-minute run

Table D-38: GCMS results for the induction period 40-minute run

Peak#	R. Time	Area	Area%	Name	Similarity	Base m/z
1	3.588	1261392	3.32	Furfural	87	96.00
2	4.981	624797	1.65	2-Cyclopenten-1-one, 2-methyl-	89	96.10
3	5.082	1189754	3.13	Ethanone, 1-(2-furanyl)-	95	95.00
4	5.825	893265	2.35	3(2H)-Furanone, 2-(1-hydroxy-1-methyl-2-oxopropyl)-2,5-dimethyl-	83	112.05
5	6.199	5424193	14.29	2-Furancarboxaldehyde, 5-methyl-	97	110.05
6	7.616	3781137	9.96	2-Cyclopenten-1-one, 2-hydroxy-3-methyl-	98	112.05
7	7.916	674078	1.78	1H-Pyrazole-4-carboxaldehyde, 1,5-dimethyl-	76	124.05
8	8.220	3203858	8.44	2-Cyclopenten-1-one, 3-ethyl-2-hydroxy-	87	126.05
9	8.946	1772836	4.67	2-Cyclopenten-1-one, 3-ethyl-2-hydroxy-	93	126.05
10	9.495	765384	2.02	2-Cyclopenten-1-one, 3-ethyl-2-hydroxy-	93	126.05
11	12.321	575854	1.52	1,2-Benzenediol, 3-methyl-	94	124.05
12	12.534	2990013	7.88	Resorcinol, 2-acetyl-	94	137.00
13	19.979	1441982	3.80	Tetradecanoic acid	95	73.05
14	20.207	1112518	2.93	6,8-Dihydroxy-3-methylisocoumarin	74	191.95
15	22.568	3009343	7.93	n-Hexadecanoic acid	95	73.05
16	27.056	937327	2.47	13-Docosenamide, (Z)-	78	59.05
17	27.404	8301333	21.87	87 Hexanedioic acid, bis(2-ethylhexyl) ester	96	129.05
		37959064	100.00			

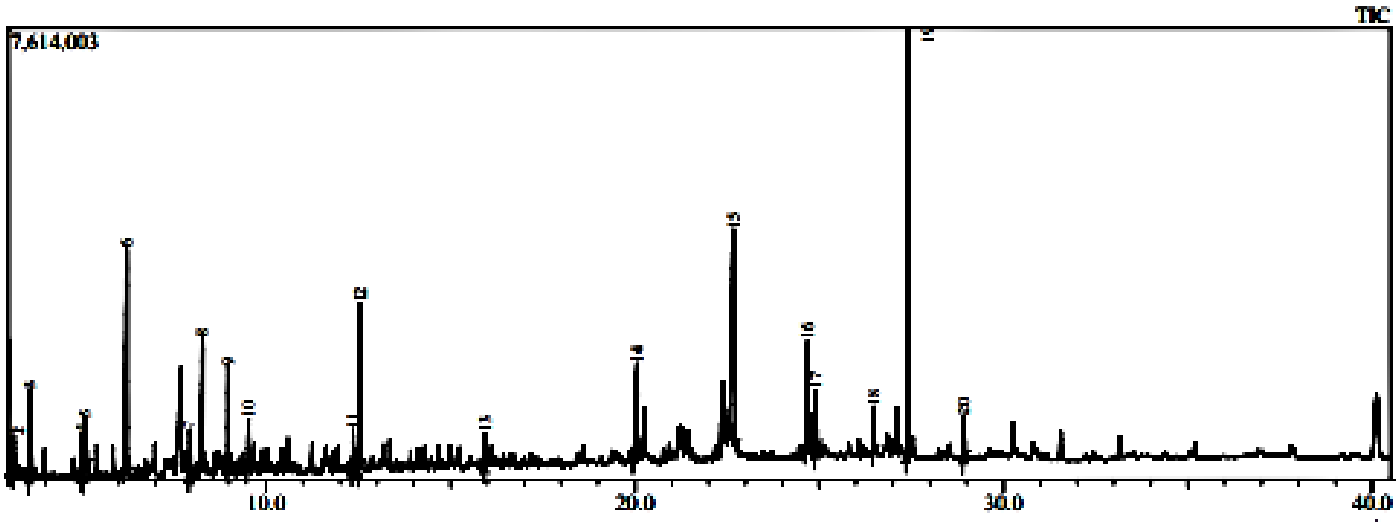

Figure D-39: GCMS analysis for the induction period 45-minute run

Table D-39: GCMS results for the induction period 45-minute run

Peak#	R. Time	Area	Area%	Name	Similarity	Base m/z
1	3.050	1039818	1.12	Propanoic acid, 2-hydroxy-2-methyl-	90	59.05
2	3.160	1192823	1.29	2-Hydroxy-3-pentanone	96	45.10
3	3.590	3010384	3.25	3,5-Dimethylpyrazole	85	96.05
4	4.981	1299127	1.40	2-Cyclopenten-1-one, 2-methyl-	90	96.10
5	5.084	2182386	2.35	Ethanone, 1-(2-furanyl)-	94	95.05
6	6.223	10793576	11.64	2-Furancarboxaldehyde, 5-methyl-	97	110.05
7	7.926	1413561	1.52	1H-Pyrazole-4-carboxaldehyde, 1,5-dimethyl-	74	124.05
8	8.259	6100664	6.58	2-Cyclopenten-1-one, 3-ethyl-2-hydroxy-	85	126.10
9	8.960	3306700	3.57	2-Cyclopenten-1-one, 3-ethyl-2-hydroxy-	92	126.10
10	9.524	2058297	2.22	2-Cyclopenten-1-one, 3-ethyl-2-hydroxy-	95	126.10
11	12.354	1553057	1.67	1,2-Benzenediol, 3-methyl-	96	124.05
12	12.555	5823906	6.28	Resorcinol, 2-acetyl-	94	137.05
13	15.940	850639	0.92	Bicyclo[3.3.1]nona-2,6-diene, 2,6-bis(acetoxy)-	78	152.10
14	20.056	5875959	6.34	Tetradecanoic acid	96	73.05
15	22.686	18327413	19.76	n-Hexadecanoic acid	95	73.05
16	24.688	5943858	6.41	Oleic Acid	94	55.05
17	24.919	2008696	2.17	Octadecanoic acid	95	73.05
18	26.482	1398230	1.51	Arachidonic acid	96	79.10
19	27.426	16920350	18.24	Hexanedioic acid, bis(2-ethylhexyl) ester	95	129.05
20	28.925	1653260	1.78	Bis(2-ethylhexyl) phthalate	71	149.00

		92752704	100.00			

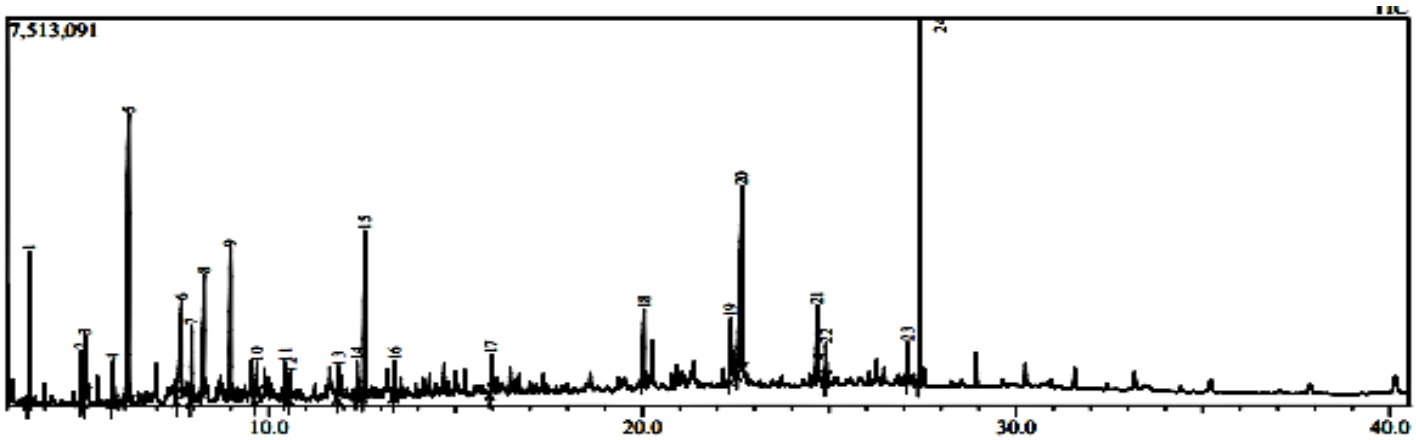

Figure D-40: GCMS analysis for the induction period 50-minute run

Table D-40: GCMS results for the induction period 50-minute run

Peak#	R. Time	Area	Area%	Name	Similarity	Base m/z
1	3.598	5634005	4.92	Furfural	94	96.00
2	4.985	1789366	1.56	1H-Imidazole-4-carboxylic acid	81	112.05
3	5.089	2383081	2.08	Ethanone, 1-(2-furanyl)-	95	95.00
4	5.829	1551342	1.36	3(2H)-Furanone, 2-(1-hydroxy-1-methyl-2-oxopropyl)-2,5-dimethyl-	83	112.05
5	6.252	19747914	17.26	2-Furancarboxaldehyde, 5-methyl-	96	110.05
6	7.673	8369189	7.32	2-Cyclopenten-1-one, 2-hydroxy-3-methyl-	98	112.05
7	7.938	2879664	2.52	Benzenemethanethiol	77	91.05
8	8.266	6631109	5.80	2-Cyclopenten-1-one, 3-ethyl-2-hydroxy-	86	126.05
9	8.978	5566789	4.87	2-Cyclopenten-1-one, 3-ethyl-2-hydroxy-	93	126.05
10	9.683	1318986	1.15	2(3H)-Furanone, 5-acetyldihydro-	95	85.00
11	10.445	1287791	1.13	2,3-Dihydroxybenzaldehyde	94	138.00
12	10.582	1052460	0.92	4,4-Dimethyl-2-propenylcyclopentanone	82	152.05
13	11.866	1077377	0.94	4-Acetyl-1-methylcyclohexene	84	138.05
14	12.366	1460719	1.28	1,2-Benzenediol, 3-methyl-	97	124.05
15	12.573	7428618	6.49	Resorcinol, 2-acetyl-	93	137.00
16	13.368	1115922	0.98	(6R,7aS)-3,6-Dimethyl-5,6,7,7a-tetrahydrobenzofuran-2(4H)-one	77	166.00
17	15.954	1236947	1.08	Bicyclo[3.3.1]nona-2,6-diene, 2,6-bis(acetoxy)-	79	152.00

18	20.045	3926150	3.43	Tetradecanoic acid	96	73.00
19	22.371	3160431	2.76	1,2-Oxathiane, 6-dodecyl-, 2,2-dioxide	84	55.05
20	22.663	15740976	13.76	n-Hexadecanoic acid	96	73.00
21	24.679	2468735	2.16	Oleic Acid	94	55.00
22	24.915	1159365	1.01	Octadecanoic acid	96	73.00
23	27.099	1763811	1.54	9-Octadecenamide, (Z)-	87	59.00
24	27.436	15649298	13.68	Hexanedioic acid, bis(2-ethylhexyl) ester	97	129.05
		114400045	100.00			

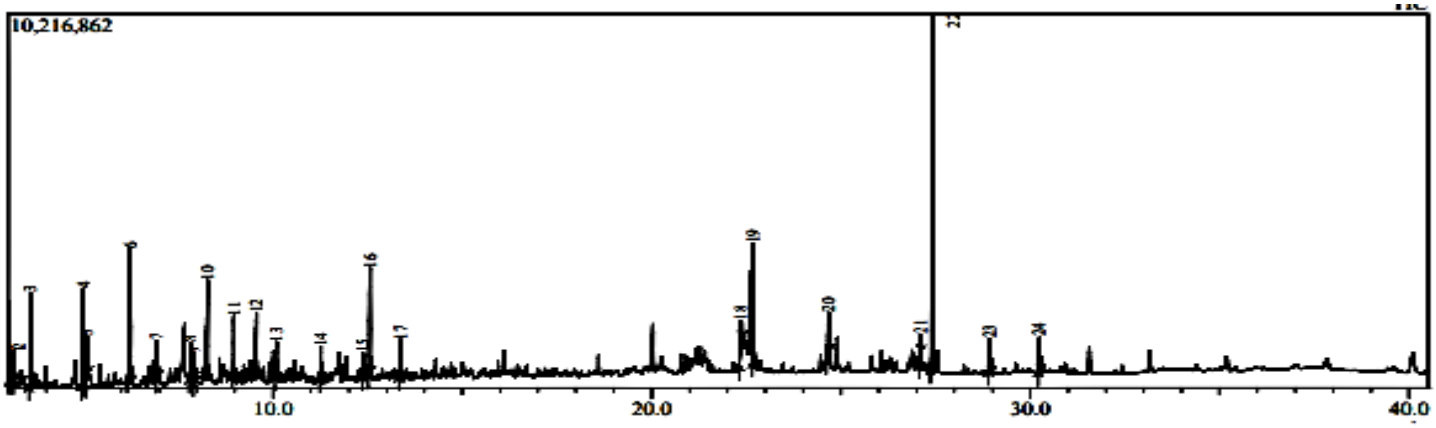

Figure D-41: GCMS analysis for the induction period 55-minute run

Table D-41: GCMS results for the induction period 55-minute run

Peak#	R. Time	Area	Area%	Name	Similarity	Base m/z
1	3.052	1361530	1.33	Propanoic acid, 2-hydroxy-2-methyl-, ethyl ester	90	59.05
2	3.163	1412616	1.38	2-Hydroxy-3-pentanone	96	45.10
3	3.599	5022621	4.92	3-Cyclopentene-1-acetaldehyde, 2-oxo-	86	82.05
4	4.993	5305506	5.20	2-Cyclopenten-1-one, 2-methyl-	92	96.05
5	5.089	2565526	2.51	Ethanone, 1-(2-furanyl)-	93	95.00
6	6.229	11687357	11.46	2-Furancarboxaldehyde, 5-methyl-	96	11.46
7	6.931	1643631	1.61	2-Cyclopenten-1-one, 2,3-dimethyl-	92	110.05
8	7.822	1890803	1.85	2-Cyclopenten-1-one, 2,3-dimethyl-	95	110.05
9	7.931	1283837	1.26	2-Benzyl-5-([(3-methoxyphenyl)amino]methyl)-2,3-dihydro-1H-1,2,4-triazol-3-one	76	124.05
10	8.270	7111244	6.97	2-Cyclopenten-1-one, 3-ethyl-2-hydroxy-	83	126.05

11	8.965	2885244	2.83	2-Cyclopenten-1-one, 3-ethyl-2-hydroxy-	92	126.05
12	9.563	4438322	4.35	2-Cyclopenten-1-one, 3-ethyl-2-hydroxy-	96	126.05
13	10.099	1868133	1.83	1,3-Cyclopentanedione, 2-ethyl-2-methyl-	79	94.05
14	11.263	1426519	1.40	2-Hydroxy-3-propyl-2-cyclopenten-1-one	85	125.05
15	12.381	1223740	1.20	1,2-Benzenediol, 3-methyl-	91	124.00
16	12.563	6062453	5.94	Resorcinol, 2-acetyl-	94	137.00
17	13.364	1809607	1.77	,4,5,6,7,8-Hexahydro-2H-chromene	79	110.05
18	22.366	2098627	2.06	6-Pentadecenoic acid, 13-methyl-, (6Z)-	91	55.05
19	22.674	6016379	5.90	n-Hexadecanoic acid	90	73.05
20	24.678	2791954	2.74	9-Octadecenoic acid, (E)-	95	55.05
21	27.096	1191166	1.17	9-Octadecenamide, (Z)-	94	59.05
22	27.440	26923013	26.39	Hexanedioic acid, bis(2-ethylhexyl) ester	95	129.05
23	28.930	2207032	2.16	Cyclononasiloxane, octadecamethyl-	66	148.95
24	30.245	1800799	1.77	Tetracosamethyl-cyclododecasiloxane	84	354.90
		102027659	100.00			

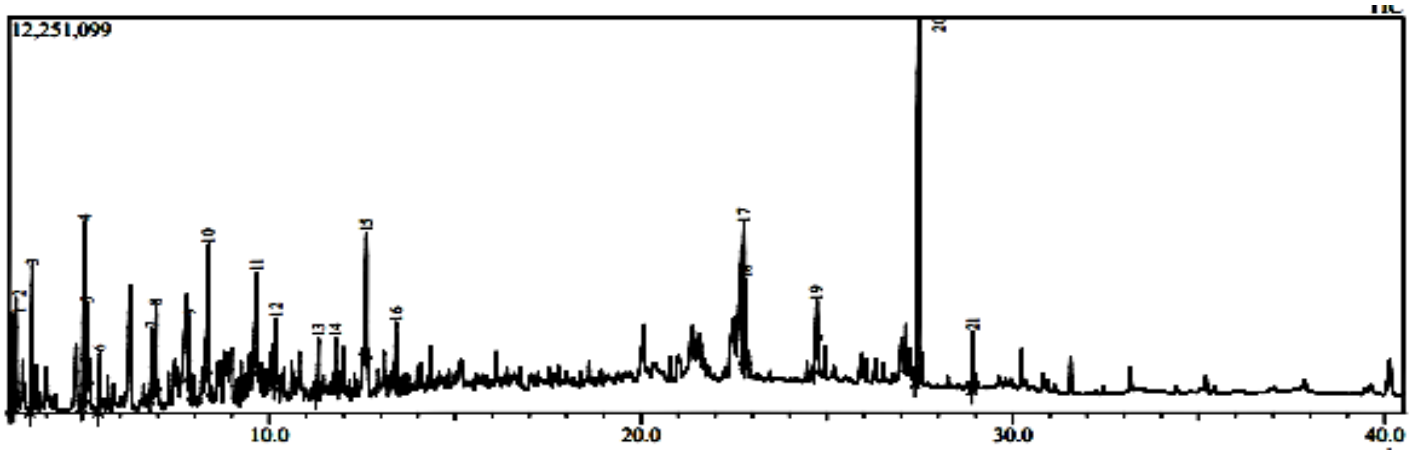

Figure D-42: GCMS analysis for the induction period 60-minute run

Table D-42: GCMS results for the induction period 60-minute run

Peak#	R. Time	Area	Area%	Name	Similarity	Base m/z
1	3.076	7866801	4.50	3-Hydroxy-3-methyl-2-butanone	90	59.05
2	3.190	7743154	4.43	2-Hydroxy-3-pentanone	96	45.05
3	3.630	10955017	6.27	2-Cyclopenten-1-one	95	82.05

4	5.038	16713405	9.57	2-Cyclopenten-1-one, 3-methyl-	92	96.05
5	5.121	3170493	1.81	Ethanone, 1-(2-furanyl)-	96	95.00
6	5.443	3424356	56 1.96	2,5-Hexanedione	98	43.05
7	6.842	5768937	3.30	2-Cyclopenten-1-one, 3,4-dimethyl-	89	95.05
8	6.959	4782850	2.74	2-Cyclopenten-1-one, 2,3-dimethyl-	94	110.05
9	7.863	4947747	2.83	2-Cyclopenten-1-one, 2,3-dimethyl-	94	110.05
10	8.372	6734275	3.85	Phenol, 2-methyl-	87	108.05
11	9.674	10132828	5.80	2-Cyclopenten-1-one, 3-ethyl-2-hydroxy-	93	126.05
12	10.189	4786792	2.74	1,3-Cyclopentanedione, 2-ethyl-2-methyl-	78	94.05
13	11.330	4540789	2.60	2-Hydroxy-3-propyl-2-cyclopenten-1-one	88	125.05
14	11.793	2664485	1.53	2-Cyclohexen-1-one, 2-hydroxy-3-methyl-6-(1-methylethyl)-	84	126.05
15	12.617	9970935	5.71	1-(2,3-Dihydroxyphenyl)ethanone	92	137.00
16	13.411	4196543	2.40	3,4,5,6,7,8-Hexahydro-2H-chromene	16 1378	110.05
17	22.773	9899505	5.67	n-Hexadecanoic acid	91	73.05
18	22.810	4673094	2.68	2,5-Piperazinedione, 3,6-bis(2-methylpropyl)-	80	170.05
19	24.732	4975934	2.85	9-Octadecenoic acid, (E	94	55.05
20	27.473	42770636	24.48	Hexanedioic acid, bis(2-ethylhexyl) ester	95	129.05
21	28.934	3975375	2.28	Bis(2-ethylhexyl) phthalate	70	148.95
		174693951	100.00			

Appendix E: Matlab Script

Main Script

```
close all
clear
clc

% Global variables
global Fin MFout c2

% Observed experimental data
Fin=xlsread('Masters Results Final.xlsx','Raw Data','C54:T56');      % initial
mass fractions for all data points
MFout=xlsread('Masters Results Final.xlsx','Raw Data','C59:T61');     % final
mass fractions for all components

NN=[1 2 3];

c1=size(MFout);
c2=c1(2);

lb=[0 0 0 0];
ub=[inf inf inf inf];

k0=[1.5 1.5 5e-05 5e-05]; %initial guess for kinetic constants and inhibition
constants [k1 k2 k3 k4]

options=optimset('Display','iter','MaxIter',100,'MaxFunEvals',5000,'TolFun',1
e-17,'TolX',1e-17,'LargeScale','on');

[k,resnorm,residual,exitflag,output,lambda,jacobian]=lsqnonlin(@myfun2021,k0,
lb,ub,options);

%initializing predicted values of final mass fractions
FS_pred=zeros(1,c2);
FO_pred=zeros(1,c2);
FA_pred=zeros(1,c2);

for c3=1:c2                    % cycle through data points


    Finp=Fin(:,c3);              % inlet mass fraction for one data point
    options=odeset('BDF','off','NonNegative',[1       2       3],'AbsTol',1e-
5,'RelTol',1e-5);

    t0=[0,c3*5]; %time span for integration
    [t,F]=ode15s(@(t,F) rates2021(t,F,k),t0,Finp,options); %integration

    c4=size(F);
    c5=c4(1);

    Fout_pred=F(c5,:);             % final mass fractions predicted by model
```

```
    Ftot_out_pred=sum(F(c5,:));     % total final mass fraction predicted by
model (should be 1)


    FS_pred(1,c3)=Fout_pred(1); %final mass fraction predicted for solids
    FO_pred(1,c3)=Fout_pred(2); %final mass fraction predicted for oil
    FA_pred(1,c3)=Fout_pred(3);  %final  mass  fraction  predicted  for  aqueous
product

end

FS_pred = [1 FS_pred];
FO_pred = [0 FO_pred];
FA_pred = [0 FA_pred];

% measured final mass fractions (from experimental data)
MS=[1 MFout(1,:)];    %solids
MO=[0 MFout(2,:)];    %oil
MA=[0 MFout(3,:)];    %aqueous product
%% ======Plotting final results =======%%%%
FFDx1=linspace(0,1);
FFDy1=linspace(0,1);
texp = 0:5:90;

figure('Name', 'Product fraction yeilds from hydrothermal liquefaction')
plot(texp, FS_pred, 'b-','LineWidth',2)
hold on
plot(texp, MS, 'bo','MarkerSize',5)
hold on
plot(texp, FO_pred, 'r-','LineWidth',2)
hold on
plot(texp, MO, 'rs','MarkerSize',6)
hold on
plot(texp, FA_pred, 'g-','LineWidth',2)
hold on
plot(texp, MA, 'g*','MarkerSize',6)
title                    ('Mass                    Fraction                    vs.
Time','FontName','Arial','FontSize',20,'FontWeight','normal')
xlabel('time(min)','FontName','Arial','FontSize',20,'FontWeight','normal')
ylabel('yield(wt%)','FontName','Arial','FontSize',20,'FontWeight','normal')
legend   ({'Solids   model','Solids   experimental',   'Bio-oil   model','Bio-oil
experimental','Aqueous   phase   product   model','Aqueous   phase   product
experimental'},'Location','northeast')
hold off
axis square

%% =====Plotting parity plot =====%%%
figure('Name','Parity plot showing fit of data')
plot(FS_pred(2:19),MS(2:19),'bo','MarkerFaceColor','blue','MarkerSize',8)
%solids data
hold on
plot(FO_pred(2:19), MO(2:19),'ro','MarkerFaceColor','red','MarkerSize',8) %oil
data
hold on
```

```
plot(FA_pred(2:19),MA(2:19),'go','MarkerFaceColor','green','MarkerSize',8)
%aqueous phase product data
hold on
plot(FFDx1,FFDy1,'k-','LineWidth',1) %x=y line for reference
title ('Parity Plot','FontName','Arial','FontSize',20,'FontWeight','normal')
xlabel('model                                                                yeild
(wt%)','FontName','Arial','FontSize',20,'FontWeight','normal')
ylabel('experimental                                                         yield
(wt%)','FontName','Arial','FontSize',20,'FontWeight','normal')
legend    ({'Solids',    'Bio-oil','Aqueous    phase    product',    'reference
line'},'Location','southeast')
hold off
axis square
```

Function 1

```
function dF = rates2021(t,F,k)

dF=zeros(3,1);
C=zeros(3,1);
 % rate constants

% solids ---> oil
k1=k(1);      %kinetic rate constant
k3=k(3);      %inhibition constant

%solids ---> aqueous phase product
k2=k(2);     %kinetic rate constant
k4=k(4);     %inhibition constant

Ftot = F(1)+F(2)+F(3);   %total fraction mass in system (dry solids + oil +
aqueous phase product) = 1

% reaction rates
r1=k1*F(1)*exp(-k3/F(1));    %reaction 1: solids ---> oil

r2=k2*F(1)*exp(-k4/F(1));    %reaction 2: %solids ---> aqueous phase product

% differential mass balances

dF(1)=-r1-r2;       % change in solids
dF(2)= r1;          % change in oil
dF(3)= r2;          % change in aqueous phase product
```

Function 2

```
function Fob=myfun2021(k)

% Global variables
global Fin MFout c2

Fob=zeros(5,c2);

for c3=1:c2                    % cycle through data points
```

```
    Finp = Fin(:,c3);              % initial mass fraction for one data point
    MFoutp = MFout(:,c3);          % final mass fraction for one data point

    %carrying out integration using ode15s
    options=odeset('BDF','off','NonNegative',[1       2       3],'AbsTol',1e-
5,'RelTol',1e-5);
    t0=[0,c3*5]; %time-span for integration
    [t,F]=ode15s(@(t,F) rates2021(t,F,k),t0,Finp,options);

    c4=size(F);
    c5=c4(1);

    Fout_pred=F(c5,:);             % outlet mass fraction predicted by model
    Ftot_out_pred=sum(F(c5,:));     % total outlet mass fraction predicted by
model

    for c6=1:3


        Fob(c6,c3)=(((Fout_pred(c6)-MFoutp(c6)))^(2))^(1); %residual function

    end

end

Fob=reshape(Fob,1,[]);
Fob=Fob';
```